Phase Behaviors of ABAC Tetrablock Terpolymers

A DISSERTATION
SUBMITTED TO THE FACULTY OF THE GRADUATE SCHOOL
OF THE UNIVERSITY OF MINNESOTA
BY

Jingwen Zhang

IN PARTIAL FULFILLMENT OF THE REQUIREMENTS
FOR THE DEGREE OF
DOCTOR OF PHILOSOPHY

Frank S. Bates, Adviser

October 2012

Acknowledgements

If I think back over the past five years now, my memories are filled with those numerous hours spent on synthesis and characterization. However, memories are selectively sieved as time passes by. I'm sure several years later, my PhD memories will consist only the excitement achieved in my research area and happiness with my colleagues and friends. I would like to thank the following people who make this possible.

First of all, I would like to thank my advisor, Prof. Frank Bates for his generous guidance, time and attention. His encourage and toleration to my ignorance and mistake is very much appreciated. He showed great enthusiasm and positive attitude towards science and research. He taught me to always pay attention to details. I greatly benefit from working with him, not only on the technical and research aspect, but also on problem-solving and interpersonal relationship, which will be very useful in my future careers.

Next, I would like to extend my appreciation to several group members, especially Michael Bluemle, who patiently taught me living anionic polymerization procedures, as well as those analytical and characterization techniques. I also want to express my gratitude to Adam Meuler, Guillaume Fleury and Sangwoo Lee for their excellent mentoring and observing me doing synthesis at my earlier research stage. I have also benefited from the discussion with many other people: Jihua Chen, Erica Redline, Brian Habersberger, Feng Zuo, Sangwon Kim, Intaek Lee, Luca Martinetti, Carmelo Declet-Perez, and Jie Lv. I would also like to thank my collaborator and polymer theorist, Scott

Sides, for his contribution and effort. I want to thank Fang Zhou for her help with the microtoming.

最后，我要感谢这些年里一直陪伴在我身边的亲人和朋友们。没有你们的鼓励和支持我不可能顺利的走到今天这一步，感谢你们所带给我的一切，欢乐与悲伤，我们一起走过，一起成长，与你们所经历的一切都是我这一生中最难得的回忆和最宝贵的财富。我尤其要感谢我的爸爸妈妈，谢谢你们在各方面对我一如既往的支持与信任，不管什么时间，都耐心地听我的电话，不厌其烦地听我唠叨和平复我的心情。我将这篇论文献给你们，我永远爱你们！

To Mom and Dad

Abstract

The thesis focuses on the composition and the asymmetric effect on the phase behaviour of the tetrablock terpolymers using poly(styrene-*b*-isoprene-*b*-styrene-*b*-ethylene oxide) (SISO) as the model system, synthesized via a living anionic polymerization method and characterized with NMR, GPC, TEM, SAXS, DSC and DMS.

In the compositional study, two series of the isoprene-rich and the styrene-rich symmetric SISO samples (the S blocks are divided equally) are studied in addition to the series with equal volume fractions of the S and I blocks. In the isoprene-rich series, the hexagonally ordered core-shell spherical and cylindrical morphologies (P_6/mmm and P_6/mm space group symmetries) have been identified with increasing O contents. The temperature dependence is examined using one specimen in the isoprene-rich series near the order-disorder boundary. A dodecagonal quasicrystalline (QC) phase has been identified to occur as an intermediate state between the simple hexagonal order (P_6/mmm) and the Frank-Kasper σ-phase (P_{4_2}/mnm) before the sample disorders, with $T_{HEX} < T_{QC} < T_\sigma < T_{ODT}$. The TEM results reveal a QC morphology with a 12-fold rotational symmetry and the existence of the local dodecagonal quasicrystalline approximants that lack of any long-range translational order.

The sequence of phases in the styrene-rich SISO series is the disordered state, spheres with a BCC lattice, liquid-like packed (LLP) spheres and the hexagonally (HEX) ordered cylinders. For SISO with f_O = 11%, LLP, 12-fold QC after shorter annealing time of 30 minutes and $Pm\bar{3}n$ phase after longer annealing time of one day, σ-phase and the disordered states are formed with increasing temperatures; and for another SISO with f_O

= 15%, the LLP spheres and HEX cylinders are formed. Changing the molecular architecture from the ISO triblocks to the SISO tetrablocks drives the preference from the hyperbolic interfaces inherent in the network morphologies to the higher, and zero Gauss, curvature surfaces present in the core-shell spheres and cylinders.

In the asymmetric study, the asymmetric parameter $\tau = N_S/(N_S+N_{S'}) = 0.21 - 0.70$ is the only variable. The core-shell spheres on a hexagonal lattice and LLP have been observed at lower temperatures; the 12-fold QC phase with shorter annealing time of 30 minutes and the $Pm\bar{3}n$ phase after longer annealing time of one day have been observed at intermediate temperatures before the Frank-Kasper σ-phase is formed at the higher temperatures before the samples disorder. The phase behaviors of the symmetric SISO and the asymmetric SIS'O tetrablock terpolymers are nearly identical.

Overall, six, and possibly more, sphere-forming phases have been identified in the SISO tetrablock terpolymers: BCC ($Im\bar{3}m$), LLP, P_6/mmm, QC, $Pm\bar{3}n$ and P_{4_2}/mnm (σ-phase). These phases indicate the great design flexibility and opportunities for the novel phase formation with the ABA'C tetrablock molecular architecture at various molecular weights and compositions.

Table of Contents

List of Tables

List of Figures

1

Introduction and Literature Review

1.1 Introduction

Homopolymers are large molecules composed of the same repeating structural units typically connected by covalent bonds. Their resultant physical and chemical properties are mainly determined by the type of constituent monomers, side groups, stereochemistry, inter- and intra-molecular bonding, etc. For example, with a T_g of 90 ^oC, poly(styrene) is rigid and transparent but brittle; with a T_g of -60 ^oC, poly(isoprene) is rubbery but easily deformed; and poly(ethylene oxide) is semicrystalline.[1] Block copolymers are formed by covalently bonding the ends of two or more homopolymers. This is a good way to combine the homopolymers together, leading to desirable overall physical and chemical properties, and to

overcome the shortcomings associated with the each individual homopolymers.

Block copolymers were first commercialized by the Shell Chemical Company in 1965 with Kraton® line of styrenic block copolymers. Over the years, polymers have grown in importance and will continue to do so with unprecedented opportunities for designing commodity materials such as shoe soles and adhesives,[2–4] along with high technology applications like state-of-art semiconductor devices[5,6] membranes with tunable nanochannels,[7–9] and nanolithography,[10,11] as well as high-end medical applications such as controlled drug delivery devices.[12–14] They are also used as additives that reduce road crack formation due to thermal expansion.[15]

Block copolymers derive utility from the ability to self-assemble into various microstructures at length scales of 5 – 50 nm.[16] This domain spacing can be precisely controlled by careful selection of monomers, molecular weights, compositions and temperature. The types of microstructures formed can be precisely controlled in AB diblock copolymers to form spheres, cylinders, lamellar and groid network morphologies. As the block architecture becomes more complicated, such as ABC triblocks, ABCD tetrablocks, ABCDE pentablocks, and star-polymers, the resultant morphologies will be more intricate. Various synthetic methods make the substitution of certain side groups possible, altering the functionality and properties of man-made materials to meet specific needs, including elasticity, toughness, processibility, optical clarity, density, permeability, etc.

According to Lodge, the current application of block copolymers is still ‘scalar’,

i.e., the useful chemical and physical properties mainly result from selected combinations of monomers, molecular weight, composition and temperature.[16] The various morphologies formed are not directly related to their eventual applications.[17] Lodge predicted that in the future more advanced value-added application of block copolymer would become 'vectorial' in nature with delicate control over microstructures formed after self-assembly, relying not only on the properties of the monomers selected, but also on the particular spatial extent, connectivity and orientation of the nanodomains.[16]

In order to learn, and eventually manipulate, block copolymer microstructures, chemists, material scientists and physicists collaborate together on the systematic study of many block copolymer systems with various molecular architectures such as AB diblocks and ABA/ABC triblocks, with the purpose to hopefully understand the fundamental interactions among various blocks and develop advanced theoretical and computational methods to explain such phase behaviors. Phase diagrams containing possible morphologies of AB diblocks (and some ABC triblocks) have been established, which serve as the foundation for theoretical model development. The highly developed self-consistent mean-field theory (SCFT) is able to calculate accurately the free energies and composition profiles of various microstructures, enabling polymer scientists to identify the most stable structure among several debated ones when the limitation of current experimental technique impairs our interpretation.

This thesis continues the systematic experimental study of ABAC type of tetrablock terpolymers using poly(styrene-*b*-isoprene-*b*-styrene-*b*-ethylene oxide) (SISO) as the model system and combines previous studies to come up with the phase map for symmetric SISO samples (S blocks divided equally). The results are then compared with the well-established ISO system to study the effect of molecular architecture alone on phase behavior. The experimentally obtained morphologies for asymmetric SIS'O samples with S blocks divided unequally are also conducted to study the effect of asymmetry. For the rest of this chapter, the thermodynamics of polymeric samples are reviewed and an overview of the thesis is presented.

1.2 Thermodynamics of Polymer Mixtures

Thermodynamics is extensively used in polymer mixtures and solutions to understand the molecular origin of certain phase equilibrium or phase transitions and explain how different blocks interact with each other. Flory-Huggins theory, modified from the regular solution theory, is often used to describe thermodynamics of polymer mixture and solutions. The Gibbs free energy of mixing of a two-component system is given as:

$$\frac{\Delta G_m}{kT} = \frac{f_A}{N_A}\ln f_A + \frac{f_B}{N_B}\ln f_B + f_A f_B \chi_{AB} \tag{1.1}$$

where k is Boltzmann constant, T is absolute temperature in K, N_A and N_B are the number of repeat units of component A and B, f_A and f_B are the volume fractions of A

and B, and χ_{AB} is the Flory-Huggins interaction parameter.[18] χ_{AB} measures the free energy cost per monomer contact between A and B.[19] The greater the χ_{AB}, the greater the repulsion, and the more favorable for components A and B to phase separate. The first two terms in Equation 1.1 account for the entropic contributions. They are always negative and favor mixing. The third term measures the enthalpic contribution. Positive χ_{AB} drives nearly all homopolymer mixtures to macrophase separate, just like oil and water. χ_{AB} is usually inversely proportional to temperature, i.e., an increase in temperature will decrease χ_{AB}, making the mixing process more favorable.

Block copolymers overcome the problem of macrophase separation by covalently bonding the end of two or more homopolymers.[20] The covalent linkage between the individual blocks forces them to remain adjacent to each other even under conditions that favor separation. Thus, block copolymers self-assemble into various micro- structures on the order of approximately 5 – 50 nm to minimize free energy.[16] The fundamental phase behavior of block copolymers is controlled by: (1) the binary Flory-Huggins interaction parameter χ (or χs), (2) architectural constraints such as the number of blocks, block sequence, and linear vs. starblock copolymers, (3) the overall degree of polymerization N, and (4) the composition of each block. In the case of symmetric AB diblock copolymers, the phase behavior is governed by the product of χN. The larger χN, the greater the tendency to microphase separate. This is because increasing χ makes contacts between chemically different blocks less

favorable while increasing N decreases the translational and configurational entropy. Increasing χN favors microphase separation.

The degree of microphase segregation among the individual blocks can be divided into three different regimes based on the value of χN: (1) weak segregation limit (WSL) for $\chi N \leq 10$, (2) strong segregation limit (SSL) for $\chi N \to \infty$ and (3) intermediate segregation region (ISR) for $10 < \chi N \leq 50$.[21] In the WSL, the individual blocks are intimately mixed with small local deviations in compositions from the bulk average values. In the SSL, the equilibrium state consists of relatively pure blocks with well-defined narrow interfaces due to enthalpic incompatibility. The Gibbs free energy of mixing is minimized under two competing factors: the enthalpic contribution to minimize the interfacial area and additional entropic contribution to stretch polymer chains to maintain this narrow interface. ISR is a region between the WSL and SSL.

1.3 Two Monomers

1.3.1 AB Diblocks

An AB diblock represents the simplest linear block copolymer architecture. At high temperature (low χ), A and B blocks mixed intimately; at low temperature (high χ), A and B blocks microphase separate to form ordered microstructures. Figure 1-1 shows the schematic drawing of AB diblocks with their equilibrium microstructures.

As the volume fraction of the minority block increases, spheres with body-centered cubic symmetry (BCC, S or Q[229]), cylinders with hexagonal symmetry (HEX, H or C), gyroid (G, Q[230] or Q_{Ia3d})[22,23] and lamellae phases(LAM or L)[19,24–30] are formed. A fifth equilibrium morphology, an *Fddd* orthorhombic network phase (O[70]), has been discovered experimentally within a very narrow composition window[31–34] and proved to be theoretically possible.[35] Another commonly reported phase is perforated lamellae (PL),[27] located between cylindrical and lamellar phases in ISR at higher χN as compared to that of G.[36–38] This phase is proved to be a long lived non-equilibrium state experimentally[39] and metastable theoretically.[35,40]

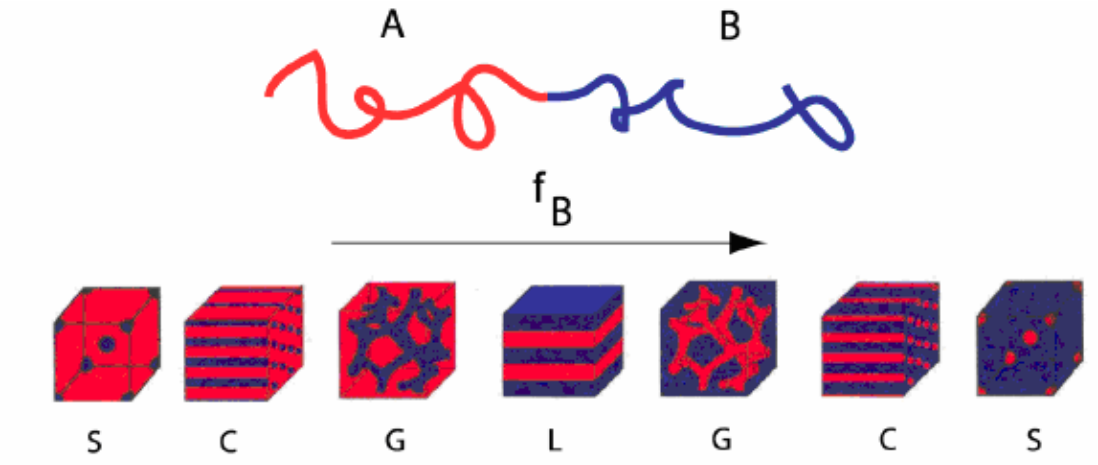

Figure 1-1 Schematic drawing of AB diblock copolymers and their associated equilibrium phase behaviors, reproduced from Bates and Fredrickson.[19]

The first molecular description of S, C and L phases was made by Meier in 1969, incorporating the concept of balancing between chain stretching (entropic) and

interfacial tension (enthalpic).[41] Based on Meier, Krause[42] and Leary and Williams,[43] Helfand and coworkers were able to extend self-consistent field theory (SCFT) to calculate the chain conformation, composition profile and the total free energy applicable to SSL with $\chi N \to \infty$.[44–46] They believed that the additional entropy penalty resulted from the chain stretching to maintain uniform density was greater than that from the localization of copolymer joints to the interfacial region in SSL. The balance between the entropic and the enthalpic contributions drove towards larger domain size, consistent with experimental results. They also correctly predicted the packing symmetry of BCC and hexagonal in spherical and cylindrical phases, respectively.

The WSL is crucial to understand the phase behavior of block copolymers near the T_{ODT}.[25] Leibler[25] pioneered the modeling of block copolymers in the WSL by adapting the random phase approximation (RPA) of deGennes[47] to a monodisperse AB diblock copolymer melt. For symmetric diblock copolymers, the order-disorder transition (ODT) was predicted to occur at χN = 10.5, where the polymer melt is expected to undergo a second order transition from disorder to lamellar state. For all other compositions, the ODT is a first order transition from disorder to spherical state, with order-order transitions (OOT) from spherical to cylindrical, cylindrical to lamellar state at increasing χN.

Experimentally, many results display non-mean-field character near the ODT.[20] A new concept of ‘fluctuation regime’ was introduced in the late 1980s by

Fredrickson and Helfand.[48] They broadened Leibler's WSL theory to include the composition fluctuation effect near the T_{ODT}, which was significant for polymer melts with finite molecular weights. Fluctuation effect altered certain T_{OOT}s, but this effect diminished in the limit of infinite molecular weights. Further away from the ODT in the ordered state with SSL, SCFT was considered to be quite reliable.[28,49]

Matsen and coworkers combined the theories of AB diblock copolymers in SSL and WSL and managed to solve the full SCFT for certain periodic phases.[50] They showed that the PL phase was unstable and the gyroid phase was the most stable among many bicontinuous cubic phases in WSL and ISR.[51] Matsen extended these calculations to SSL by adding more Fourier terms to represent polymer segment profiles, leading to more favorable comparison between theoretical prediction and experimental results.[28,52]

Figure 1-2 shows the theoretical universal phase diagram for AB diblock copolymers calculated based on SCFT,[30] in which the formation of different equilibrium phases is correlated by two parameters, f_A and $\chi_{AB}N$. An experimentally obtained phase diagram for poly(styrene-*b*-isoprene) is also shown, roughly consistent with the theoretical prediction.[27]

1.3.2 ABA Symmetric Triblocks

Symmetric ABA triblock terpolymers are the simplest extension of AB diblock

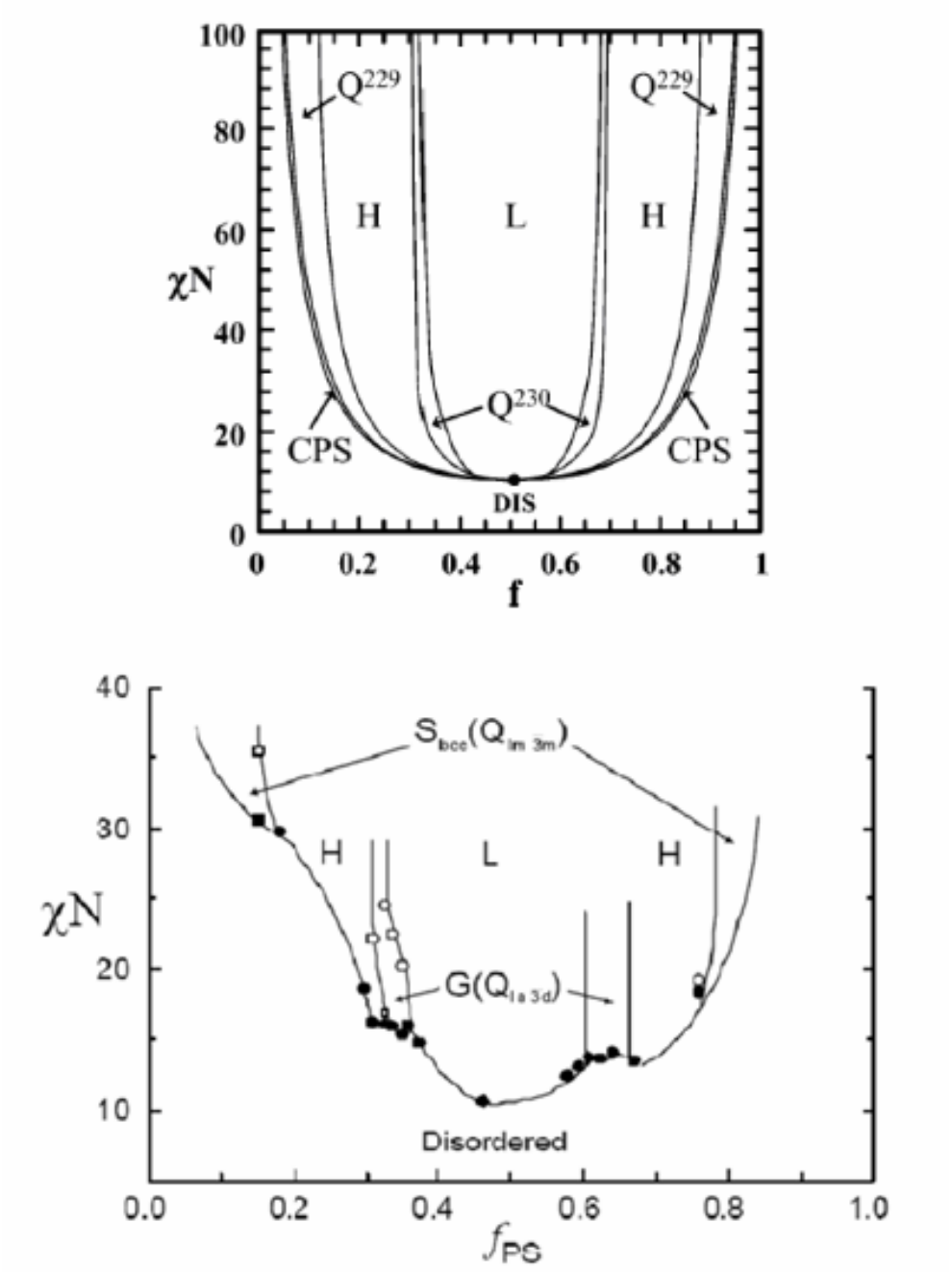

Figure 1-2 Comparison of (top) theoretical phase portrait calculated using SCFT reproduced from Cochran *et al.*[30] and (bottom) experimentally determined phase portrait of poly(styrene-*b*-isoprene) reproduced from Khandpur *et al.*[27] and Ryu *et al.*.[53]

copolymers in terms of linear block copolymer architecture. For diblock copolymers, Leibler predicted the ODT to occur at $\chi N = 10.5$;[25] for triblock terpolymers, the value was predicted to be $\chi N = 18$.[54–58] The experimental results broadly confirmed the theory, including homologous pairs of SI and SIS, PEP-PE_E and PEP-PE_E-PEP and others.[53,59–65] Furthermore, theory predicts that near the ODT, polymer chains will stretch more to produce larger domain spacing in ABA triblock systems as compared to that of the AB diblocks.[56–58]

Another difference between AB diblock and ABA triblock copolymers is the presence of the bridge and loop configuration in the latter. In the bridge configuration, two A blocks are distributed in two different A domains; in the loop configuration, both A blocks are located in the same A domain (see Figure 1-3). The bridge configuration improves the mechanical properties of the ABA triblock tremendously and the enhanced mechanical performance is affected by the bridge-to-loop ratio.[53,60] Matsen and Thompson predicted the bridging fraction is independent of χN, but dependent on morphology: slightly less than 0.8 for spherical micelles, 0.6 for cylindrical micelles and 0.45 for lamellar melts.[58] These theoretical predictions were very similar to the experimental results using the model system of SIS: 0.6 for spherical micelles[66] and 0.4 for lamellar melts.[67]

Despite these differences in AB diblock and ABA triblock systems, they have nearly identical phase behavior. Mayes and Olvera de la Cruz extended Leibler's theory[25] in diblock copolymer system to both symmetric and asymmetric ABA

triblock melts in WSL and computed fluctuation correction in 1991.[54,55] In 1999, Matsen and Thompson mapped out the theoretical phase map for symmetric ABA triblock system, shown in Figure 1-4 (b). Figure 1-4 (a) illustrates a similar theoretical phase map for a homologous AB diblock system. Their similarity is obvious, with S, C, G and L phases formation at increasing values of f_A. In addition, the domain spacings in homologous diblock and triblock melts further away from ODT are found to be quite similar,[69,70] consistent with theoretical predictions. However, there are some differences. The critical χN value for ABA triblock is higher due to the increased likelihood of penetration of the longer B chains in the A domains. Also, the phase diagram become asymmetric as f_A increases because of the same reason, releasing longer B chains from their domain to form disordered state.

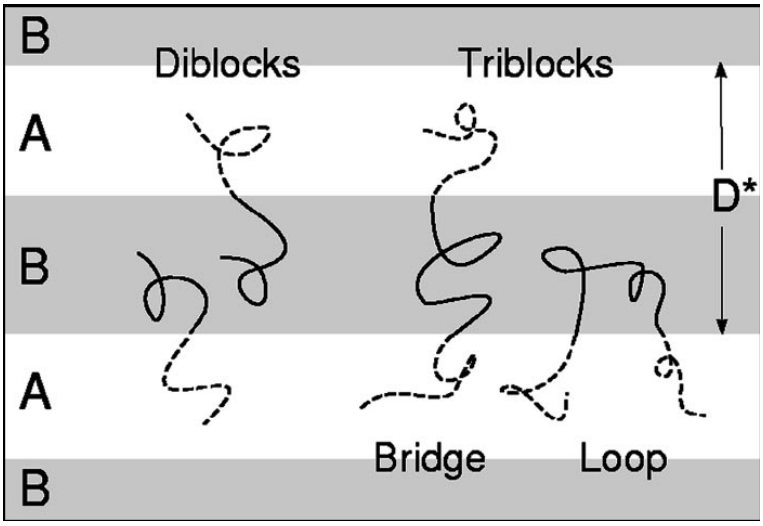

Figure 1-3 Typical configurations of AB diblock and ABA triblock systems in lamellar phase. Triblock molecules are shown in both bridge and loop configurations. Reproduced from Matsen and Thompson.[58]

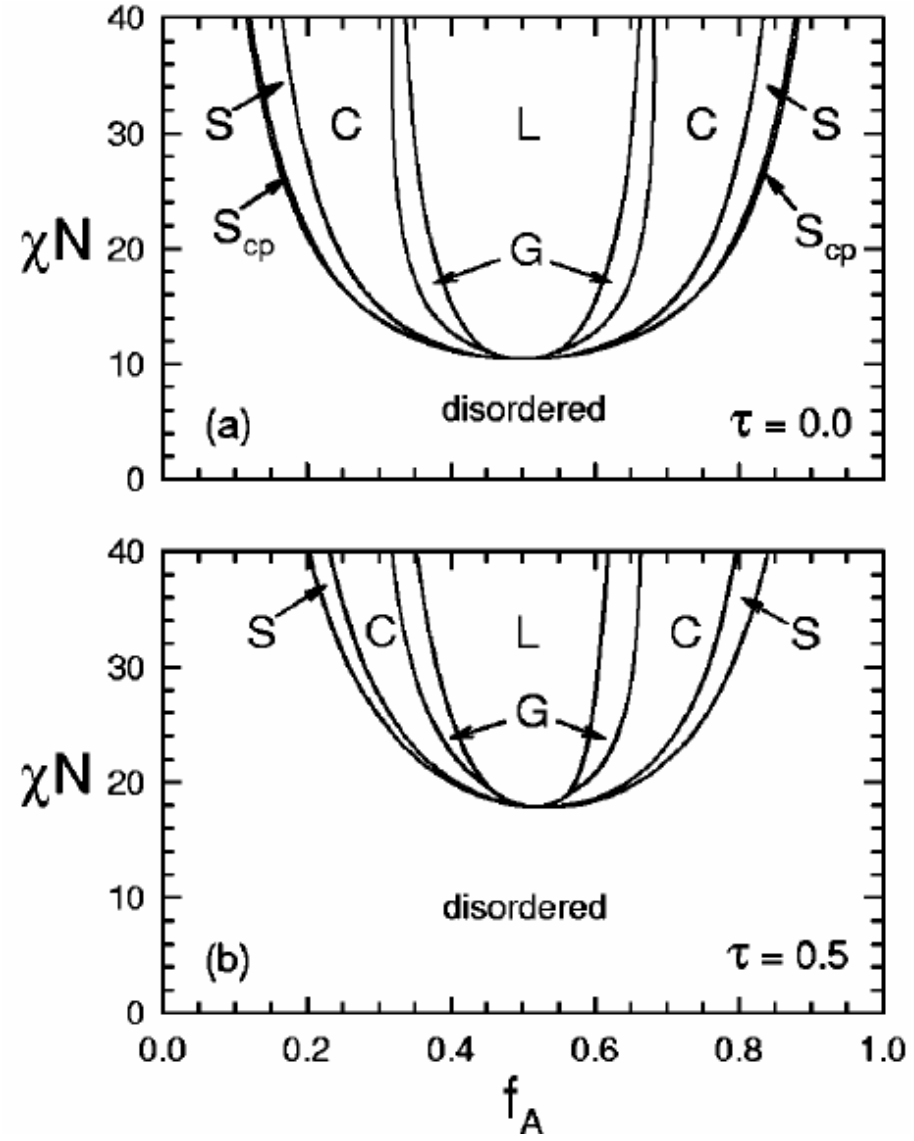

Figure 1-4 Mean-field phase diagrams for block copolymer melts of (a) AB diblock and (b) symmetric ABA triblock plotted in terms of segregation χN and composition f_A calculated with SCFT. Both systems have nearly identical phase behavior except the critical χN value is higher the phase diagram becomes asymmetric as f_A increases for ABA triblock. Reproduced from Matsen.[68]

1.3.3 ABABA Pentablocks

As the number of blocks continues to increase in the linear block copolymers containing two types of blocks, A and B, we obtain ABABA pentablock, ABABABA septablock, ABABABABA nonablock, etc. Similar to ABA triblock, bridge and loop configurations are present in these alternating multiblock copolymers. Experiments show that the failure mode changes from brittle to ductile upon changing the molecular architecture from a lamellae-forming triblock copolymer (with bridge configuration only in B domain) to a lamellae-forming pentablock copolymer (with bridge configuration in both A and B domains) (see Figure 1-5) in homologous pairs of CEC and CECEC,[71,72] and SBS and SBSBS.[73] This increased bridge-to-loop ratio in ABABA pentablock copolymers is believed to enhance other physical properties such as elasticitity and fracture toughness, either in lamellar[71–73] or cylindrical

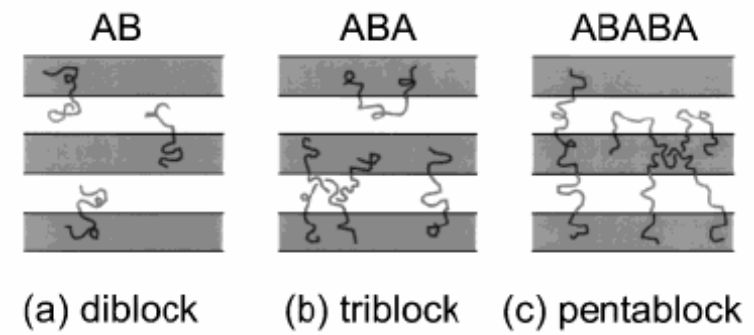

Figure 1-5 Typical configurations of AB diblock, ABA triblock and ABABA pentablock systems in lamellar phase. Triblock and pentablock molecules are shown in both bridge- and loop-type configurations. Reproduced from Vigild *et. al.*.[76]

phases.[74] In theory, Drolet and Fredrickson suggested that manipulating the bridging fraction in ABABA pentablock copolymers can potentially optimize the toughness and strength based on SCFT.[75]

Not surprisingly, increasing the number of blocks in alternating multiblock copolymers does not dramatically influence the associated phase behaviors between symmetric ABA and ABABA systems. We could view ABA triblocks as produced from cutting the symmetric ABABA pentablock in the middle (see Figure 1-5), leaving the free energy of both systems virtually the same.[45] In symmetric alternating mutiblock copolymers copolymers (ABA, ABABA, etc.), increasing the number of blocks can lead to enhanced physical and mechanical properties, but the associated phase behaviours are not dramatically affected.

1.3.4 ABA' Asymmetric Triblocks

In addition to the conventional parameters such as f, χ and N that influences the block copolymers phase behavior in AB diblock and symmetric ABA triblock copolymers, another parameter of asymmetry τ comes into effect when we examine the asymmetric ABA' triblock copolymers (A blocks are of different lengths) (see Figure 1-6) with $\tau = N_A/(N_A+N_{A'})$. For AB diblock copolymers, $\tau = 0$; for symmetric ABA triblock copolymers, $\tau = 0.5$. $0 \leq \tau \leq 0.5$ controls the asymmetry.

In 2000, Matsen extended the theoretical analysis from symmetric ABA triblock

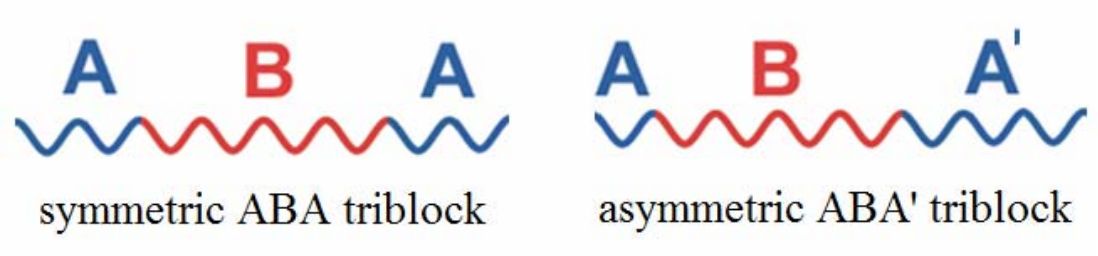

Figure 1-6 Schematic drawing of symmetric ABA and asymmetric ABA' triblock copolymers.

to asymmetric ABA' triblock copolymers.[68] Figure 1-7 shows the phase diagram of asymmetric ABA' triblock copolymers in τ vs f_A at different degrees of segregations, χN = 20, 30 and 40. As asymmetric parameter decreases from τ = 0.5 to τ = 0 (asymmetry increases), the phase diagram changes from symmetric triblock system in Figure 1-4 (b) to diblock system in Figure 1-4 (a). As χN increases, the OOT seems to occur at higher f_A. Since diblocks are better ordered than symmetric triblocks of same molecular weight, the ordered region is wider as asymmetry decreases, especially when χN is small (see Figure 1-7 (a)). The phase behavior of asymmetric ABA triblocks is dominated by the usual L, G, C and S morphologies, but S_{cp}, as opposed to the normal BCC packing, is predicted to present in an unusually large region by self-consistent field theory (SCFT) at intermediate τ and small f_A. Perforated-lamellar (PL) phase favors asymmetry as the increased softness and thickness of the majority domain reduces the packing frustration.[68]

Two new effects are introduced as asymmetry increases: first, the elastic energy of the A domains decreases; second, high asymmetry pulls the short A block into the

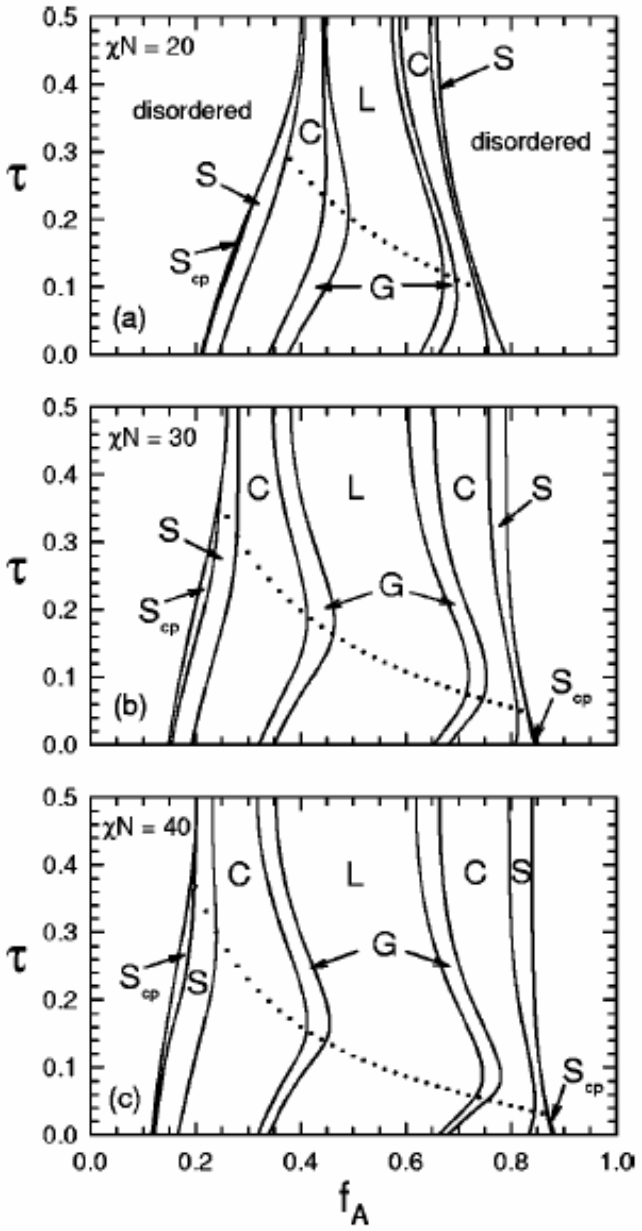

Figure 1-7 Mean-field phase diagrams for asymmetric ABA triblocks spanning between the diblock ($\tau = 0.0$) and symmetric triblock ($\tau = 0.5$) limits at segregations of (a) $\chi N = 20$, (b) $\chi N = 30$, and (c) $\chi N = 40$ calculated with SCFT. $0 \leq \tau \leq 0.5$ controls the asymmetry. The dotted curves indicate the critical asymmetries τ_c predicted by SST beyond which short A blocks are extracted from their domains. Reproduced from Matsen.[68]

B domain, lowering the stretching energies of B domains. These two factors significantly increase the domain size, influence packing frustration and cause large shifts in the phase boundaries. The gyroid phase can be shifted by $\Delta fA \approx \pm 0.1$ in theory, and observed experimentally in AB diblock blends with A blocks of different lengths, which behaved similarly as the asymmetric ABA' triblocks. While maintaining constant volume fraction, segment-segment interaction and molecular weight, the asymmetric parameter τ offers additional control over the packing symmetry in ABA' triblock terpolymer melts.

1.4 Three Monomers

1.4.1 ABC Triblocks

Addition of a third chemically distinct C block to an AB diblock copolymer yields an ABC triblock terpolymer shown in Figure 1-8. Additional parameters are introduced such as volume fractions (f_B), Flory-Huggins interaction parameters (χ_{BC} and χ_{AC}) and block sequences (ABC, ACB and BAC). As a result, the phase behaviour for ABC terpolymers becomes much more complicated than that of AB diblocks. Unlike AB diblocks, there is no theory able to predict the phase behaviour of any arbitrary ABC triblock terpolymer. Most researchers adopt the systematic approach to carry out a lot of synthesis to explore the large parameter space, discover new morphologies and determine the fundamental information about the interactions

among these three blocks.

The first reported linear ABC block terpolymers were synthesized using living anionic polymerization by Fielding-Russell and Pillai,[77] Cooper *et al.*,[78] and Price *et al.*[79] in 1974. Fielding-Russell and Pillai studied the phase behaviour of benzene cast films of poly(α-methylstyrene-*b*-butadiene-*b*-styrene). The phase behavior analysis was limited to characterization techniques available at that time. They concluded that microphase separation occurred in two microdomains with glassy α-methylstyrene and styrene blocks dispersed randomly in the rubbery butadiene domains. Similar conclusions about phase behavior were derived by Cooper *et al.* and Price *et al.* using other systems. With the development of TEM and SAXS beginning in the late 1960s, phase behavior analysis became feasible. So far, more than 30 equilibrium morphologies in ABC linear triblock terpolymers have been reported with many more to be identified in the future.[19,80–94] Bates and Fredrickson summarized some of the observed morphologies, for which changes in the controlling parameters completely alter the phase behaviour (see Figure 1-8).

In ABC terpolymers, the effect of block sequences on phase behaviour can be examined based on the morphologies formed in ABC, ACB and BAC triblock terpolymers with similar molecular weight and composition. The effect of block sequences cannot be studied in AB diblock or ABA triblock copolymers because altering the block sequence will yield the same copolymers, respectively. Systems such as poly(isoprene-*b*-styrene-*b*-vinylpyridine) (ISP)/SIP,[80,95] poly(styrene-*b*-

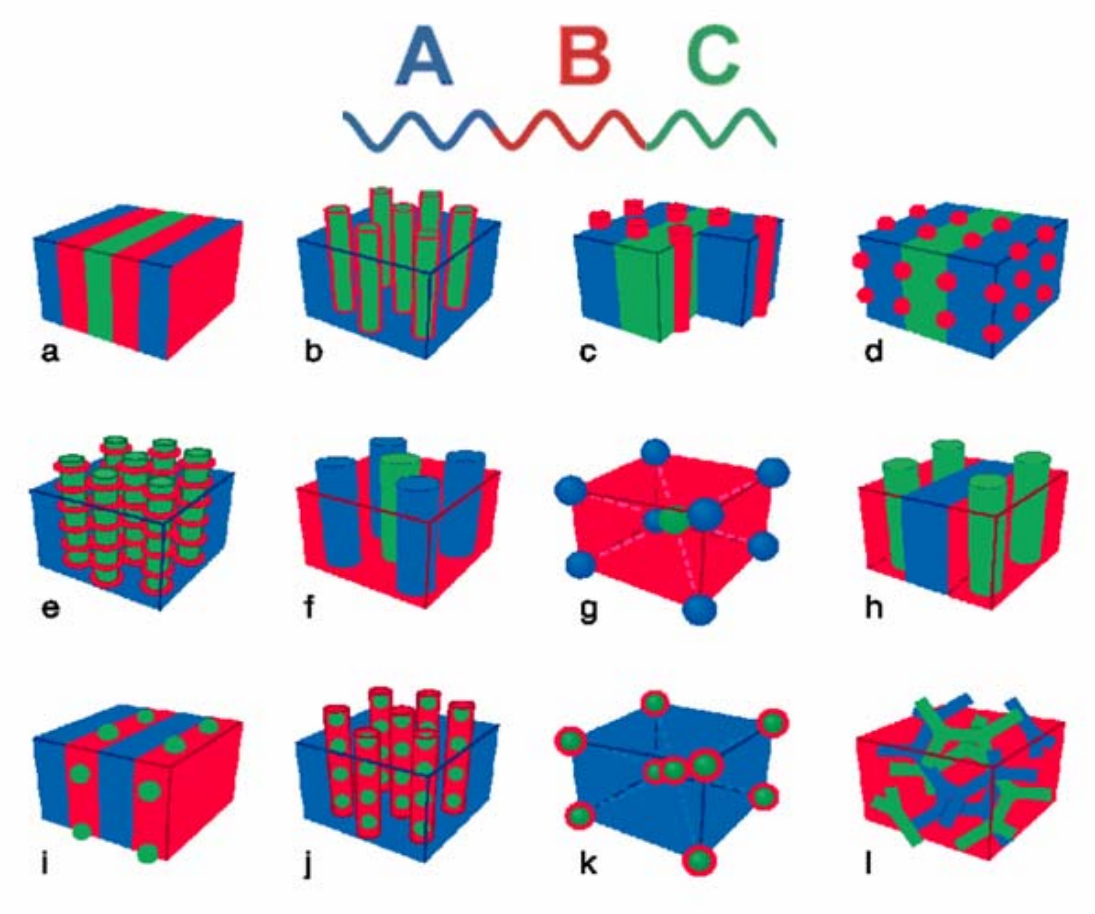

Figure 1-8 (top) Schematic drawing of ABC triblock terpolymers. (bottom) Illustrations of various types of morphologies that are formed in ABC triblock terpolymers. Reproduced from Bates and Fredrickson.[19]

butadiene-*b*-isoprene) (SBI)/BSI,[92,96] poly(styrene-*b*-isoprene-*b*-ethylene oxide) (SIO)/ISO,[1,90,97] and poly(styrene-*b*-isoprene-*b*-dimethylsiloxane) (SID)/ISD[87,98,99] have been studied and block sequences have been shown to have profound effects on terpolymer phase behaviour.

Taking SIO/ISO terpolymers as an example, with $\chi_{IO} >> \chi_{IS} \approx \chi_{SO}$, the repulsion between the I and O blocks is the greatest as compared to S/O and S/I pairs. In SIO,

I/O interface is mandatory due to covalent bond connectivity. It is the most unfavorable and has highest degree of curvature. In ISO, I and O blocks are not directly bonded, thus I/O interface is unlikely to form in order to minimize chain packing frustrations. In SIO, the sequence of ordered morphologies formed with $f_S = f_I$ and increasing f_O is: two-domain lamellae (LAM_2), pillared lamellar structure, core-shell cylinders (hexagonal) (CSC), core-shell gyroid, semi-perforated three-domain lamellae and three-domain lamellae (LAM_3).[100] This contrasts sharply with the ISO system, in which two-domain (LAM_2), orthorhombic network with *Fddd* symmetry (O^{70}), and three-domain (LAM_3) lamellae are formed with $f_S = f_I$ and increasing f_O.

1.4.2 ISO Triblocks

The most thoroughly investigated linear ABC triblock system is poly(isoprene - *b*-styrene-*b*-ethylene oxide) (ISO) by the Bates group.[1,32,93,97,98,101–105] In 2002, Bailey *et al.* compared the phase behavior of ISO with the homologous SIO system (see Section 1.4.1).[97] In 2003, Epps *et al.* studied the effect on phase behavior after doping SIO/ISO with lithium perchlorate.[101] For SIO, only four morphologies remain after doping, namely, LAM_2, pillared lamellar structure, CSC, and LAM_3 at increasing f_O. For ISO, three phases are formed: LAM_2, CSC, and LAM_3 at increasing f_O.

In 2004, Epps *et al.* introduced three network morphologies observed in ISO system: an orthorhombic network phase (O^{70}) with *Fddd* space group symmetry and two cubic network phases of core-shell double gyroid (Q^{230}) with $Ia\bar{3}d$ space group symmetry and alternating gyroid (Q^{214}) with $I4_132$ space group symmetry (see Figure 1-9).[102] Soon afterwards, they interpreted these results with modeling techniques and confirmed the assignment of these network morphologies.[93] Level set models show that each network consists of ordered arrays with trivalent connected 10-node loops which form triply periodic structures with hyperbolic interfacial surfaces.

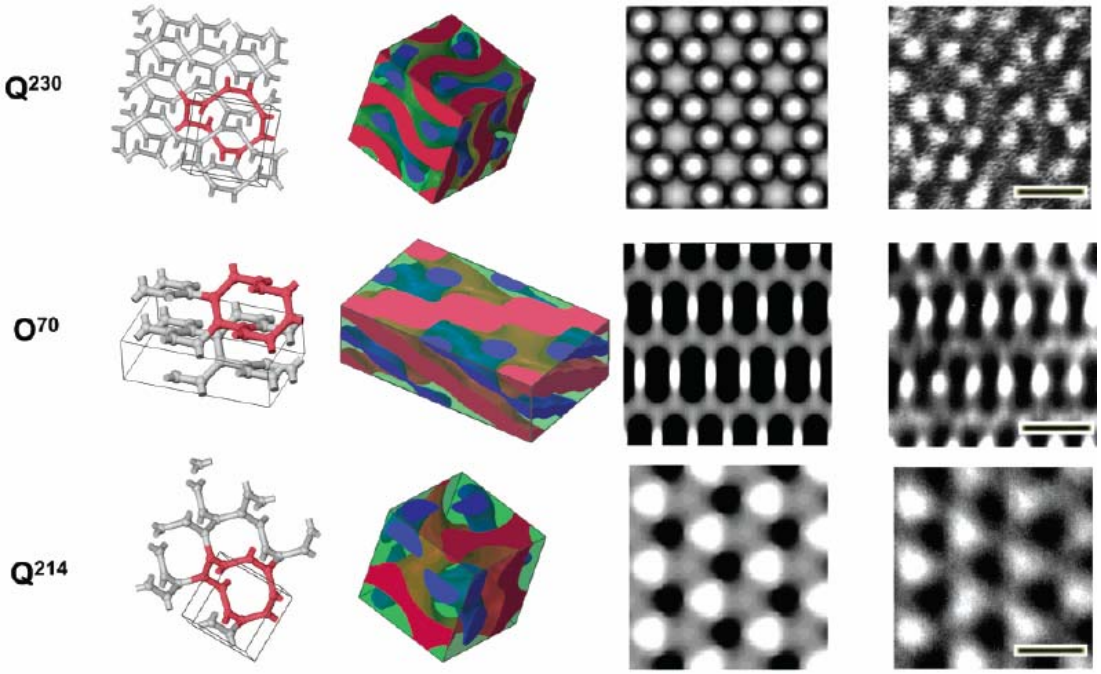

Figure 1-9 Network lattice structures, 3-D morphologies, 2-D projections derived from level set constructions and TEM images for core-shell doubly gyroid network Q^{230}, *Fddd* orthorhombic network O^{70} and alternating gyroid network Q^{214}. PI is blue, PS is green and PEO is red. TEM scale bar is 30 nm. Reproduced from Epps *et al.*.[102]

In 2005, Epps *et al.* described the effect of mixing ISO with PS or PI homopolymers near the composition window where the network morphologies were found.[103] Phase transitions of $Q^{230} \rightarrow O^{70}$ and $Q^{214} \rightarrow O^{70}$ occurred after adding either homopolymer, and transition of $LAM_3 \rightarrow O^{70}$ occurred after adding both homopolymers. Overall, pure ISO and ISO/PS/PI mixtures formed similar morphologies.

In 2006, the effects of molecular weight on network formation were investigated by Epps *et al.*.[104] Increasing the molecular weight to 1.5 ~ 2 times of the previous reported value disrupted the long-range order within the composition window where network phases were used to form. Higher molecular weight leads to reduction in molecular diffusion. As a result, equilibrium phases are hard to achieve due to higher kinetic barriers.

In 2007, Chatterjee *et al.* summarized a total of 44 ISO samples across the phase map compositions near the WSL to ISR (see Figure 1-10).[1] Six equilibrium phases were reported: three aforementioned network morphologies, Q^{230}, Q^{214} and O^{70}, lamellae, hexagonally ordered cylinders and body-centered cubic (BCC) spheres. This comprehensive phase map sets the foundation for polymer theorists to come up with theoretical models to explain the phase behaviors of linear ABC triblock terpolymers.

Theoretical studies to account for the ISO phase behavior were conducted by Cochran *et al.* in 2003 using random phase approximation (RPA)[98] and Tyler *et al.* in

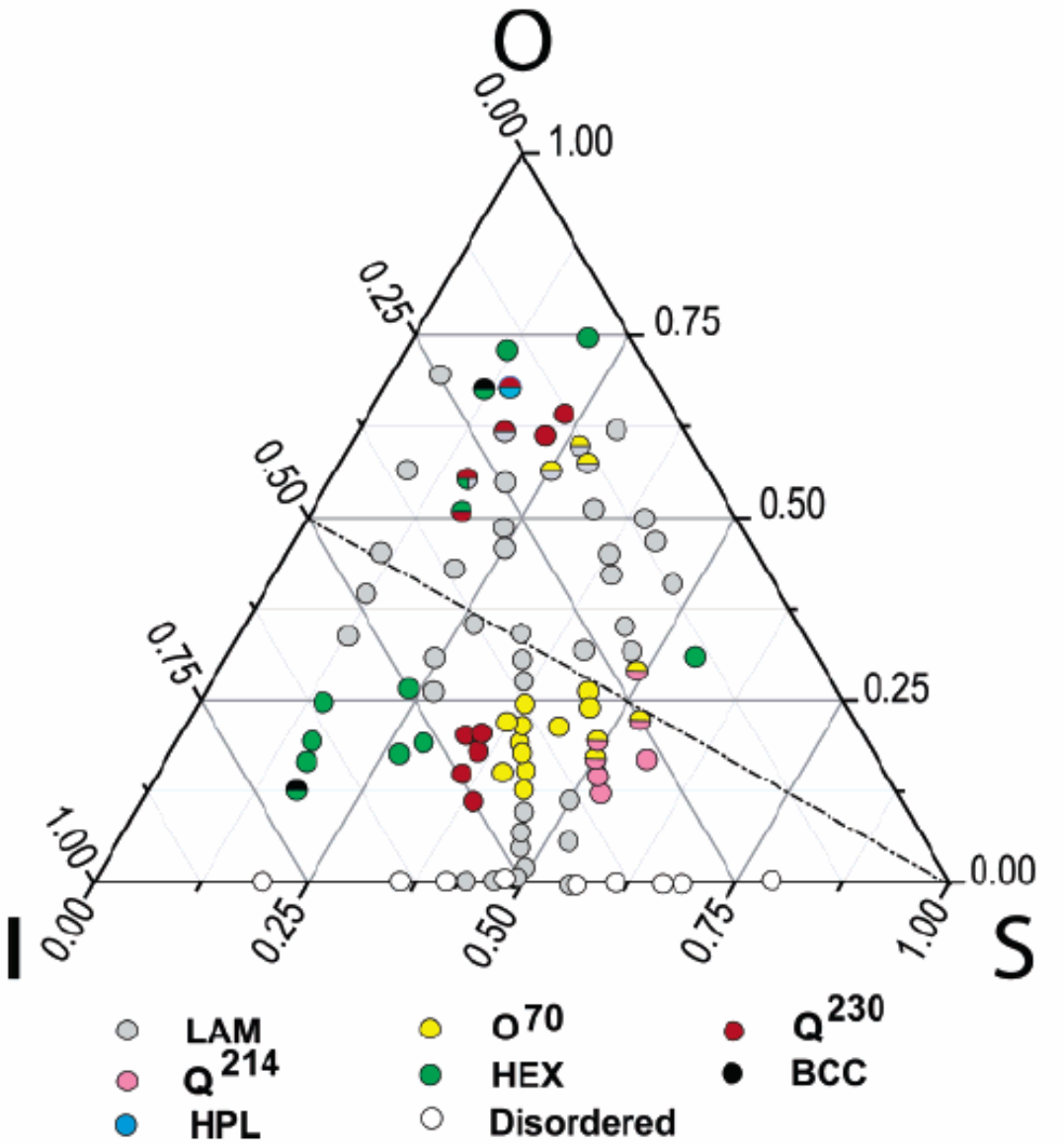

Figure 1-10 Phase map for ISO with axes representing volume fractions of each block. Samples with OOT are represented with two different colors with the upper half showing the higher temperature state. The dashline represents the $f_I = f_O$ isopleth. Reproduced from Chatterjee *et al.*.[1]

2007 using SCFT.[32] Tyler *et al.* focused on ABC triblock terpolymers with $\chi_{AC} >> \chi_{AB} \approx \chi_{BC}$. These systems tend to form continuous B phase without A/C interface. Both symmetric ($\chi_{AB} = \chi_{BC}$) and slightly asymmetric model similar to ISO system ($\chi_{IS} \approx \chi_{SO}$) were developed, leading to different morphological distributions across the phase map. Theoretical models also accounted for the existence of O^{70} phase and its sensitivity in phase behavior with respect to Flory-Huggins interaction parameters.

1.4.3 ABAC Tetrablocks

Increasing the number of blocks to $n > 2$ while fixing the type of blocks to $k = 2$ generates alternating multiblock copolymers with similar phase behavior as that of the AB diblock. Increasing to $n = 3$ enhances the mechanical and physical properties of the multiblock copolymers for new opportunities at marginal or no added cost. Thermoplastic elastomers such as poly(styrene-*b*-isoprene-*b*-styrene) (SIS) are the most successful block copolymer product worldwide. Increasing the type of blocks to $k = 3$ quickly expands and complicates the phase behavior with the formation of more than thirty equilibrium morphologies,[19] providing many new opportunities. Bates *et. al.* claim that virtually any morphology can be achieved at the length scale between 5 nm and 1 μm using block copolymers. Every (n, k) enumeration has the potential to produce a unique structure.[106] However, these tempting goals are challenged by complexity. As n or k increases, the parameter space controlling block

copolymer phase behavior expands tremendously, resulting in difficulties to carry out the systematic study approach most researchers adopt to study block copolymer phase behavior. A minor extrapolation in molecular architecture to $n = 4$ and $k = 3$ offers additional control and provides a glimpse to block copolymer phase behavior after decoupling domain geometry and ordering symmetry without exacerbating the multiblock complexity enormously.

The sequence ABA'C is one of nine possible tetrablock terpolymer enumerations, where A and A' represent chemically identical blocks as shown in Figure 1-11. It breaks the molecular symmetry by inserting part of the A block between B and C blocks, introducing flexibility in diverse morphology formation while keeping molecular weight and composition constant as compared to ABC triblocks. At marginal or no added cost, we could change the morphology by changing the molecular architecture alone. The asymmetry factor is measured by $\tau = N_A / N_{A'}$ where N_A and $N_{A'}$ are the number of repeat units for A blocks.

Figure 1-11 Schematic drawing of symmetric ABAC and asymmetric ABA'C tetrablock copolymers.

In 2009, Bluemle *et al.* studied the poly(cyclohexylethylene-*b*-ethylene-*b*-

cyclohexyl-ethylene-*b*-dimethylsiloxane) (CECD) tetrablock terpolymers with $f_C : f_E = 3 : 7$ and $\tau = 1$.[107] Sequence of hexagonally packed cylinders, O^{52} network with *Pnna* space group symmetry and core-shell cylinders was reported at increasing f_D. The new O^{52} network morphology is unlike those networks found in ISO triblocks. The tetrablock molecular architecture and block interactions were accountable for the formation of this unique phase.

In 2010, Bluemle *et al.* published the preliminary result of the systematic study using poly(styrene-*b*-isoprene-*b*-styrene-*b*-ethylene oxide) (SISO) with $f_S = f_I$ and $\tau = 1$.[108] Liquid-like packing of spheres and hexagonally packed core-shell cylinders were reported at increasing f_O. One particular sample with $f_O = 0.08$ was later found to form Frank-Kasper σ-phase at elevated temperatures.[109] This phase has a unit cell with 30 atoms (see Figure 1-12) and is known as the 'periodic approximate' to certain dodecagonal quasicrystals.[110]

ABCA' is another possible tetrablock molecular architecture with $n = 4$ and $k = 3$. In the early 2000s, Takano reported the presence of noncentrosymmetric (NCS) lamellar phase (with sequence …ABCDABCD…) using poly(isoprene-*b*-styrene-*b*-2-vinylpyridine-*b*-isoprene) even though the long-range ordering was not as good as the regular centrosymmetric (CS) lamellar phase (with sequence ..ABCDDCBA…).[111] Subsequent theoretical works showed that NCS phase was stable and direct transitions from disorder to NCS states were possible, even though the local free energy between NCS and CS was similar.[112,113] Kaga *et al.*

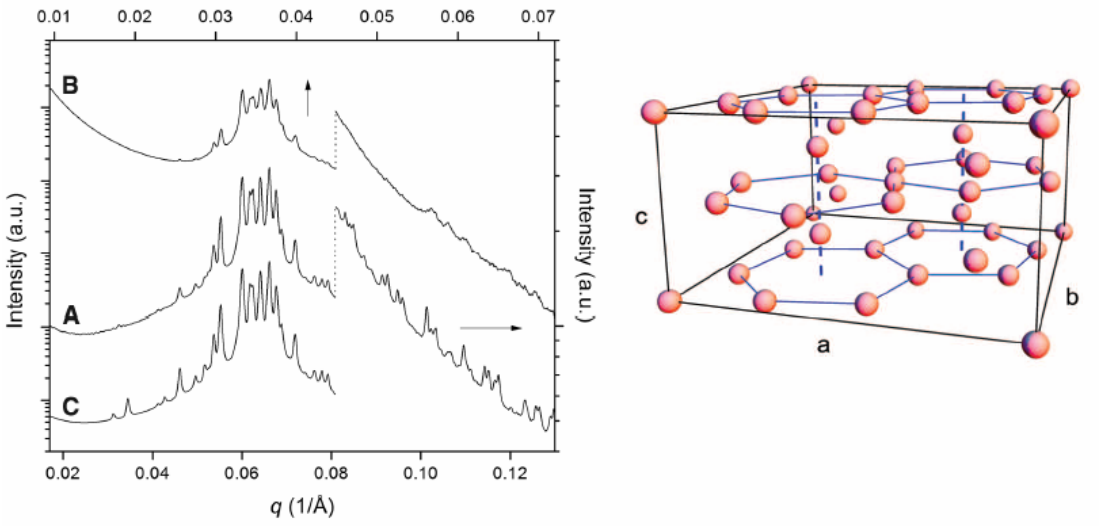

Figure 1-12 (left) Synchrotron SAXS powder patterns of Frank-Kasper σ-phase from poly(isoprene-*b*-lactide) diblock (A), SISO tetrablock(B) and model simulation (C). (right) Unit cell for σ-phase based on Rietveld analysis. Reproduced from Lee *et al.*.[109]

derived free-energy functions and kinetic equations for ABCA' tetrablock copolymers and explained how NCS was selected.[113]

This thesis continues the systematic study of ABA'C type of tetrablock copolymers using SIS'O as the model system. Throughout this thesis, SISO is used when $\tau = 1$ (S blocks are divided equally) and SIS'O is used in general unless specified otherwise ($\tau \neq 1$). The goal is to study the effect of molecular architecture and asymmetry on phase behavior. A similar phase portrait for SISO is set up and compared with that of the well established ISO system. The experimental phase portrait lays the foundation for polymer theorists to come up with theoretical models to predict future phase behavior for other tetrablock terpolymers, which will greatly

expedite their future experimental work. It also provides guidance and interpretation on the interactions among different blocks in these tetrablock terpolymers.

SIS'O tetablock terpolymer is chosen as the model system because: PS homopolymer is rigid and transparent but brittle; PI homopolymer is rubbery but easily deformed; PEO homopolymer is semicrystalline.[1] SIS'O tetrablock copolymer yields the desirable overall physical and chemical properties while overcoming the limitations associated with the each individual homopolymers. Two-step synthetic method is used. Hydroxyl-terminated SIS'-OH triblock copolymers allows reinitiation and growth of PEO with different lengths from the same parent triblock.[114] As a result, systematic studies of phase behavior along series with different volume ratios of PS and PI blocks can be conducted. In order to enhance the contrast under TEM, SIS'O samples can be stained with the vapour from a 4% aqueous solution of OsO_4. The metal oxide selectively reacts with the double bonds in the PI block, resulting in darker PI domain than those of PS and PEO domains.[1,115]

1.5 Thesis Review

In Chapter 2, the general principles of the various characterization methods such as nuclear magnetic resonance, size exclusion chromatography, dynamic mechanical spectroscopy, small angle x-ray scattering, transmission electron microscopy, and differential scanning calorimetry are described. In Chapter 3, the general living

anionic polymerization method and the experimental techniques/procedures are described and the molecular characterization results of all the polymers used in this thesis are summarized. Chapter 4 describes the phase behavior of symmetric isoprene-rich SISO samples with $f_S : f_I = 2 : 3$ and $f_O = 0 – 32\%$. Chapter 5 discusses the temperature effect in one particular sample near the order-disorder boundary from the symmetric isoprene-rich SISO sample with $f_S : f_I = 2 : 3$ and $f_O = 9\%$. Chapter 6 describes the phase behavior of symmetric styrene-rich SISO samples with $f_S : f_I = 3 : 2$ and $f_O = 0 – 35\%$, as well as the temperature effect. A phase map for symmetric SISO samples is developed and compared with that of the ISO samples. Chapter 7 describes the phase behavior of asymmetric SIS'O samples targeted at the same molecular weight and composition with only variable, $\tau = 0.21 – 0.70$. The temperature effect is also investigated. Chapter 8 summarizes and compares the results obtained.

1.6 References

(1) Chatterjee, J.; Jain, S.; Bates, F. S. *Macromolecules* **2007**, *40*, 2882.

(2) Chin, S. S. *United State Patent* **1992**, 5118762.

(3) Chin, S. S.; St. Clair, D. J.; Talbott, R. L. *United State Patent* **1993**, 5194500.

(4) Fischer, C. A.; Simmons, E. R.; Kroll, M. S.; Lindquist, J. S. *United State*

Patent **1999**, 5863977.

(5) Moffitt, M.; Vali, H.; Eisenberg, A. *Chemistry of Materials* **1998**, *10*, 1021.

(6) Black, C. T.; Guarini, K. W.; Milkove, K. R.; Baker, S. M.; Russell, T. P.; Tuominen, M. T. *Applied Physics letters* **2001**, *79*, 409.

(7) Lee, J. S.; Hirao, A.; Nakahama, S. *Macromolecules* **1989**, *22*, 2602.

(8) Liu, G. J.; Ding, J. F.; Guo, A.; Herfort, M.; BazettJones, D. *Macromolecules* **1997**, *30*, 1851.

(9) Hashimoto, T.; Tsutsumi, K.; Funaki, Y. *Langmuir* **1997**, *13*, 6869.

(10) Mansky, P.; Chaikin, P.; Thomas, E. L. *Journal of Materials Science* **1995**, *30*, 1987.

(11) Park, M.; Harrison, C.; Chaikin, P. M.; Register, R. A.; Adamson, D. H. *Science* **1997**, *276*, 1401.

(12) Rosler, A.; Vandermeulen, G. W. M.; Klok, H.-A. *Advanced Drug Delivery Reviews* **2001**, *53*, 95.

(13) Kumar, M. N. V. R. *Journal of Pharmacy & Pharmaceutical Sciences* **2000**, *3*, 234.

(14) Kataoka, K.; Harada, A.; Nagasaki, Y. *Advanced Drug Delivery Reviews* **2001**, *47*, 113.

(15) Lach, R.; Adhikari, R.; Weidisch, R.; Huy, T. A.; Michler, G. H.; Grellmann, W.; Knoll, K. *Journal of Materials Science* **2004**, *39*, 1283.

(16) Lodge, T. P. *Macromolecular Chemistry and Physics* **2003**, *204*, 265.

(17) Holden, G.; Legge, N. R.; Quirk, R.; Schroeder, H. E. *Thermoplastic Elastomers*; 2nd ed.; Hanser/Gardner: Cincinnati, 1996.

(18) Hiemenz, P. C.; Lodge, T. P. *Polymer Chemistry*; Taylor & Francis Group: University of Minnesota: Minneapolis, MN, 2007.

(19) Bates, F. S.; Fredrickson, G. H. *Physics Today* **1999**, *52*, 32.

(20) Bates, F. S.; Fredrickson, G. H. *Annual Review of Physical Chemistry* **1990**, *41*, 525.

(21) Fredrickson, G. H.; Bates, F. S. *Annual Review of Materials Science* **1996**, *26*, 501.

(22) Hajduk, D. A.; Harper, P. E.; Gruner, S. M.; Honeker, C. C.; Kim, G.; Thomas, E. L. *Macromolecules* **1994**, *27*, 4063.

(23) Schulz, M. F.; Bates, F. S.; Almdal, K.; Mortensen, K. *Physical Review Letters* **1994**, *73*, 86.

(24) Lazzari, M.; Liu, G.; Lecommandoux, S. *Block Copolymers in Nanoscience*; John Wiley & Sons: Betz-druck GmbH, Darmstadt, 2007.

(25) Leibler, L. *Macromolecules* **1980**, *13*, 1602.

(26) Matsen, M. W.; Schick, M. *Macromolecules* **1994**, *27*, 4014.

(27) Khandpur, A. K.; Foerster, S.; Bates, F. S.; Hamley, I. W.; Ryan, A. J.; Bras, W.; Almdal, K.; Mortensen, K. *Macromolecules* **1995**, *28*, 8796.

(28) Matsen, M. W.; Bates, F. S. *Macromolecules* **1996**, *29*, 1091.

(29) Floudas, G.; Vazaiou, B.; Schipper, F.; Ulrich, R.; Wiesner, U.; Iatrou, H.;

Hadjichristidis, N. *Macromolecules* **2001**, *34*, 2947.

(30) Cochran, E. W.; Garcia-Cervera, C. J.; Fredrickson, G. H. *Macromolecules* **2006**, *39*, 2449.

(31) Tyler, C. A.; Morse, D. C. *Physical Review Letters* **2005**, *94*, 208302.

(32) Tyler, C. A.; Qin, J.; Bates, F. S.; Morse, D. C. *Macromolecules* **2007**, *40*, 4654.

(33) Takenaka, M.; Wakada, T.; Akasaka, S.; Nishitsuji, S.; Saijo, K.; Shimizu, H.; Kim, M. I.; Hasegawa, H. *Macromolecules* **2007**, *40*, 4399.

(34) Kim, M. I.; Wakada, T.; Akasaka, S.; Nishitsuji, S.; Saijo, K.; Hasegawa, H.; Ito, K.; Takenaka, M. *Macromolecules* **2008**, *41*, 7667.

(35) Matsen, M. W.; Bates, F. S. *Macromolecules* **1996**, *29*, 7641.

(36) Zhao, J.; Majumdar, B.; Schulz, M. F.; Bates, F. S.; Almdal, K.; Mortensen, K.; Hajduk, D. A.; Gruner, S. M. *Macromolecules* **1996**, *29*, 1204.

(37) Foerster, S.; Khandpur, A. K.; Zhao, J.; Bates, F. S.; Hamley, I. W.; Ryan, A. J.; Bras, W. *Macromolecules* **1994**, *27*, 6922.

(38) Hamley, I. W.; Koppi, K. A.; Rosedale, J. H.; Bates, F. S.; Almdal, K.; Mortensen, K. M. L. *Macromolecules* **1993**, *26*, 5959.

(39) Hajduk, D. A.; Takenouchi, H.; Hillmyer, M. A.; Bates, F. S.; Vigild, M. E.; Almdal, K. *Macromolecules* **1997**, *30*, 3788.

(40) Qi, S.; Wang, Z. G. *Macromolecules* **1997**, *30*, 4491.

(41) Meier, D. J. *Journal of Polymer Science, Part C: Polymer Symposia* **1969**,

26, 81.

(42) Krause, S. *Journal of Polymer Science, Polymer Physics Edition* **1969**, *7*, 249.

(43) Leary, D. F.; Williams, M. C. *Journal of Polymer Science, Polymer Letters Edition* **1970**, *8*, 335.

(44) Helfand, E. *Macromolecules* **1975**, *8*, 552.

(45) Helfand, E.; Wasserman, Z. R. *Macromolecules* **1976**, *9*, 879.

(46) Helfand, E.; Tagami, Y. *Journal of Chemical Physics* **1972**, *56*, 3592.

(47) DeGennes, P. G. *Scaling Concepts in Polymer Physics*; Cornell University Press: Ithaca, NY, 1979.

(48) Fredrickson, G. H.; Helfand, E. *Journal of Chemical Physics* **1987**, *87*, 697.

(49) Whitmore, M. D. *Encyclopedia of Materials: Science and Technology*; Elsevier Science: Oxford, 2001.

(50) Matsen, M. W.; Schick, M. *Macromolecules* **1994**, *27*, 7157.

(51) Matsen, M. W.; Schick, M. *Physical Review Letters* **1994**, *72*, 2660.

(52) Matsen, M. W.; Bates, F. S. *Journal of Chemical Physics* **1997**, *106*, 2436.

(53) Ryu, C. Y.; Lee, M. S.; Hajduk, D. A.; Lodge, T. P. *Journal of Polymer Science Part B* **1997**, *35*, 2811.

(54) Mayes, A. M.; Olvera de la Cruz, M. *Journal of Chemical Physics* **1989**, *91*, 7228.

(55) Mayes, A. M.; Olvera de la Cruz, M. *Journal of Chemical Physics* **1991**, *95*,

4670.

(56) Matsen, M. W.; Schick, M. *Macromolecules* **1994**, *27*, 187.

(57) Matsen, M. W. *Journal of Chemical Physics* **1995**, *102*, 3884.

(58) Matsen, M. W.; Thompson, R. B. *Journal of Chemical Physics* **1999**, *111*, 7139.

(59) Koberstein, J. T.; Russell, T. P.; Walsh, D. J.; Pottick, L. *Macromolecules* **1990**, *23*, 877.

(60) Gehlsen, M. D.; Almdal, K.; Bates, F. S. *Macromolecules* **1992**, *25*, 939.

(61) Adams, J. L.; Graessley, W. W.; Register, R. A. *Macromolecules* **1994**, *27*, 6026.

(62) McKay, K. W.; Gros, W. A.; Diehl, C. F. *Journal of Applied Polymer Science* **1995**, *56*, 947.

(63) Riise, B. L.; Fredrickson, G. H.; Larson, R. G.; Pearson, D. S. *Macromolecules* **1995**, *28*, 7653.

(64) Nakatani, A. I.; Morrison, F. A.; Douglas, J. F.; Mays, J. W.; Jackson, C. L.; Muthukumar, M.; Han, C. C. *Journal of Chemical Physics* **1996**, *104*, 1589.

(65) Kim, J. K.; Lee, H. H.; Gu, Q.-J.; Chang, T.; Jeong, Y. H. *Macromolecules* **1998**, *31*, 4045.

(66) Watanabe, H.; Sato, T.; Osaki, K. *Macromolecules* **2000**, *33*, 2545.

(67) Karatasos, K.; Anastasiadis, S.; Pakula, T.; Watanabe, H. *Macromolecules* **2000**, *33*, 523.

(68) Matsen, M. W. *Journal of Chemical Physics* **2000**, *113*, 5539.

(69) Matsushita, Y.; Nomura, M.; Watanabe, J.; Mogi, Y.; Noda, I.; Imai, M. *Macromolecules* **1995**, *28*, 6007.

(70) Mai, S.; Mingvanish, W.; Turner, S. C.; Chaibundit, C.; Fairclough, J. P. A.; Heatley, F.; Matsen, M. W.; Ryan, A. J.; Booth, C. *Macromolecules* **2000**, *33*, 5124.

(71) Hermel, T.; Hahn, S.; Chaffin, K.; Gerberich, W.; Bates, F. S. *Macromolecules* **2003**, *36*, 2190.

(72) Mori, Y.; Lim, L. S.; Bates, F. S. *Macromolecules* **2003**, *36*, 9879.

(73) Adhikari, R.; Michler, G. H. *Progress in Polymer Science* **2004**, *29*, 949.

(74) Ryu, C.; Ruokolainen, J.; Fredrickson, G. H.; Kramer, E. J.; Hahn, S. *Macromolecules* **2002**, *35*, 2157.

(75) Drolet, F.; Fredrickson, G. H. *Macromolecules* **2001**, *34*, 5317.

(76) Vigild, M. E.; Chu, C.; Sugiyama, M.; Chaffin, K. A.; Bates, F. S. *Macromolecules* **2001**, *34*, 951.

(77) Fielding-Russell, G. S.; Pillai, P. S. *Polymer* **1974**, *15*, 97.

(78) Cooper, W.; Hale, P. T.; Walker, J. S. *Polymer* **1974**, *15*, 175.

(79) Price, C.; Lally, T. P.; Stubbersfield, R. *Polymer* **1974**, *15*, 541.

(80) Mogi, Y.; Mori, K.; Matsushita, Y.; Noda, I. *Macromolecules* **1992**, *25*, 5412.

(81) Mogi, Y.; Nomura, M.; Kotsuji, H.; Ohnishi, K.; Matsushita, Y.; Noda, I.

Macromolecules **1994**, *27*, 6755.

(82) Beckmann, J.; Auschra, C.; Stadler, R. *Macromolecular Rapid Communications* **1994**, *15*, 67.

(83) Stadler, R.; Auschra, C.; Beckmann, J.; Krappe, U.; Voight-Martin, I.; Leibler, L. *Macromolecules* **1995**, *28*, 3080.

(84) Breiner, U.; Krappe, U.; Stadler, R. *Macromolecular Rapid Communications* **1996**, *17*, 567.

(85) Matsushita, Y.; Suzuki, J.; Seki, M. *Physica. B, Condensed Matter* **1998**, *248*, 238.

(86) Breiner, U.; Krappe, U.; Jakob, T.; Abetz, V.; Stadler, R. *Polymer Bulletin (Berlin)* **1998**, *40*, 219.

(87) Shefelbine, T. A.; Vigild, M. E.; Matsen, M. W.; Hajduk, D. A.; Hillmyer, M. A.; Cussler, E. L.; Bates, F. S. *Journal of the American Chemical Society* **1999**, *121*, 8457.

(88) Seki, M.; Sujuki, J.; Matsushita, Y. *Journal of Applied Crystallography* **2000**, *33*, 285.

(89) Suzuki, J.; Seki, M.; Matsushita, Y. *Journal of Chemical Physics* **2000**, *112*, 4862.

(90) Bailey, T. S.; Pham, H. D.; Bates, F. S. *Macromolecules* **2001**, *34*, 6994.

(91) Ludwigs, S.; Boeker, A.; Voronov, A.; Rehse, N.; Magerle, R.; Krausch, G. *Nature Materials* **2003**, *2*, 744.

(92) Avgeropoulos, A.; Paraskeva, S.; Hadjichristidis, N.; Thomas, E. L. *Macromolecules* **2003**, *35*, 4030.

(93) Epps III, T. H.; Cochran, E. W.; Bailey, T. S.; Waletzko, R. S.; Hardy, C. M.; Bates, F. S. *Macromolecules* **2004**, *37*, 8325.

(94) Cochran, E. W.; Bates, F. S. *Physical Review Letters* **2004**, *93*, 087802.

(95) Matsushita, Y.; Tamura, M.; Noda, I. *Macromolecules* **1994**, *27*, 3680.

(96) Neumann, C.; Loveday, D. R.; Abetz, V.; Stadler, R. *Macromolecules* **1998**, *31*, 2493.

(97) Bailey, T. S.; Hardy, C. M.; Epps III, T. H.; Bates, F. S. *Macromolecules* **2002**, *35*, 7007.

(98) Cochran, E. W.; Morse, D. C.; Bates, F. S. *Macromolecules* **2003**, *36*, 782.

(99) Hardy, C. M.; Bates, F. S.; Kim, M.-H.; Wignall, G. D. *Macromolecules* **2002**, *35*, 3189.

(100) Bailey, T. S. *Ph.D. Dissertation*; University of Minnesota: Minneapolis, 2001.

(101) Epps III, T. H.; Bailey, T. S.; Waletzko, R. S.; Bates, F. S. *Macromolecules* **2003**, *36*, 2873.

(102) Epps III, T. H.; Cochran, E. W.; Hardy, C. M.; Bailey, T. S.; Waletzko, R. S.; Bates, F. S. *Macromolecules* **2004**, *37*, 7085.

(103) Epps III, T. H.; Chatterjee, J.; Bates, F. S. *Macromolecules* **2005**, *38*, 8775.

(104) Epps III, T. H.; Bates, F. S. *Macromolecules* **2006**, *39*, 2676.

(105) Meuler, A. J.; Ellison, C. J.; Evans, C. M.; Hillmyer, M. A.; Bates, F. S. *Macromolecules* **2007**, *40*, 7072.

(106) Bates, F. S.; Hillmyer, M. A.; Lodge, T. P.; Bates, C. M.; Delaney, K. T.; Fredrickson, G. H. *Science* **2012**, *336*, 434.

(107) Bluemle, M. J.; Fleury, G.; Lodge, T. P.; Bates, F. S. *Soft Matter* **2009**, *5*, 1587.

(108) Bluemle, M. J.; Zhang, J.; Lodge, T. P.; Bates, F. S. *Macromolecules* **2010**, *43*, 4449.

(109) Lee, S.; Bluemle, M. J.; Bates, F. S. *Science* **2010**, *330*, 349.

(110) Keys, A. S.; Glotzer, S. C. *Physical Review Letters* **2007**, *99*, 235503.

(111) Takano, A.; Soga, K.; Suzuki, J.; Matsushita, Y. *Macromolecules* **2003**, *36*, 9288.

(112) Jaffer, K. M.; Wickham, R. A.; Shi, A.-C. *Macromolecules* **2004**, *37*, 7042.

(113) Kaga, M.; Ohta, T. *Journal of the Physical Society of Japan* **2006**, *75*, 043002.

(114) Hillmyer, M. A.; Bates, F. S. *Macromolecules* **1996**, *29*, 6994.

(115) Meuler, A. J.; Fleury, G.; Hillmyer, M. A.; Bates, F. S. *Macromolecules* **2008**, *41*, 5809.

2

Material Synthesis and Experimental/ Characterization Techniques

This chapter summarizes the synthesis procedures and the various characterization techniques used to identify the phase behaviour of poly(styrene- *b*-isoprene-*b*-styrene-*b*-ethylene oxide) (SISO) tetrablock terpolymers. Synthesis procedures for poly(isoprene-*b*-styrene-*b*-ethylene oxide) (ISO) triblock terpolymers are well established in our group using the sequential living anionic polymerization methods.[1–5] I made slight modifications to synthesize the SISO tetrablock compounds. The characterization techniques used in this research work are: nuclear magnetic resonance (NMR) spectroscopy, size exclusion chromatography (SEC), dynamic mechanical spectroscopy (DMS), small angle X-ray scattering (SAXS), transmission electron microscopy (TEM), and differential scanning calorimetry (DSC).

2.1 Living Anionic Polymerization

2.1.1 General Aspects of Living Anionic Polymerization

There are two broad types of polymerization, step-growth and chain-growth polymerization. Living cationic or anionic polymerization is a special case of chain-growth polymerization. In particular, the living anionic polymerization method has gained great popularity in phase behaviour studies due to its ability to control the molecular weight, architecture, composition, to reduce synthetic workload, and most importantly, to limit molecular weight distribution (PDI < 1.1 for most samples). Polydispersity has been shown to have effects on block copolymer phase behaviour.[6,7] Narrow molecular distribution minimizes such effect and enables polymer theorists to develop theoretical models to explain phase behaviour as theory often assumes PDI = 1. The living anionic polymerization technique was first developed by Szwarc in 1956, who successfully polymerized styrene and isoprene via electron transfer of sodium naphthanalide to styrene.[8]

Living anionic polymerization is characterized by the lack of undesired transfer and termination steps in the absence of impurities such as water and oxygen.[9,10] It consists of four steps: dissociation of the initiator, initiation via nucleophilic attack, propagation by transferring the active site to another monomer, and termination. These steps are shown below taking alkyllithium as the initiator. The charged species were shown as ion pairs even though they might be in the form of free ions.[11]

Dissociation: $(I-Li)_n \xrightarrow{k_d} nI^- + nLi^+$

Initiation: $Li^+I^- + M \xrightarrow{k_i} (I-M)^- Li^+$

Propagation: $(I-M)^- Li^+ + M \xrightarrow{k_p} (I-M_2)^- Li^+$

$$(I-M_N)^- Li^+ + M \xrightarrow{k_p} (I-M_{N+1})^- Li^+$$

Termination: $(I-M_N)^- Li^+ + X-Y \xrightarrow{k_t} Li^+Y^- + (I-M_N-X)$

The rate of initiation, R_i, after ignoring the association effects, can be expressed as:

$$R_i = k_i[I][M] \tag{2.1}$$

where k_i is the initiation rate constant, [I] is the initiator concentration and [M] is the concentration of the monomer.

The rate of propagation of polymerization, R_p, is:

$$R_p = k_p[M^-][M] \tag{2.2}$$

where k_p is the apparent propagation rate constant and $[M^-]$ is the total concentration of the propagating anionic species.[11] Under the assumption that all initiators dissociated and rapid initiation, the number of initiator ions is equal to the number of polymer chains and Equation 2.2 becomes:

$$R_p = k_p[I]_o[M] \tag{2.3}$$

Without any chain transfer or termination, the average number of monomers in each polymer chain, also called number-average degree of polymerization, $\overline{\chi_n}$, equals to the ratio of the concentration of reacted monomer to that of the initial initiator:

$$\overline{X_n} = \frac{p[M]_o}{[I]_o} \tag{2.4}$$

where p is the fractional conversion of monomer at any time.

Flory postulated that the ideal narrow molecular weight distribution was given by the Poisson distribution if all the polymer chains grew uniformly to the same length and the rate of propagation was much less than the rate of initiation, with

$$PDI = \frac{M_w}{M_n} = 1 + \frac{\overline{X_n}}{\left(\overline{X_n} + 1\right)^2} \approx 1 + \frac{1}{\overline{X_n}} \tag{2.5}$$

where M_w is the weight-average molecular weight and M_n is the number-average molecular weight. In practice, if the reactor is void of oxygen, water and other impurities, chain transfer and chain termination reactions will not occur. The propagating species remain 'alive' and grow as long as there is still monomer left in the reactor. By exploiting this lack of termination and by sequential adding various types of monomers, block copolymers such as AB, ABC, ABA, ABAC, ABCBA etc can be produced.

2.1.2 Materials

2.1.2.1 Initiators

Alkyllithium compounds are commonly used initiators in living anionic polymerization. They are efficient, commercially available and soluble in many solvents, including hydrocarbons.[12] The alkyllithium initiator used in my research is

***sec*-butyllithium** (1.3M solution in cyclohexane, Aldrich). It is stored in a glove box under argon atmosphere and is injected into the polymerization reactor using air-tight syringes. The concentration stated on the initiator bottle provids a good estimate of the initiator concentration and the exact value is back calculated from the volume of the initiator, mass of the first monomer and the M_n of the first block obtained from the synthesis carried out in the previous weeks prior to my own synthesis.

Potassium naphthalenide is used to initiate SIS-OH triblock. It is prepared by reacting potassium and naphthalene in THF. Potassium chunks (Aldrich) are cut into small pieces (about 1g) and the surface oxidized layer is scratched off using a knife, then transferred into a conical flask while purging with argon; the flask is subjected to several vacuum-argon cycles to remove impurities and flamed with a butane torch to remove moisture prior to introduction of the potassium. Ten times molar excess of naphthalene (99%, Aldrich) is added and the reactor is sealed with a septum. Anhydrous THF is then transferred into the conical flask via a cannular and the mixture is stirred for 24 hours using a glass stir bar. Formation of potassium naphthalanide results in the development of a dark green color. The potassium naphthalanide solution is not titrated because we can catch the moment when all SIS-OH triblocks are reinitiated by the persistent color change from colorless to dark green.

2.1.2.2 Monomers

Only certain types of monomers can be polymerized using the living anionic polymerization method. They are vinyl monomers containing carbon-carbon double bond (such as butadiene, isoprene and styrene), heterocyclic monomers (such as cyclic oxides like ethylene oxide, butylenes oxide, cyclic sulphides), and monomers containing carbon-heteroatom double or triple bonds. The reactivity of vinyl monomer increases as the stability of the corresponding anion increases. For example, if a monomer contains an electrophilic substituent that withdraws some electron density from the double-bond, which stabilizes the carbanion via resonance, the reactivity increases. However, it is not desirable to make the substituents reactive, as termination and side chain reactions can occur. The following substituents are ranked in the order of increasing reactivity:[11]

$$-CN > -CO_2R > -Ph, -CH=CH_2 > -H$$

Other than reactivity, proper sequencing of the monomers is also very important. Monomers should be added in the order of equal, if not increasing, stability of the corresponding carbanion, to ensure efficient crossover from one carbanion to another. For example, a polystyryl carbanion can initiate the polymerization of ethylene oxide but not vice-versa. Thus, we need to synthesis SIS-OH in the first step and add PEO block later. Since the stabilities of polystyryl and polyisopryl carbanions are comparable, so the sequence of monomer addition can be interchanged. We can add a PI block to a first PS block and then add a second PS block to the living $(PS\text{-}PI)^-Li^+$

diblocks.

The monomers used in my research are styrene, isoprene and ethylene oxide. **Styrene** (99%, 10-15 ppm *p-tert*-butylcatechol inhibitor, Aldrich) is freeze-pump-thawed three times and then purified by two distillations over solvent-dried dibutylmagnesium (1M solution in heptanes, Aldrich) (0.1 mmol/g styrene) at 40 ^{o}C for one hour each. The styrene is received into a single ended burette then covered with aluminium foil to prevent photo polymerization and stored at room temperature. **Isoprene** (99+ %, 100 ppm *p-tert*-butylcatechol inhibitor, Acros) is also freeze-pump- thawed three times and purified by two distillations over solvent-dried *n*-butyllithium (0.1 mmol/g isoprene) at 0 ^{o}C for one hour each. The isoprene burette is immersed inside a dry-ice/isopropanol bath (-78 ^{o}C) to avoid explosion since isoprene is highly volatile with a low boiling point of 34 ^{o}C. **Ethylene oxide** (EO) (99.5+ %, compressed gas, Aldrich) is freeze-pump-thawed three times and purified by two distillations over solvent-dried butylmagnesium chloride (0.2 mm/g EO) at 0 ^{o}C for 30 minutes each. The monomer burettes are stored in a dry-ice/isopropanol bath.

All these monomers can be harmful upon exposure. Ethylene oxide is the most dangerous, being genotoxic, carcinogenic, mutagenic, extremely flammable and explosive (flash point = -20 ^{o}C). It is in gaseous state at room temperature (boiling point = 10.7 ^{o}C). Extreme care is needed to prevent explosion of ethylene oxide since it can self-polymerize violently under exposure to heat, acids or bases.

2.1.2.3 Solvents

A good solvent in living anionic polymerization should readily dissolve the initiator and polymer chains, but be inert to the carbanions and not become involved in any chain transfer or termination reactions. Solvents can affect the polymerization rate and resulting regiochemistry of the polymer. Non-polar solvents result in relatively slow polymerizations due to aggregation of the initiator and the formation of anion-cation contact pairs. Polar solvents such as tetrahydrofuran (THF) generally increase the rate of polymerization but lead to different microstructures upon polymerizing dienes such as isoprene and butadiene. Isoprene polymerization in THF yields mainly 3, 4- and 1, 2-addition, while in non-polar solvents like cyclohexane, predominately 1, 4-addition occurs.[13]

The solvents used in my research are cyclohexane and tetrahydrofuran. **Cyclohexane** (HPLC grade, Fischer Scientific) is purified by passing through a column of activated alumina followed by a column of copper redox catalyst (CU-0226S, Engelhard) to remove residual oxygen. **Tetrahydrofuran** (HPLC grade, Fischer Scientific) is stored under argon (15 psi) and protic impurities are removed from THF by passing through two columns containing activated alumina (A15 grade, LaRoche).

2.1.2.4 Other Chemicals

The purification agents, ***n*-butyllithium** (2.5M solution in hexanes, Aldrich),

dibutylmagnesium (1M solution in heptanes, Aldrich) are received as solutions and the solvents are removed under vacuum before use. Exposure to air is prevented by storing and handling under an argon atmosphere in a glove box. High-purity **argon** to provide inert condition is passed through an OMI-2 organometallic Nanochem® resin indicator/purification column (Air Products). The termination reagent **Methanol** (reagent grade, Aldrich) is degassed by purging with argon for 30 minutes to remove oxygen, which could cause potential coupling to form undesired products. All other chemicals are used as purchased.

2.1.3 SISO Tetrablock Copolymer Synthesis

2.1.3.1 Reaction Strategy

Synthesis of SIS-OH triblock. Figure 2-1 shows the reaction scheme to synthesize hydroxyl terminated SIS-OH triblock via living anionic polymerization by sequentially adding monomers of styrene, isoprene and styrene, followed by an addition of a single ethylene oxide unit before end-capped with a methanol group. The initiator is *sec*-butyllithium and the solvent is cyclohexane. Each monomer is allowed to react for 8 hours at 40 ^{o}C. In order to prevent undesired termination or chain transfer of the propagating chains, all materials are purified and reactions are conducted under an argon environment. 8 hours are long enough to reach nearly complete conversion (99.9%) but not too long to spread the molecular weight

distribution undesirably. An aliquot of the first styrene block (in 10 mL reaction solution) is collected in degassed methanol (100mL), decanted the methanol, dried under vacuum and analyzed using SEC in order to determine its M_n and PDI.

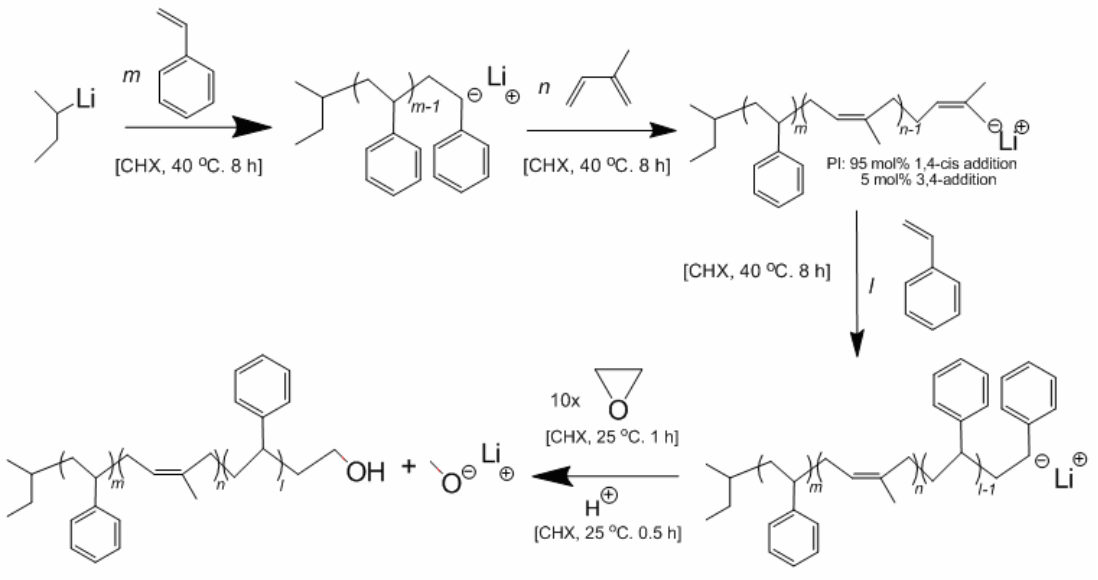

Figure 2-1 Reaction scheme to synthesize SIS triblock terpolymers.

Ten times molar excess ethylene oxide (EO) is purified and added into the reactor after complete conversion of the second styrene block leading to the addition of one EO unit per polymer chain. EO does not polymerize in non-polar cyclohexane because of the low nucleophilicity of the lithium alkoxide base-pair.[14] After one hour, degassed methanol (10mL) is added to terminate the reaction, and the polymer solution is poured into 3 L methanol (reagent grade, Aldrich). White polymer precipitated out and settled down. The solution is decanted and discarded. The precipitate is dried in a vacuum oven at room temperature until it reaches constant

mass. Typically, 50 grams of SIS-OH triblock is prepared in this manner.

Synthesis of SISO tetrablock copolymer. Figure 2-2 shows the reaction scheme used to synthesize SISO tetrablock terpolymers from the SIS-OH triblock. The SIS-OH triblock is reinitiated using potassium naphthalenide to abstract the proton from the terminal –OH group. Tetrahydrofuran (THF) is used as the solvent to increase the reactivity of the oxanions towards EO. Even so, the polymerization rate is lower than that of styrene and isoprene, thus, 48 hours is required to achieve suitable conversions. The reaction is terminated using degassed methanol. SISO tetrablock terpolymers are recovered from solutions using several washes with sodium bicarbonate solution and distilled water. The resulting SISO samples are stored in tightly capped jars at 3-4 ^{o}C for further characterization.

2.1.3.2 Reaction Procedures

Synthesis of SIS-OH. All the detailed experimental setups are described elsewhere.[15] A 3L spherical glass reactor with 5 or 6 ports (size 5, Ace Glass) is used with a target yield of SIS-OH of 50 g. Other glassware such as a thermocouple holder, an airlock, a solvent flask containing 1 L of cyclohexane, and a three-port connector to vacuum and argon are attached to the reactor using ½" OD tubings. Teflon ferrules (Ace Glass) and nylon bushings (Ace Glass) are used to prevent leakage. A teflon coated magnetic stir bar (Chemglass) is used. The assembled empty reactor is subjected to six cycles of dynamic vacuum (<100 millitorr) and pressurized argon (3

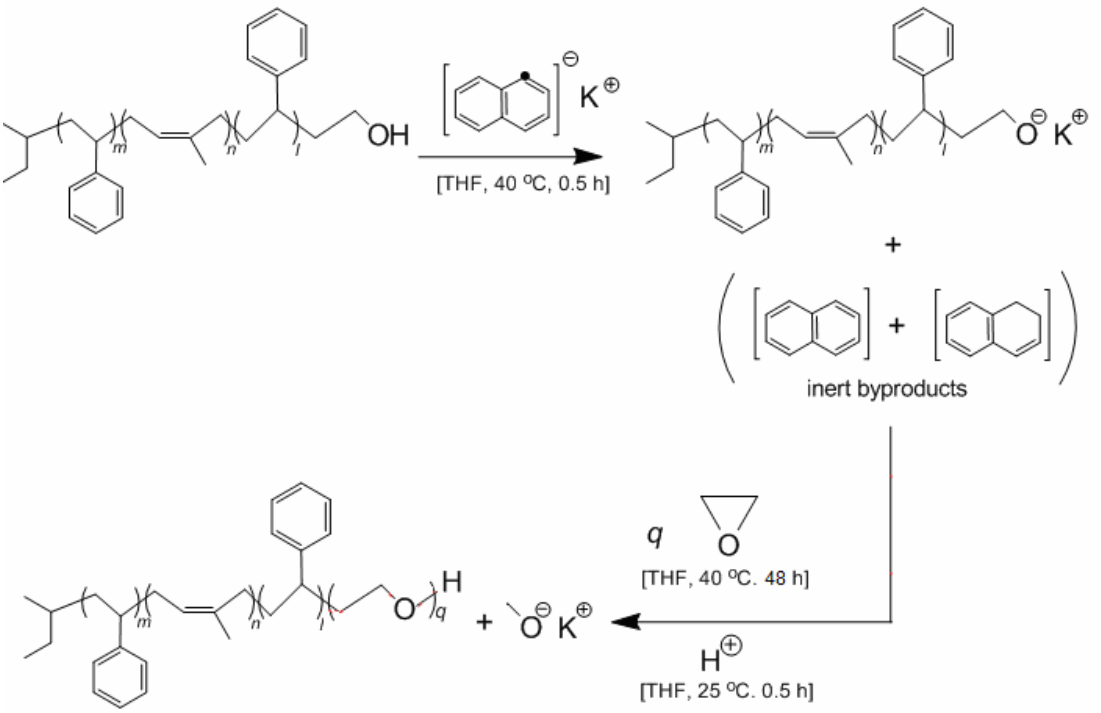

Figure 2-2 Reaction scheme to synthesize SISO tetrablock terpolymers from SIS-OH triblock.

psi), while being heated with a butane torch to remove air and moisture from the interior of the reactor glass wall. The sealed reactor is left under positive argon (3psi) overnight to check for leaks. Solvent is added to the reactor which is immersed in water bath regulated at 40 ^{o}C with a circulating heater. Once the temperature of the solvent and the reactor are stabilized, *sec*-butyllithium initiator is injected through the central septum port using a 5-mL gas tight syringe (SGE international) and a 12'' long needle (18 gauge SS needle). Then the mixture is stirred for 30 minutes to reach constant initiator concentration before a calculated amount of purified styrene monomer is added through an airlock. Polymerization of styrene is indicated by a colour change from colourless to deep orange. The reaction proceeds for 8 hours.

Before adding the isoprene monomer, an aliquot (10 mL) is extracted using a syringe and a needle and injected into degassed methanol. This precipitated polystyrene specimen is dried under vacuum and analyzed by SEC to determine the molecular weight and the PDI. Subsequently, isoprene and styrene monomers are added sequentially and allowed to react for 8 hours each. The solution changes to light yellow upon addition of isoprene and changes back to deep orange upon addition of the second styrene block. Ethylene oxide is added in small amounts to prevent excessive build up of pressure (max. 7 psig). The solution turnes colourless immediately. After one hour, the reaction is terminated by injecting 10 mL of degassed methanol and wait for 30 minutes. The reactor is allowed to vent excess EO and other gases in the fume hood overnight. To avoid contact of EO with skin in the event of an equipment failure, the hood window is closed immediately after opening one port of the reactor.

On the following day, the solution is poured into a beaker with 3L methanol (reagent grade, Aldrich). White polymer precipitates out and settles down. The solution is decanted and discarded. The precipitate is dried in a vacuum oven at room temperature until it reaches a constant mass.

Synthesis of SISO tetrablock terpolymer. Several series of SISO tetrablocks are synthesized using a single master batch of SIS-OH triblock. In any particular series, different amounts of PEO are grown from the same SIS-OH triblock. The only variable in that series is the PEO block length. A smaller reactor (1L) is set up in a

similar way described above. A solvent flask containing 500 mL THF is attached to one of the five ports of the reactor. Calculated amount of SIS-OH triblock (5.0 g) is added to the reactor, after it is subjected to six cycles of dynamic vacuum (<50 millitorr) and pressurized argon (3 psi), and heated with a butane torch to remove air and moisture adsorbed to the interior of the reactor. After ensuring that the reactor is leak-proof, THF is added into the reactor and stirred with a glass magnetic stir bar while maintained at 40 ^{o}C using a water bath. After waiting for one hour for the SIS-OH to dissolve completely, it is reinitiated with potassium naphthalenide. The conical flask containing potassium naphthalenide is connected to an argon/vacuum manifold and pressurized with argon while the initiator solution is transferred into the reactor through the septum port and a long annular (18 GA needle, 2 ft, double tipped SS with non-coring deflection tips, Aldrich). The solution turns from colourless to pale green. The titration end point is established by a persistent pale green colour, indicating complete activation of chain ends on the SIS-OH triblock. The solution is allowed to stir for 30 minutes before EO is added. The purified ethylene oxide burette is connected to the reactor via an airlock having two ½" OD tubings connected by flexible metal tubing. EO burettes are submerged in an ice water bath before addition for safety. The solution turns colourless upon addition of EO. Polymerization of EO proceeds for 48 hours at 40 ^{o}C. The reaction is terminated by injecting 10 mL degassed methanol and stirring for 30 minutes. The reactor is allowed to vent excess EO and other gases in the fume hood overnight. To avoid

contact of EO with skin in the event of equipment failure, the hood window is closed immediately after opening one port of the reactor.

On the following day, the reaction solution is dried using a rotary evaporator to remove the THF solvent. The concentrated SISO samples are dissolved in dichloromethane and washed with saturated sodium bicarbonate solution using a separation funnel. Four additional washes with distilled water are conducted to remove acidity and residual salts. The heavier polymer-containing dichloromethane solution is collected at the bottom port each time. The light portion of bicarbonate solution and distilled water are discarded. Finally, the dichloromethane is removed using a rotary evaporator. The SISO polymers are dissolved into a small amount of THF (20 mL) and precipitated in a 3:1 isopropanol (reagent grade, Aldrich) to methanol mixture in a 4 L beaker. White SISO polymer precipitates and the solution is decanted and discarded. The precipitate is dried via a filtration method using a vacuum pump. The polymer is then dissolved in benzene (reagent grade, Aldrich) (typically 2 mL benzene for 1 g of SISO polymer), with addition of 0.5 wt% butylated hydroxytoluene (BHT) to prevent isoprene degradation. The solution is frozen in liquid nitrogen before transferring to a high vacuum oven (60-80 millitorr) to remove benzene until the sample reaches a constant mass. The polymer is stored in tightly capped jar at 3-4 ^{o}C for future characterization.

2.2 Synthesis and Molecular Characterization Results

Table 2-1 summarizes the molecular characterization results for all the SISO polymers discussed in this thesis. Terpolymer volume fractions, f_S, f_I, and f_O, were estimated through the NMR analysis. Number average molecular weights, M_N, were calculated from the molecular weight of the first S block (determined through SEC) and the terpolymer weight fractions. The PDI values were determined by SEC. The asymmetric factor τ is defined as $Ns/(Ns + Ns')$.

2.3 Nuclear Magnetic Resonance Spectroscopy

Nuclear magnetic resonance spectroscopy is used widely in polymer chemistry to identify the molecular structure and to quantitatively analyze the ratio of each monomer in multiblock copolymers. This technique utilizes the magnetic properties of nuclei such as ^{1}H, ^{13}C, ^{9}F and ^{15}P which have characteristic spin angular momentum with spin quantum number of ± ½. Among them, ^{1}H and ^{13}C are especially relevant to polymer chemists. When the spinning nuclei are aligned with the external magnetic field, they have lower energy than opposed to it.[16] In NMR, short pulses of radio frequencies are used to promote nuclei to a higher energy state, and allowed to relax back to a lower energy state. The energy released is measured as free induction decay (FID) in the time domain, which is converted via Fourier transform to obtain a reasonable plot in the frequency domain. Each proton has a

Table 2-1 The symmetric SISO and asymmetric SIS'O polymer characterization data. SIS'O-0.50 was synthesized and characterized by another group member.[17,18]

Sample	M_n/kDa	PDI	f_S	f_I	f_O
Symmetric SISO samples					
f_S:f_I = 2:3					
SIS-OH	23.3	1.03	0.39	0.61	0.00
SISO-1	23.6	1.04	0.38	0.60	0.02
SISO-2	24.4	1.04	0.35	0.56	0.09
SISO-3	25.0	1.08	0.34	0.53	0.12
SISO-4	26.1	1.06	0.32	0.50	0.19
SISO-5	29.0	1.07	0.27	0.41	0.32
f_S:f_I = 3:2					
SIS-OH	23.1	1.07	0.60	0.40	0.00
SISO-4	23.6	1.07	0.58	0.38	0.04
SISO-9	24.2	1.07	0.54	0.37	0.09
SISO-11	24.6	1.05	0.52	0.37	0.11
SISO-15	25.2	1.06	0.49	0.36	0.15
SISO-31	28.5	1.14	0.40	0.29	0.31
SISO-35	29.7	1.10	0.37	0.28	0.35

Asymmetric SIS'O	$\tau=N_S/(N_S+N_{S'})$	M_n/kDa	PDI	f_S	f_I	f_O
SIS'O-0.21	0.21	19.7	1.04	0.40	0.44	0.16
SIS'O-0.32	0.32	19.1	1.07	0.48	0.46	0.07
SIS'O-0.39	0.39	17.0	1.04	0.46	0.47	0.07
SIS'O-0.50	0.50	23.0	1.04	0.46	0.46	0.08
SIS'O-0.61	0.61	24.2	1.05	0.45	0.46	0.09
SIS'O-0.70	0.70	20.7	1.14	0.43	0.45	0.12

resonance frequency (Larmor frequency) at which maximum intensity is obtained. This frequency depends on the applied magnetic field strength and the local chemical environment the proton is exposed to. Electron shielding occurs when the induced magnetic field opposes the applied field and vice versa. Neighboring protons generate local magnetic fields which either reinforce or oppose the applied field.

These effects interact and result in a slight shift in the resonance frequency of each proton, known as chemical shift, δ. For ^{1}H NMR, the δ scale ranges from 0-12 ppm (parts per million). For ^{13}C, it ranges from 0-220 ppm. By convention, all chemical shifts of protons in ^{1}H NMR are compared with protons in tetramethylsilane, which is considered to be at 0.0 ppm. The chemical shifts of other protons are calculated as:

$$\delta = \frac{v_{sample} - v_{spectrometer}}{v_{spectrometer}} \tag{2.6}$$

where v_{sample} and $v_{spectrometer}$ are the sample frequency and the NMR spectrometer one.

In this study, ^{1}H NMR spectra are obtained at room temperature from 10 mg/mL polymer solutions in deuterated chloroform ($CDCl_3$) (Cambridge) using a Varian 300 MHz instrument, equipped with an autosampler. The ^{1}H NMR characteristic shifts of various chemical environments related to the characterization of SISO tetrablock

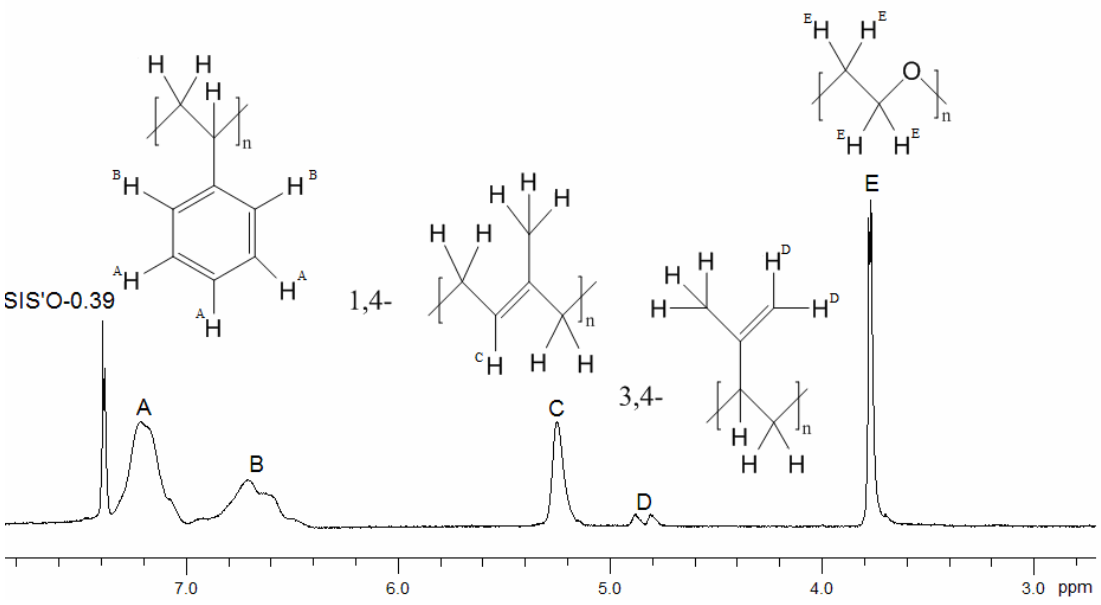

Figure 2-3 ^{1}H NMR spectra for SIS'O-0.39 samples obtained at room temperature.

terpolymers, namely polystyrene, polyisoprene and poly(ethylene oxide) are different, as shown in Figure 2-3.

These characteristic peaks enable us to monitor the successfulness of each monomer addition process. The volume fractions of each monomer in SISO tetrablock terpolymers are calculated by taking the ratio of the integrated area under peaks at their corresponding chemical shifts. The mole fraction of each monomer is calculated as:

$$x_S = \frac{\frac{A+B}{5}}{\frac{A+B}{5}+C+\frac{D}{2}+\frac{E}{4}} \tag{2.7}$$

$$x_{I(1.4)} = \frac{C}{\frac{A+B}{5}+C+\frac{D}{2}+\frac{E}{4}} \tag{2.8}$$

$$x_{I(3,4)} = \frac{\frac{D}{2}}{\frac{A+B}{5}+C+\frac{D}{2}+\frac{E}{4}} \tag{2.9}$$

$$x_O = \frac{\frac{E}{4}}{\frac{A+B}{5}+C+\frac{D}{2}+\frac{E}{4}} \tag{2.10}$$

where *A, B, C, D* and *E* are the areas under peaks at various chemical shifts labeled on Figure 2-3. *S, $I_{(1,4)}$, $I_{(3,4)}$* and *O* represent styrene, 1,4-isoprene, 3,4-isoprene and ethylene oxide respectively.

The weight fractions of the four blocks are then calculated as:

$$w_i = \frac{x_i \times M_i}{\sum_i x_i \times M_i} \tag{2.11}$$

where M_i is the molecular weight for each monomer unit. The volume fraction is

estimated from w_i and published homopolymer densities at 140 ^{o}C:[19]

$$\rho_I = 0.830 \text{ g/cm}^3, \rho_S = 0.969 \text{ g/cm}^3, \rho_O = 1.064 \text{ g/cm}^3 \quad (2.12)$$

2.4 Size Exclusion Chromatography (SEC)

Size exclusion chromatography, also known as gel permeation chromatography (GPC), measures the molecular weight and the molecular weight distribution of macromolecules. Polymer samples are dissolved in a solvent (~1 mg/mL) and allowed to pass through columns packed with porous particles of various sizes. Higher molecular weight polymer chains have greater hydrodynamic volume, proportional to their radius of gyration R_g. They cannot enter most of the pores, and thus travel faster and exit the column earlier. Shorter chains are retained in the pores for longer time and exit the column later. The eluting solution is monitored using a refractive index (RI) or UV absorption detector to record its concentration as a function of retention volume, V_R, volume of solvent passing through the column prior to a particular molecular weight. Sometimes, light scattering and/or viscometric detectors are used to measure exact M_w values.[20] However, these detectors are not used for block copolymers as their dependence of refractive index on solution concentration varies with compositions.

The column is calibrated with polymers of known molecular weights to find out the relationship between V_R and M_w or M_n. A polynomial function can be fitted to

assign a specific molecular weight to each retention volume. Therefore, M_w and M_n can be calculated as:

$$M_n = \frac{\sum_{i=1}^{n} n_i M_i}{\sum_{i=1}^{n} n_i} = \frac{\sum_{i=1}^{n} c_i}{\sum_{i=1}^{n} \frac{c_i}{M_i}} \tag{2.13}$$

$$M_w = \frac{\sum_{i=1}^{n} n_i M_i^2}{\sum_{i=1}^{n} n_i M_i} = \frac{\sum_{i=1}^{n} c_i M_i}{\sum_{i=1}^{n} c_i} \tag{2.14}$$

where c_i and M_i are concentration and molecular weight of the i^{th} slice of the chromatogram respectively.

Different polymers have different relationships between V_R and M. To determine the molecular weight of polystyrene needs to use polystyrene as the standards. This creates a problem for block copolymers, because there is no suitable standard and their composition and molecular architecture relationship between V_R is not clear. Universal calibration is used to solve this problem by assuming the retention volume is directly related to the hydrodynamic volume, which is in turn related to the solution's intrinsic viscosity, [η], regardless of the molecular structure. It could be expressed in the following equation:

$$[\eta] \sim \frac{V_h}{M} \sim \frac{V_R}{M} \tag{2.15}$$

Also, the Mark-Houwink relationship states that,

$$[\eta] = kM^a \tag{2.16}$$

where k and a are Mark-Houwink's parameters.[20]

Combining Equation 2.15 and Equation 2.16 yields:

$$V_R \sim kM^{1+a} \tag{2.17}$$

This equation is used to calculate the molecular weight of any polymer, as long as the Mark-Houwink's parameters are known for both the unknown and standard polymers.

The first PS aliquot and the resulting SISO samples are measured using SEC instrument that contains 5 mm Phenomenex Phenogel columns with a Waters 717 plus autosampler, Waters 590 programmable HPLC pump, and a Waters 410 differential refractometer. Chloroform (0.1~1 mg/mL) is used as the solvent. Ten EasiCal PS-2 polystyrene standards from Polymer Laboratories are used for calibration. A multi-angle light scattering detector (Wyatt Technology DAWN) is used to determine the absolute weight average molecular weight, $M_{w,S}$ of the first PS block. The molecular weights of the SISO tetrablock terpolymers are calculated from $M_{w,S}$ of the first PS block, combined with the mole fractions of each monomer block obtained from NMR. Molecular weight distribution in terms of PDI values, however, is solely determined from the SEC data. Figure 2-4 shows the representative SEC results obtained at the room temperature for the PS aliquot, the SIS-OH triblock precursur and the resulting SISO-11 tetrablock terpolymer, respectively.

2.5 Dynamic Mechanical Spectroscopy (DMS)

Dynamic mechanical spectroscopy (DMS), also called dynamic mechanical analysis (DMA), is used to determine the viscoelastic behaviour of polymers over a

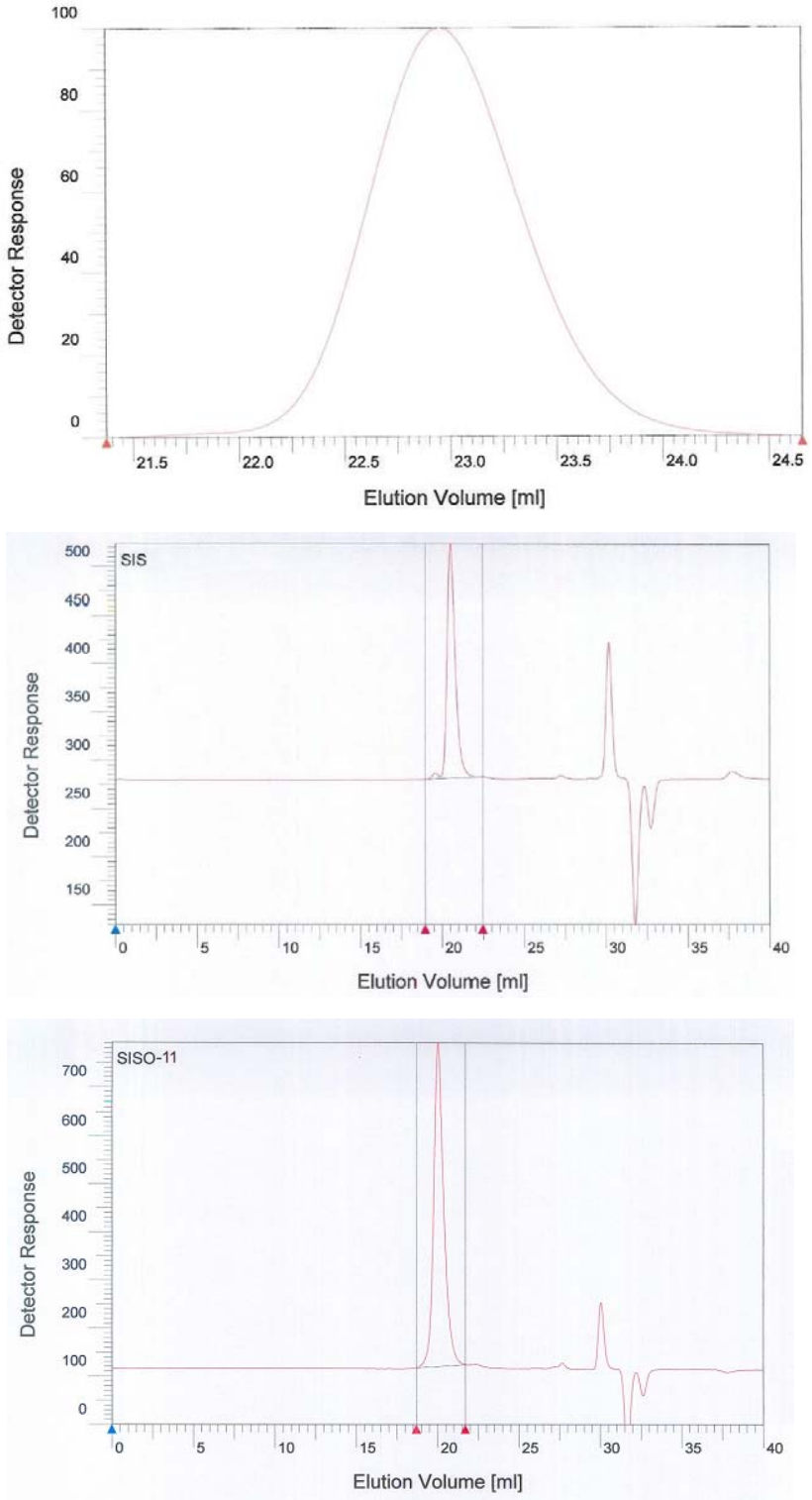

Figure 2-4 GPC data for the PS homopolymer (top), the SIS-OH triblock (middle), and the SISO-11 tetrablock terpolymers (bottom) obtained at room temperature.

wide range of frequencies and temperatures.[21] The main purpose of using DMS in

my research is to study the relationship between rheology and phase behaviour of SISO tetrablock terpolymers. These block copolymers usually have long relaxation times. Thus, at low frequencies, their linear viscoelastic response offers information about the underlying nanostructures.[22,23] While SAXS and TEM are used mainly to investigate the structural details on space group symmetry or spatial organization of the ordered structures, DMS is used as a complementary technique to determine the temperatures of morphological transitions (T_{ODT} and T_{OOT}).[1]

Block polymers behave both like elastic solids and viscous liquids, affecting their mechanical properties, such as strength and performance. There are two limiting responses when they are subject to strain: viscous response and elastic response. Shear modulus is generally a function of time, temperature and strain. However, when the strain is very small (1 – 10 %), the shear modulus is independent of strain, i.e., the system is within the linear viscoelastic regime. It is important to operate the DMS in the linear regime, i.e., with the oscillating strain amplitude γ_o within this limit.

As shown in Figure 2-5, for viscous liquid, the strain and stress are 90^o out of phase and for elastic solid, they are in phase. For viscoelastic polymers, they show characteristics of both types. The stress and strain are out of phase with a phase angle, δ between 0^o and 90^o. Let the strain function for viscoelastic material be:

$$\gamma(t) = \gamma_o \sin(\omega t) \tag{2.18}$$

where ω is the frequency at which the sinusoidal time-varying strain is applied.

The stress function is then given by:

$$\tau(t) = \tau_o \sin(\omega t + \delta)$$

$$\tau(t) = \frac{\tau_o}{\gamma_o}\cos(\delta)\gamma_o \sin(\omega t) + \frac{\tau_o}{\gamma_o}\sin(\delta)\gamma_o \cos(\omega t) \qquad (2.19)$$

$$\tau(t) = G'\gamma_o \sin(\omega t) + G''\gamma_o \cos(\omega t)$$

$$\text{with } G' = \frac{\tau_o}{\gamma_o}\cos(\delta),\ G'' = \frac{\tau_o}{\gamma_o}\sin(\delta) \qquad (2.20)$$

G' is associated with the component that is in phase with the strain, called the storage or elastic modulus; G'' is associated with the component that is out of phase with strain, in phase with strain rate, called the loss or viscous modulus, reflecting the viscous response. Both G' and G'' can be obtained from DMS data. The phase angle is sometimes presented in the form of a loss angle, the ratio of viscous modulus to elastic modulus:[20]

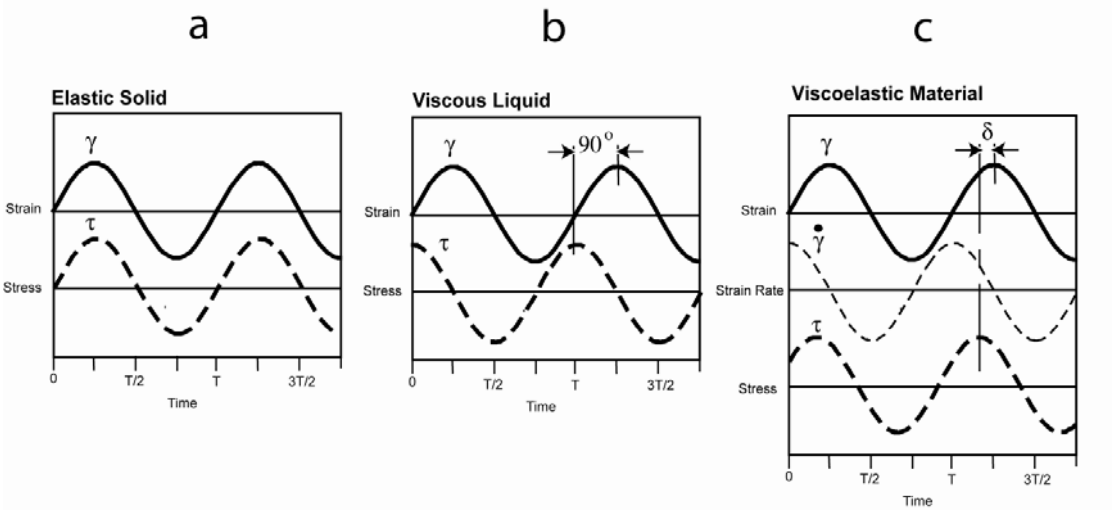

Figure 2-5 Stress and strain functions when sinusoidal strain is applied to an elastic solid (left), a viscous liquid (middle) and a viscoelastic material (right).

$$\tan\delta = \frac{G''}{G'} \tag{2.21}$$

For rheologically simple polymers, such as homopolymers, G'(ω) and G"(ω) frequency obtained at various temperatures can be shifted to produce a master-curve with a reference temperature, T_r. This technique is referred to as time-temperature superposition (TTS).[24] This principle does not apply if there is a phase transition within the temperature range. It is important to note that TTS breaks down in the case of block copolymers,[25] since each polymer block is characterized by a different set of shift factors. Often, master curves can still be constructed for block copolymers by superimposing the response obtained at high frequencies (over which the response is independent of phase behavior). The master curve identifies the critical frequency below which the response will be affected by phase structure. In the disordered state, the block copolymers behave like a liquid at low frequencies, with $G'\sim\omega^2$ and $G''\sim\omega$. In the ordered state, different phases behave differently. For triply periodic solid structures such as the gyroid, O^{70} orthorhombic network and body-centered spherical phase, G' is independent of ω, indicating solid-like response.[2,3,5,26,27] For singly periodic (such as lamellae) or doubly periodic (such as cylinders) structures, they show intermediate behavior between liquid and solid. For the lamellae phase, $G'\sim G''\sim\omega^{1/2}$;[25,26,28–30] and for hexagonally order cylindrical phase, $G'\sim G''\sim\omega^{1/3}$,[31,32] although these low frequency responses may vary between systems. Therefore, by monitoring G' and G" with respect to ω in the low frequency regime, phase transitions can be identified. At high frequencies, the viscoelastic responses are

dominated by single chain dynamics and/or chain entanglements and do not reflect the underlying morphology.

All DMS measurements are made on a Rheometric Scientific ARES strain-controlled instrument. A schematic diagram of the experimental setup is shown in Figure 2-6. Polymer samples are hot pressed at 130 ^{o}C and 1000 psi for 5 minutes between Teflon-covered plates to form circular disks, 25 mm in diameter and 1 mm in thickness. Then the sample disk is placed between parallel circular plates that are fixed to the rheometer; one is forced to oscillates with controllable frequency and a set strain amplitude while the resulting torque is measured in the other plate. Nitrogen is used as a purging gas to prevent oxidative degradation and crosslinking of polyisoprene block in the SISO samples. The measurements are taken between 100 ^{o}C and 250 ^{o}C. The lower value is limited by the glass transition temperature of polystyrene and the upper value is limited by thermal degradation of the material.

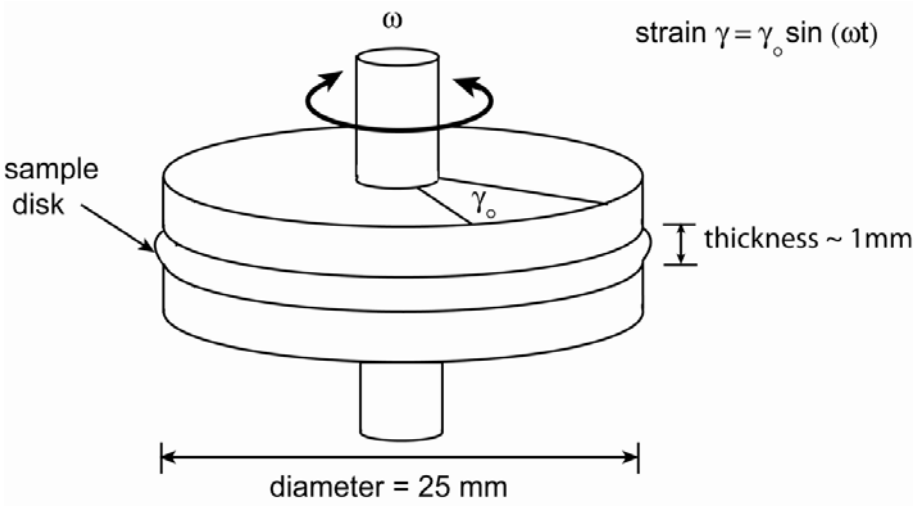

Figure 2-6 Experimental setup for the DMS experiment.

The following protocols are used during DMS measurements. Strain sweeps for all samples are first conducted at 110 ^{o}C to make sure that at 1% strain, the specimen is within their linear viscoelastic region. A frequency of 1 rad/s is used in all experiments, assuming phase behavior is independent of this low frequency of 1 rad/s. The sample is first undergone a faster temperature ramp at 10 ^{o}C/min to locate the T_{ODT}. The T_{ODT} measures the transition from ordered to disordered state and is identified by a sudden decrease in the elastic modulus across several orders of magnitudes.[1,25,30,33–37] If the T_{ODT} is below 250 ^{o}C, the sample is heated to approximately 10 ^{o}C higher than T_{ODT} for 5 minutes to erase any thermal history, and then cooled back to 100 ^{o}C. Another slower temperature ramp at 2 ^{o}C /min is carried out to determine the exact T_{ODT}.

2.6 Small Angle X-Ray Scattering (SAXS)

In my research, x-ray scattering is used as the primary technique to determine block copolymer phase behavior. Incident x-rays excite electrons in a material which reemit as 'scattered' photons with spherical symmetry. If there is no energy exchange (i.e., the incident and emitted wavelength (λ) are equal), the scattering event is referred to as elastic. The incident and scattering wave vectors are denoted by $\vec{k}_i$ and $\vec{k}_s$, respectively, where $\left|\vec{k}_i\right| = \left|\vec{k}_s\right| = 2\pi/\lambda$ for elastic scattering events. The magnitude of the scattering wave vector is described geometrically in Figure 2-7, where

$\vec{q} = \vec{k_i} - \vec{k_s}$ and

$$|\vec{q}| = \frac{4\pi}{\lambda}\sin(\frac{\theta}{2}) \tag{2.22}$$

where θ is the scattering angle defined by the experimental equipment.

Scattering from a collection of atoms (e.g. bulk materials) leads to the superposition of many scattered waves, resulting in an interference pattern that depends on the atomic structure of the material. If the material is a perfectly periodic crystal, constructive and destructive interference occurs depending on the crystal orientation, symmetry and planar spacings. The Bragg's law describes the criterion for constructive interference and illustrates how scattering patterns provide structural information for ordered materials.[38] Constructive interference will occur only when the path difference between waves scattering at a given angle θ from different planes separated by a distance d is equal to an integral multiple of the wavelength:

$$n\lambda = 2d\sin(\frac{\theta}{2}) \tag{2.23}$$

where n is an integer value representing diffraction order, d is the inter-planar

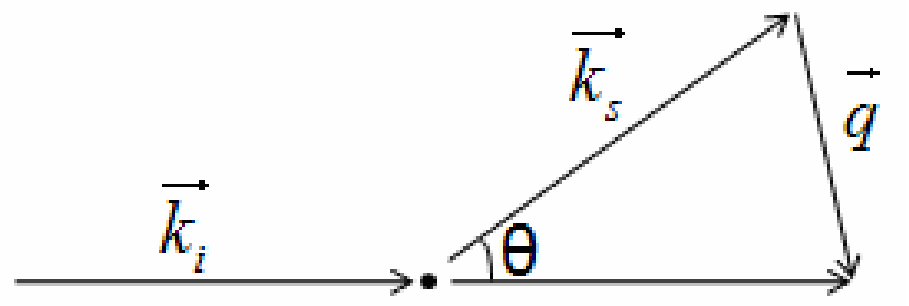

Figure 2-7 Incident plane waves hit a point scatterer and spherical waves are re-emitted. $\vec{q}$ is the scattering vector and θ is the scattering angle.

spacing, and *θ/2* is the angle between incident and reflecting plane. Domain spacings can be probed by scanning θ at fixed λ and identifying the scattering angles where constructive interference (i.e. strong scattered intensity) is obtained.

Block copolymers produce ordered structures with periodic spacings of about 5 – 50 nm. Based on synchrotron x-ray sources, λ is on the order of 0.1 nm. Thus, the scattering angle must be less than 5^o to access the relevant domain spacings. This is referred to as small-angle x-ray scattering. Ordered block copolymer morphologies produce scattering patterns and ratios of higher order scattering wave vectors to the first order peak (q^*). Combing Bragg's law (Equation 2.22) and Equation (2.23) yields:

$$q_{hkl} = \frac{2\pi n}{d_{hkl}} \tag{2.24}$$

This equation shows that the interplanar spacing, d_{hkl} of specific space group is inversely proportional to the scattering wave vector, q_{hkl}. This equation can be expressed as a function of Miler indices and the unit cell dimensions as shown in the equation below:

$$\frac{q_{hkl}}{2\pi} = \frac{1}{d_{hkl}} = \sqrt{\frac{h^2}{a^2} + \frac{k^2}{b^2} + \frac{l^2}{c^2} + 2\frac{hk}{ab}\cos\gamma + 2\frac{hl}{ac}\cos\beta + 2\frac{lk}{cb}\cos\alpha} \tag{2.25}$$

For cubic lattice, $a = b = c$ and $\alpha = \beta = \gamma = 90^o$:

$$d_{hkl} = \frac{a}{\sqrt{h^2 + k^2 + l^2}} \tag{2.26}$$

For hexagonal lattice, $a = b \neq c$ and $\alpha = \beta = 90^o, \gamma = 60^o$:

$$d_{hkl} = \frac{a}{\sqrt{h^2 + k^2 + hk}} \tag{2.27}$$

For orthorhombic lattice, $a \neq b \neq c$ and $\alpha = \beta = \gamma = 90^o$:

$$d_{hkl} = \frac{1}{\sqrt{\frac{h^2}{a^2} + \frac{k^2}{b^2} + \frac{l^2}{c^2}}} \tag{2.28}$$

There are seven lattice groups consisting of 230 space groups in Bravais lattices. Once the lattice is determined, the space group can be determined by identifying various symmetry elements such as mirror planes, screw axes, inversion centers etc. These factors set up constraints for the allowed reflections by the lattice symmetry, i.e., reflections allowed by the lattice symmetry might be absent due to the addition of the symmetry elements in each space group. Therefore, we could not eliminate a proposed space group because certain reflection is missing; however, the proposed space group should be eliminated if a reflection appears at forbidden locations. Reflection conditions for all 230 space groups are listed in the International Tables for Crystallography.[39] Different space group symmetries determine the block copolymer morphology. The possible reflections for some common block copolymer morphologies are listed in Table 2-2.

Most SAXS data presented in this research are obtained at the Advanced Photon Source in Argonne National Laboratory. Experiments are conducted in station DND-SAT-5ID-D in the DuPont-Northwestern-Dow Synchrotron Research Center (more details are described on the website www.aps.anl.gov). Figure 2-8 shows the schematic diagram of the SAXS experiment. The wavelengths of the synchrotron x-

ray is adjustable between 0.73 – 1.54 Å as the energy changes between 10 – 17 keV. The sample detector distance is varied from 3 – 6.6 m. The sample temperature is controlled to within ± 1 ^{o}C with a Linkam DSC chamber under a helium purge. MarCCD area detector with 133 mm in diameter and a resolution of 2048×2048 pixels is used. The ordered block copolymer samples are annealed at 120 ^{o}C in vacuum (≈ 150 torr) oven for a day, quenched in liquid nitrogen to preserve their morphologies, stored in a refrigerator of 4 ^{o}C at laboratory and reheated to various acquisition temperatures at Argonne facilities. All samples were annealed at the targeted temperature for 5 – 10 minutes prior to data collection, unless otherwise specified. The diffraction data were azimuthally averaged and represented as the intensity vs. the scattering wave vector $q=|\mathbf{q}|=4\pi/\lambda \sin(\theta/2)$, where θ is the scattering angle.

Table 2-2 Possible reflections for several common block copolymer morphologies.

Block Copolymer Morphology	**q/q***
Lamellar (LAM)[40]	1, 2, 3, 4, 5, 6,…
Hexagonally packed cylinders(HEX)[41]	$\sqrt{1}, \sqrt{3}, \sqrt{4}, \sqrt{7}, \sqrt{9}, \sqrt{12}$,…
BCC spheres(S)[42]	$\sqrt{1}, \sqrt{2}, \sqrt{3}, \sqrt{4}, \sqrt{5}, \sqrt{6}$,…
Core-shell gyroid (Q^{230})[43]	$\sqrt{6}, \sqrt{8}, \sqrt{14}, \sqrt{16}, \sqrt{20}, \sqrt{22}$,…
Alternating gyroid (Q^{214})[2]	$\sqrt{2}, \sqrt{6}, \sqrt{8}, \sqrt{10}, \sqrt{12}, \sqrt{14}$,…
Orthorhombic Network (O^{70})[3]	Depends on lattice dimension

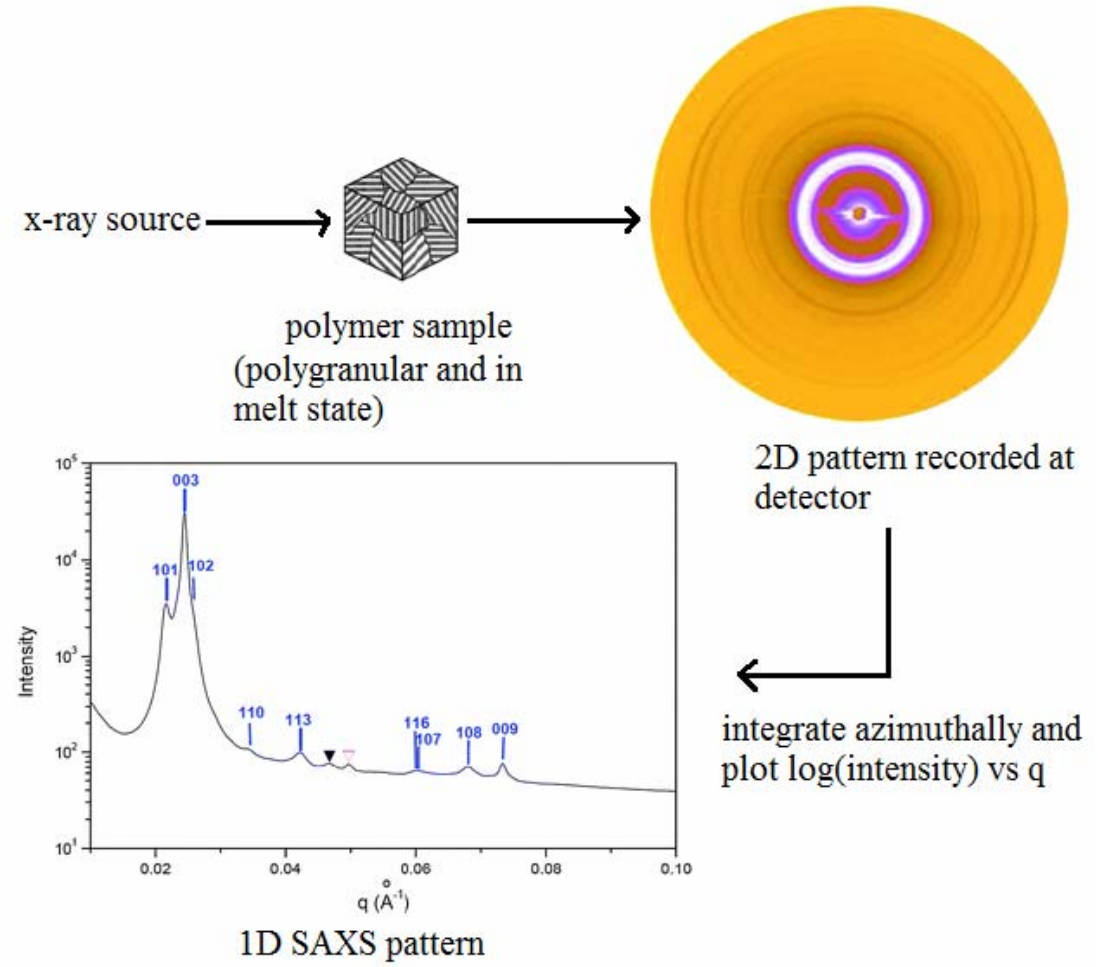

Figure 2-8 Schematic diagram of SAXS experiment.

2.7 Transmission Electron Microscopy (TEM)

Transmission electron microscopy (TEM) provides direct visual images of block copolymers phase behavior on a nanometer scale and complements reciprocal space images obtained by SAXS. This method has been used for block copolymer characterization for many years.[44] A beam of electrons are used to image the specimen in TEM. A high voltage (typically 40-400 kV) electron beam is generated

by an electron gun and focused onto the sample with electromagnetic lenses. Upon interaction with the sample, the electron beam is either reflected or transmitted through the sample. The latter passes through a series of lens and apertures and gets magnified and recorded on a phosphor viewing screen. The image is a two-dimensional projection of the sample cross section with 10,000-1,000,000 times enlarged. While x-rays interact with the electron cloud surrounding the nuclei, the electron beam in TEM interacts primarily with the nuclei in a polymer (or other materials) at modest or low magnification; heavier nuclei produce more Rutherfold scattering leading to Z-contrast.[45] Thus, sections of a material containing higher z elements will appear darker in a TEM image. Thicker portions of a specimen also result in darker image since fewer electrons reach the detector due to more scattering event occurring with a greater number of nuclei. Typical specimen thicknesses used in TEM are about 50 – 70 nm to allow for adequate transmission of electrons. It is important that samples have uniform thickness so that dark and light areas represent change in material composition instead of sample thickness.[46]

In the case of block copolymers which contain mainly carbon, hydrogen, and oxygen, most nuclei are light (low z), resulting in very little contrast between the micro-domains. In order to enhance the contrast, SISO samples were stained with the vapour from a 4% aqueous solution of OsO_4 for 5 to 10 minutes, depending on the thickness of the sample and the volume fraction of the PI block. The metal oxide selectively reacts with the double bonds in the PI block, introducing Z-contrast. After

staining, PI block domain appears darker than those of PS and PEO block in the TEM images.[4,5]

There are certain limitations when using TEM to analyze block copolymer samples. First, TEM images are two-dimensional representations of a three-dimensional structure; the micrograph depends on the sample orientation with respect to the principal axes present in a specific morphology. Also, TEM provides information on a local state of order less than 1 μm^2 in size. Relying on TEM as a sole characterization technique to determine the sample morphology can lead to incorrect conclusions.[47–53] Other complementary characterization techniques should be used to conclusively determine the sample morphology such as SAXS, rheology and DSC. They are generally used to provide statistically averaged information about the bulk state of order.[43,54,55]

The instrument used in this study is a Tecnai T12 microscope operated at 120 kV with a magnifying ratio as high as 700,000 times. A Gatan Multiscan CCD camera (1024 × 1024) is used for digital image collection. The images are then analyzed with DigitalMicrographs version 3.3.1. Block copolymers are first annealed under vacuum for a specified period of time at desired temperatures, followed by a liquid nitrogen quench to preserve the morphology. Then samples are microtomed at -70 ^{o}C into 0.3 cm × 0.3 cm × 70 nm pieces with a Reichart Ultramicrotome equipped with a Microstar diamond knife. The thickness is chosen to be about 50 – 70 nm so that the sample is thin enough for adequate electron transmission but thick

enough for optimum contrast in the images. The cutting temperature is chosen at -70 ^{o}C (lower than the lowest glass transition, for polyisoprene T_g = -60 ^{o}C)[56] so that the sample is completely glassy to prevent possible deformation of the nanostructures during the cutting process. Usually 5 – 10 slices are collected on a copper grid (uncoated and 400 mesh-size, Ted Pella) using an eye-lash.

2.8 Differential Scanning Calorimetry

Differential scanning calorimetry is a thermal analysis technique, used to measure the glass transition temperature, melting temperature, and percent crystallinity in block copolymers containing a semicrystalline block. The glass transition and melting temperatures establish the use and processing temperatures above which the materials could be easily molded.[20,57,58] A small amount (10 mg) of the polymer sample is placed in an aluminum pan with another empty pan as the reference. Both pans are quickly heated to 10 ^{o}C above T_{ODT} or 250 ^{o}C, whichever is lower to minimize any thermal history, and then cooled back to -100 ^{o}C. Then they are heated and cooled at specified heating/cooling rates. DSC measures the differences in heat flow to these two pans in order to keep them at the same temperature, using a resistive heating element. Magnitude and direction (exothermic or endothermic) of the heat flows are recorded and plotted as a function of temperature. The slope of this curve is C_p. It changes whenever the sample undergoes

a thermal transition. A pseudo-step increase suggests a glass transition, an exothermic peak blow the curve suggests some crystallization, and an endothermic peak above the curve represents melting. Polymer usually melts over a range of temperatures and the peak melting temperature is taken as the melting point. The segregation of domains in block copolymers leads to the presence of multiple glass transitions. Integrating the exothermic and endothermic peaks yields the latent heats of crystallization and melting, respectively. These values can be used to determine the crystallinity (X_c) of a semicrystalline block as shown below:

$$X_c = \frac{\Delta H_s}{\Delta H_m \times w_c} \tag{2.29}$$

where ΔH_s is the heat of fusion of the polymer, ΔH_m is heat of fusion of the pure crystal phase, and w_c is the weight fraction of the semicrystalline block.

The DSC experiments were conducted on a TA Instruments Q1000 DSC. Approximately 5 – 10 mg polymer samples were heated to 150 ^{o}C to erase any thermal history before cooling to -100 ^{o}C at 10 ^{o}C/min. Data were acquired upon heating a second time at 10 ^{o}C/min.

2.9 References

(1) Hillmyer, M. A.; Bates, F. S.; Almdal, K.; Mortensen, K.; Ryan, A. J.; Fairclough, J. P. A. *Science* **1996**, *271*, 976.

(2) Bailey, T. S.; Hardy, C. M.; Epps III, T. H.; Bates, F. S. *Macromolecules*

2002, *35*, 7007.

(3) Epps III, T. H.; Cochran, E. W.; Bailey, T. S.; Waletzko, R. S.; Hardy, C. M.; Bates, F. S. *Macromolecules* **2004**, *37*, 8325.

(4) Chatterjee, J.; Jain, S.; Bates, F. S. *Macromolecules* **2007**, *40*, 2882.

(5) Meuler, A. J.; Fleury, G.; Hillmyer, M. A.; Bates, F. S. *Macromolecules* **2008**, *41*, 5809.

(6) Meuler, A. J.; Ellison, C. J.; Evans, C. M.; Hillmyer, M. A.; Bates, F. S. *Macromolecules* **2007**, *40*, 7072.

(7) Meuler, A. J.; Ellison, C. J.; Hillmyer, M. A.; Bates, F. S. *Macromolecules* **2008**, *41*, 6272.

(8) Szwarc, M. *Nature* **1956**, *178*, 1168.

(9) Lodge, T. P. *Macromolecular Chemistry and Physics* **2003**, *204*, 265.

(10) Hadjichristidis, N.; Pitsikalis, M.; Iatrou, H. *Advances in Polymer Science* **2005**, *189*, 1.

(11) Odian, G. *Principles of Polymerization*; Wiley: New York, 2004.

(12) Hadjichristidis, N.; Iatrou, H.; Pispas, S.; Pitsikalis, M. *Journal of Polymer Science Part A: Polymer Chemistry* **2000**, *38*, 3211.

(13) Cochran, E. W. *Ph.D. Dissertation*; University of Minnesota, 2004.

(14) Quirk, R. P.; Ma, J.-J. *Journal of Polymer Science Part A: Polymer Chemistry* **1988**, *26*, 2031.

(15) Ndoni, S.; Papadakis, C. M.; Bates, F. S.; Almdal, K. *Review of Scientific*

Instruments **1995**, *66*, 1090.

(16) Silverstein, R. M.; Webster, F. X.; Kiemle, D. J. *Spectrometric Identification of Organic Compounds*; John Wiley & Sons: Hoboken, NJ, 2005.

(17) Bluemle, M. J.; Fleury, G.; Lodge, T. P.; Bates, F. S. *Soft Matter* **2009**, *5*, 1587.

(18) Lee, S.; Bluemle, M. J.; Bates, F. S. *Science* **2010**, *330*, 349.

(19) Fetters, L. J.; Lohse, D. J.; Richter, D.; Witten, T. A.; Zirkel, A. J. *Macromolecules* **1994**, *27*, 4639.

(20) Hiemenz, P. C.; Lodge, T. P. *Polymer Chemistry*; Taylor & Francis Group: University of Minnesota: Minneapolis, MN, 2007.

(21) Macosko, C. W. *Rheology: Principles, Measurements and Applications*; Wiley-VCH: New York, 1994.

(22) Fredrickson, G. H.; Bates, F. S. *Annual Review of Materials Science* **1996**, *26*, 501.

(23) Colby, R. H. *Current Opinion in Colloid and Interface Science* **1996**, *1*, 454.

(24) Williams, M. L.; Landel, R. F.; Ferry, J. D. *Journal of the American Chemical Society* **1955**, *77*, 3701.

(25) Rosedale, J. H.; Bates, F. S. *Macromolecules* **1990**, *23*, 2329.

(26) Zhao, J.; Majumdar, B.; Schulz, M. F.; Bates, F. S.; Almdal, K.; Mortensen,

K.; Hajduk, D. A.; Gruner, S. M. *Macromolecules* **1996**, *29*, 1204.

(27) Kossuth, M. B.; Morse, D. C.; Bates, F. S. *Journal of Rheology* **1999**, *43*, 167.

(28) Bates, F. S.; Rosedale, J. H.; Fredrickson, G. H. *The Journal of Chemical Physics* **1990**, *92*, 6255.

(29) Koppi, K. A.; Tirrell, M.; Bates, F. S.; Almdal, K.; Colby, R. H. *Journal de Physique II* **1992**, *2*, 1941.

(30) Patel, S. S.; Larson, R. G.; Winey, K. I.; Watanabe, H. *Macromolecules* **1995**, *28*, 4313.

(31) Morrison, F. A.; Winter, H. H.; Gronski, W.; Barnes, J. D. *Macromolecules* **1990**, *23*, 4200.

(32) Ryu, C. Y.; Lee, M. S.; Hajduk, D. A.; Lodge, T. P. *Journal of Polymer Science Part B* **1997**, *35*, 2811.

(33) Almdal, K.; Rosedale, J. H.; Bates, F. S. *Macromolecules* **1990**, *23*, 4336.

(34) Almdal, K.; Bates, F. S.; Mortensen, K. *The Journal of Chemical Physics* **1992**, *96*, 9122.

(35) Winter, H. H.; Scott, D. B.; Gronski, W.; Okamoto, S.; Hashimoto, T. *Macromolecules* **1993**, *26*, 7236.

(36) Foerster, S.; Khandpur, A. K.; Zhao, J.; Bates, F. S.; Hamley, I. W.; Ryan, A. J.; Bras, W. *Macromolecules* **1994**, *27*, 6922.

(37) Sakamoto, N.; Hashimoto, T.; Han, C. D.; Kim, D.; Vaidya, N. Y.

Macromolecules **1997**, *30*, 1621.

(38) Stout, G. H.; Jensen, L. H. *X-Ray Structure Determination*; John Wiley & Sons: New York, 1989.

(39) *International Tables for Crystallography, Volume B: Reciprocal Space*; Shmueli, U., Ed.; 1st ed.; Springer, 1993.

(40) Ryan, A. J.; Hamley, I. W.; Bras, W.; Bates, F. S. *Macromolecules* **1995**, *28*, 3860.

(41) Bailey, T. S.; Pham, H. D.; Bates, F. S. *Macromolecules* **2001**, *34*, 6994.

(42) Breiner, U.; Krappe, U.; Abetz, V.; Stadler, R. *Macromolecular Chemistry and Physics* **1997**, *198*, 1051.

(43) Hajduk, D. A.; Harper, P. E.; Gruner, S. M.; Honeker, C. C.; Kim, G.; Thomas, E. L. *Macromolecules* **1994**, *27*, 4063.

(44) Drzewinski, M. A.; Cohen, R. E. *Polymeric Materials Science and Engineering* **1985**, *52*, 437.

(45) Pennycook, S. J.; Jesson, D. E. *Ultramicroscopy* **1991**, *37*, 14.

(46) Williams, D. B.; Carter, C. B. *Transmission Electron Microscopy: A Textbook for Materials Science*; Plenum Press: New York, 1996.

(47) Alward, D. B.; Kinning, D. J.; Thomas, E. L.; Fetters, L. J. *Macromolecules* **1986**, *19*, 215.

(48) Thomas, E. L.; Alward, D. B.; Kinning, D. J.; Martin, D. C.; Handlin Jr., D. L.; Fetters, L. J. *Macromolecules* **1986**, *19*, 2197.

(49) Herman, D. S.; Kinning, D. J.; Thomas, E. L.; Fetters, L. J. *Macromolecules* **1987**, *20*, 2940.

(50) Hasegawa, H.; Tanaka, H.; Yamasaki, K.; Hashimoto, T. *Macromolecules* **1987**, *20*, 1651.

(51) Mogi, Y.; Mori, K.; Matsushita, Y.; Noda, I. *Macromolecules* **1992**, *25*, 5412.

(52) Xie, R.; Yang, B.; Jiang, B. *Macromolecules* **1993**, *26*, 7097.

(53) Matsushita, Y.; Tamura, M.; Noda, I. *Macromolecules* **1994**, *27*, 3680.

(54) Matsushita, Y.; Suzuki, J.; Seki, M. *Physica. B, Condensed Matter* **1998**, *248*, 238.

(55) Matsen, M. W. *The Journal of Chemical Physics* **1998**, *108*, 785.

(56) Brandrup, J.; Immergut, E. H. *Polymer Handbook*; 3rd ed.; John Wiley & Sons: New York, 1989.

(57) Campbell, D.; White, J. R. *Polymer Characterization: Physical Techniques*; Chapman and Hall: New York, 1989.

(58) Wetton, R. E. *Polymer Characterization*; Blackie Academic & Professional: New York, 1993.

3

Hexagonal Spherical Phase in Isoprene-rich SISO Tetrablock Terpolymers

* Reproduced in part with permission from Zhang J.; Sides S. W.; Bates, F. S. *Macromolecules* **2012**, *45*, 256-265.

3.1 Introduction

Over the past forty years, people have devoted much research attention to the phase behaviour of block copolymers. Remarkably, due in part to the limitations in the available quantitative characterization tools, a comprehensive understanding of the phase behaviour of the simplest form of block copolymers, linear AB diblock copolymers, took more than forty years to achieve. Six equilibrium phases have been discovered: spheres, cylinders, gyroid, lamellae, and more recently the O^{70} and the σ-phase.[1–14] And there is no guarantee that more surprises remain, e. g., the discovery of the O^{70} and the σ-phase in diblocks. Self-consistent field theory (SCFT) has

accounted for all but the σ-phase. Highly asymmetric AB diblocks with minority volume fraction of 10 to 15 % form spherical phase with BCC symmetry in the matrix consisting the majority block. The phase behaviour of ABC triblocks was much more complex with more than 30 equilibrium morphologies discovered and many more to be identified in the future.[5,15–23] In ABC triblocks with $\chi_{AC} > \chi_{AB}$ and $\chi_{AC} > \chi_{CB}$, core-shell spheres are formed with BCC symmetry as well.[24–27]

Symmetric ABAC tetrablock terpolymers break the molecular symmetry by inserting half of the A block between the B and C blocks, introducing flexibility in diverse morphology formation. Without altering the molecular weights and compositions as those of the ABC triblocks, we can change the morphology by changing the molecular architecture alone. So far, two ABA'C tetrablock terpolymers have been investigated: poly(cyclohexylethylene-*b*-ethylene-*b*-cyclohexylethylene-*b*-dimethylsiloxane) CECD and poly(styrene-*b*-isoprene-*b*-styrene-*b*-ethylene oxide) SISO.[28,29] In a preliminary study, Lee *et. al.* reported an unanticipated sphere-forming σ-phase in SISO with $f_S = f_I$ and f_O = 8%.[13] In another preliminary study, Bluemle *et. al.* reported the various morphologies along the same isopleth with $f_S = f_I$.[29]

In this chapter, we explore a set of SISO tetrablock terpolymers (listed in Table 3-1) with $f_S : f_I$ = 2 : 3, τ = 1 and f_O = 0 – 32%. The molecular structure is shown in Figure 3-1 (a). The SIS-OH triblock is disordered above 80 °C. With $\chi_{SI} \leq \chi_{SO} << \chi_{IO}$, the repulsion between the I and O blocks is the greatest. Since the I and O blocks are

not directly bonded to each other, it is unlikely to form I/O interfaces. Therefore, core-shell spheres are formed with an O core, a shell of internal and terminal S blocks, in an I-rich matrix (see Figure 3-1 (b)).[29] These spheres form a new hexagonal packing symmetry (P_6/mmm or P_6/mm space group symmetry). By tailoring the composition ratio between the S and I blocks, we expect to see subtle yet significant effects on the equilibrium morphologies based on the changes in composition alone.

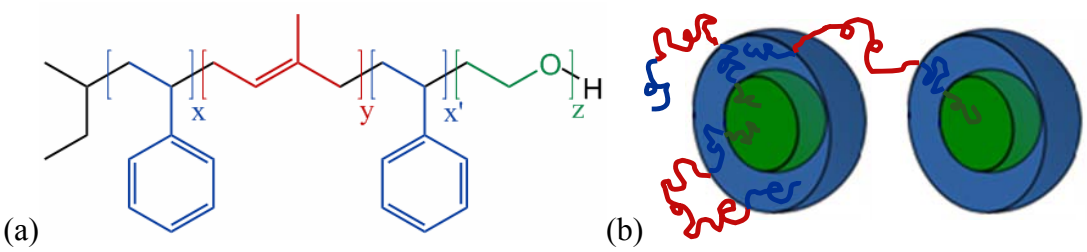

Figure 3-1 (a) Molecular structure of SISO tetrablock terpolymers with x = x'. (b) core-shell spherical morphology. Unfavorable interactions between the O (core) and I (matrix) blocks are screened by S blocks (shell).

3.2 Results and Analysis

Figure 3-2 shows the phase portrait of the SISO tetrablock terpolymers. The effects of the molecular weight are not reflected on this map. Results from the middle series (containing equal volume fractions of S and I) were described elsewhere.[29] This chapter focuses on the series with $f_S : f_I = 2 : 3$, as indicated by the black line.

Five SISO tetrablock terpolymers with different f_Os were synthesized from the same SIS-OH triblock. Molecular characterization data, lattice dimensions, degree of crystallinity, T_{ODT}'s and morphology assignments based on SAXS, TEM, DSC and DMS are listed in Table 3-1.

Estimation of T_{ODT} for SIS-OH triblock. Since the PS blocks have a glass transition temperature around 90 °C[30] and the PI blocks tend to degrade above 250 °C, the molecular weight of the SIS-OH triblock needs to be carefully designed so that the corresponding T_{ODT}s of the SISO tetrablock terpolymers are between 100 and 250 °C for the morphological behavior to be within the weak to intermediate segregation regime. For diblock copolymers, $(\chi N)_{ODT} = 10.5$;[1] for symmetric triblock copolymers $(\chi N)_{ODT} = 18.0$.[31] Thus, the molecular weight of the SIS-OH triblock should be about 1.8 times of that of the IS-OH diblock in order to achieve similar T_{ODT}s between the SISO tetrablocks and the ISO triblocks. With reference to a previous study for the ISO triblocks prepared from a IS-OH diblock with f_S = 0.42 and M_n = 12.7 kg/mol,[22] our SIS-OH triblock was targeted to have N_{total} = 291 with $N_{S_1} = N_{S_2} = 49$, and N_I= 193. At T_{ODT}, $\chi_{ODT} = 18.0 N_{total}^{-1} = 0.0618$ and the associated Flory-Huggins interaction parameters are reported as:

$$\begin{aligned} \chi_{IS}(T) &= 26.4T^{-1} - 0.0287 \\ \chi_{SO}(T) &= 29.8T^{-1} - 0.0229 \\ \chi_{IO}(T) &= 90.0T^{-1} - 0.0579 \end{aligned} \qquad (3.1)$$

based on a common segment volume of 118 A^3.[32] Therefore, the T_{ODT} of the SIS-OH triblock is calculated to be 19 °C. Upon addition of the PEO blocks, the T_{ODT}s of the

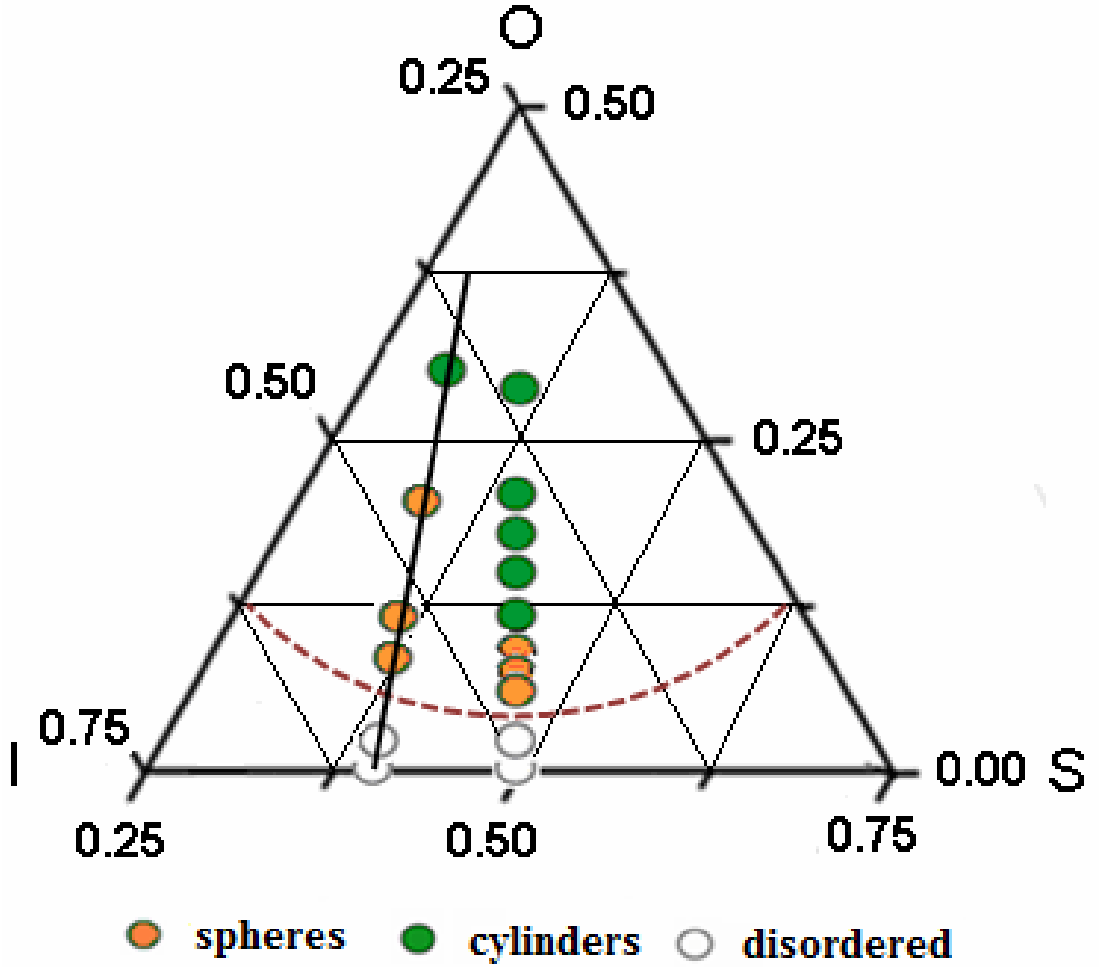

Figure 3-2 Poly(styrene-*b*-isoprene-*b*-styrene-*b*-ethylene oxide) (SISO) phase portrait in the vicinity of the order-disorder transition, indicated by the dashed brown curve. Filled and open circles indicate ordered and disordered states, respectively, within the experimental temperature range of $110 \leq T \leq 250$ ^{o}C. Specimens considered in this work were identified by the black line and prepared by adding O blocks of different lengths to the same SIS-OH triblock containing 40 % S and 60 % I by volume.

Table 3-1 SIS-OH and SISO Characterization Data.

Sample	M_n/kDa	PDI	f_S[a]	f_I[a]	f_O[a]	Phase[b]	d/nm[c,d]	% Cryst.[e]	T_{ODT}/°C[f]
SIS-OH	23.3	1.03	0.39	0.61	0.00	DIS	-	0.0	<80
SISO-1	23.6	1.04	0.38	0.60	0.02	DIS	-	36.2	<80
SISO-2	24.4	1.04	0.35	0.56	0.09	HEX	21.8, 18.9	39.8	213±2
SISO-3	25.0	1.08	0.34	0.53	0.12	HEX	25.8, 22.3	55.3	>250
SISO-4	26.1	1.06	0.32	0.50	0.19	HEX	29.7, 25.7	68.3	>250
SISO-5	29.0	1.07	0.27	0.41	0.32	HEX	35.5	70.8	>250

[a]Volume fractions calculated with from densities at 140 °C. [b]HEX-hexagonally packed spheres for SISO-2, -3, -4 and hexagonally packed cylinders for SISO-5. [c]Temperature is 120 °C. [d]Lattice dimensions listed for SISO-2, -3, -4 correspond to *a* and *c* and characteristic morphological length scale ($d_{100}=2\pi/q^*$) for SISO-5. [e]Percent crystallinity of the O domains was determined by differential scanning calorimetry. [f]Order-disorder transition temperatures were determined by dynamic mechanical spectroscopy.

corresponding SISO tetrablock terpolymers are within the desired temperature window over a range of compositions.

SAXS. Synchrotron SAXS powder patterns for the SIS-OH triblock and five SISO tetrablocks are presented in Figure 3-3. SIS and SISO-1 were annealed at 110 ^{o}C for five minutes before the data were taken. A single and broad peak indicates a disordered state. Samples SISO-2 to -5 were annealed under vacuum for a day at 120 ^{o}C, quenched in liquid nitrogen to preserve the morphologies and reheated to120 ^{o}C at the Argonne facilities. Data were taken every 5 minutes until no further changes were recorded, typically a total of 3 – 5 scans. The scattering patterns display peaks at $q/q^{*} = \sqrt{1}, \sqrt{3}, \sqrt{4}$, and $\sqrt{7}$ with q^{*} being the principal peak location. These peak ratios are consistent with hexagonal (HEX) symmetry.

DMS. Order versus disorder of the samples can also be determined by dynamic mechanical spectrometry as shown in Figure 3-4. Dynamic elastic (G') and loss (G") moduli were measured as a function of frequency at 110 ^{o}C for SISO-1 and at 120 ^{o}C for SISO-2 to -5. Only SISO-1 with f_O = 2% shows terminal viscoelastic behavior (G'~ ω^2 and G"~ ω), indicating a disordered state at 110 ^{o}C, just above the glass transition temperature of the PS blocks. SISO-2 with f_O = 9% to SISO-5 with f_O = 32% have elastic modulus G' almost independent of frequency at 120 ^{o}C, characteristic of triply periodic ordered structures. This indicates that the O block length plays a key role in fixing the T_{ODT} of the resultant SISO samples.

TEM. While SAXS data indicate a hexagonal symmetry for the SISO specimens (except SISO-1), TEM images allow us to characterize the detailed morphologies, i.e.

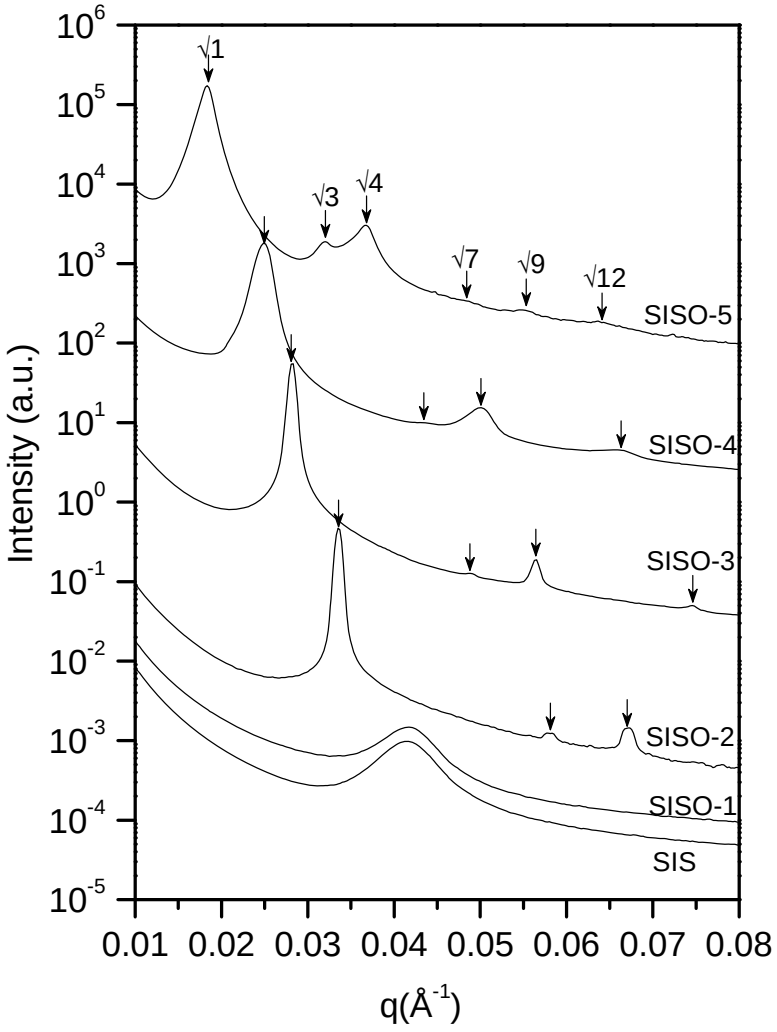

Figure 3-3 Synchrotron SAXS data for the series of SISO tetrablock terpolymers with f_S : f_I = 2 : 3 and f_O = 0 – 32%. SIS-OH and SISO-1 samples were annealed at 110 ^oC before data was taken. SISO-2 to -5 were prepared by annealing under vacuum at 120 ^oC for one day, quenched in liquid nitrogen to preserve the morphology. At Argonne facilities, samples were reheated and annealed at 120 ^oC for five minutes before taking the measurements. The arrows identify the relative peak positions associated with a hexagonal symmetry. Scattering patterns are shifted vertically for clarity.

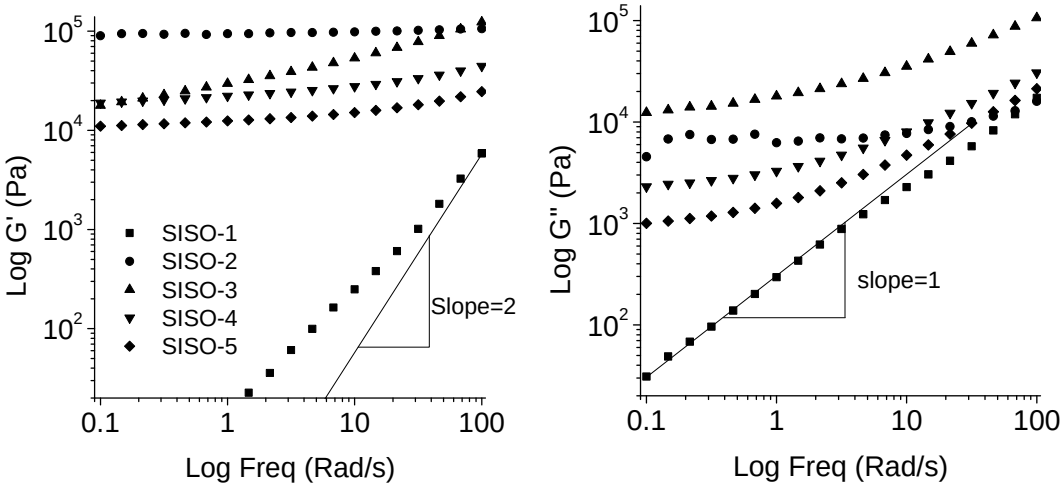

Figure 3-4 Dynamic elastic (G') and loss (G") modulus measured at 120 °C (110 °C for SISO-1) as a function of frequency. These results indicate states of order except for SISO-1, which is disordered.

whether they are spheres or cylinders as shown in Figure 3-5. Samples were annealed in a vacuum oven (1 day at 160 °C for SISO-2, 1 day at 120 °C for SISO-3, and -4, 3 days at 160 °C for SISO-5) prior to quenching into liquid nitrogen to preserve the melt morphologies. The PI domains react preferentially with OsO_4 and appear darker in these images, while the unstained S and O blocks appear lighter. The images in Figure 3-5 (A), (B), (C) and (D) were generated from SISO-2, -3, -4, and -5 respectively. SISO-5 with f_O = 32% forms cylinders as evidenced by a strand-like morphology. Based on the SAXS result (Figure 3-3), the hexagonal unit cell spacing for SISO-5 is $d_{100} = 2\pi/q^* = 35.5$ nm based on the principal peak position of $q^*=0.0117 Å^{-1}$.

The TEM images for SISO-2, -3, and -4 reveal very different structures. The specimen thickness is about 70 nm, approximately three times the domain spacing (~26

nm, Table 3-1), so there are about three layers of spheres in depth. The absence of anisotropic domains eliminates the possibility of a cylindrical morphology. Panels A, B and C in Figure 3-5 contain assemblies of white spheres ordered in a continuous black matrix. On the top of panel B, spheres seem to align into straight lines. This is because the grains are tilted at an angle to the electron beam in the microscope. Areas with 6-fold and 4-fold symmetries are identified by the circled regions in panel A. Grain rotation in panel A reveals a continuous transition from the 6-fold to 4-fold regions, suggesting an underlying hexagonal lattice with either P_6/mmm (No.191) or P_{6_3}/mmc (HCP, No. 194) space group symmetry (see Figure 3-7). A distinct grain boundary is evident in panel B. This arrangement of spheres resembles the structure of the Frank-Kasper σ-phase reported in another SISO sample with $f_S = f_I = 46\%$ and $f_O = 8\%$.[13]

DSC. Figure 3-6 displays the DSC curves for SISO tetrablock terpolymers. All samples have nearly identical $T_{g,I}$ = -61.3 ^{o}C. Endotherms between 20 and 70 °C exhibit that all SISO tetrablock terpolymers have an O melting peak, consistent with segregation of the O blocks in a core-shell morphology. The corresponding melting temperature of SISO-2 to -4 increases with increasing f_O. SISO-1 is an exception since its melting temperature increases with decreasing f_O. This phenomenon might be attributed to crystals formed from the homogeneous melt. The fractional crystallinity of the O blocks (X_c) is calculated from integrating the baseline-corrected melting peak and normalizing this value to the heat of fusion of bulk PEO,

$$X_c = \frac{\Delta H_m}{w_{PEO}\Delta H^o_{m,PEO}} \tag{3.2}$$

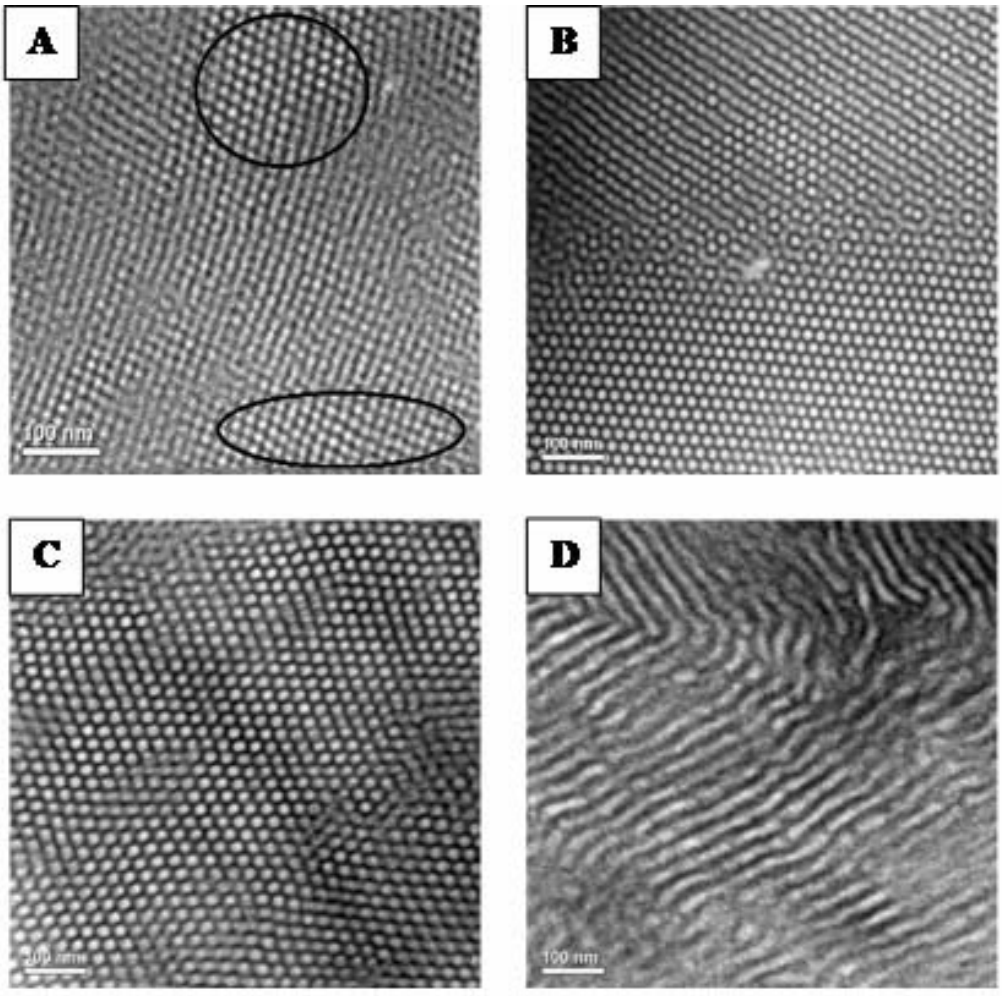

Figure 3-5 TEM micrographs obtained from OsO_4 stained SISO tetrablock terpolymers for (A) SISO-2 (160 ^{o}C, 1day), (B) SISO-3 (120 ^{o}C, 1day), (C) SISO-4 (120 ^{o}C for 1 day), and (D) SISO-5 (160 ^{o}C for 3 days), where the temperatures and the times in the parentheses indicate the annealing conditions prior to microtoming. Panel A, B, and C contain ordered arrays of spherical microdomains while D is consistent with a cylindrical morphology. Transition from 6-fold to 4-fold symmetric projections (circled in A) that share common planes of spheres is consistent with a simple hexagonal lattice. B contains two large grains separated by an unusual grain boundary structure.

where w_{PEO} is the weight fraction of O blocks in the tetrablock terpolymer and $\Delta H^{o}_{m,PEO}$ is the heat of fusion of bulk PEO ((213 J/g).[33] The X_c is calculated from data obtained during the second heating ramp upon minimizing the thermal history; the values range from 36 to 71 % as listed in Table 3-1. Surprisingly enough, given only about 11 EO units in SISO-1, it shows a fractional crystallinity as high as 36%. These results demonstrate the segregation of the O blocks in the melt state for SISO-2 to -4. Segregation of S blocks is subtle, as shown in the inset in Figure 3-6 with a $T_{g,S}$ = 64.1 ^{o}C, indicating fluctuation effects[34] or possibility of microphase separation

below 80 ^{o}C.

3.3 Discussion

In addition to the simple hexagonal symmetry (No. 191), hexagonal close- packed structure (HCP, No. 194) with P_{6_3}/mmc space group symmetry is also consistent with the SAXS pattern shown in Figure 3-3. In order to make the comparison between them clearer, the Jade program was used to simulate the images for SISO-3 with the simple hexagonal and the HCP symmetry (see Figure 3-7). The second row shows the simulated images for the (100) plane with the 6-fold symmetry. Due to the alternating ABABAB… stacking of the spheres in HCP, certain gaps are filled by the spheres from the layers underneath, resulting in the black domains on the white matrix. In the simple hexagonal symmetry, the spheres stack directly on top of each other, resulting in the white domains on the black matrix, consistent with the actual TEM results. In the last row, rotation

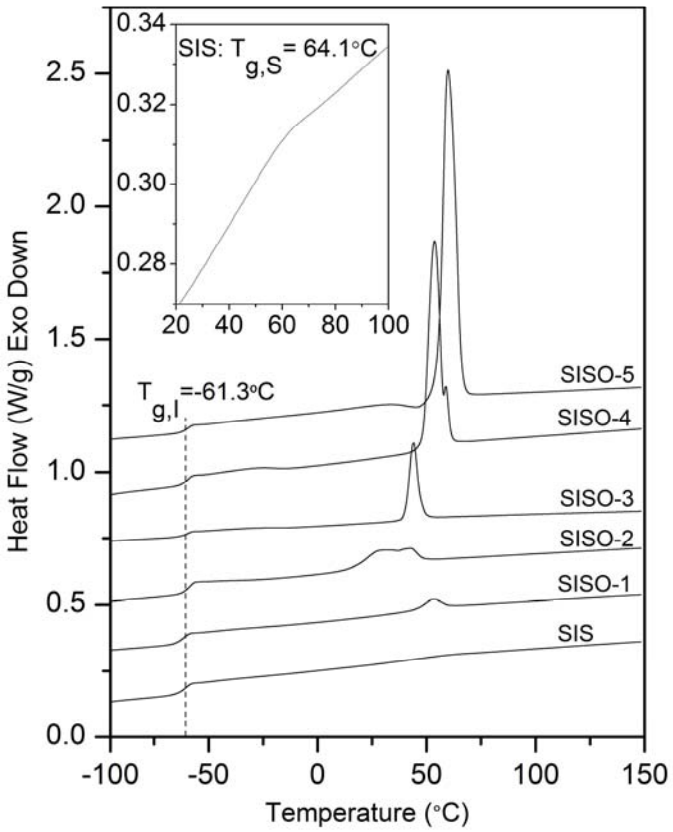

Figure 3-6 DSC traces obtained from the SIS-OH triblock and SISO tetrablock terpolymers. Endotherms between 20 and 70 °C reflect melting of PEO consistent with segregation of the O blocks in a core-shell morphology. The small peak at 55 °C for SISO-1 is attributed to crystals formed from the homogeneous melt. All the specimens display a glass transition at -61 °C, which is associated with PI. The inset shows evidence of a PS glass transition in SIS-OH, suggestive of composition fluctuations or segregation at T < 65 °C for this specimen. Curves have been shifted vertically for clarity.

around the [100] direction for the HCP symmetry fails to produce the 4-fold projections as shown in Figure 3-5 (A). The simulated images for the (010)/(001) planes with the simple hexagonal symmetry generate the square projections consistent with the experimental results.

The lattice dimensions of SISO-2 to -4 can be determined after the relationship between *a* and *c* is established. The first four peaks of SISO-2 to -4 shown in Figure 3-3 correspond to the (100), (110), (200) and (210) planes of reflections respectively, similar to the case of the cylindrical morphology with hexagonal symmetry and $c \rightarrow \infty$. However, in the case of the spherical morphology with a finite value of *c*, additional peaks corresponding to (001), (101), (111)… planes of reflections are expected. The hexagonal lattice dimensions can be determined as:

$$\frac{1}{d^2} = \frac{4}{3}\left(\frac{h^2 + hk + k^2}{a^2}\right) + \frac{l^2}{c^2} \tag{3.3}$$

where *d* is the distance between adjacent planes in the set (*hkl*).[35] The ratio between *a* and *c* affects the peak positions, q (= 2π/*d*).

Table 3-2 lists the first nine allowed reflections for different ratios between *a* and *c*: $c = a$, $c = a\sqrt{3/2}$, $c = a/2$ (for P_6/mmm symmetry) and $c = 1.63a$ (for P_{6_3}/mmc symmetry). By comparing the theoretically allowed peak positions and the experimentally obtained values, we can rule out the possibility of $c = a$ and $c = 1.63a$ because many peaks are missing at positions where the diffraction signals are expected to be strong (shown in italic font in Table 3-2). The actual *a* and *c* are directly measured in Figure 3-5 (A) to be 20.0 ± 0.8 nm and 16.7 ± 0.4 nm respectively, suggesting a

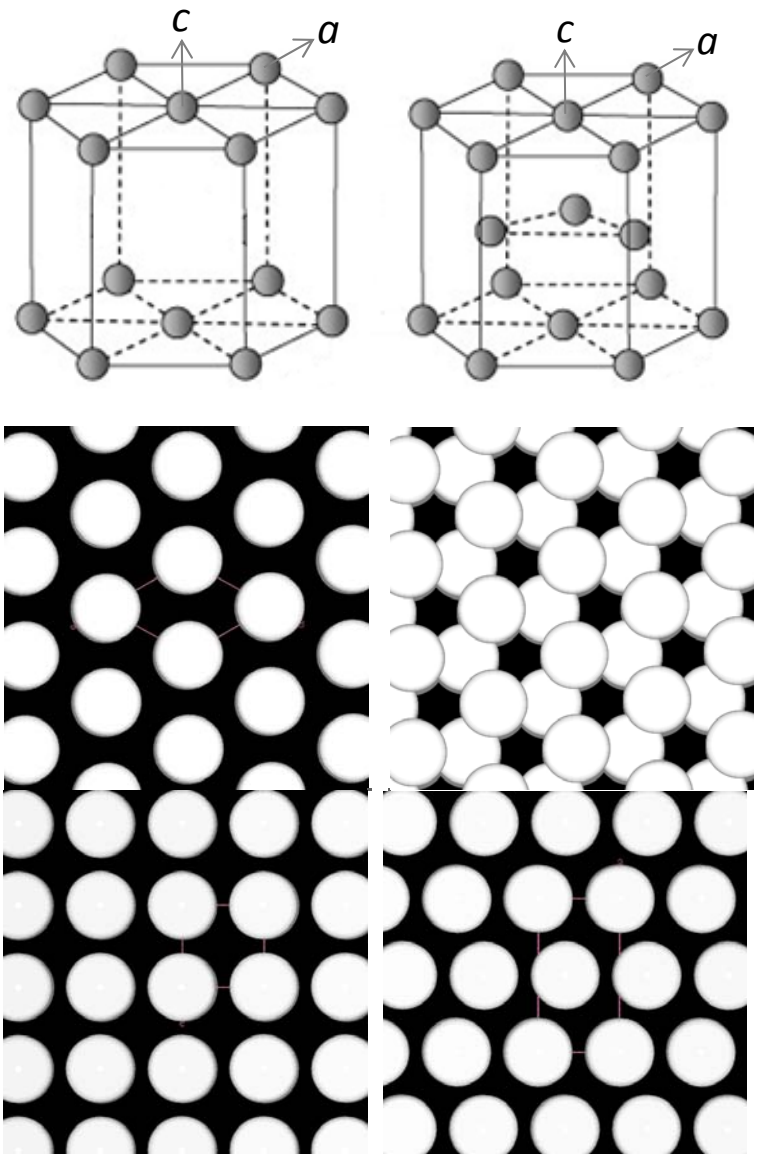

Figure 3-7 Simulated images of hexagonal crystal structures formed from spherical domains: P_6/mmm with $c = a\sqrt{3/2}$ (left) and P_{6_3}/mmc (right). The second row represents projections along the 6-fold (*c*) axis, while the bottom row represents projections along the *a* axis, i.e., after rotating the crystal by 90°. Comparison of these images with the TEM results in Figure 3-5 indicates that the spheres pack on a simple hexagonal lattice.

Table 3-2 Allowed reflections for different *a* and *c* relationships.

	(100)	**(001)**	**(110)**	**(101)**	**(111)**	**(200)**	**(002)**	**(201)**	**(210)**
Expt. data	√1	√1	√3	-	√4	√4	√4	-	√7
c=a	√1	√*1.5*	√3	√*3.5*	√*7.5*	√4	√3	√*9.5*	√7
c=a√3/2	√1	√1	√3	√*2*	√4	√4	√4	√*5*	√7
c=a/2	√1	√3	√3	√4	√*6*	√4	√3	√7	√7
c=1.63*a*	√1	-	√3	√*1.28*	-	√4	√*1.13*	√*4.3*	√7

relationship of $c = a\sqrt{3/2}$.

Missing peaks are also observed with $c = a\sqrt{3/2}$ ($\sqrt{2}$ and $\sqrt{5}$) and c = a / 2 ($\sqrt{6}$). One possible explanation for the missing peaks is that the diffraction signals are too weak as compared to the existing ones. The correlations along the 6-fold axis in the [001] direction is much weaker than the strong in-plane (hk0) long-range order. However, such correlation is not completely lost as a certain degree of correlation is clearly observed in TEM (Figure 3-5 (A)) where the rotation around the (100) plane with the 6-fold axis leads to the (010)/(001) planes with the 4-fold axis. Nonetheless, the 6-fold packing is much more prominent as compared to the 4-fold packing in these images, explaining the low scattering peak intensities. The assignment of P6/mmm space group symmetry with $c = a\sqrt{3/2}$ is based on a combination of SAXS and TEM results and used in the rest of this chapter. In this case, the (001) peak overlaps with the (100) peak, and the (101), (111) and (200) peaks overlap. However, we cannot rule out the possibility of other unit cell

dimension relationships or space group symmetries due to the lack of (hkl) diffraction data.

The SISO tetrablock terpolymer molecular architecture adds more complexity in the block interactions and phase behaviors as compared to the ISO triblock terpolymers, including segregations between O, internal and terminal S blocks from the I-rich matrix. Figure 3-8 shows three possible limiting configurations. In configuration 1, spheres are formed by the O blocks alone. Both S blocks mix with the I blocks to form the matrix. The theoretical spherical volume fraction is the volume fraction of the O blocks, i.e., $f_{sphere} = f_O$. In configuration 2, the core-shell spheres are formed with an O core and a shell of the internal S blocks in the I-rich matrix mixed with the terminal S blocks. In this case, $f_{sphere} = f_O + f_S / 2$. In configuration 3, both S blocks contribute to the shell, leaving the I blocks alone to form the matrix, with $f_{sphere} = f_O + f_S$. The theoretical spherical volume fractions for SISO-2 to -4 are listed in Table 3-3. The lattice dimension a (measured from TEM), the sphere diameter d (measured from TEM), and the experimental spherical volume fractions (calculated based on $c = a\sqrt{3/2}$) are listed in Table 3-3. Within the experimental error, configuration 2 is the most likely configuration. The experimental spherical volume fractions are less than $f_S + f_I$, possibly due to the selectively staining with OsO_4 of the I domains. In configuration 2, we expect a sharp but continuous gradient of the I blocks from the matrix towards the O/S interface. Assuming the staining process partially penetrates the shell of the S blocks and reacts with the I blocks in the interfacial region, the estimated core volume fractions are roughly consistent with the theoretical values.

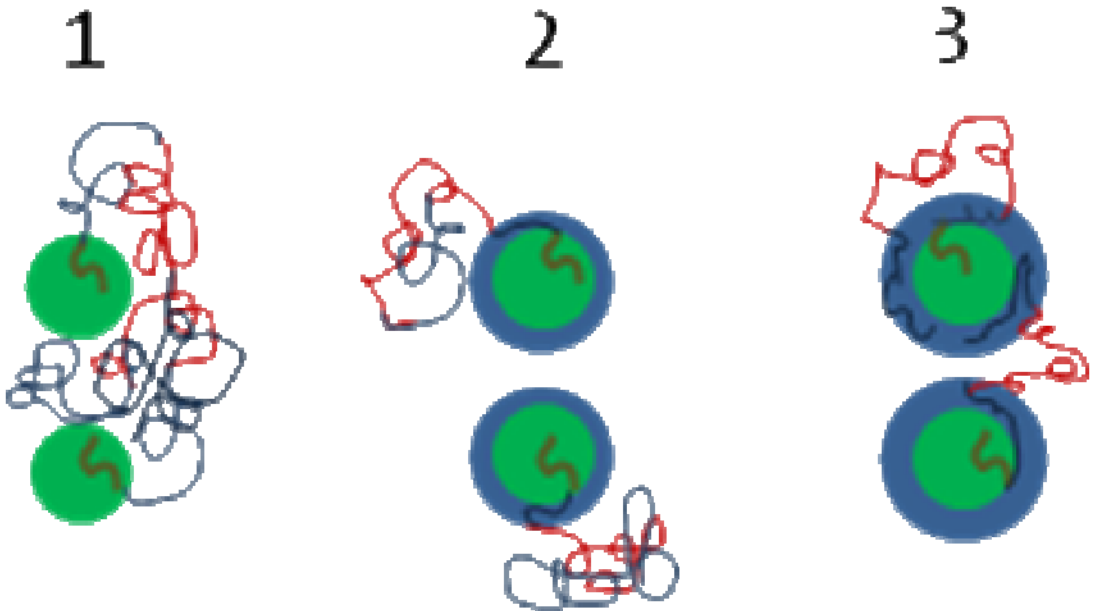

Figure 3-8 Discreet states of microphase separation for sphere-forming SISO samples. 1) segregation of the O blocks from the mixed S and I blocks. 2) segregation with an O core surrounded by a shell of the internal S blocks in a matrix of the I and the terminal S blocks. 3) segregation with an O core surrounded by a shell of segregated internal and terminal S blocks embedded in a matrix of the I blocks. SCFT calculations indicate that the actual morphology is a hybrid of configuration 2 and 3.

Self consistent mean field theoretical calculations were performed by Scott Sides (Tech-X Research Corporation) for several SISO compositions and molecular weights. A detailed discussion about the associated theory and assumptions made can be found elsewhere.[36,37] Figure 3-9 illustrates the SCFT simulated density profiles of the O, the internal S and the terminal S blocks of SISO-3 with f_O = 12% at 120 ^oC against the position variable *r* along two different unit cell directions of a BCC lattice: the [111]

Table 3-3 Comparison between calculated and experimental spherical volume ratios.

Calculated volumes %[a]				Experimental results		
Sample	PEO	PEO+1/2PS	PEO+PS	a(nm)[bc]	d(nm)[bc]	Vol %[d]
SISO-2	9	27	44	20.0±0.8	13.3±1.0	20±5
SISO-3	12	29	46	22.6±1.2	16.0±1.2	25±7
SISO-4	19	35	51	27.2±0.7	20.6±1.2	30±6

[a]Calculated spherical volume fractions based on experimental data from Table 3-1. [b]Lattice dimension and sphere diameter are obtained from TEM images for SISO-2, -3, and -4 respectively. c is calculated using $c = a\sqrt{3}/2$. [c]Temperature is 120 °C. [d]Volume fractions are the volume ratios between the spheres and the hexagonal unit cells.

direction denoted by the red line in the inset (top) and the [100] direction denoted by the blue line in the inset (bottom). The densities of the internal S blocks midway between the O core centers at the ½, ½, 0 position along the [100] direction and at the ¼, ¼, ¼ position along the [111] direction are almost the same, indicating they disperse quite uniformly around the O core. We believe such constraints imposed on the positioning of the two S blocks are responsible for the formation of the novel symmetry of P_6/mmm. The density of the terminal S blocks is higher than that of the internal S blocks midway between the O core centers, showing the affinity of the terminal S blocks mixing with the I blocks to form the matrix, i.e. a hybrid of configurations 2 and 3 shown in Figure 3-8.

Figure 3-10 illustrates simulated density profiles of the O, the internal S and the terminal S blocks of SISO-5 with f_O = 32% at 120 °C as a function of the position variable r along the [100] direction denoted by the red line in the inset. These calculations were also performed by Dr. Scott Sides; Cylindrical morphology is formed by an O core, a shell of the internal S and the terminal S blocks, and an I-rich matrix mixed with more

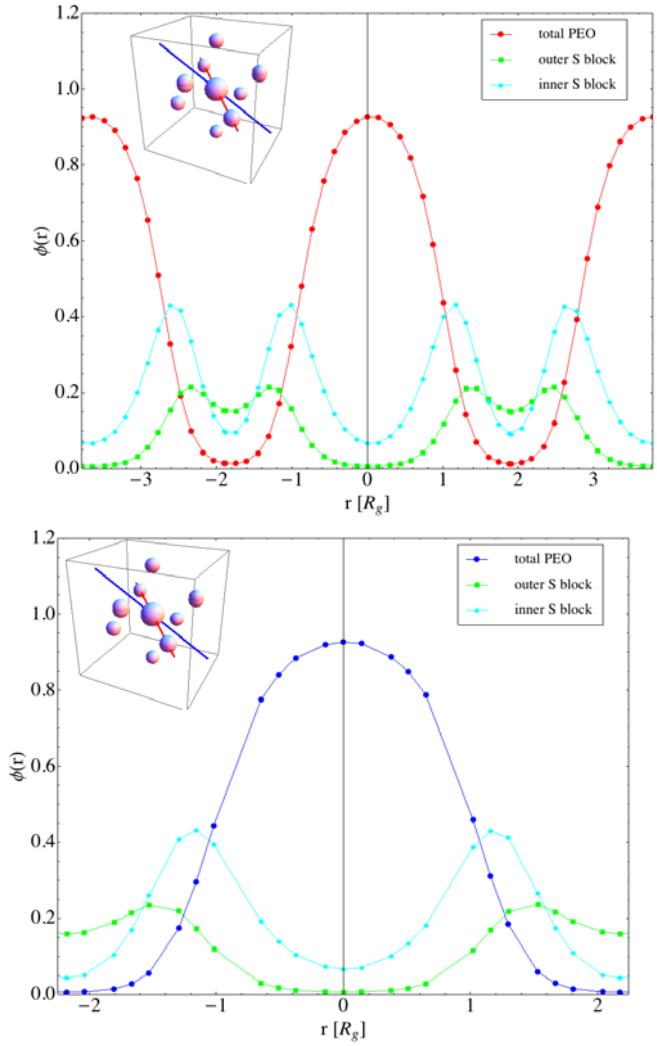

Figure 3-9 SCFT simulated density profiles of the O, the internal S and the external S blocks of SISO-3 against the position variable, *r*. The calculation yields a BCC symmetry, contrary to the experimental result, which is attributed to the mean-field nature of the theory. Top panel: [111] direction denoted by the red line in the inset. Bottom panel: [100] direction denoted by the blue line in the inset. These results indicate that the SISO tetrablock terpolymers segregate with a distribution of blocks that is a hybrid of configurations 2 and 3 as illustrated in Figure 3-8. We thank S. W. Sides for generating these results and this figure.

of the terminal S than the internal S blocks, similar to the asymmetrical distribution of the S blocks in the spherical morphology.

The SCFT theory correctly predicts the transition from the spherical (see Figure 3-9) to the cylindrical (see Figure 3-10) symmetry as f_O increases. It also provides useful insights to the interactions among various blocks, especially the distribution of the two S blocks in the O core, the shell and the matrix, which is hard to decipher based on the experimental TEM or SAXS results. However, the theory fails to account for the formation of the (simple) hexagonal symmetry and predicts the BCC symmetry instead. This discrepancy might arise due to the Gaussian chain model used in the SCFT

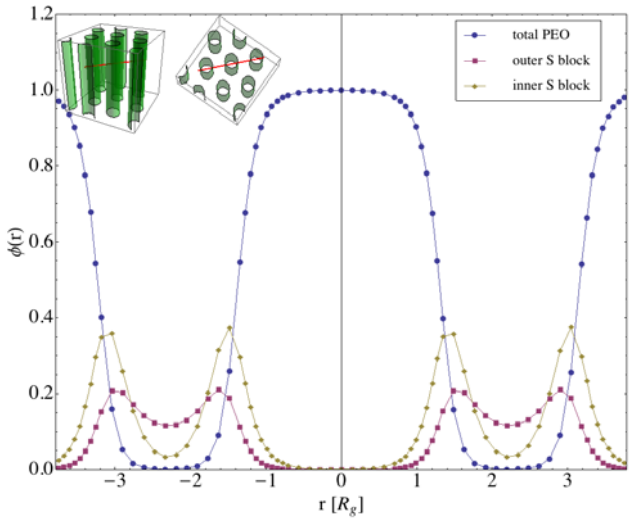

Figure 3-10 SCFT simulated density profiles of the O, the internal S and the terminal S blocks of SISO-5 against the position variable, *r*, along the [100] unit cell direction denoted by the red line in the inset. Cylindrical morphology is formed, with similar asymmetrical distribution of the S blocks in the I-rich matrix to the spherical morphology. We thank S. W. Sides for generating these results and this figure.

algorithms. Theory predicts the BCC symmetry based on an infinite chain length, which is unrealistic for our SISO model system with N_{total} = 300 ~ 400. Including finite-chain length effects can change the effective interactions among different blocks by introducing anisotropic forces between these spherical domains. This is similar to the unusual crystalline order observed in some metals with large atomic number and anisotropic outer shell electron orbitals.

Before the discovery of this hexagonally ordered spherical phase, the sphere-forming block copolymers are known almost exclusively to form the BCC symmetry.[1] Soft matters such as block copolymers prefer this because chain stretching and compression are minimized to maintain uniform density due to incompressibility. Close-packed spherical packing such as the HCP and the face-centered cubic (FCC) symmetries were reported theoretically possible in polymers by Matsen and Bates.[4,38] Experimentally, the FCC symmetry has been reported in a few cases such as disordered micelles,[39] certain homopolymers[40] and triblocks[41] under specific conditions.

This is the first time that the P_6/mmm space group symmetry is observed in block copolymers. Given its simplicity, it is surprising to find out that such lattice does not occur in most of the natural materials. Across the periodic table, most elements form the BCC, FCC or HCP symmetries. Certain covalently bonded molecules such as Cl_2, O_2 and sulfur crystallize with orthorhombic symmetry, and carbon forms diamond or graphite. Some group VB elements crystallize with rhombohedral (As, Sb, Bi and Hg) and tetragonal symmetry (In and Sn). The only simple cubic packing is observed in polomiun, due to relativistic corrections to the effective mass of valence electrons.[42] Uranium and

tantalum form Frank-Kasper σ-phase with 30 atoms per unit cell.[43] P_6/mmm symmetry has not been observed in single component, but has been observed in certain intermetallic compounds such as $CaCu_5$.[44]

3.4 Conclusion

Hexagonally ordered spherical and cylindrical morphologies (P_6/mmm and P_6/mm space group symmetries) have been identified in the bulk SISO tetrablock terpolymers with $f_S : f_I = 2 : 3$ and $f_O = 9 – 32\%$. SCFT calculations predict correctly the core (O) and shell (S) domain geometries and provide insight to the distribution of the block segments, especially the asymmetric placement of the internal and the terminal S blocks within the core, the shell and the matrix, but fail to account for the simple hexagonal symmetry. These results, together with an earlier publication on Frank-Kasper σ-phase[13] and the dodecagonal quasicrystalline phase,[14] offer a new approach to independently control the domain shape and packing in block copolymer melts through manipulation of the magnitude and the sequencing of the binary segment-segment interactions ($\chi_{SI} \leq \chi_{SO} << \chi_{IO}$), which dictate core segregation and the effective inter-domain interactions.

Acknowledgements. This work was supported by the U.S. Department of Energy, Basic Energy Sciences, Division of Materials Science and Engineering, under contract number DEAC05-00OR22725 with UT-Battelle LLC at Oak Ridge National Laboratory. Some of the facilities employed derived support from the University of Minnesota

Materials Research Science and Engineering Center (MRSEC) (NSF-DMR-0819885). Portions of this work were performed at the DuPont-Northwestern-Dow Collaborative Access Team (DND-CAT) located at Sector 5 of the Advanced Photon Source (APS). DND-CAT is supported by E.I. DuPont de Nemours & Co., the Dow Chemical Company, and the State of Illinois. Use of the APS was supported by the U.S. Department of Energy, Office of Science, Basic Energy Sciences, under contract No. DE-AC02-06CH11357. Parts of this work were carried out in the University of Minnesota College of Science and Engineering Characterization Facility, which receives partial support from NSF through the NNIN program. We thank Fang Zhou for her assistance in microtoming the TEM sections.

3.5 References

(1) Leibler, L. *Macromolecules* **1980**, *13*, 1602.

(2) Matsen, M. W.; Schick, M. *Macromolecules* **1994**, *27*, 4014.

(3) Khandpur, A. K.; Foerster, S.; Bates, F. S.; Hamley, I. W.; Ryan, A. J.; Bras, W.; Almdal, K.; Mortensen, K. *Macromolecules* **1995**, *28*, 8796.

(4) Matsen, M. W.; Bates, F. S. *Macromolecules* **1996**, *29*, 1091.

(5) Bates, F. S.; Fredrickson, G. H. *Physics Today* **1999**, *52*, 32.

(6) Floudas, G.; Vazaiou, B.; Schipper, F.; Ulrich, R.; Wiesner, U.; Iatrou, H.; Hadjichristidis, N. *Macromolecules* **2001**, *34*, 2947.

(7) Cochran, E. W.; Garcia-Cervera, C. J.; Fredrickson, G. H. *Macromolecules*

2006, *39*, 2449.

(8) Hajduk, D. A.; Harper, P. E.; Gruner, S. M.; Honeker, C. C.; Kim, G.; Thomas, E. L. *Macromolecules* **1994**, *27*, 4063.

(9) Schulz, M. F.; Khandpur, A. K.; Bates, F. S.; Almdal, K.; Mortensen, K.; Hajduk, D. A.; Gruner, S. M. *Macromolecules* **1996**, *29*, 2857.

(10) Matsen, M. W.; Schick, M. *Physical Review Letters* **1994**, *72*, 2660.

(11) Takenaka, M.; Wakada, T.; Akasaka, S.; Nishitsuji, S.; Saijo, K.; Shimizu, H.; Kim, M. I.; Hasegawa, H. *Macromolecules* **2007**, *40*, 4399.

(12) Tyler, C. A.; Morse, D. C. *Physical Review Letters* **2005**, *94*, 208302.

(13) Lee, S.; Bluemle, M. J.; Bates, F. S. *Science* **2010**, *330*, 349.

(14) Zhang, J.; Bates, F. S. *Journal of the American Chemical Society* **2012**, *134*, 7636.

(15) Mogi, Y.; Mori, K.; Matsushita, Y.; Noda, I. *Macromolecules* **1992**, *25*, 5412.

(16) Mogi, Y.; Nomura, M.; Kotsuji, H.; Ohnishi, K.; Matsushita, Y.; Noda, I. *Macromolecules* **1994**, *27*, 6755.

(17) Stadler, R.; Auschra, C.; Beckmann, J.; Krappe, U.; Voight-Martin, I.; Leibler, L. *Macromolecules* **1995**, *28*, 3080.

(18) Matsushita, Y.; Suzuki, J.; Seki, M. *Physica. B, Condensed Matter* **1998**, *248*, 238.

(19) Shefelbine, T. A.; Vigild, M. E.; Matsen, M. W.; Hajduk, D. A.; Hillmyer, M. A.; Cussler, E. L.; Bates, F. S. *Journal of the American Chemical Society* **1999**, *121*, 8457.

(20) Seki, M.; Sujuki, J.; Matsushita, Y. *Journal of Applied Crystallography* **2000**, *33*, 285.

(21) Bailey, T. S.; Pham, H. D.; Bates, F. S. *Macromolecules* **2001**, *34*, 6994.

(22) Epps III, T. H.; Cochran, E. W.; Bailey, T. S.; Waletzko, R. S.; Hardy, C. M.; Bates, F. S. *Macromolecules* **2004**, *37*, 8325.

(23) Cochran, E. W.; Bates, F. S. *Physical Review Letters* **2004**, *93*, 087802.

(24) Breiner, U.; Krappe, U.; Abetz, V.; Stadler, R. *Macromolecular Chemistry and Physics* **1997**, *198*, 1051.

(25) Tyler, C. A.; Qin, J.; Bates, F. S.; Morse, D. C. *Macromolecules* **2007**, *40*, 4654.

(26) Qin, J.; Bates, F. S.; Morse, D. C. *Macromolecules* **2010**, *43*, 5128.

(27) Wang, J. F.; Mueller, M.; Wang, Z. G. *Journal of Chemical Physics* **2009**, *130*, 154902.

(28) Bluemle, M. J.; Fleury, G.; Lodge, T. P.; Bates, F. S. *Soft Matter* **2009**, *5*, 1587.

(29) Bluemle, M. J.; Zhang, J.; Lodge, T. P.; Bates, F. S. *Macromolecules* **2010**, *43*, 4449.

(30) Hiemenz, P. C.; Lodge, T. P. *Polymer Chemistry*; Taylor & Francis Group: University of Minnesota: Minneapolis, MN, 2007.

(31) Wu, L.; Cochran, E. W.; Lodge, T. P.; Bates, F. S. *Macromolecules* **2004**, *37*, 3360.

(32) Frielinghaus, H.; Hermsdorf, N.; Almdal, K.; Mortensen, K. M. L.; Corvazier, L.; Fairclough, J. P. A.; Ryan, A. J.; Hamley, I. W. *Europhysics Letters* **2001**, *53*, 680.

(33) Brandrup, J.; Immergut, E. H. *Polymer Handbook*; 3rd ed.; John Wiley & Sons: New York, 1989.

(34) Bates, F. S.; Rosedale, J. H.; Fredrickson, G. H.; Glinka, C. J. *Physical Review Letters* **1988**, *61*, 2229.

(35) Cullity, B. D.; Stock, S. R. *Elements of X-Ray Diffraction*; Third.; Addison-Wesley Publishing Company, Inc: Reading, MA, 1956.

(36) Zhang, J.; Scott, S. W.; Bates, F. S. *Macromolecules* **2012**, *45*, 256.

(37) Sides, S. W.; Fredrickson, G. H. *Polymer* **2003**, *44*, 5859.

(38) Semenov, A. N. *Macromolecules* **1989**, *22*, 2849.

(39) Huang, Y. Y.; Hsu, J. Y.; Chen, H. L.; Hashimoto, T. *Macromolecules* **2007**, *40*, 406.

(40) Huang, Y. Y.; Hsu, J. Y.; Chen, H. L.; Hashimoto, T. *Macromolecules* **2007**, *40*, 3700.

(41) Imaizumi, K.; Ono, T.; Kota, T.; Okamota, S.; Sakurai, S. *Journal of Applied Crystallography* **2003**, *36*, 976.

(42) Dominik, L.; Martin, F.; Mojmir, S. *Physical Review Letters* **2007**, *99*, 106402.

(43) Jiang, A.; Yohannan, A.; Nnolim, N. O.; Tyson, T. A.; Axe, L.; Lee, S.; Cote, P. *Thin Solid Films* **2003**, *437*, 116.

(44) Fornasini, M. L.; Manfrinetti, P.; Mazzone, D. *Journal of Solid State Chemistry* **2006**, *179*, 2012.

4

Dodecagonal Quasicrystalline Phase in an Isoprene-rich SISO Tetrablock Terpolymer

4.1 Introduction

Careful examination of the TEM micrograph of the SISO-3 samples with $f_S : f_I = 2 : 3$, $\tau = 1$ and $f_O = 12$ % in Figure 3-5 (B) reveals an unusual packing arrangement at the boundary between two spherical grains with (simple) hexagonal symmetry (P_6/mmm or perhaps P_6/mm space group symmetry). This unusual packing arrangement resembles the

structure of the Frank-Kasper σ-phase (P_{4_2}/mnm space group symmetry) discovered in another SISO tetrablock terpolymer system with $f_S = f_I$, M_n = 23 kg/mol, f_O = 8 % and PDI = 1.04, as an intermediate state between the liquid-like packing of spheres at lower temperatures and the disordered state at higher temperatures.[1,2] The Frank-Kasper σ-phase was found in another diblock system of poly(isoprene-*b*-lactide) (IL) with M_n = 3.89 kg/mol, f_I = 78%, and PDI = 1.12, indicating certain degree of universal presence of this phase.[1] With 30 atoms in the unit cell, it is known as the crystal approximant to quasicrystals (QC).[3]

Motivated by the unusual packing arrangement at the grain boundary in Figure 3-5 (B) and its similarity to the Frank-Kasper σ-phase, the temperature dependence of the block copolymer phase behavior is considered in this chapter using another SISO specimen along the same isoprene-rich series, SISO-2, as denoted by the blue arrow in Figure 4-1. Experiments were conducted between 120 and 215 ^{o}C, with T_{ODT} = 213 ^{o}C (± 3 ^{o}C). Figure 4-2 (a) shows the molecular architecture of an SISO tetrablock terpolymer, with two S blocks of equal molecular weight, i.e., x = x'. Detailed molecular characterization data, lattice dimensions, T_{ODT} and morphology assignment for this particular sample are listed in Table 3-1. With $\chi_{SI} \leq \chi_{SO} << \chi_{IO}$, the repulsion between the I and O blocks is the greatest. Since the I and O blocks are not directly bonded to each other, it is unlikely to form the I/O interfaces. Therefore, the core-shell spheres are formed with an O core, a shell of the internal and terminal S blocks, in an I-rich matrix (see Figure 4-2 (b)).[2] These spheres form a hexagonal packing symmetry described in detail in Chapter 3.[4] SISO-2 was heated and cooled to a series of temperatures and

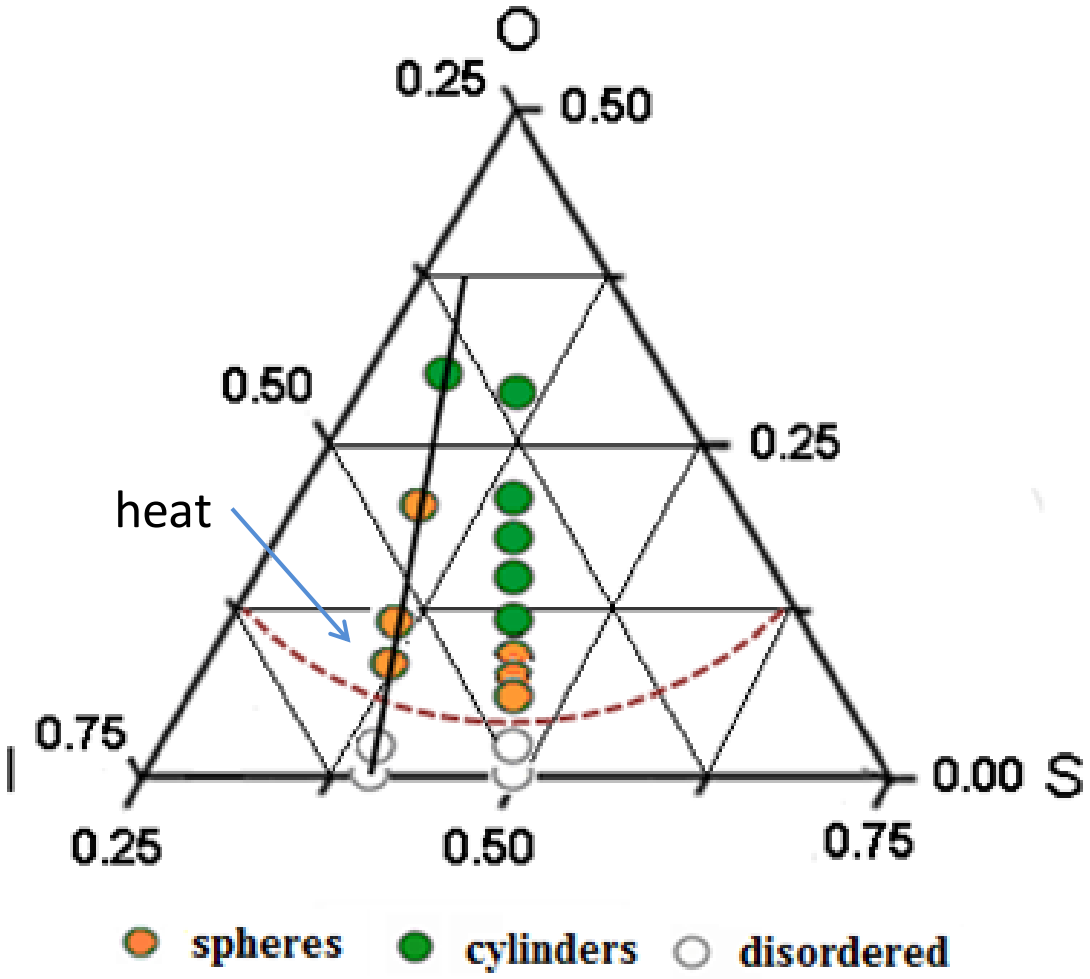

Figure 4-1 Poly(styrene-*b*-isoprene-*b*-styrene-*b*-ethylene oxide) (SISO) phase portrait. Filled and open circles indicate the ordered and disordered states, respectively, within the experimental temperature range of $110 \leq T \leq 250$ °C. The temperature effect on block copolymer phase behavior is examined using SISO-2, with $f_S : f_I = 2 : 3$, $\tau = 1$ and $f_O = 9$ %, as identified by the blue arrow. This sample is chosen because it is near the vicinity of the order-disorder boundary, as indicated by the dashed brown curve.

investigated using well-established SAXS, TEM and DMS techniques,[2,4] leading to the identification of a dodecagonal quasicrystalline morphology as an intermediate state between the hexagonally ordered spherical phase at lower temperatures and the Frank-Kasper σ-phase at higher temperatures before the SISO-2 samples disorder.[5]

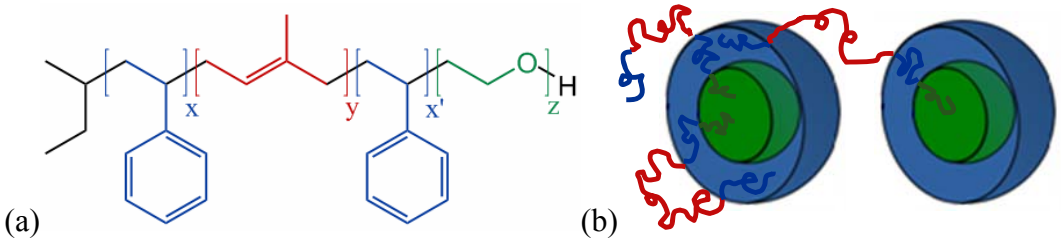

Figure 4-2 (a) Molecular structure of SISO-2 tetrablock terpolymer, with x = x'. (b) Core (O) – shell(S) spherical morphology. Unfavorable interactions between the O (core) and the I (matrix) blocks are screened by the S blocks (shell).

4.2 Results and Analysis

Figure 4-3 shows the linear dynamic elastic shear modulus G' for the SISO-2 samples obtained during the heating and cooling processes at a heating/cooling rate of 2 ^{o}C/min and ω = 1 rad/s. The order-order transition (OOT) occurs when there is a sudden change of G', indicating changes of the underlying morphologies. The order-disorder transition (ODT) occurs when G' decreases suddenly across several orders of magnitude to almost zero, indicating the loss of order within the specimen.

Over the temperature window of 150 – 166 ^{o}C, G' remains at a plateau value of about 5×10^{3} Pa upon heating, indicating the absence of OOT in between. In a previous

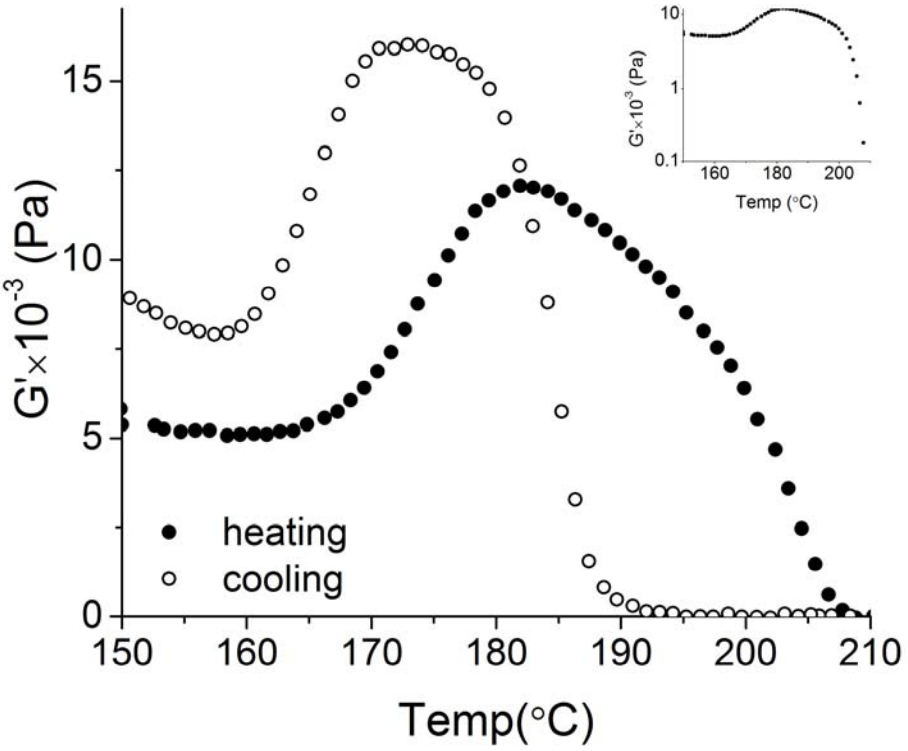

Figure 4-3 Dynamic elastic shear modulus G' for SISO-2 determined during the heating and cooling processes at a heating/cooling rate of 2 ^{o}C/min and ω = 1 rad/s. Changes in G' beginning at 166 ^{o}C and 183 ^{o}C during the heating process are interpreted as the order-order transitions.[6] Hysteresis in G'(T) is indicative of the first-order phase transitions. Inset shows the same dynamic elastic shear modulus G' in the log scale. A dramatic decrease of G' across several orders of magnitude at 208 ^{o}C indicates the order-disorder transition.

study, SISO-2 was reported to form a hexagonally ordered spherical morphology with the P_6/mmm space group symmetry at 120 ^oC.[4] Figure 4-4 shows the TEM micrographs obtained after annealing the SISO-2 samples at (a) 140 ^oC and (b) 160 ^oC under vacuum for a day prior to microtoming and TEM imaging. Both micrographs contain assemblies of white spheres ordered in a continuous black matrix. In panel (a), some spheres seem to align into straight lines because certain grains tilt at an angle to the electron beam in the microscope. When the electron beam is parallel to the *c* axis, we see regions with discrete spheres arranged on a hexagonal lattice. Grain rotation in (b) reveals a continuous transition from the 6-fold to the 4-fold regions (identified by the circled regions), suggesting an underlying hexagonal lattice. More details are described in Chapter 3. Based on a combination of the TEM and the DMS results, we can conclude that the SISO-2 samples form a hexagonally ordered spherical morphology over the temperature window of 120 – 166 ^oC.

At 166 ^oC, G' starts to increase (see Figure 4-3) and at 183 ^oC, G' reaches a maximum value of about 1.4×10^4 Pa, before dropping to almost zero at 208 ^oC. The two T_{OOT}s are measured to be 166 ^oC and 183 ^oC (each ± 1 ^oC), suggesting the presence of two additional ordered phases at higher temperatures besides the hexagonally ordered spherical morphology discovered at lower temperatures, before the sample disorders. T_{ODT} is better illustrated when the elastic modulus G' is plotted on the log scale with a dramatic decrease of G' across several orders of magnitude at 208 ± 1 ^oC (see the inset). Upon cooling, G' remains around zero till 190 ^oC, before increasing to a maximum of 1.6×10^4 Pa at 175 ^oC, then decreases to 7.5×10^3 Pa at 160^oC followed by a little

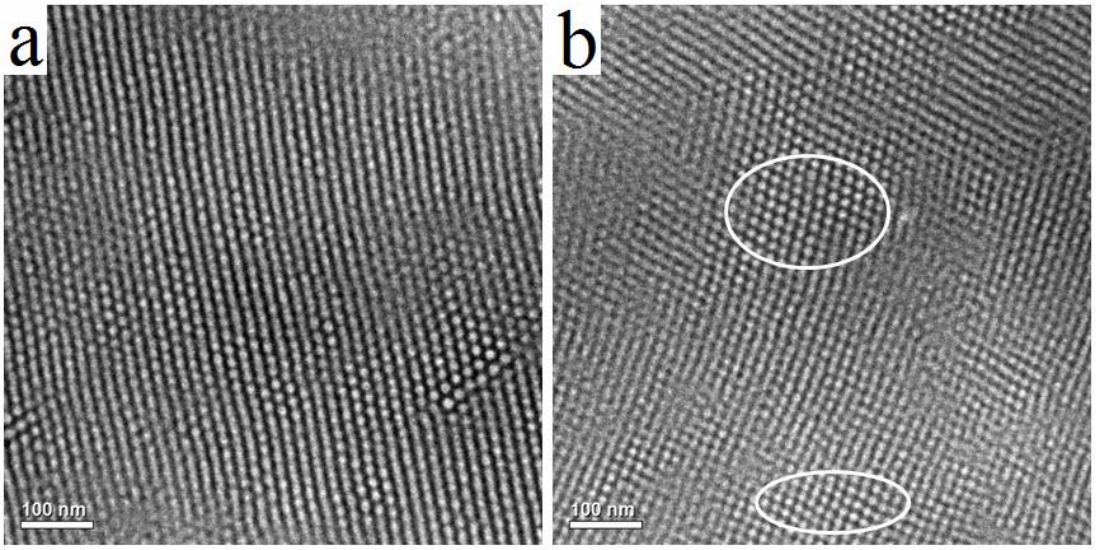

Figure 4-4 TEM micrographs obtained from OsO_4 stained SISO-2 tetrablock terpolymer after annealing under vacuum for a day at (a) 140 ^{o}C and (b) 160 ^{o}C prior to microtoming. Both images contain ordered arrays of spherical microdomains.[4] Transition from 6-fold to 4-fold symmetric projections (circled in panel (b)) that share common planes of spheres is consistent with a simple hexagonal lattice with P_6/mmm space group symmetry.

increment to 8.5×10^3 Pa at 150 ^{o}C. Even though the ODT and OOTs occur at lower temperatures during cooling than those during heating, the trend is consistent with hysteresis in G' measurements due to the nucleation kinetics associated with the first-order phase transitions.

Guided by the T_{OOT}s (166 and 183 ^{o}C) and T_{ODT} (208 ^{o}C) obtained from the DMS experiments, we design a temperature series of 120 → 175 → 190 → 175 → 210 → 215 ^{o}C along which the SAXS data were collected. At least one temperature is chosen from each temperature window separated by the T_{OOT}s and T_{ODT} values, i.e., 120 – 166 ^{o}C, 166 – 183 ^{o}C, and 183 – 208 ^{o}C. In each temperature window, an ordered morphology is

expected to be present. The SAXS data obtained along the designed temperature series are shown in Figure 4-5.

At 120 ^{o}C, the diffraction peaks for the SISO-2 samples (also shown in Figure 3-3) with the relative positions of $(q/q^*)^2$ = 1, 3 ,4,…, where q* represents the first-order reflection, indicates a state of the hexagonal order, consistent with the assigned core-shell hexagonally ordered spherical morphology with a core of the O blocks and a shell of the S blocks in an I-rich matrix mixed with the S blocks discussed previously.[7]

Upon heating to 175 ^{o}C, at least four new peaks appear with two peaks above and two peaks below the primary peak. The √3 peak disappears and the √4 peak broadens with a decreased intensity. These limited reflections at 175 ^{o}C cannot be indexed with any specific space group symmetry. Further heating to 190 ^{o}C leads to dramatic changes in the reflection patterns around q*. The primary peak broadens with the appearance of multiple peaks around q* and two prominent peaks on each shoulder. Additional higher-order peaks become apparent as well. Cooling back from 190 ^{o}C to 175 ^{o}C reverses these changes, suggesting this unique phase obtained at 175 ^{o}C is stable.

Upon further heating from 175 ^{o}C to 210 ^{o}C, a characteristic scattering pattern consistent with the Frank-Kasper σ-phase[1] is obtained before the sample disorders at 215 ^{o}C with the disappearance of all the Bragg peaks. The single broad scattering peak with a maximum at q* is interpreted as the correlation hole scattering from the disordered samples. The order-disorder transition temperature based on the SAXS is 213 ± 3 ^{o}C.

In a previous study, the Frank-Kasper σ-phase (P_{4_2}/mnm space group symmetry) was discovered in another SISO sample with a number-average molecular weight of

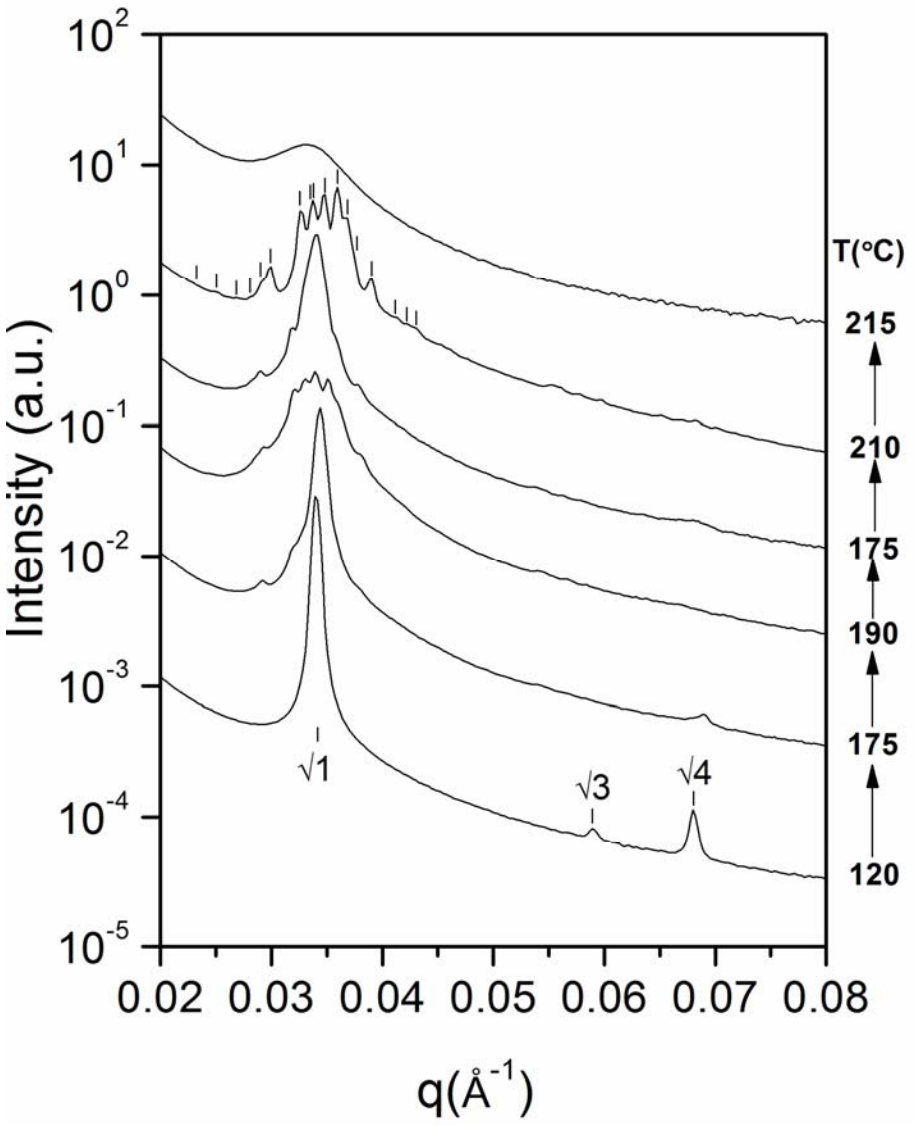

Figure 4-5 Representative synchrotron SAXS data obtained from SISO-2. Hexagonal and tetragonal (σ-phase) order, and disorder, are identified with the results at 120 ^{o}C, 210 ^{o}C, and 215 ^{o}C, respectively. Relative σ-phase peak positions, reported previously for another SISO material[7] are identified with the SISO-2 scattering pattern. A distinctly different structure is indicated by the thermally reversible scattering patterns obtained at 175 ^{o}C. Scattering patterns have been shifted vertically for clarity.

M_n = 23 kg/mol, PDI = 1.04, containing 46 % S (divided equally), 46 % I and 8 % O by volume (each ± 1 %) at 200 ^oC with a tetragonal symmetry and the unit cell dimensions of a = 77.7 nm and c = 41.1 nm based on the Rietveld analysis.[1] The SAXS scattering pattern is presented as the bottom red curve in Figure 4-6. The top black curve is the SAXS scattering data of our SISO-2 samples after annealing for 5 – 10 minutes at 200 ^oC. The positions of the diffraction peaks are consistent with the Frank-Kasper σ-phase with the unit cell dimensions of a = 80.2 nm and c = 42.6 nm based on the Rietveld analysis. A slightly larger unit cell is formed because of its higher molecular weight (24.4 kg/mol for SISO-2 vs. 23.0 kg/mol for SISO). All the theoretically calculated peak positions for the Frank-Kasper σ-phase are labeled using short strokes and the Miller indices for the experimentally observed prominent peaks are also identified. A quick comparison of the peak positions and the intensities shows that our SISO-2 samples contain the Frank-Kasper σ-phase at 200 ^oC. These nearly identical SAXS results found in our SISO-2 samples[5] and the previously published SISO samples[1] with similar molecular weight and composition, as well as in another diblock system of poly(isoprene-*b*-lactide) (IL), indicate certain degree of the universal presence of this unique ordered morphology.

In order to learn more about the thermally reversible distinctly different structure formed at 175 ^oC based on the SAXS results, representative TEM images are obtained after annealing the SISO-2 samples under vacuum at 175 ^oC for a day. At 120 ^oC, SISO-2 forms a hexagonally ordered spherical morphology.[4] One representative TEM image is shown in Figure 4-7 (a) for easy comparison. The sphere diameter is about 13.3 ± 1.0 nm (see Table 3-3).

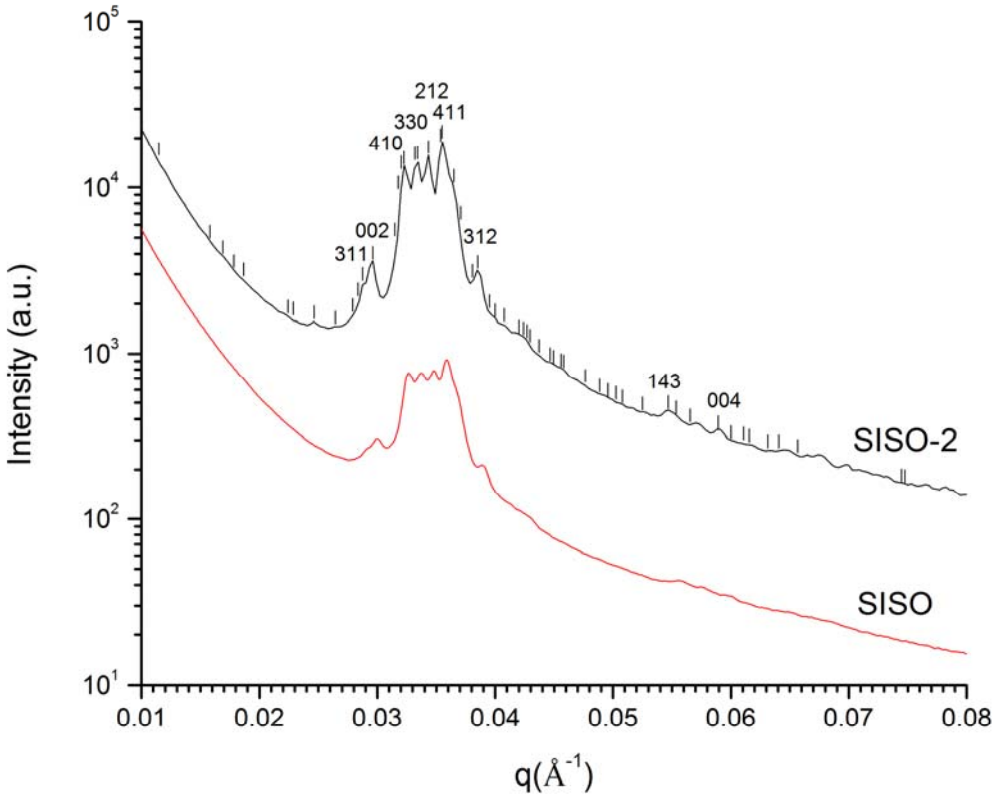

Figure 4-6 Synchrotron SAXS powder patterns at 200 ^{o}C from (top) SISO-2 containing 35 % S, 56 % I and 9 % O by volume, and (bottom) SISO containing 46 % S, 46 % I and 8 % O by volume. SISO has been verified to be the Frank-Kasper σ-phase with tetragonal symmetry.[1] For SISO-2, all the calculated peak positions based on these unit cell dimensions for Frank-Kasper σ-phase were labeled using short strokes and Miller indices for experimentally observed prominent peaks were also identified. A quick comparison of peak position and intensities also showed that the SISO-2 samples form the Frank-Kasper σ-phase at 200 ^{o}C.

Changing the annealing temperature to 175 ^{o}C reveals a dramatically different TEM result shown in Figure 4-7 (b). It contains many scattered rings with the white spherical cores surrounded by the grey shells separated with the black linings. The diameter of the white spherical cores is about 13 nm, similar to the value obtained at 120 ^{o}C with the P_6/mmm space group symmetry. The rings in the larger rectangular box seem to exhibit certain level of order, i.e., an 'H-element'(see Figure 4-11). However, such local order does not extend to other regions outside the box, i.e., they do not have any long-range translational order.

One abovementioned core-shell ring midway between the bottom line of the 'H-element' is surrounded by many white spheres enclosed in the black linings. Even though some of these spheres cannot be observed distinctively, the total number can be counted to be twelve assuming similar spherical diameters. The inset in Figure 4-7 (b) shows a fast Fourier Transform image with the clear presence of a twelve-fold rotational symmetry. We assign it as the dodecagonal quasicrystalline phase. Note that even though this unique arrangment of the spheres is only observed in limited regions under the TEM microscope, we are able to identify similar patterns in other regions of the same thin specimen section, as well as to reproduce similar results in the other thin sections microtomed from the same SISO-2 material, suggesting the credibility of the presence of this distinctive order. A comparison between the TEM images obtained at 120 ^{o}C and 175 ^{o}C indicates that temperature plays a key effect on the block copolymer phase behavior.

In order to illustrate the origins of the rotational order, Figure 4-7 (b) is tilited 90^{o} out of the plane of view, as demenstrated in Figure 4-8, with straight white undulating

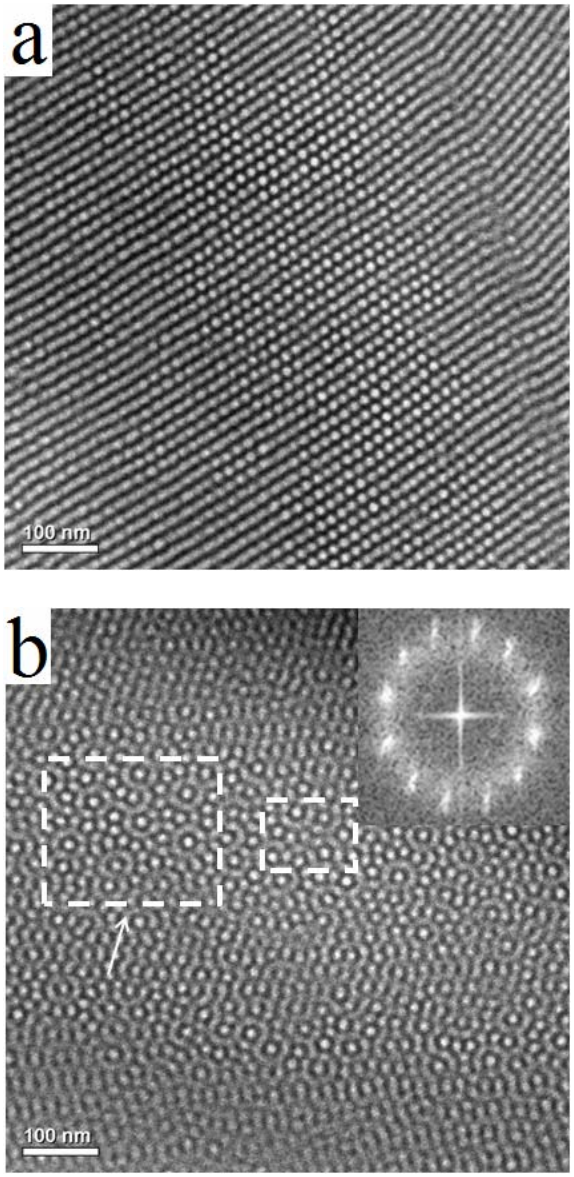

Figure 4-7 TEM images from OsO_4 stained SISO-2 samples after annealing for 1 day at (a) 120 ^{o}C and (b) 175 ^{o}C. Both images contain spherical domains with a core of the O blocks. The long-range order in (a) is associated with the simple hexagonal symmetry.[4] (b) contains clear evidence of local (ca. 50 – 100 nm) coordination of spheres, but lacks the long-range translational order. A Fourier transform (inset) reveals a 12-fold rotational symmetry consistent with a dodecagonal QC order.

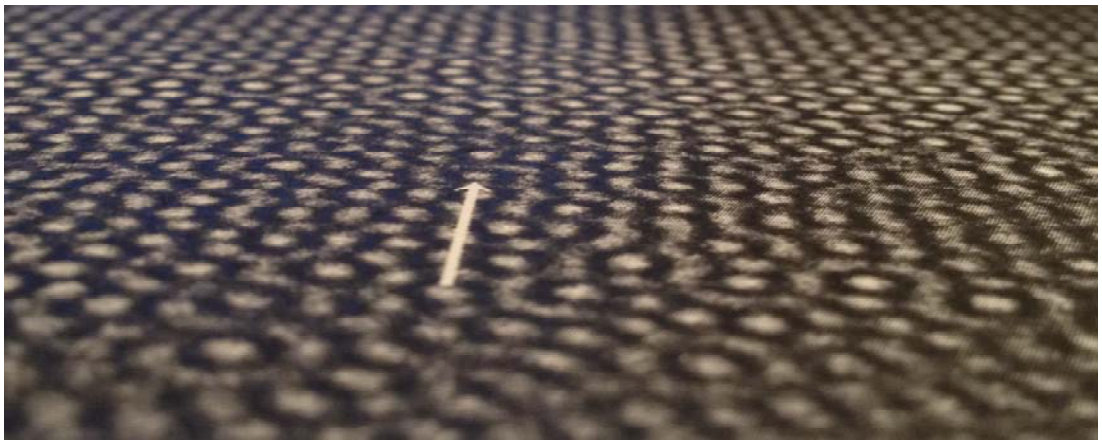

Figure 4-8 Image with planes of (uncorrelated) spheres obtained after rotating Figure 4-7 (b) out of the plane of view; the arrow identifies the orientation.

lines along one of the twelve rotational symmetries, as indicated by the white arrows in Figure 4-7 (b) and Figure 4-8. If we continue to rotate Figure 4-8 around the normal, for every $360^{o} / 12 = 30^{o}$ rotation, similar images are obtained.

4.3 Discussion

Prior to the twentieth century, scientists believed that the periodic filling of space with regular arrangement of tiles was only possible with 2-, 3-, 4- and 6-fold rotational symmetries. Not until 1961, did mathematicians start the quest to fill space with the aperiodic patterns. In 1963, 'Wang tiles' were invented, which can fill space in an aperiodic fashion with 13 tile types.[8] Sir Roger Penrose made a great leap forward in 1974 by showing that just two tile types (shown in two colors in Figure 4-9), related by the 'Golden ratio,' are required to fill space completely without leaving gaps or

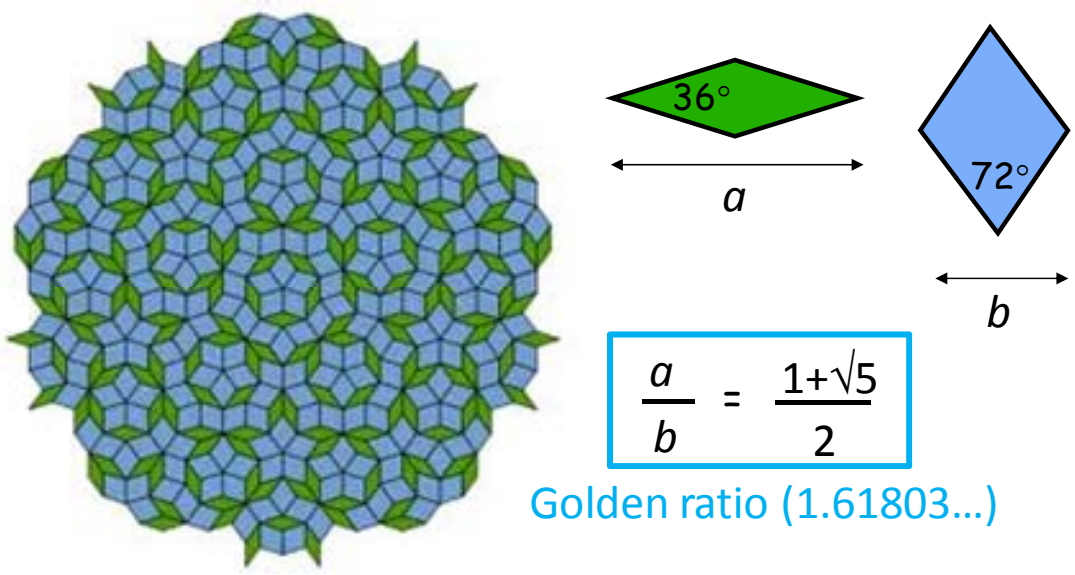

Figure 4-9 Penrose Tiling with just two tile types related by the golden ratio (Image is obtained from the internet: http://en.wikipedia.org/wiki/Penrose_tiling)

overlapping regions.[9] This resulting aperiodic pattern lacks of any translational order but contains a five-fold rotational symmetry. Another remarkable property is that Penrose tilings are self-similar, i.e., the pattern repeats at different length scales. Penrose tilings can be viewed as the two-dimensional slices of the five-dimensional hypercubic structures.[10] A Penrose tilling is an example of a 2-dimensional QC.

The first experimental QC was found in the lab setting in the binary Al-Mn metallic alloys with a five-fold rotational symmetry after rapid cooling from the liquid state by Dan Shechtman and coworkers in 1982. Shechtman was awarded the Nobel Prize in Chemistry in 2011 for this discovery. This work was jointly published with Ilan Blech's computer simulated result of the diffraction patterns in 1984,[11] together with another paper[12] demonstrating the spontaneous assembly of certain metallic alloys into structures

with an unusual rotational symmetry and lack of any long-range translational order. The word ‘quasicrystal’ was first used by Levine and Steinhardt in 1984.[13] Soon after this, Ishimasa *et al.* reported a twelve-fold symmetry in Ni-Cr binary metallic alloys[14] and Wang *et al.* reported an eight-fold symmetry in V-Ni-Si and Cr-Ni-Si ternary metallic alloys.[15] Over the years, hundreds of QCs have been discovered in the lab setting in the binary and ternary metallic alloys with different compositions and rotational symmetries.[16–24] Not until 2009, was the first natural quasicrystalline icosahedrite, $Al_{63}Cu_{24}Fe_{13}$, discovered in a mineral found near the Khatyrka River in eastern Russia.[25] Interestingly, the analysis shows that this natural QC might come from a part of a meteorite from the outer space formed in the early solar system about 4.5×10^9 light years ago.[26] The unique physical properties of QCs are currently under vigorous study. Most notably is that even though most QCs are alloys of two or more metals, they are poor conductors of heat and electricity.

There are two types of quasicrystals: polygonal and icosahedral. Polygonal QCs consist of octagonal (local 8-fold symmetry), decagonal (10-fold) and dodecagonal (12-fold) quasicrystals. They are quasiperiodic in two dimensions with one periodic direction perpendicular to the quasiperiodic layers. For regular crystals with three-dimensional periodicity, only three integer values, known as the Miller indices, are needed to label the observable reflections. In polygonal QCs, five linearly independent vectors are needed, 3 unit vectors in the external space and 2 in the internal space. Icosahedral QCs with local 20-fold symmetry are quasiperiodic in all three dimensions without any periodic direction, requiring six linearly independent vectors to index each peak, 3 unit vectors each in the

external and the internal spaces. A third type, also called the new type, has been reported with a broken symmetry.[27]

The thermal stability of QCs depends on the fabrication processes; stable QCs are formed by slow cooling or casting with subsequent annealing. Metastable QCs are formed by melt-spinning or crystallization of the amorphous phase.[24] Except for the Al-Li-Cu system, all stable QCs are well-ordered and almost free of defects and disorder, as evidenced by the sharp X-ray or electron diffraction peaks. Metastable QCs form regular crystals upon heating. Local icosahedral order is a common feature for both stable and metastable QCs. It is in equilibrium in the liquid state for stable ones[28] and prevails in the undercooled liquid state for the metastable ones[29]. It is the stability and the density of this local icosahedral order in a liquid that governs the thermal stability of the QCs.

Classical crystals have point lattices where each point can be viewed as the center of mass of the corresponding identical units. A similar concept of quasilattices is used in the QCs with more than one type of unit. The crystal structure is analyzed by defining an associated group. The term groupoids is used as the appropriate tool to study the QCs.[30] Software package was developed by Yamamoto to build models, refine structures and provide detailed structure analysis of the QCs,[22] greatly facilitating the experimentalists' task to construct and analyze the QC structures.

Besides the metal alloys, QCs are also found in a few organic materials,[31–33] including polymers[31]. As early as 1959, Frank and Kasper[34] pointed out the possibility of polymers to form the 'Frank-Kasper' phases, also known as the 'periodic approximant' to certain dodecagonal quasicrystals,[3] using the closed-pack tetrahedral units of the

spherical domains with the packing symmetries such as P_{4_2}/mnm (σ-phase), $Pm\bar{3}n$, and $Fd\bar{3}m$. In 2003, Ungar and coworkers[35] observed the formation of the Frank-Kasper σ-phase and the dodecagonal QC phase in wedge-shaped dendrimer molecules that self-assemble into approximately spherical particles,[31] as a result of the molecular packing frustration.[36] SAXS results illustrate the sequence of phases formed being QC → σ-phase → disorder with increasing temperatures.[31]

In 1992, Dzugutov[37] generated a potential curve from a special form of pair potential employed in monatomic liquid lead. Similar to the classical 6-12 Lennard Jones potential, this potential curve has a short-range repulsion and a nearest neighbor attraction with a minimum at r = 1.13σ. In addition, Dzugutov potential has a maximum repulsion peak at r = 1.63σ, encouraging the formation of the local icosahedral order,[38,39] as well as the Frank-Kasper phases,[37] which remains stable over a wide range of temperature frame.

In 2007, Keys and Glotzer reported the growth of the dodecagonal QC phase with the dense uniformly sized hard spheres simulated based on the Dzugutov potential (see Figure 4-10 (a)),[3] which agrees well with our experimental results shown in Figure 4-7 (b). The image on the right shows the aperiodic tiles formed by connecting the centers of the dodecagonal rings of atoms. In Figure 4-10 (b), unit cells of various QC approximants are listed: the σ-element (a periodic 2-dimensional Archimedean tiling's formed by a distinctive pattern of $3^2.4.3.4$ triangular and square elements), the Z-element (six triangular elements), the H-element (three triangular and two square elements) and the A15 element (four square elements).

A detailed examination of Figure 4-7 (b) shows the intermediate scale structures that

support the assignment of the QC morphology. Dodecagonal QCs are characterized by the irregular tiling patterns, which include a mixture of various approximants shown in Figure 4-10 (b). The smaller dashed box in Figure 4-7 (b) is enlarged in Figure 4-11 (a), with the Frank-Kasper σ-element identified.[1] The larger dashed box in Figure 4-7 (b) is enlarged in Figure 4-11 (b), with the H-element identified.[3,34] These are characteristic elements for the QCs. The scale bars represent 100 nm. Interestingly, these two elements have different tiling length scales, which is another characteristic feature of the QC phase.

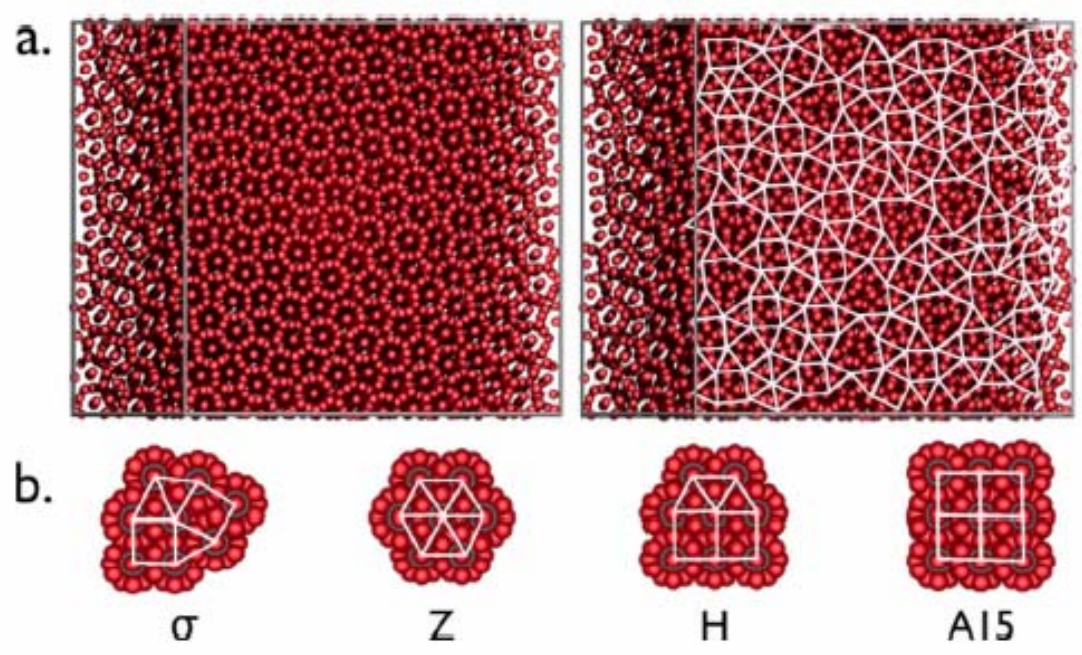

Figure 4-10 Dodecagonal QC and approximants. (a) Simulated dodecagonal QC formed by the Dzugutov system. The image on the right shows the aperiodic tiles formed by connecting the centers of the dodecagonal rings of atoms. (b) Unit cells of various QC approximants. Reproduced from Keys and Glotzer.[3]

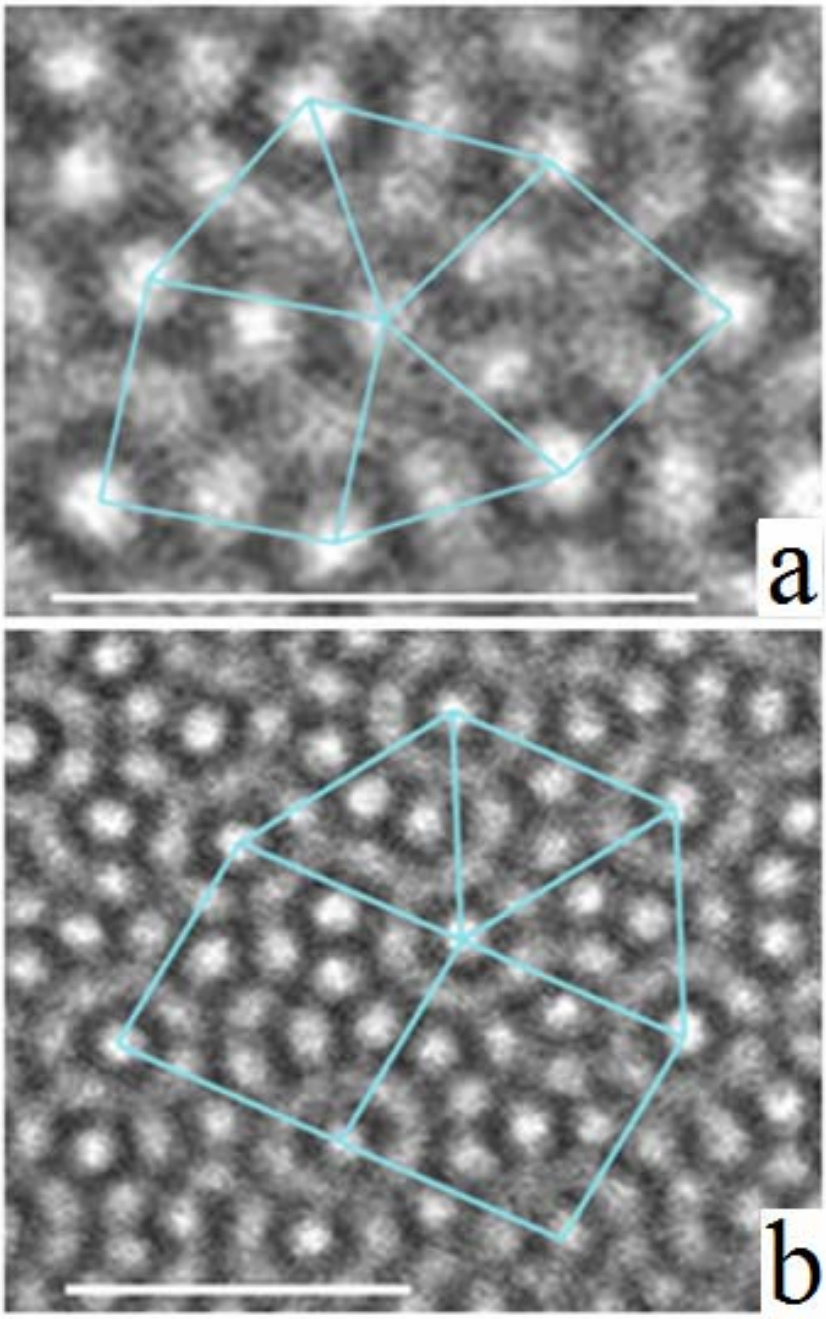

Figure 4-11 Clusters displaying (a) the σ-element and (b) the H-element quasicrystal approximant tilings, located within the smaller and the larger dashed rectangular boxes in Figure 4-7 (b), are magnified and highlighted respectively. The scale bars represent 100 nm.

Based on the TEM analysis, we believe that the SISO-2 samples form a 2-dimensional dodecagonal QC phase at 175 ^{o}C. Dodecagonal QCs are one type of the polygonal QCs. They are quasiperiodic in two dimensions with one periodic direction perpendicular to the quasiperiodic layers, i.e., the pattern shown in Figure 4-7 (b) is repeated periodically in the normal direction.[31] In the TEM micrographs, we see regions with a translational order, a QC order and disorder, consistent with this assignment. For an anisotropic specimen with a polydomain texture, the probability of slicing a thin section with the QC morphology similar to Figure 4-7 (b) is very low, explaining the limited QC images obtained from the TEM observations.

In single component block copolymer melts, polymer chains get stretched and compressed in order to maintain a uniform density.[40] In sphere-forming diblock copolymers with the mean-field limit, spheres are arranged on a body-centered cubic (BCC) lattice.[41,42] However, recent results showed that low molecular weight sphere-forming diblock copolymers can form the Frank-Kasper σ-phase, after modifying the inter-particle interactions due to the non-Gaussian corona block chain statistics.[1]

The inter-particle interactions, which can be tuned by the molecular architecture, are also responsible for coordinating the polymer chains into the local icosahedral or the dodecahedral order necessary for the QC formation.[35,36,43] By changing the molecular architecture from AB diblocks or ABC triblocks to ABAC tetrablock terpolymers, we expand the parameter space greatly to control the basic domain geometry (e.g., spherical or cylindrical domains) and the inter-particle interactions, which can be uniquely tunable among soft matters via elastic deformations at constant overall density, allowing the

formation of novel and potentially valuable crystalline and quasicrystalline phases. Taking the model system SISO as an example, the formation of the core-shell spherical structure, with the O blocks forming the core and the S blocks forming the shell in an I-rich matrix, shields the unfavorable interaction of the I/O blocks (see Figure 4-2 (b)), offering direct control over the effective inter-particle potential. Enthalpic interactions between the dissimilar blocks can be designed to be uniformly mixed, partially segregated or microphase separated by altering the Flory-Huggins interaction parameters and degree of polymerizations.

The SAXS and TEM results suggest that the dodecagonal QC phase obtained at 175 ^{o}C is stable, providing new opportunities for creating materials with as yet unexplored properties. So far, SISO tetrablock copolymers have been reported to form unique structures such as simple hexagonally ordered spherical phase,[4] the Frank-Kasper σ-phase[1] and the QC phase,[5] which are dramatically different from the network structures reported for the analogous ISO compounds (ABC triblock terpolymers).[44–50] These recently discovered structures explore only very limited region of the vast parameter space offered in the ABAC tetrablock copolymers. The cause-effect relationships between the tetrablock terpolymers molecular parameters and their corresponding phase behaviors remain elusive.

4.4 Conclusion

A dodecagonal quasicrystalline phase is identified in a SISO tetrablock terpolymer, named SISO-2 in Chapter 3, based on the SAXS, TEM and rheology measurements. The

QC state occurs as an intermediate state between the simple hexagonal order (P_6/mmm) and the σ-phase (P_{4_2}/mnm) before the sample disorders, with $T_{HEX} < T_{QC} < T_{\sigma} < T_{ODT}$. The core-shell spherical domains are formed in all three ordered morphologies, with the O blocks being the core and the internal S blocks forming the shell in an I-rich matrix, shielding the unfavourable I/O block interactions. The TEM results reveal a QC morphology with a 12-fold rotational symmetry and the existence of the local dodecagonal quasicrystalline approximants but devoid of any long-range translational order. The ABAC tetrablock molecular architecture offers a new approach to independently control domain shape and packing in block copolymer melts by changing the magnitude and sequence of the binary segment-segment interactions.

4.5 References

(1) Lee, S.; Bluemle, M. J.; Bates, F. S. *Science* **2010**, *330*, 349.

(2) Bluemle, M. J.; Zhang, J.; Lodge, T. P.; Bates, F. S. *Macromolecules* **2010**, *43*, 4449.

(3) Keys, A. S.; Glotzer, S. C. *Physical Review Letters* **2007**, *99*, 235503.

(4) Zhang, J.; Scott, S. W.; Bates, F. S. *Macromolecules* **2012**, *45*, 256.

(5) Zhang, J.; Bates, F. S. *Journal of the American Chemical Society* **2012**, *134*, 7636.

(6) Hillmyer, M. A.; Bates, F. S.; Almdal, K.; Mortensen, K.; Ryan, A. J.; Fairclough, J. P. A. *Science* **1996**, *271*, 976.

(7) Lee, S.; Bluemle, M. J.; Bates, F. S. *Science* **2010**, *330*, 349.

(8) Wang, H. *Bell Systems Technical Journal* **1961**, *40*, 1.

(9) Penrose, R. *Bulletin of the Institute of Mathematics and its Applications* **1974**, *10*, 266.

(10) de Bruijn, N. *Nederlandse Akademie Wetenschappen Proc.* **1981**, *A84*, 39.

(11) Shechtman, D.; Blech, I.; Gratias, D.; Cahn, J. *Physical Review Letters* **1984**, *53*, 1951.

(12) Cahn, J. W.; Shechtman, D.; Gratias, D. *Materials Research* **1986**, *1*, 13.

(13) Levine, D.; Steinhardt, P. J. *Physical Review Letters* **1984**, *53*, 2477.

(14) Ishimasa, T.; Nissen, H.-U.; Fukano, Y. *Physical Review Letters* **1985**, *55*, 511.

(15) Wang, N.; Chen, H.; Kuo, K. *Physical Review Letters* **1987**, *59*, 1010.

(16) Janot, C. *Quasicrystals: A Primer*; 2nd ed.; Oxford University Press: New York, 1994.

(17) Yamamoto, A. *Acta Crystallographica* **1996**, *A52*, 509.

(18) DiVincenzo, D. P.; Steinhardt, P. J. *Quasicrystals: The State of the Art*; World Scientific: Singapore, 1991.

(19) Lifshitz, R. *Physical Review Letters* **1998**, *80*, 2717.

(20) Wolf, R. M.; Aalst, W. *Acta Crystallographica* **1972**, *28*, 111.

(21) Kleinert, H.; Maki, K. *Fortschritte der Physik* **1981**, *29*, 219.

(22) Yamamoto, A. *Science and Technology of Advanced Materials* **2008**, *9*, 013001.

(23) Macia, E. *Reports on Progress in Physics* **2006**, *69*, 397.

(24) Tsai, A. P. *Science and Technology of Advanced Materials* **2008**, *9*, 013008.

(25) Bindi, L.; Steinhardt, P. J.; Yao, N.; Lu, P. J. *Science* **2009**, *324*, 5932.

(26) Bindi, L.; Eiler, J. M.; Guan, Y.; Hollister, L. S.; MacPherson, G.; Steinhardt, P. J.; Yao, N. *Proceedings of the National Academy of Sciences of the United States of America* **2012**, *109*, 1396.

(27) Abe, E.; Saitoh, K.; Takakura, H.; Tsai, A. P.; Steinhardt, P. J.; Jeong, H.-C. *Physical Review Letters* **2000**, *84*, 4609.

(28) Klein, H.; Audier, M.; Simonet, V.; Hippert, F.; Bellissent, R. *Physica. B, Condensed Matter* **1998**, *964*, 241.

(29) Jones, H. *Proceedings of the Physical Society* **1937**, *49*, 250.

(30) Paterson, A. L. T. *Groupoids, Inverse Semigroups, and Their Operator Algebras*; Springer: Boston, MA, 1999.

(31) Zeng, X.; Ungar, G.; Liu, Y.; Percec, V.; Dulcey, A. E.; Hobbs, J. K. *Nature* **2004**, *428*, 157.

(32) Hayashida, K.; Dotera, A.; Takano, A.; Matsushita, Y. *Physical Review Letters* **2007**, *98*, 195502.

(33) Ceolin, R.; Agafonov, V.; Fabre, C.; Rassat, A.; Dworkin, A.; Andre, D.; Szwarc, H.; Schierbeek, A. J.; Bernier, P.; Zahab, A. *Journal De Physique* **2004**, *428*, 157.

(34) Frank, F. C.; Kasper, J. S. *Acta Crystallographica* **1959**, *12*, 483.

(35) Ungar, G.; Liu, Y.; Zeng, X.; Percec, V.; Cho, W. D. *Science* **2003**, *299*, 1208.

(36) Ungar, G.; Zeng, X. *Soft Matter* **2005**, *1*, 95.

(37) Dzugutov, M. *Physical Review A* **1992**, *46*, R2984.

(38) Dzugutov, M. *Physical Review Letters* **1993**, *70*, 2924.

(39) Doye, J. P. K.; Wales, D. J.; Zetterling, F. H. M.; Dzugutov, M. *Journal of Chemical Physics* **2003**, *118*, 2792.

(40) Matsen, M. W.; Bates, F. S. *Macromolecules* **1996**, *29*, 7641.

(41) Leibler, L. *Macromolecules* **1980**, *13*, 1602.

(42) Bates, F. S.; Cohen, R. E.; Berney, C. V. *Macromolecules* **1982**, *15*, 589.

(43) Rosen, B. M.; Wilson, D. A.; Wilson, C. J.; Peterca, M.; Won, B. C.; Huang, C.; Lipski, L. R.; Zeng, X.; Ungar, G.; Heiney, P. A.; Percec, V. *Journal of the American Chemical Society* **2009**, *131*, 17500.

(44) Bailey, T. S.; Hardy, C. M.; Epps III, T. H.; Bates, F. S. *Macromolecules* **2002**, *35*, 7007.

(45) Epps III, T. H.; Cochran, E. W.; Hardy, C. M.; Bailey, T. S.; Waletzko, R. S.; Bates, F. S. *Macromolecules* **2004**, *37*, 7085.

(46) Cochran, E. W.; Bates, F. S. *Physical Review Letters* **2004**, *93*, 087802.

(47) Epps III, T. H.; Cochran, E. W.; Bailey, T. S.; Waletzko, R. S.; Hardy, C. M.; Bates, F. S. *Macromolecules* **2004**, *37*, 8325.

(48) Chatterjee, J.; Jain, S.; Bates, F. S. *Macromolecules* **2007**, *40*, 2882.

(49) Bluemle, M. J.; Fleury, G.; Lodge, T. P.; Bates, F. S. *Soft Matter* **2009**, *5*, 1587.

(50) Tyler, C. A.; Qin, J.; Bates, F. S.; Morse, D. C. *Macromolecules* **2007**, *40*, 4654.

5

Phase Behavior of Polystyrene-rich SISO Tetrablock Terpolymers

5.1 Introduction

The model system of the SISO tetrablock terpolymer is an extension of the ISO triblock terpolymer system. We intend to study the effect of the volume fraction and the molecular architecture on the block copolymer phase behaviour. In a previous study, the SISO terpolymers along the composition channel containing equal volume fractions of the S and I blocks were synthesized[1] and the cylinders on HEX lattice, the Frank-Kasper σ-phase,[2] the disordered state and the tentatively assigned liquid-like packing (LLP) of

spherical phases were reported. In Chapter 3, the SISO samples along the isoprene-rich composition channel containing $f_S : f_I = 2 : 3$ are described and the spheres on HEX lattice, the cylinders on HEX lattice and disordered states are reported.[3] In Chapter 4, the temperature dependence of one particular sample from the same isoprene-rich composition channel is studied in detail and the spheres on HEX lattice, the dodecagonal quasicrystalline phase, the Frank-Kasper σ-phase and the disordered phases are observed with increasing temperatures.[4]

In this chapter, we explore the same SISO system along the styrene-rich composition channel containing $f_S : f_I = 3 : 2$ (the S blocks are divided equally, i.e., x = x') and f_O between 0 and 35 % (see Figure 5-1). With $\chi_{SI} \leq \chi_{SO} << \chi_{IO}$, the repulsion between the I and the O blocks is the greatest. The S blocks shield the unfavourable I/O interaction. Increasing the volume fractions of the shielding S blocks leads to dramatic changes in the morphological behaviours when we compare the phases reported along the styrene-rich channel, the isoprene-rich channel, and the channel with equal S and I blocks, indicating the key effect of the composition on the block copolymer phase behaviour. Combining the results observed from the three channels of SISO tetrablock terpolymers and comparing that with the well-established ISO system, we could study the effect of

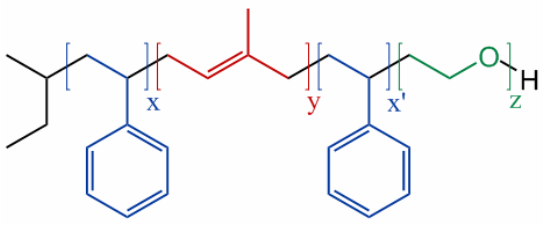

Figure 5-1 Molecular structure of SISO tetrablock terpolymers.

molecular architecture on the phase behaviours.

5.2 Results and Analysis

Figure 5-2 shows the phase portrait of the SISO tetrablock terpolymers. The effect of the molecular weight is not reflected in this map, but all the polymers have similar molecular weights ranging from 21.7 to 31.1 kg/mol (see Table 5-1). The middle channel contains equal S and I volume fractions[1] and the left isoprene-rich channel[3,4] contains f_S : f_I = 2 : 3. The right styrene-rich channel containing f_S : f_I = 3 : 2 is the focus of this chapter. Six SISO tetrablock terpolymers with narrow overall molecular weight distributions were synthesized from the same parent SIS-OH triblock precursor and the only difference is the lengths of the O blocks. Molecular characterization data, degree of crystallinity, T_{ODT}'s and morphology assignments based on SAXS, TEM, DSC and DMS are listed in Table 5-1.

SIS-OH and SISO-4. Synchrotron SAXS powder patterns for the SIS-OH triblock and the SISO-4 tetrablock terpolymer are presented in Figure 5-3. Both samples were annealed at 110 ^{o}C for 5 minutes before the SAXS data were taken. The single broad scattering peak with a maximum at q* is interpreted as the correlation hole scattering from the disordered state for both samples.

SISO-9. Synchrotron SAXS data of the SISO-9 samples at various temperatures during the heating and cooling processes are shown in Figure 5-4. Samples were taken out of the freezer (see Chapter 2.1 for the detailed sample preparation methods) and

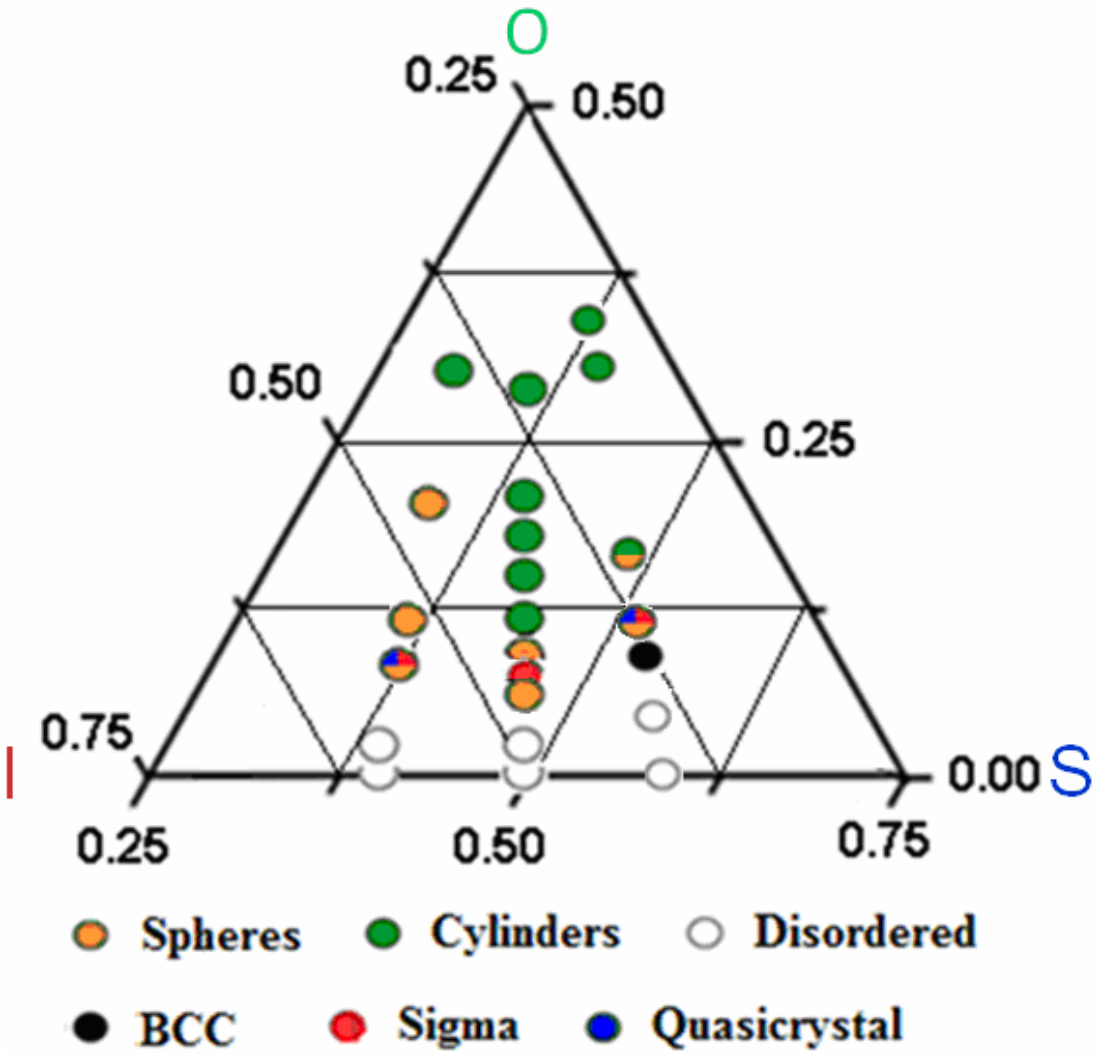

Figure 5-2 Poly(styrene-*b*-isoprene-*b*-styrene-*b*-ethylene oxide) (SISO) phase portrait in the vicinity of the order-disorder transition. Filled and open circles indicated ordered and disordered states, respectively, within the experimental temperature range of $110 \leq T \leq 250\ ^{o}C$. Specimens considered in this chapter were prepared by adding O blocks to a SIS-OH triblock containing 60 vol% S and 40 vol% I on the right isopleth.

Table 5-1 SIS-OH and SISO Characterization Data.

Sample	M_n/kDa	PDI	f_S[a]	f_I[a]	f_O[a]	Phase[b]	% Cry.[c]	T_{ODT}/°C[d]
SIS-OH	23.1	1.07	0.60	0.40	0.00	DIS	0	<80
SISO-4	23.6	1.07	0.58	0.38	0.04	DIS	0	<80
SISO-9	24.2	1.07	0.54	0.37	0.09	BCC	27	162
SISO-11	24.6	1.05	0.52	0.37	0.11	LLP, QC, σ	42	245
SISO-15	25.2	1.07	0.49	0.36	0.15	LLP,HEX	52	>250
SISO-31	28.5	1.14	0.40	0.29	0.31	HEX	56	>250
SISO-35	29.7	1.10	0.37	0.28	0.35	HEX	74	>250

[a]Volume fractions calculated with from densities at 140 °C. [b]HEX-hexagonally packed cylinders for SISO-15, -31 and -35. [c]Percent crystallinity of the O domains was determined by differential scanning calorimetry. [d]Order-disorder transition temperatures were determined by small-angle x-ray scattering for SISO-9 and -11, and dynamic mechanical spectroscopy for the other samples.

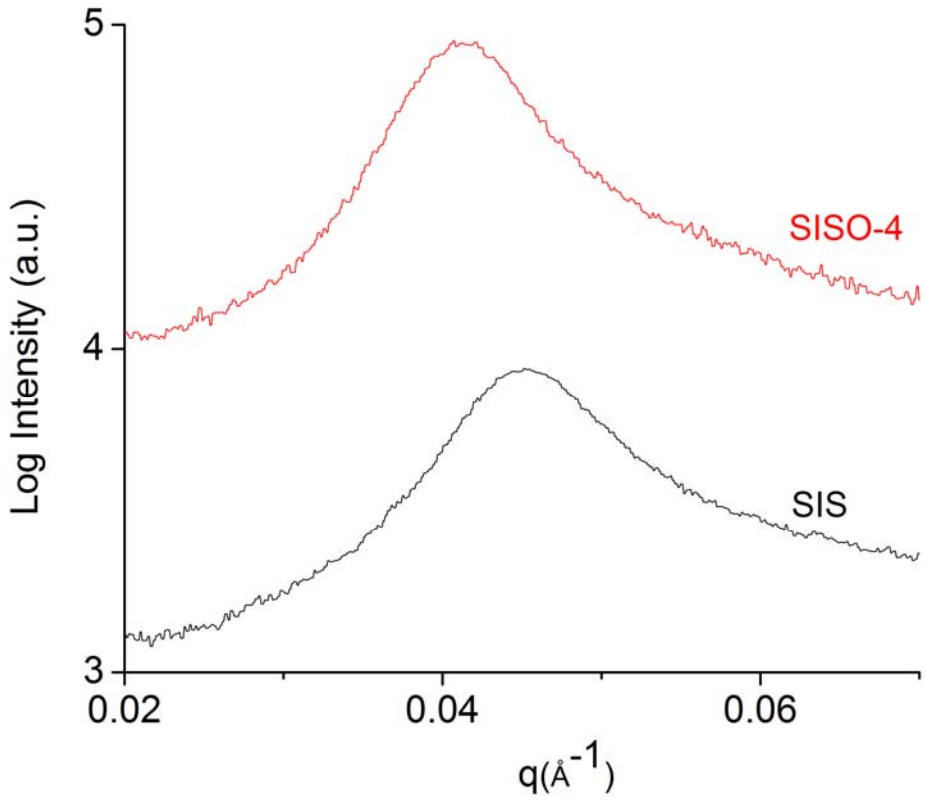

Figure 5-3 Synchrotron SAXS data for SIS-OH and SISO-4 samples. Both samples show disordered state. Scattering patterns are shifted vertically for clarity.

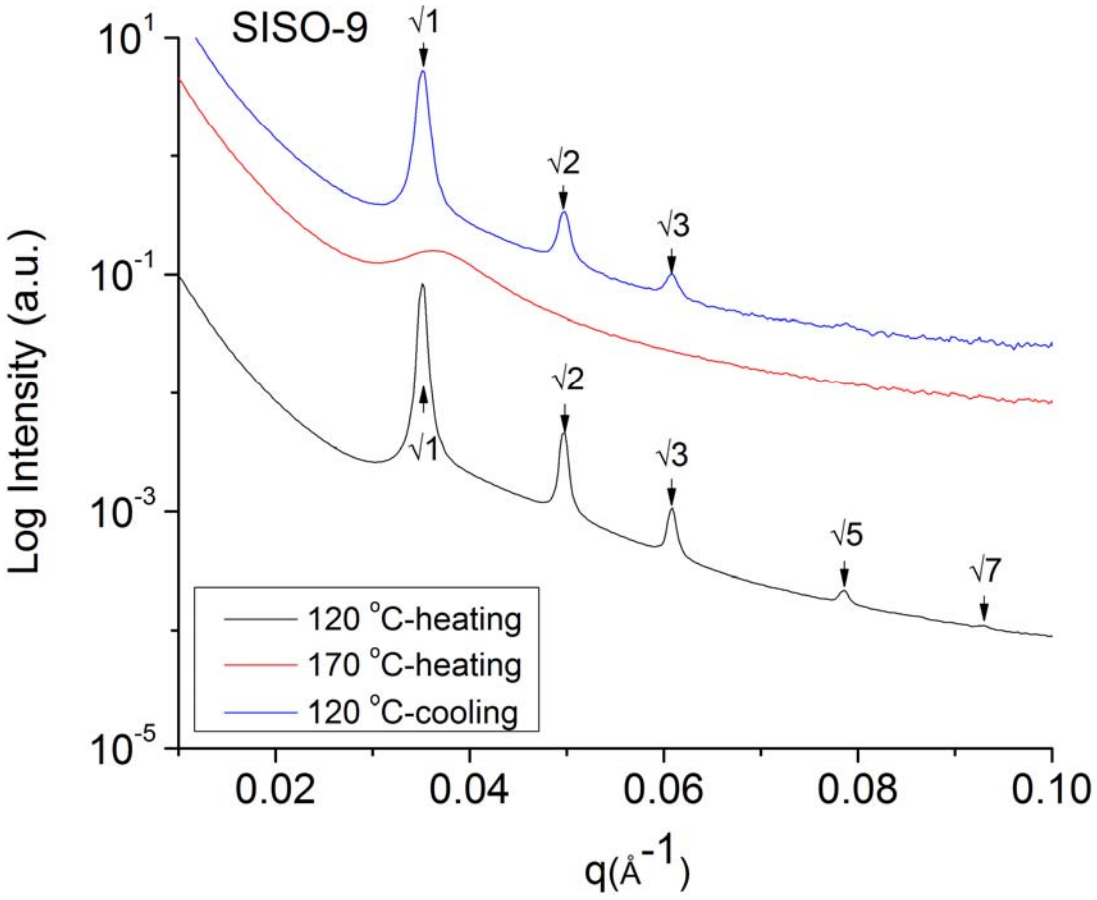

Figure 5-4 Representative synchrotron SAXS data obtained from SISO-9. The BCC symmetry and the disorder states are identified after annealing at 120 °C and 170 °C for a day and 5 minutes, respectively. The BCC structure obtained at 120 °C is indicated as thermally reversible. Scattering patterns have been shifted vertically for clarity.

annealed under vacuum at 120 °C for one day followed by a liquid nitrogen quench to preserve the morphology. At the Argonne facility, samples were heated and annealed at specific temperatures while the measurements were taken every five minutes until there were no further changes. The same procedures were carried out for the SISO-11, -15, -31 and -35 samples.

At 120 ^{o}C, the scattering pattern displays peaks at $q/q^{*} = \sqrt{1}, \sqrt{2}, \sqrt{3}, \sqrt{5}$, and $\sqrt{7}$ with q* being the principal peak location. These peak ratios are consistent with the BCC symmetry, except that the $\sqrt{4}$ peak is missing. We attribute this to the form factor extinctions due to the destructive interference. At 170 ^{o}C, the single and broad peak indicates the disordered state. Cooling the samples back to 120 ^{o}C, the ordered phase consistent with the BCC symmetry is recovered, indicating it is a stable state.

Representative TEM images for the SISO-9 samples after annealing at 120 ^{o}C are presented in Figure 5-5. Samples were annealed under vacuum at 120 ^{o}C for one day, quenched in liquid nitrogen to preserve the morphology, before being microtomed into thin slices (ca. 50 – 70 nm) for TEM imaging. After staining with OsO_4, the I domains appear dark and the S and O domains appear bright. The same sample preparations procedures for TEM imaging were carried out for the SISO-11, -15, -31 and -35 samples at specified annealing temperatures.

All the images in Figure 5-5 have regions of white spherical domains with diameters of 16 ± 3 containing a core of the O blocks with either a 3- or a 4-fold axis, consistent with the assignment of the BCC symmetry. Panel (a) and (b) display regions of the black spherical domains (approximately 16 nm in diameter) in a grey matrix with similar domain spacings as the white spherical domains (ca. 20 – 25 nm), possibly resulting from the different contrasts in the TEM microscope. The white spherical domains exhibit longer range of the translational order than the black ones, as shown in panel (c) and (d). In panel (d), we see the clear boundaries where three large grains cross. The top grain is tilted such that the planes of spheres are slightly off the axis resulting in a projection that

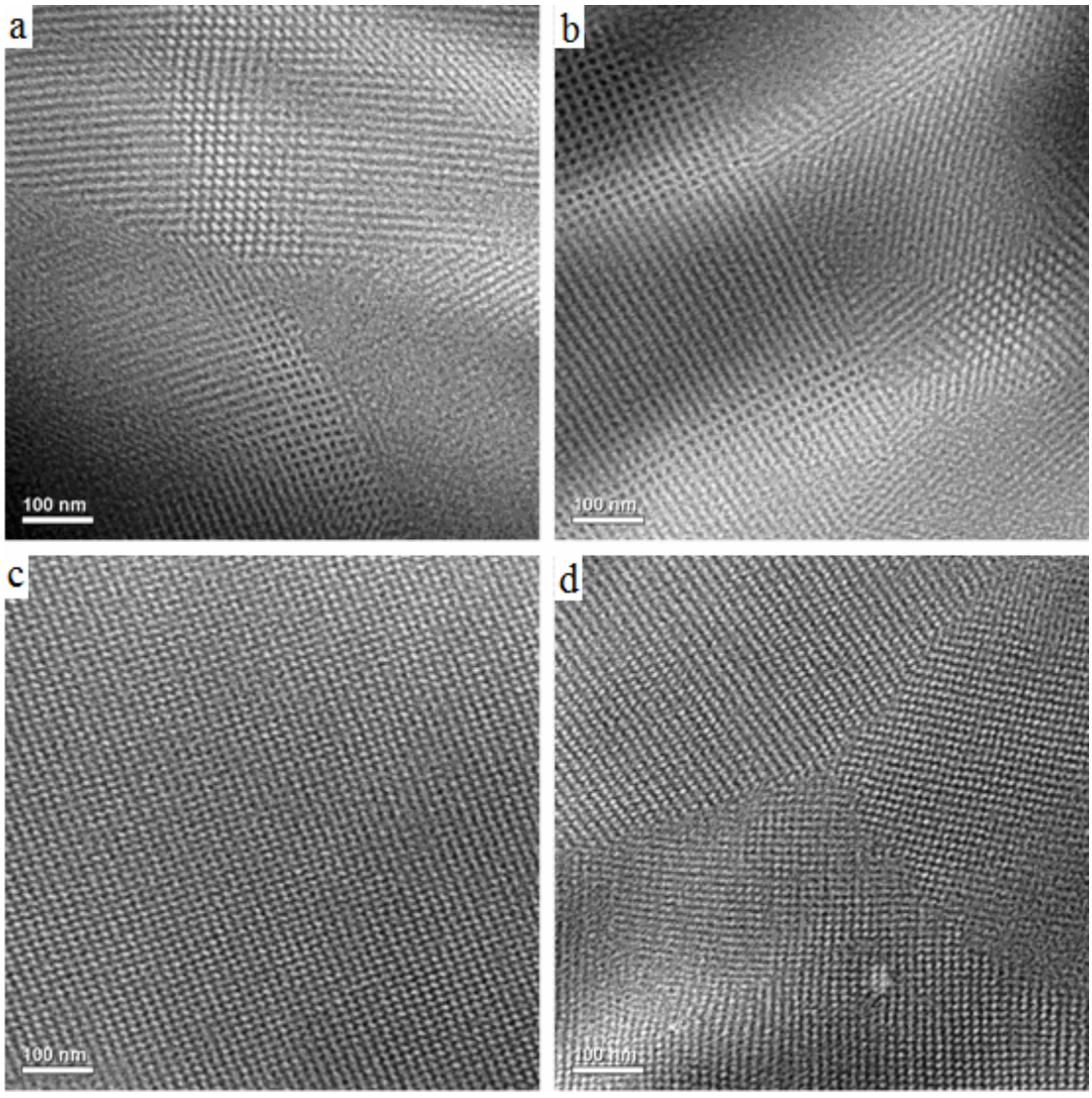

Figure 5-5 Representative TEM micrographs obtained from OsO_4 stained SISO-9 samples after annealing for one day at 120 ^oC. All the scale bars represent 100 nm. All images have regions with the white spherical domains containing a core of the O blocks with either a 3- or 4-fold axis. Panel (a) and (b) have regions of the black spherical domains in a grey matrix with similar domain spacing as the white spherical domains, possibly due to the differences in contrasts under the microscope.

reveals the black and modulated white layers with certain regions showing the dicrete spheres dispersed in a continuous black matrix with a distinct 3-fold symmetry. The other two grains contain the white spherical domains with a 4-fold symmetry, consistent with the assignment of the BCC symmetry.

SISO-11. Synchrotron SAXS data for the SISO-11 samples at various temperatures during the heating process are shown in Figure 5-6. From 120 to 200 ^{o}C, samples exhibit

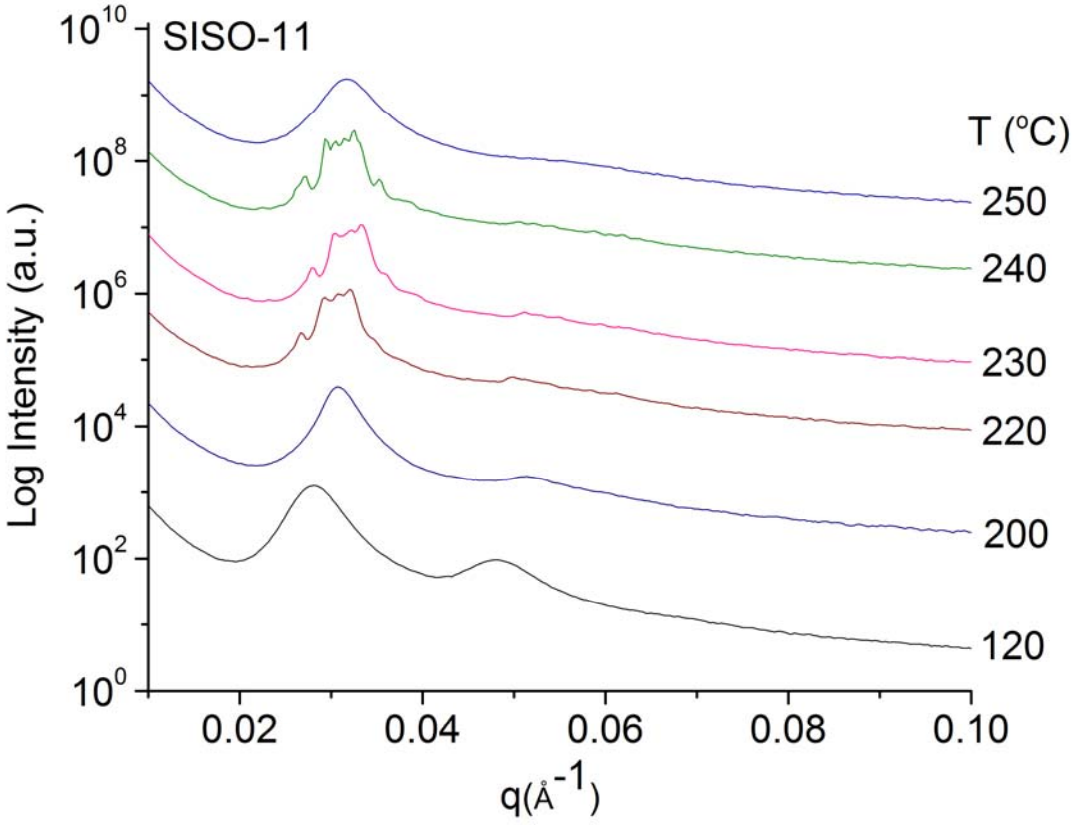

Figure 5-6 Representative synchrotron SAXS data obtained from SISO-11 during the heating process. Liquid-like packing of spheres, QC phase, tetragonal Frank-Kasper σ-phase, and disorder, are identified.

nearly identical SAXS patterns with two broad peaks, indicating limited long-range structural order. We attribute these results to the liquid-like packing of the spheres,[5–12] which are corroborated by the TEM measurements (see Figure 5-8).

At 220 to 230 ^{o}C, the SAXS patterns change dramatically with three closely spaced strong peaks and a weak peak close to this triplet at the position where the primary peak q* is used to be at lower temperatures. Higher order peaks become prominent as well. These peak positions and the relative intensity distribution of the peaks are very similar to the diffraction pattern of the QC phase (see Figure 5-14).[13,14] Upon further heating to 240 ^{o}C, a characteristic scattering pattern consistent with the Frank-Kasper σ-phase[2] is obtained before the sample disorders at 250 ^{o}C with the disappearance of all the Bragg peaks. The single broad scattering peak with its maximum at q* is interpreted as the correlation hole scattering from the disordered sample. The order-disorder transition temperature based on the SAXS data is 245 ± 5 ^{o}C.

Figure 5-7 shows the SAXS patterns obtained during the cooling process for the SISO-11 samples. When the samples were cooled back from the disordered state to 210 ^{o}C, the SAXS patterns consistent with the QC phase are recovered, indicating the QC phase is stable. Upon further cooling to 120 ^{o}C, the samples remain at the QC phase. However, when the samples were cooled directly from the disordered state to 120 ^{o}C, the stable LLP phase is recovered. The LLP phase cannot be recovered upon cooling from 210 ^{o}C after the formation of the QC phase, suggesting the kinetic barrier is too high to overcome.

Representative TEM images for SISO-11 after annealing at 120 ^{o}C for one day are

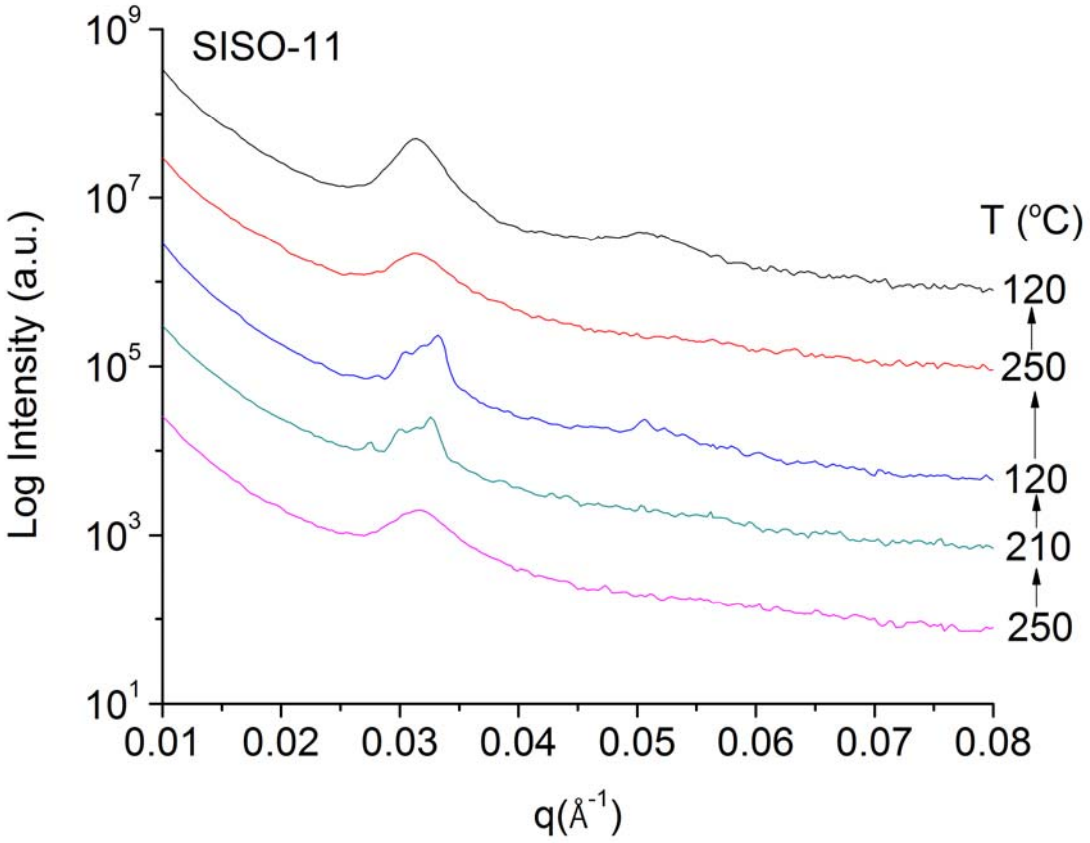

Figure 5-7 Representative synchrotron SAXS data obtained from SISO-11 during the cooling processes. The LLP and the QC phases are obtained upon cooling from the disordered state, indicating these phases are stable. Once the QC phase is obtained at 210 ^{o}C, it remains till further cooling to 120 ^{o}C. However, when the samples are cooled directly to 120 ^{o}C from the disordered state, the LLP phase is obtained.

shown in Figure 5-8. In panel (a), the dark circular regions associated with the I blocks with a bright core of the O blocks and the S shields appear to be dispersed without any long-range order in a grey matrix, possibly a mix of the S and the I blocks. However, close examination reveals certain restricted regions with the short-range micro-domain periodicity as shown in the white box (enlarged in panel (b)). Additional TEM images are

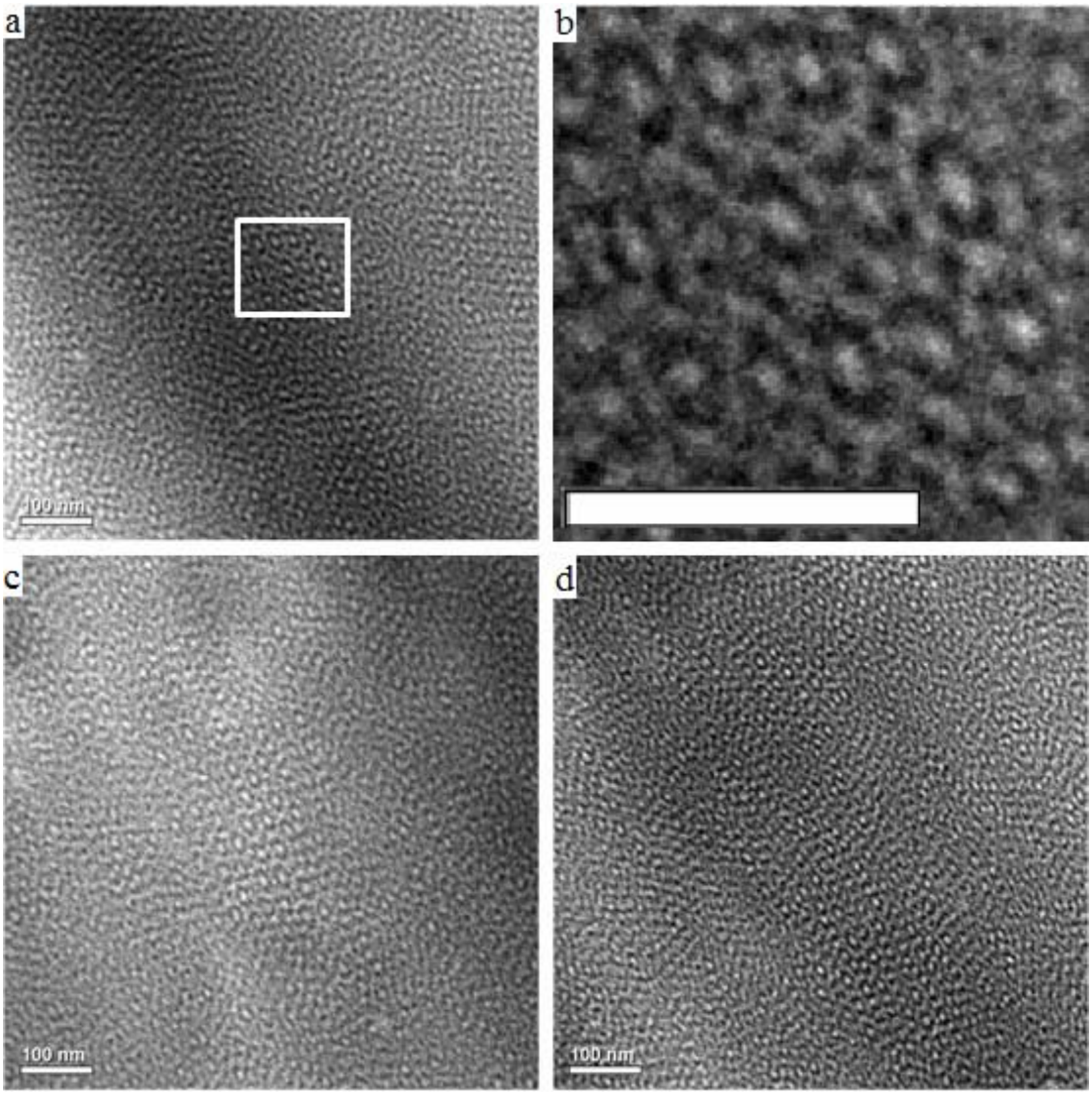

Figure 5-8 TEM micrographs generated from SISO-11 at 120 ^{o}C. The dark regions result from the selective staining of the I blocks with OsO_4. The I domains are microphase separated from the brighter S and O domains, but there is limited long-range order in the specimen. Panel (b) is the magnified view of the area marked with a square in panel (a), displaying the short-range periodic order. All the scale bars denote 100 nm.

shown in panel (c) and (d), both displaying certain regions with the short-range order of the circular domains with the black linings, void of any long-range translational or rotational order, consistent with the assignment of the LLP phase as identified in the SAXS results. Due to the high annealing temperatures and narrow temperature ranges of the QC phase (220 – 230 ^{o}C) and the Frank-Kasper σ-phase (240 ^{o}C), these morphologies could not be trapped in the quenched specimens for TEM analysis.

SISO-15. Synchrotron SAXS data for the SISO-15 samples from 120 to 250 ^{o}C are shown in Figure 5-9. From 120 – 220 ^{o}C, the SAXS data shows two broad peaks, indicating limited long-range structural order, similar to that of SISO-11. We attribute these results to the liquid-like packing of spheres.[5–12] At 240 – 250 ^{o}C, the scattering patterns display peaks at $q/q^{*} = \sqrt{1}, \sqrt{3}$ and $\sqrt{4}$, consistent with a hexagonal symmetry.

Representative TEM images for SISO-15 after annealing at 120 ^{o}C are shown in Figure 5-10. In panel (a), the bright spherical domains on a hexagonal lattice with a diameter of 16 ± 4 nm appear to be dispersed without any long-range order in the dark matrix of the I domains. In panel (b), the wavy white continuous lines arrange in parallel (periodicity = 13 nm) in the dark I matrix without any long-range order, indicating the possibility of limited regions with the hexagonally ordered cylindrical microdomains. However, these hexagonal cylindrical domains do not present the majority of the TEM images (see panel (c)). Instead, the liquid-like packing of the spherical domains with the black linings without any long-range order is observed in most TEM images such as panel (d). Due to the high annealing temperatures and the narrow temperature windows of the hexagonally ordered cylindrical phase (240 – 250 ^{o}C), these morphologies could

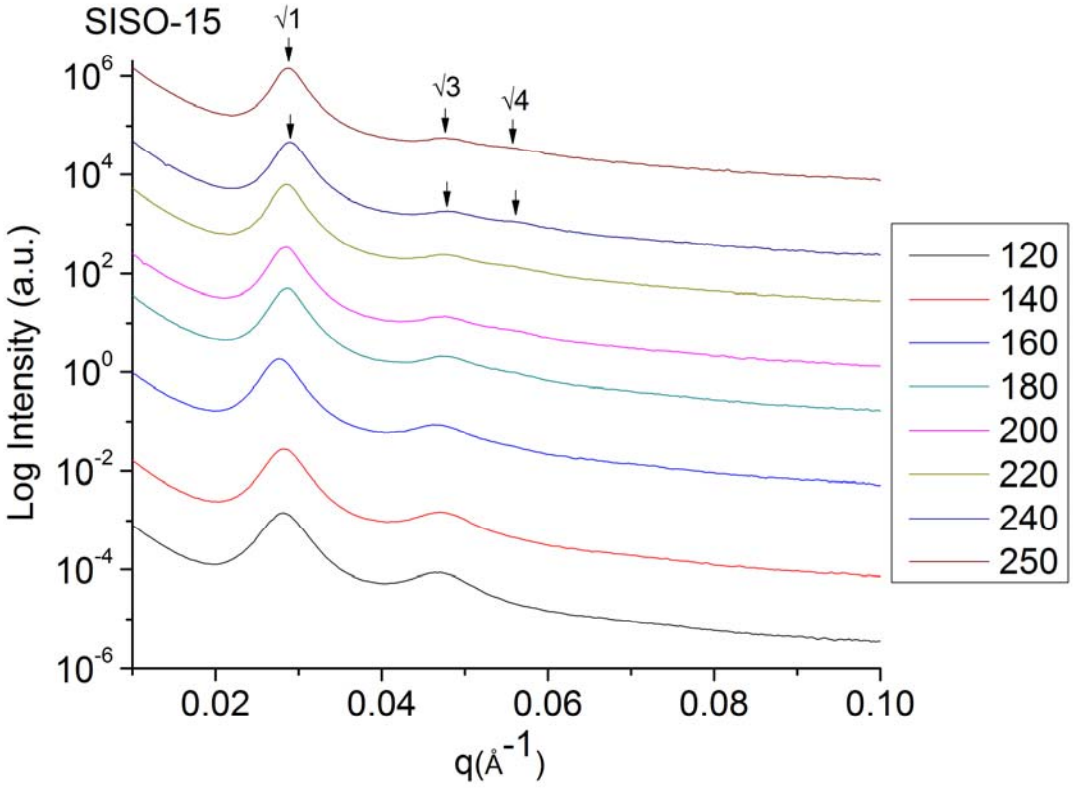

Figure 5-9 Representative synchrotron SAXS data obtained from SISO-15. Liquid-like packing of spheres and hexagonally ordered cylindrical phases are identified with the results at 120 – 220 ^{o}C, and 240 – 250 ^{o}C, respectively. Scattering patterns have been shifted vertically for clarity.

not be trapped in the quenched specimens for TEM analysis.

SISO-31 and SISO-35. Synchrotron SAXS data for SISO-31 at 240 ^{o}C and SISO-35 at 120 ^{o}C are shown in Figure 5-11. For SISO-31, the scattering patterns display peaks at $q/q^{*} = \sqrt{1}, \sqrt{3}$ and $\sqrt{4}$. These peak ratios are consistent with a hexagonal symmetry. The relatively broad peaks signify the limited long-range order. Higher temperature of

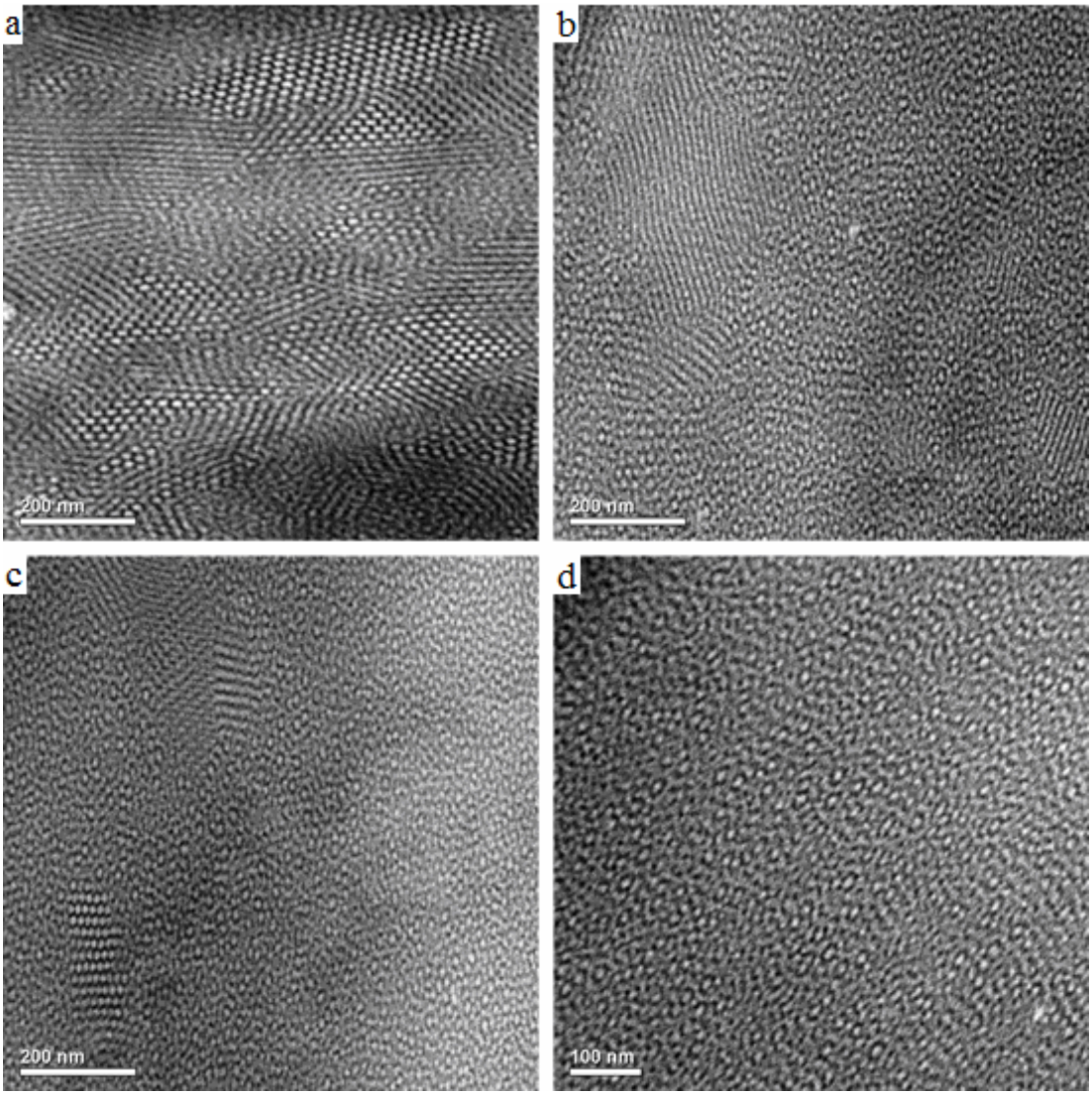

Figure 5-10 TEM micrographs generated from SISO-15 at 120 ^{o}C. The dark regions resulted from selective staining of the I blocks with OsO_4. I domains were microphase separated from the lighter S and O domains, but there was limited long-range order in the specimen. The scale bars denoted 200 nm for panel (a) – (c) and 100 nm for (d), respectively.

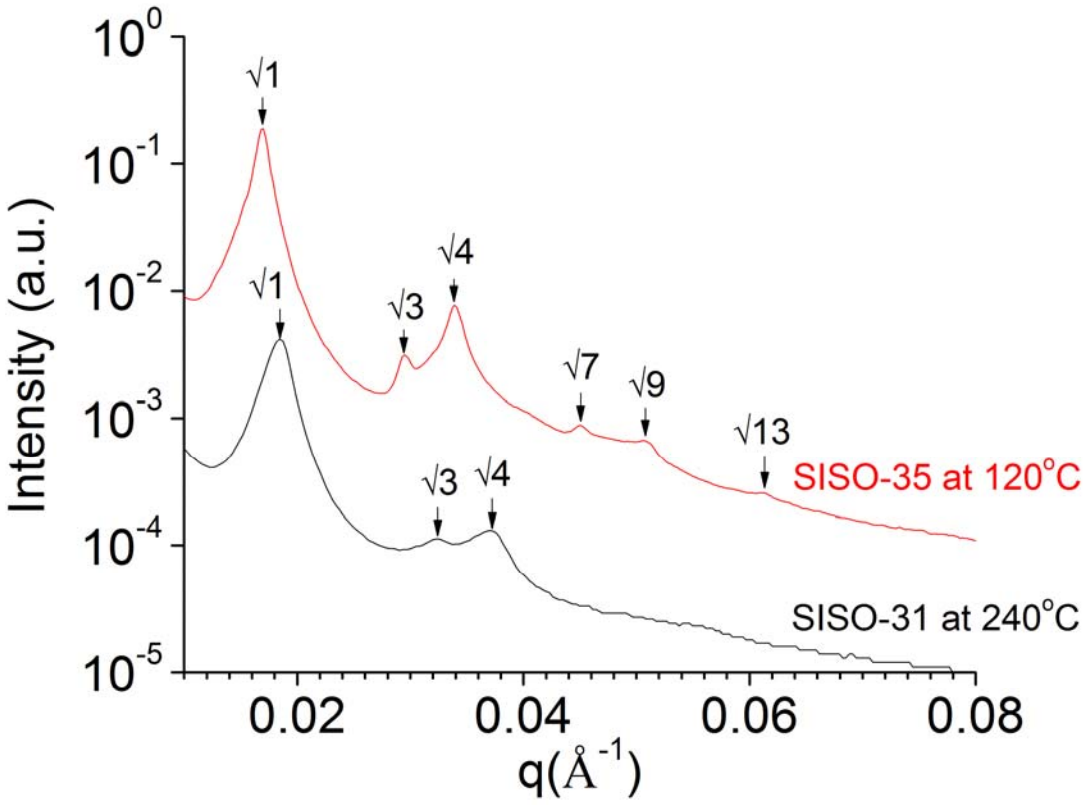

Figure 5-11 Representative synchrotron SAXS data obtained from (bottom) SISO-31 at 240 °C and (top) SISO-35 at 120 °C, respectively. Their Bragg reflections are consistent with a hexagonal symmetry. Scattering patterns have been shifted vertically for clarity.

240 °C is necessary to overcome the kinetic barriers for the polymer chains to arrange into well-defined long-range hexagonal order. For SISO-35, the narrow peaks with ratios at $q/q^* = \sqrt{1}, \sqrt{3}, \sqrt{4}, \sqrt{7}, \sqrt{9}$ and $\sqrt{13}$ are consistent with a hexagonal symmetry. A lower temperature of 120 °C is required to achieve the well-defined long-range order. The primary q* for SISO-35 is lower than that of SISO-31, indicating the larger domain spacing with higher f_O (about 36.9 nm for SISO-35 vs. 33.6 nm for SISO-31).

Figure 5-12 (a) and (b) show the TEM images of SISO-31 after annealing at 240 °C,

and (c) and (d) for SISO-35 after annealing at 120 ^{o}C. SISO-31 samples were annealed at 240 ^{o}C for 3 hours to minimize the degradation of the I blocks and SISO-35 samples are annealed at 120 ^{o}C for a day, prior to quenching into liquid nitrogen to preserve the melt morphologies. Both samples show TEM images consistent with the hexagonal symmetry identified by SAXS and the allowed assignment of the cylindrical phases (orthogonal views of the long axis are shown in panel (a) and (d)). Regions of the S and the O domains are arranged either in the form of the spheres or the cylinders within the continuous I matrix, with SISO-35 displaying longer range of translational order in accordance with its relatively narrow diffraction peaks in SAXS. These results provide the definitive evidence of the inverted phases with the majority constituents (the S and the O blocks) forming spheres and cylinders.

5.3 Discussion

Based on the SAXS and TEM characterization results, the sequence of the phases associated with the styrene-rich channel of the SISO tetrablock terpolymers is: disordered state ($f_O \leq 4\%$), spheres with BCC lattice ($f_O = 9\%$), liquid-like packing of (LLP) spheres ($f_O = 11 - 15\%$) and hexagonally (HEX) ordered cylinders ($f_O = 31 - 35\%$). For SISO samples with $f_O = 11\%$, LLP, QC, σ-phase and the disordered states are formed with increasing temperatures; for SISO with $f_O = 15\%$, the LLP of spheres and the HEX cylinders are formed. Lack of the long-range order in LLP might occur due to slow equilibrium kinetics. Cavicchi and Lodge suggested that the process of forming well-

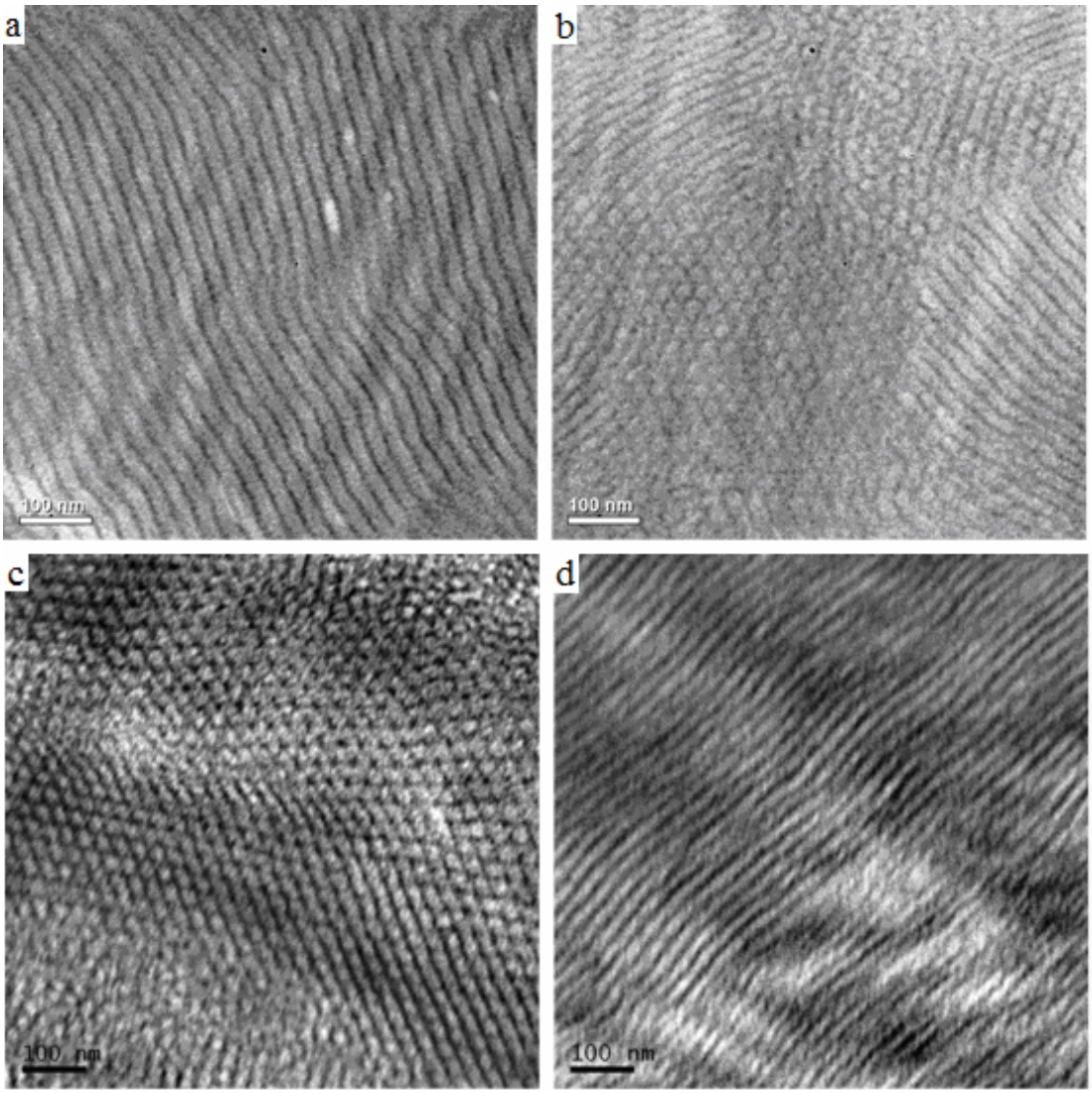

Figure 5-12 TEM micrographs generated (a, b) from SISO-31 at 240 ^{o}C and (c, d) from SISO-35 at 120 ^{o}C. The dark regions resulted from selective staining of the I blocks with OsO_4. Hexagonal packing of unstained S and O blocks with the I matrix was apparent for both samples. (a) and (d) showed the orthogonal view of the long axis of the cylinders for SISO-31 and SISO-35, respectively. All the scale bars denoted 100 nm.

ordered BCC lattice in the sphere-forming block copolymers is hindered by the expulsion and reinsertion of the polymer chains from one sphere into another during the equilibration.[15] The SISO tetrablock molecular architecture exacerbates this process. Annealing at higher temperatures or longer durations is necessary to achieve the well-defined long-range ordered microstructures.

Based on the TEM measurements of the SISO-9 samples, the diameters of the spheres in the regions with a 3-fold axis are 16 ± 3 nm. Figure 5-13 shows the SAXS patterns with the simulated form factor distribution with a sphere diameter of 16 nm. The form factor extinction occurs at the position where the $\sqrt{4}$ peak is expected to appear, explaining its zero intensity, consistent with the assignment of the BCC symmetry to the SISO-9 samples.

Figure 5-14 shows the SAXS patterns for two different samples. The top curve is obtained from one triphenylene functionalized with benzyl ether and phenyl propyl ether dendrons, with the scattering wave vector q labeled at the top horizontal axis. It shows three closely spaced strong peaks and a weak peak close to this triplet with indexing of these planes of reflections. This sample has been identified to be a 12-fold quasicrystalline phase,[14] similar to several other ones.[13,16–18] The bottom curve is the SAXS patterns obtained from the SISO-11 samples after annealing at 220 ^{o}C for about 20 – 30 minutes at the Argonne facility. Its scattering wave vector q is labeled as the bottom horizontal axis. A comparison between these two SAXS patterns shows that they have almost identical peak positions and peak intensities, suggesting that our SISO-11 samples also form the QC phase. One thing noteworthy is the formation of this QC phase occurs

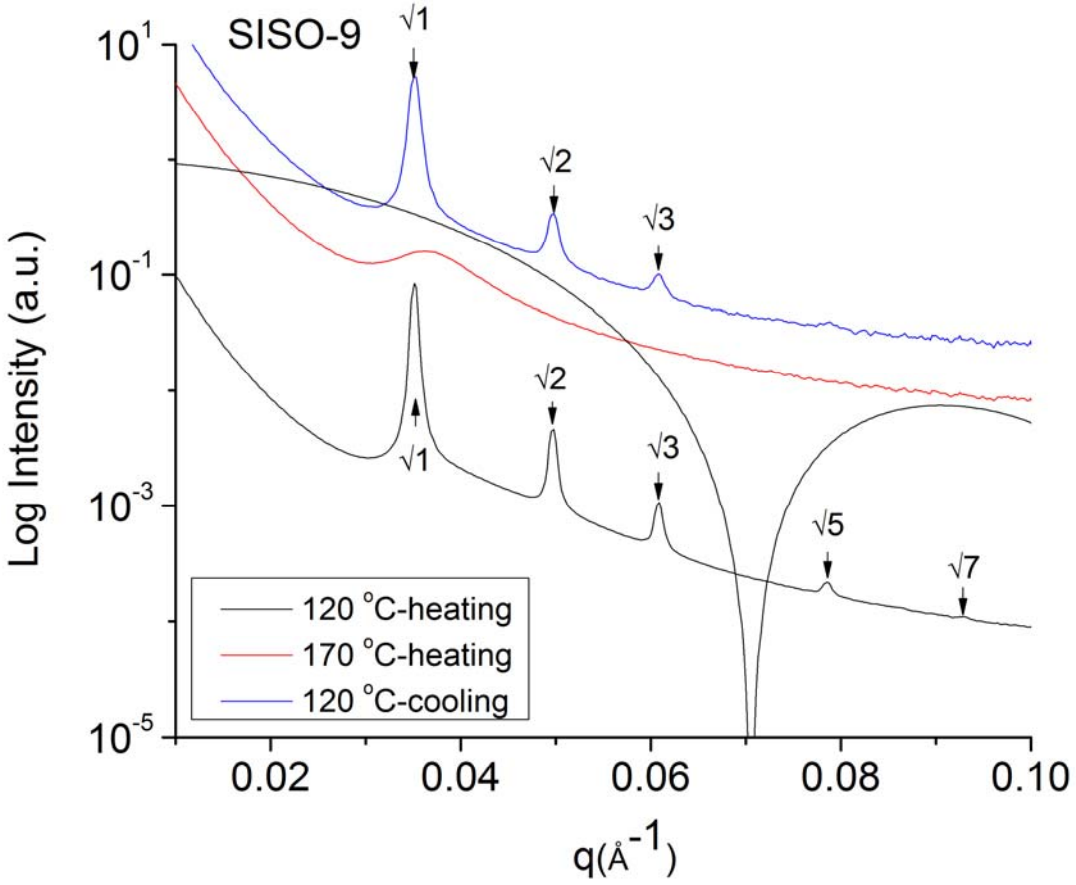

Figure 5-13 Representative synchrotron SAXS data obtained from SISO-9. The black curve is the form factor distribution with a sphere diameter of 16 nm and a spherical volume fraction of 29%.

right below the formation temperature of the Frank-Kasper σ-phase, i.e., $T_{QC} < T_{\sigma} < T_{disorder}$, similar to the temperature dependence of the isoprene-rich SISO-2 samples discussed in Chapter 4.

The percent crystallinities of the samples are listed in Table 5-1 (the experimental results are shown in the appendix of this chapter), increasing with the increasing f_Os.

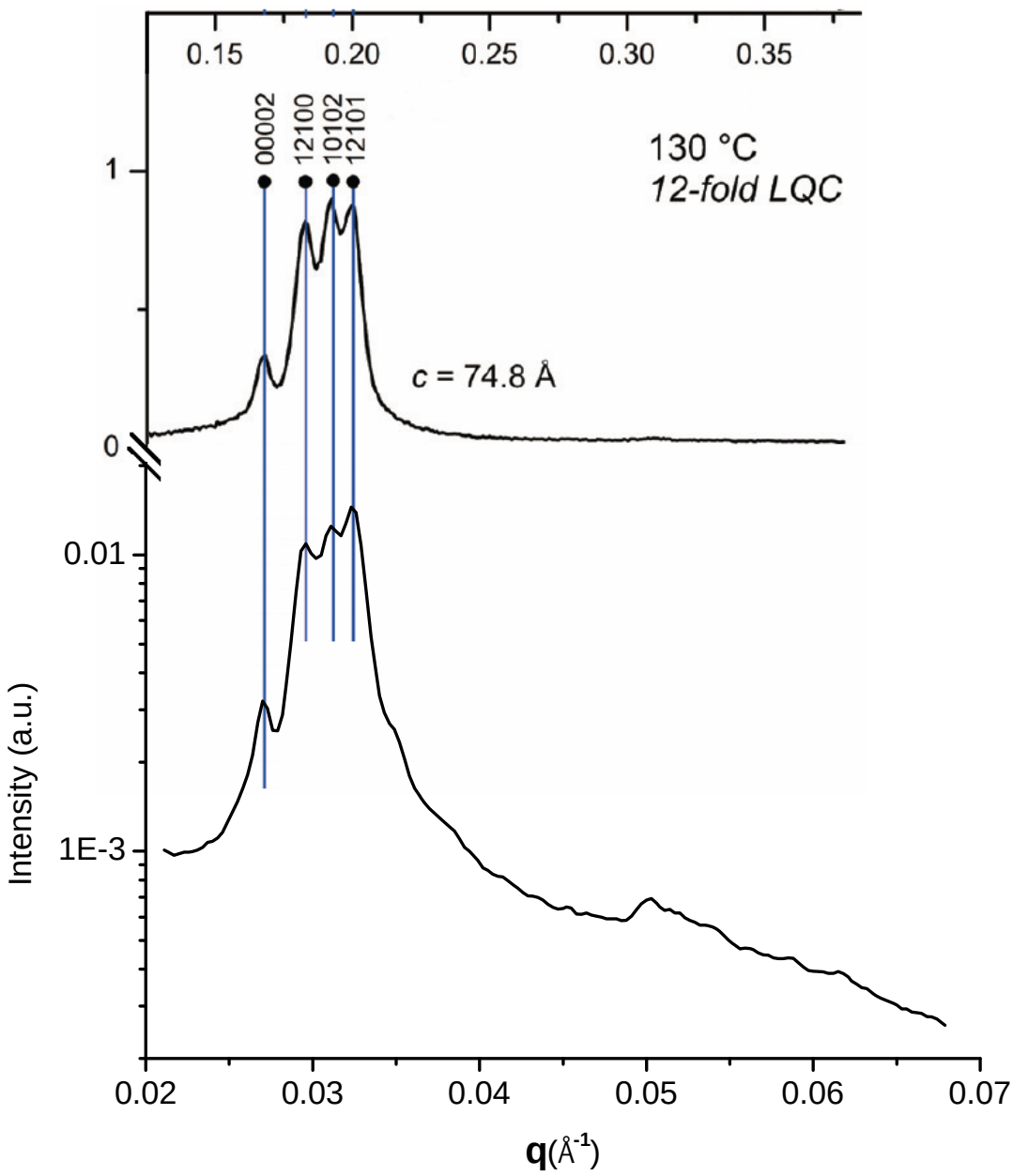

Figure 5-14 SAXS patterns for (top) one triphenylene functionalized with benzyl ether and phenyl propyl ether dendrons which has already been identified as the 12-fold QC phase, with q labeled at the top axis;[14] (bottom) the SISO-11 samples which show almost identical phase positions and the intensities with q labeled at the bottom axis, suggesting that SISO-11 forms the QC phase after annealing at 220 ^{o}C.

These DSC results suggest that the core-shell spheres[3,4] and cylinders[1] are formed in the ordered states. A significant increase in the amount of the cystallinity from 0% in the disordered SISO-4 samples to 27% in the ordered SISO-9 samples with the BCC lattice indicates that the S and the O blocks at least partial segregated. In the HEX cylindrical phases, the amount of crystallinity ranges from 52 to 74 %, similar to those values reported in the series of ISO triblock terpolymers with the well-segregated O domains.[19] It is possible that the S blocks mixed with the O blocks at elevated temperatures with decreasing enthalpic penalty between these blocks. Order-order transitions from the 'three-domain' to the 'two-domain' structures have been reported in several ABC triblock terpolymer systems.[20–22]

The morphologies of the SISO tetrablock terpolymers differ dramatically from the morphologies of the ISO triblock counterparts containing comparable compositions and molecular weights. Figure 5-15 (a) displays the various phases reported in the ISO triblock terpolymers.[23,24] Overall, clusters of common phases with similar compositions reflect certain ordering tendencies. Lamellae (LAM) dominates the central portion extending from the left to the right across the entire phase map, i.e., from the symmetric IO diblocks to the symmetric SO diblocks. Network morphologies of the double gyroid (Q^{230}), the alternating gyroid (Q^{214}) and the *Fddd* orthorhombic structure (O^{70}) appear in both the O-lean and the O-rich regions, with Q^{214} more concentrated in the O-lean, S-rich region, Q^{230} more concentrated in the O-lean, I-rich region and O^{70} towards the IS boundary. The hexagonally ordered cylindrical phase (HEX) is evident in three locations: the I-rich, O-rich and S-rich. The BCC symmetry is found in two samples with relatively

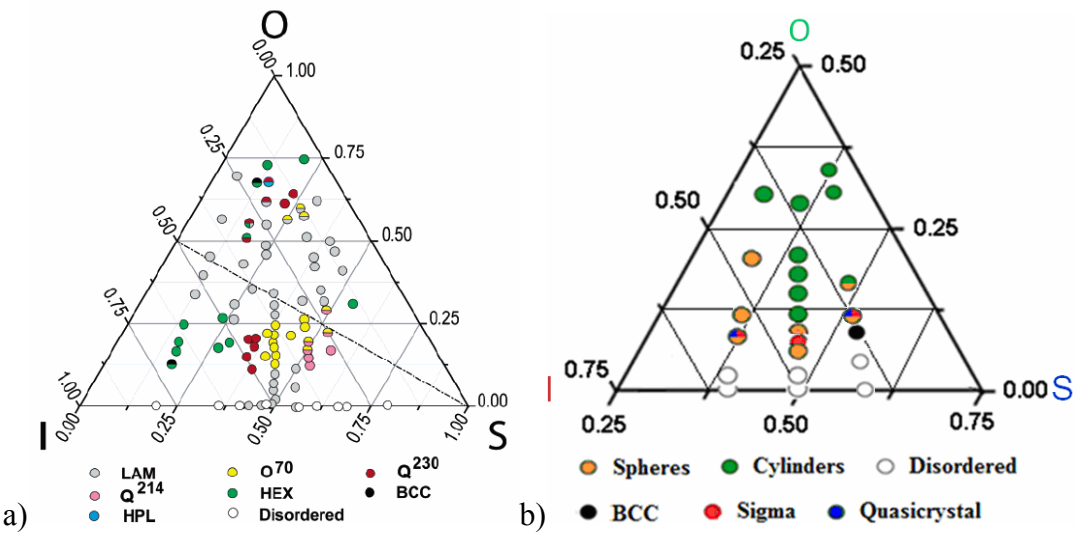

Figure 5-15 (a) The phase map for the ISO triblocks with the axes representing the volume fractions of each block in the vicinity of the order-disorder transition. The filled and open circles indicate the ordered and the disordered states, respectively, within the experimental temperature range of $90 \leq T \leq 250$ °C. Samples with OOT are represented with two different colors with the upper half showing the higher temperature state. The dashline represents the $f_I = f_O$ isopleth. Reproduced from Chatterjee *et al.*.[23] (b) SISO phase portrait within $110 \leq T \leq 250$ °C. Reproduced from Figure 5-2 for easy comparison.

low f_S, at high and low f_I, sandwiched between the HEX and the disordered states.

Figure 5-15 (b) shows the various morphologies observed in the SISO tetrablock terpolymers.[1–4] The disorder, spherical and cylindrical phases are formed with increasing f_Os for all three composition channels. The spheres with the (simple) hexagonal symmetry (P_6/mmm) are evident in the I-rich region and the liquid-like packing of spheres are concentrated on the S-rich region and the IS boundary. The BCC symmetry is found in one sample in the S-rich region. The dodecagonal quasicrystalline phase is found in two

samples: I-rich and S-rich, sandwiched between the simple hexagonal symmetry (I-rich) or the LLP (S-rich) and the Frank-Kasper σ-phase, respectively. The Frank-Kasper σ-phase is found in three channels with similarly low f_Os (= 8 – 11 %). The hexagonally ordered cylindrical phase is common for all channels with high f_Os.

In the SISO tetrablock system, the morphologies presented in the ISO triblocks such as the two-domain, three-domain LAM, and the network morphologies (Q^{230}, Q^{214} and O^{70} with *Fddd* orthorhombic symmetry) are not reported; instead, the core-shell spheres and cylinders are documented across the entire phase map developed so far. The interfacial curvature increases from the LAM to the network to the core-shell morphologies. For the ABC triblocks with the symmetric AB diblocks and a small amount of the C block, the two-domain LAM are reported and with similar volume fractions among these three blocks, the three-domain LAM are formed with zero interfacial curvature. With an intermediate amount of the C block addition to the symmetric AB diblocks, the network morphologies are prevalent evidenced in the case of the ISO triblocks,[19,23–28] as well as many other ABC triblock systems.[29–39] While the symmetric A and B blocks prefer the flat interfaces, an intermediate amount of the C block addition favours the B/C interfaces with certain spontaneous curvature, creating competing packing constraints. Negative interfacial Gauss curvature found in network morphologies satisfies both conditions simultaneously under the constraint of constant density, driving the formation of the three-dimensional network morphologies. Changing the molecular architecture from the ISO triblocks to the SISO tetrablocks drives a preference from the hyperbolic interfaces inherent in the network morphologies to the

higher, and zero Gauss, curvature surfaces present in the spheres and the cylinders.

The core-shell cylindrical morphology is preferred even when f_O approaches f_I and f_S in all three channels presented in the SISO phase map. Similar inverted cylindrical phases have been identified in the SIO triblocks,[40] poly(isoprene-*b*- styrene-*b*-dimethylsiloxane)[21] and diblock/triblock copolymer blends,[41] in which the segment-segment interaction parameters are asymmetric ($\chi_{BC} > \chi_{AB} \approx \chi_{AC}$), but not in ISO ($\chi_{AC} > \chi_{AB} \approx \chi_{BC}$). In SISO, even though $f_S = f_I$, the S blocks are divided into half. With the terminal S blocks having the freedom to fill space and release entropic tension, SISO tetrablocks behave similarly to the ISO triblocks with shorter S blocks in terms of morphologies behaviours and should resemble the S-lean region of the ISO phase map, consistent with the phase behaviours shown in Figure 5-15.

5.4 Conclusion

In conclusion, the spheres with the BCC, LLP, QC, Frank-Kasper σ-phase and cylinders with hexagonal lattice have been identified in the bulk S-rich SISO tetrablock terpolymers. The core (O) – shell (S) domain geometries are formed in both spheres and cylinders with the asymmetric distributions of the internal and the terminal S blocks within the core, the shell and the matrix. The SISO tetrablock terpolymers exhibit different phase behaviours as the ISO counterparts with similar compositions, molecular weights and segregation strengths. While ISO samples form the network morphologies over a wide range of compositions, the SISO samples form the core-shell spheres and

cylinders. Molecular architecture plays a key role in the block copolymers phase behaviours.

5.5 References

(1) Bluemle, M. J.; Zhang, J.; Lodge, T. P.; Bates, F. S. *Macromolecules* **2010**, *43*, 4449.

(2) Lee, S.; Bluemle, M. J.; Bates, F. S. *Science* **2010**, *330*, 349.

(3) Zhang, J.; Scott, S. W.; Bates, F. S. *Macromolecules* **2012**, *45*, 256.

(4) Zhang, J.; Bates, F. S. *Journal of the American Chemical Society* **2012**, *134*, 7636.

(5) Kinning, D. J.; Thomas, E. L. *Macromolecules* **1984**, *17*, 1712.

(6) Winey, K. I.; Thomas, E. L.; Fetters, L. J. *Macromolecules* **1992**, *25*, 2645.

(7) Schwab, M.; Stuehn, B. *Physical Review Letters* **1996**, *76*, 924.

(8) Adams, J. L.; Quiram, D. J.; Graessley, W. W.; Register, R. A.; Marchand, G. R. *Macromolecules* **1996**, *29*, 2929.

(9) Sakamoto, N.; Hashimoto, T.; Han, C. D.; Kim, D.; Vaidya, N. Y. *Macromolecules* **1997**, *30*, 1621.

(10) Han, C. D.; Vaidya, N. Y.; Kim, D.; Shin, G.; Yamaguchi, D.; Hashimoto, T. *Macromolecules* **2000**, *33*, 3767.

(11) Dormidontova, E. E.; Lodge, T. P. *Macromolecules* **2001**, *34*, 9143.

(12) Wang, X.; Dormidontova, E. E.; Lodge, T. P. *Macromolecules* **2002**, *35*, 9687.

(13) Zeng, X.; Ungar, G.; Liu, Y.; Percec, V.; Dulcey, A. E.; Hobbs, J. K. *Nature* **2004**, *428*, 157.

(14) Percec, V.; Imam, M. R.; Peterca, M.; Wilson, D. A.; Graf, R.; Spiess, H. W.; Balagurusamy, V. S. K.; Heiney, P. A. *The Journal of American Chemical Society* **2009**, *131*, 7662.

(15) Cavicchi, K. A.; Lodge, T. P. *Journal of Polymer Science Part B: Polymer Physics* **2003**, *41*, 715.

(16) Percec, V.; Ahn, C.-H.; Ungar, G.; Yeardley, D. J. P.; Moller, M.; Sheiko, S. S. *Nature* **1998**, *391*, 161.

(17) Rosen, B. M.; Wilson, D. A.; Wilson, C. J.; Peterca, M.; Won, B. C.; Huang, C.; Lipski, L. R.; Zeng, X.; Ungar, G.; Heiney, P. A.; Percec, V. *The Journal of the American Chemical Society* **2009**, *131*, 17500.

(18) Ungar, G.; Liu, Y.; Zeng, X.; Percec, V.; Cho, W. D. *Science* **2003**, *299*, 1208.

(19) Bailey, T. S.; Hardy, C. M.; Epps III, T. H.; Bates, F. S. *Macromolecules* **2002**, *35*, 7007.

(20) Neumann, C.; Abetz, V.; Stadler, R. *Polymer Bulletin* **1996**, *36*, 43.

(21) Hardy, C. M.; Bates, F. S.; Kim, M.-H.; Wignall, G. D. *Macromolecules* **2002**, *35*, 3189.

(22) Hashimoto, T.; Yamauchi, K.; Yamaguchi, D.; Hasegawa, H. *Macromolecular Symposia* **2003**, *201*, 65.

(23) Chatterjee, J.; Jain, S.; Bates, F. S. *Macromolecules* **2007**, *40*, 2882.

(24) Epps III, T. H.; Cochran, E. W.; Bailey, T. S.; Waletzko, R. S.; Hardy, C. M.;

Bates, F. S. *Macromolecules* **2004**, *37*, 8325.

(25) Epps III, T. H.; Cochran, E. W.; Hardy, C. M.; Bailey, T. S.; Waletzko, R. S.; Bates, F. S. *Macromolecules* **2004**, *37*, 7085.

(26) Cochran, E. W.; Bates, F. S. *Physical Review Letters* **2004**, *93*, 087802.

(27) Bluemle, M. J.; Fleury, G.; Lodge, T. P.; Bates, F. S. *Soft Matter* **2009**, *5*, 1587.

(28) Tyler, C. A.; Qin, J.; Bates, F. S.; Morse, D. C. *Macromolecules* **2007**, *40*, 4654.

(29) Bates, F. S.; Fredrickson, G. H. *Physics Today* **1999**, *52*, 32.

(30) Breiner, U.; Krappe, U.; Abetz, V.; Stadler, R. *Macromolecular Chemistry and Physics* **1997**, *198*, 1051.

(31) Huckstadt, H.; Goldacker, T.; Gopfert, A.; Abetz, V. *Macromolecules* **2000**, *33*, 3757.

(32) Huckstadt, H.; Gopfert, A.; Abetz, V. *Polymer* **2000**, *41*, 9089.

(33) Mogi, Y.; Nomura, M.; Kotsuji, H.; Ohnishi, K.; Matsushita, Y.; Noda, I. *Macromolecules* **1994**, *27*, 6755.

(34) Seki, M.; Sujuki, J.; Matsushita, Y. *Journal of Applied Crystallography* **2000**, *33*, 285.

(35) Suzuki, J.; Seki, M.; Matsushita, Y. *Journal of Chemical Physics* **2000**, *112*, 4862.

(36) Avgeropoulos, A.; Paraskeva, S.; Hadjichristidis, N.; Thomas, E. L. *Macromolecules* **2003**, *35*, 4030.

(37) Shefelbine, T. A.; Vigild, M. E.; Matsen, M. W.; Hajduk, D. A.; Hillmyer, M. A.; Cussler, E. L.; Bates, F. S. *Journal of the American Chemical Society* **1999**,

121, 8457.

(38) Mogi, Y.; Mori, K.; Matsushita, Y.; Noda, I. *Macromolecules* **1992**, *25*, 5412.

(39) Matsen, M. W. *The Journal of Chemical Physics* **1998**, *108*, 785.

(40) Bailey, T. S.; Pham, H. D.; Bates, F. S. *Macromolecules* **2001**, *34*, 6994.

(41) Goldacker, T.; Abetz, V. *Macromolecules* **1999**, *32*, 5165.

6

Phase Behavior of the Asymmetric SIS'O Tetrablock Terpolymers

6.1 Introduction

Block copolymers receive great research attention because they can self-assemble into various ordered periodic morphologies at a nanometer scale of 5 – 100 nm.[1] Furthermore, polymer scientists can precisely control the parameters of the model systems to explore and ultimately manipulate the resulting morphologies. The most important and conventional parameters that can influence the block copolymer phase

behaviours are f, χ and N, where f is the volume fraction, χ is the Flory-Huggins interaction parameter, and N is the total degree of polymerization.[2,3] These influences are already well captured in the simplest AB diblock molecular architecture.[4–6] As the asymmetry (measured by f in the case of the AB diblocks) increases, the spontaneous curvature produces the usual transition from the lamellar (L), the gyroid (G), the cylindrical (C), and the spherical (S) morphologies.

As the molecular architecture changes from the AB diblocks to the symmetric ABA triblocks (A blocks are divided equally), the phase behaviours are nearly identical.[7,8] Even though more complicated chain configurations such as bridge and loop occur,[9–11] they mainly affect the mechanical properties,[12–16] but not the phase behaviours. The ABA triblocks are expected to have higher T_{ODT}s theoretically due to the likelihood of the penetration of the longer B block in the A domains,[8–10,17,18] which is confirmed experimentally.[12–16,19–21] Because of the same reason, the phase diagram of the ABA triblocks becomes more asymmetric as f_A increases.[22]

Another parameter of the asymmetry τ comes into effect when we examine the asymmetric ABA' triblock copolymers (A blocks are of different lengths) with the asymmetric parameter $\tau = N_A/(N_A+N_{A'})$. As τ changes from 0.5 to 0, i.e., the asymmetry increases, two new effects are introduced: first, the elastic energy of the A domains decreases; second, high asymmetry pulls the short A blocks into the B domain, lowering their stretching energies. These two factors significantly increase the domain size, influence packing frustration and cause large shifts in the phase boundaries.[22] Since the AB diblocks are better ordered than the symmetric ABA triblocks of the same molecular

weight, the ordered region is wider as the asymmetry parameter decreases, especially when χN is small. The phase behavior of the asymmetric ABA triblocks is dominated by the usual L, G, C and S morphologies, but the S_{cp}, as opposed to the normal BCC packing, is predicted to present in an unusually large region by the self-consistent field theory (SCFT) at intermediate τ and small f_A.

To the best of the author's knowledge, the asymmetric effect on the ABA'C tetrablock terpolymers has not received any research attention, with the only limited attention focusing on the diblock[23–29] and triblock[22,30] systems. In Chapter 3 – 5, we have demonstrated the important effect of the volume fraction *f* on the phase behavior of the symmetric ABAC tetrablock terpolymer (A blocks are divided equally), using poly(styrene-*b*-isoprene-*b*- styrene-*b*-ethylene oxide) (SISO) as the model system, i.e., x = x' in Figure 6-1 (a). In the sphere-forming symmetric SISO samples, the core-shell spheres are formed with the O blocks being the core and the S blocks being the shell, in a matrix of the I and the S blocks ($T_{g,I} \approx -70\ ^oC$), as shown in Figure 6-1 (b). In this chapter, we keep the conventional parameters such as *f*, χ and *N* constant and study the effect of the asymmetry alone on the tetrablock terpolymer phase behaviours. The asymmetric parameter τ is defined as $N_S/(N_S+N_{S'})$. For the ISO triblocks, $\tau = 0$; for the symmetric SISO tetrablocks, $\tau = 0.5$; for the SIO triblocks, $\tau = 1$. By changing $0 \leq \tau \leq 1$, we can control the asymmetry.

In the ISO triblocks with $\tau = 0$, $\chi_{IO} >> \chi_{IS} \approx \chi_{SO}$, the repulsion between the I and the O blocks is the greatest as compared to the S/O and S/I pairs. Since the I and the O blocks are not directly bonded, the I/O interface is unlikely to form in order to minimize chain

packing frustrations. We call this type of system 'nonfrustrated'.[31–38] In the nonfrustrated ABC triblock systems, two interfaces of A/B and B/C balance the interfacial strengths to accommodate two equally important contributions to the free energy.[36] In the 'frustrated' SIO triblocks with $\tau = 1$, the I/O interface is mandatory due to the covalent bonding between the I and the O blocks, leading to the formation of three interfaces.[31,39–43] With comparable volume fractions and similar molecular weights, both the nonfrustrated ISO[45] and the frustrated SIO[47] triblock terpolymers form the lamellar phase with two and three interfaces, respectively.

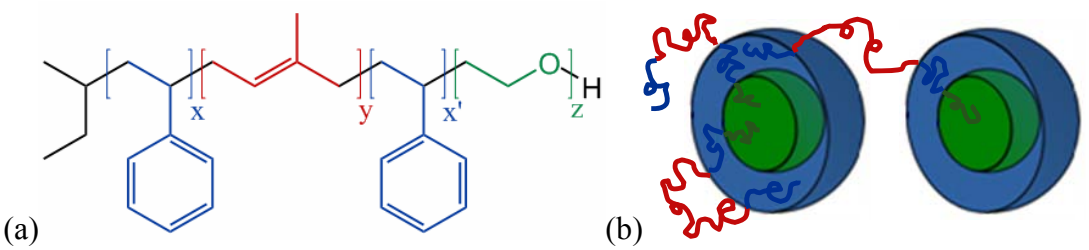

Figure 6-1 (a) Molecular structure of SIS'O tetrablock terpolymers. (b) core-shell spherical morphology. Unfavorable interactions between the O (core) and I (matrix) blocks are screened by S blocks (shell).

By altering the asymmetric parameter τ in the SIS'O tetrablock terpolymers, we can monitor how the morphological changes are taking place from the nonfrustrated ISO to the frustrated SIO triblock systems. In this chapter, we synthesize a series of the asymmetric SIS'O tetrablock terpolymers ($\tau = 0.21 – 0.70$) and characterize the resulting morphologies with SAXS, TEM and DMS. The focus is on the SIS'O samples containing equal volume fractions of the S and I blocks with lower f_Os (= 7 – 19 %), near the

composition window where the interesting spherical morphologies such as the (simple) hexagonal,[44] the dodecagonal quasicrystalline,[45] the Frank-Kasper σ-phase,[45,46] the liquid-like packing of spheres[47] and the BCC symmetries are reported in the symmetric SISO samples.[44–47] These results presented in this chapter expand our understanding of the fundamental phase behavior of the block copolymers.

6.2 Experimental Section

Polymer Synthesis. All the SIS'O tetrablock terpolymers are targeted to have the same molecular weight and volume fraction. The only difference is the ratio between the lengths of the first S and the second S' blocks. The SIS'-OH triblocks were synthesized via a living anionic polymerization method. For the subsequent addition of the O blocks, three reactors were set up simultaneously, each containing a small amount (5 g) of the same SIS'-OH triblock, to ensure that at least one of the SIS'O samples contains the desired f_Os, due to the inconsistent yield of the O block addition. The detailed reaction scheme and strategies are described elsewhere.[38,40,48,49]

6.3 Results and Analysis

Six asymmetric SIS'O tetrablock terpolymers with similar molecular weights and volume fractions, and the asymmetric parameter τ ranging from 0.21 to 0.70, were synthesized. The molecular characterization data, morphology assignments based on a

combination of SAXS, TEM, and DMS, together with the T_{ODT}'s determined by SAXS are listed in Table 6-1.

SIS'O-0.21 and SIS'O-0.32. Synchrotron SAXS data for the SIS'O-0.21 samples and the SIS'O-0.32 samples at various temperatures during the heating process are shown in Figure 6-2 (a) and (b), respectively. The samples were annealed under vacuum at 120 ^{o}C for one day, followed by a liquid nitrogen quench to preserve the morphologies. At the synchrotron facility at Argonne, the samples were reheated and annealed at specific temperatures for 5 – 10 minutes before the measurements were taken every five minutes until there were no further changes. The same procedures were carried out for the SIS'O-0.39, -0.61 and -0.70 samples.

Throughout the temperature window of 100 – 250 ^{o}C for SIS'O-0.21 and 100 – 150 ^{o}C for SIS'O-0.32, the scattering patterns display peaks at $q/q^{*} = \sqrt{1}, \sqrt{3}$ and $\sqrt{4}$ with q*

Table 6-1 SIS'O Characterization Data.

Sample	τ	*Mn*/kDa	PDI	f_S[a]	f_I[a]	f_O[a]	Phase[b]	T_{ODT}/^{o}C[d]
SISO-0.21	0.21	19.7	1.04	0.40	0.44	0.16	HEX	>250
SISO-0.32	0.32	19.1	1.07	0.48	0.46	0.07	HEX	153
SISO-0.39	0.39	17.0	1.04	0.46	0.47	0.07	HEX,σ	130
SISO-0.50[c]	0.50	23.0	1.04	0.46	0.46	0.08	LLP,σ	224
SISO-0.61	0.61	24.2	1.05	0.45	0.46	0.09	LLP, QC,σ	177
SISO-0.70	0.70	20.7	1.14	0.43	0.45	0.12	QC,σ	177

[a]Volume fractions calculated with from densities at 140 ^{o}C. [b]HEX-hexagonally packed spheres for SISO-0.21, -0.32 and -0.39. [c]Detailed characterization for this sample could be found elsewhere.[ref] [d]Order-disorder transition temperatures were determined by small-angle x-ray scattering for all samples and confirmed with dynamic mechanical spectroscopy.

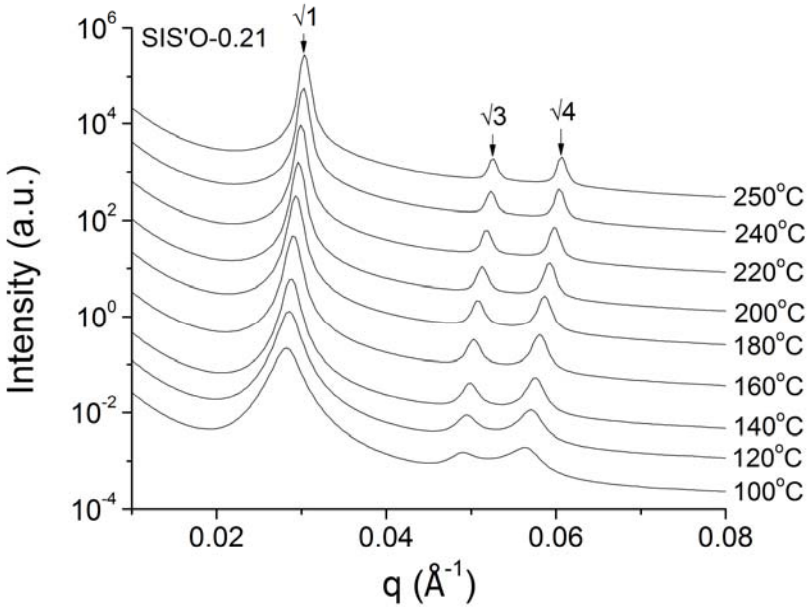

(a)

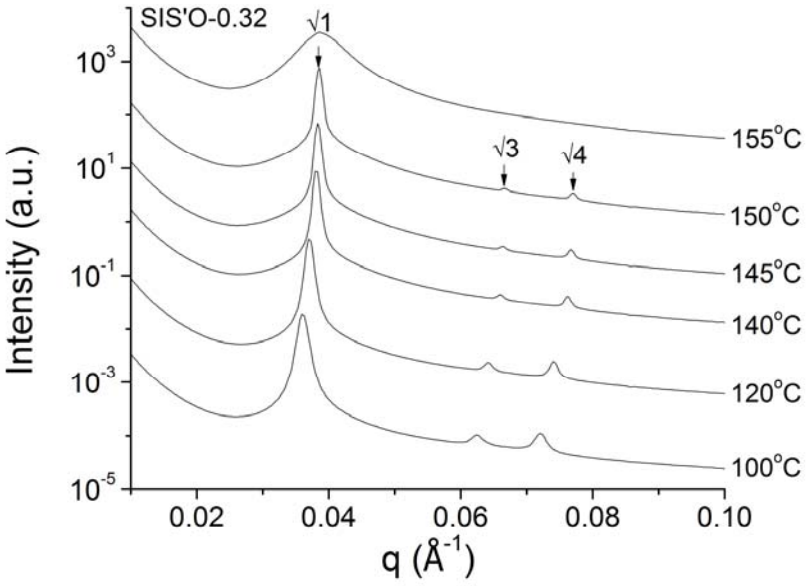

(b)

Figure 6-2 Synchrotron SAXS data for the asymmetric (a) SIS'O-0.21 and (b) SIS'O-0.32 tetrablock copolymers with equal volume fractions of the S and the I blocks respectively. The arrows identify the relative peak positions associated with a hexagonal symmetry. Scattering patterns have been shifted vertically for clarity.

being the principal peak location. These peak ratios are consistent with a hexagonal symmetry. Their primary q* values increase with temperatures, indicating their domain spacing decreases. At 155 ^{o}C, the SIS'O-0.32 samples display a single broad scattering peak with a maximum at q*, indicating the sample is disordered. Its order-disorder transition temperature based on the SAXS is 153 ± 3 ^{o}C.

While the SAXS data provide the long-range ordered hexagonal symmetry, the TEM images allow us to characterize the detailed morphological information, i.e. whether they are the spheres or the cylinders (see Figure 6-3). The SIS'O samples were annealed in a vacuum oven for 1 day at 120 ^{o}C for SIS'O-0.21, and at 140 ^{o}C for SIS'O-0.32, prior to quenching into liquid nitrogen to preserve the melt morphologies. Panel (a) and (b) are generated from SIS'O-0.21, and panel (c) and (d) are generated from SIS'O-0.32. All four panels exhibit array of spherical domains that are associated with the bright S and O blocks. There is no evidence of cylinders. At the bottom of panel (d), the spheres arrange into a well-ordered pattern with a six-fold symmetry. As the grain tilts away from the electron beam under the microscope, we see the projection of the black and modulated white layers.

The specimen thickness is about 60 nm, more than three times of the domain spacing (about 17 nm for both SIS'O-0.21 and -0.32), i.e., there are at least three layers of the spheres in depth in each specimen. At the bottom of the panel (a) and (d), as well as the majority region of the panel (b) and (c), the clear and sharp boundaries between the bright spheres and the dark matrix are observed, suggesting the formation of the simple hexagonal lattice with a P_6/mmm (No.191) space group symmetry. This assignment is

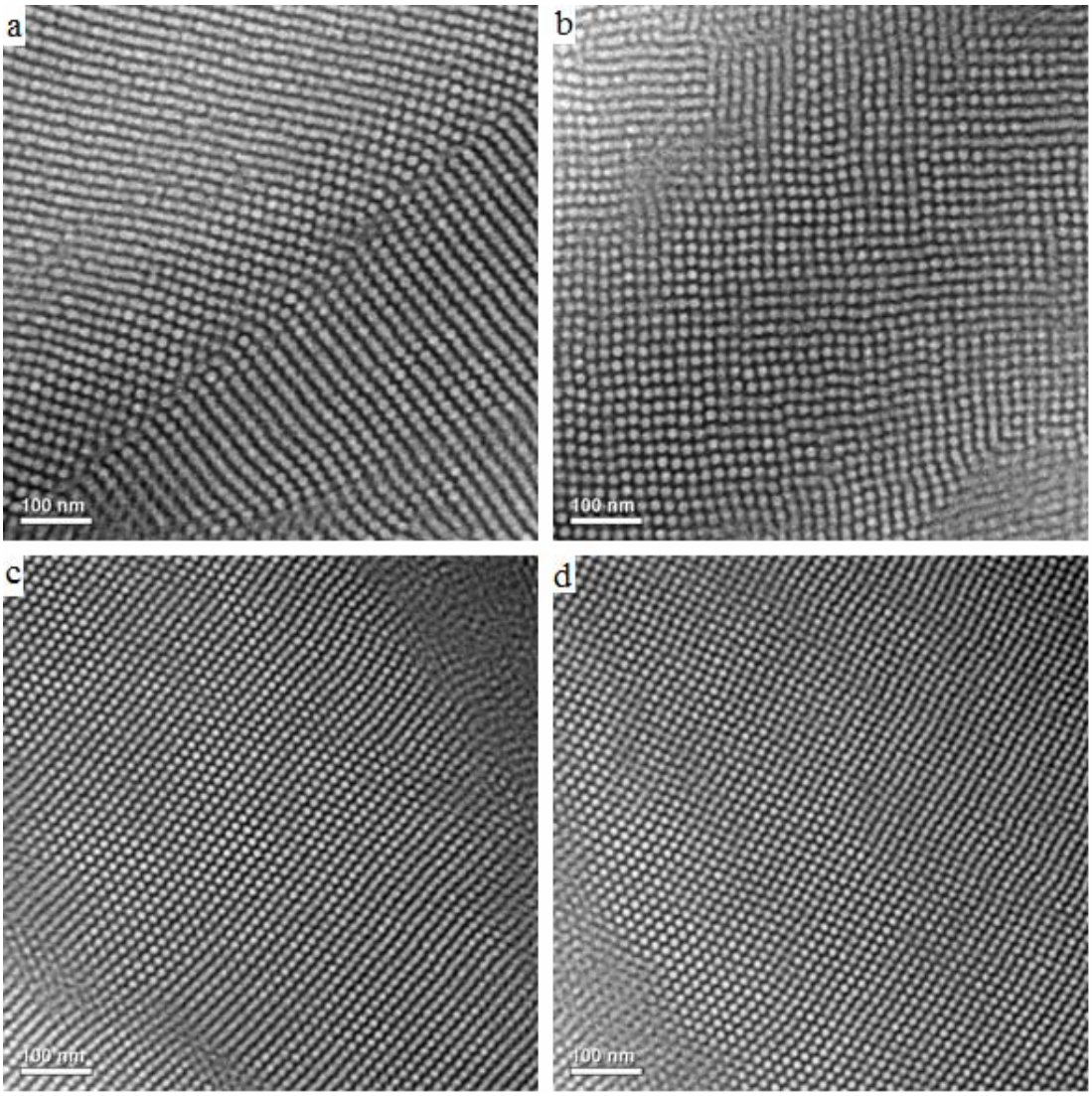

Figure 6-3 TEM micrographs obtained from OsO_4 stained asymmetric SIS'O tetrablock copolymers of (a, b) SIS'O-0.21 annealed at 120 ^{o}C and (c, d) SIS'O-0.32 annealed at 140 ^{o}C for one day. All panels contain the ordered arrays of the spherical microdomains. Panel (a) contains two large grains with similar white straight parallel lines consisted of the spherical microdomains. Panel (a), (c) and (d) contain regions of the six-fold symmetric projections and panel (b) contains regions of the four-fold symmetric projections, consistent with a simple hexagonal lattice.

also supported by panel (d). At the top right corner, we see the four-fold region of the (010)/(001) plane and as the sample tilts 90^{o}, we see the six-fold region of the (100) planes at the bottom left corner in the same TEM micrograph.

The SIS'O-0.21 samples have larger sphere diameter (about 15 nm) than that of SIS'O-0.32 (about 12 nm), possibly due to the higher PEO volume fraction (16 % in SIS'O-0.21 vs. 7 % in SIS'O-0.32). Another possible explanation is the high asymmetry of τ = 0.21 in SIS'O-0.21 which permits some of the I blocks to lower their stretching energies by pulling the shorter terminal S blocks into the I domain, significantly increasing the spherical domain sizes.[22]

SIS'O-0.39. Synchrotron SAXS data for SIS'O-0.39 from 100 – 140 ^{o}C during the heating process are shown in Figure 6-4. At 100 ^{o}C, the scattering patterns display peaks at $q/q^{*} = \sqrt{1}, \sqrt{3}$ and $\sqrt{4}$ with q* being the principal peak location. These peak ratios are consistent with a hexagonal symmetry. The peaks are relatively broader, indicating the limited long-range order possibly due to either lower annealing temperatures or shorter annealing durations. Upon further heating to 120 ^{o}C, a characteristic scattering pattern consistent with the Frank-Kasper σ-phase[46] is observed before the sample disorders at 140 ^{o}C with the disappearance of all the Bragg peaks. The single broad scattering peak with the maximum at q* is interpreted as the correlation hole scattering from the disordered sample. The order-disorder transition temperature based on the SAXS is 130 ± 10 ^{o}C.

Representative TEM images for SIS'O-0.39 at 100 ^{o}C and 120 ^{o}C are shown in Figure 6-5 (a) and (b), respectively. In panel (a), the bright spherical domains arranged

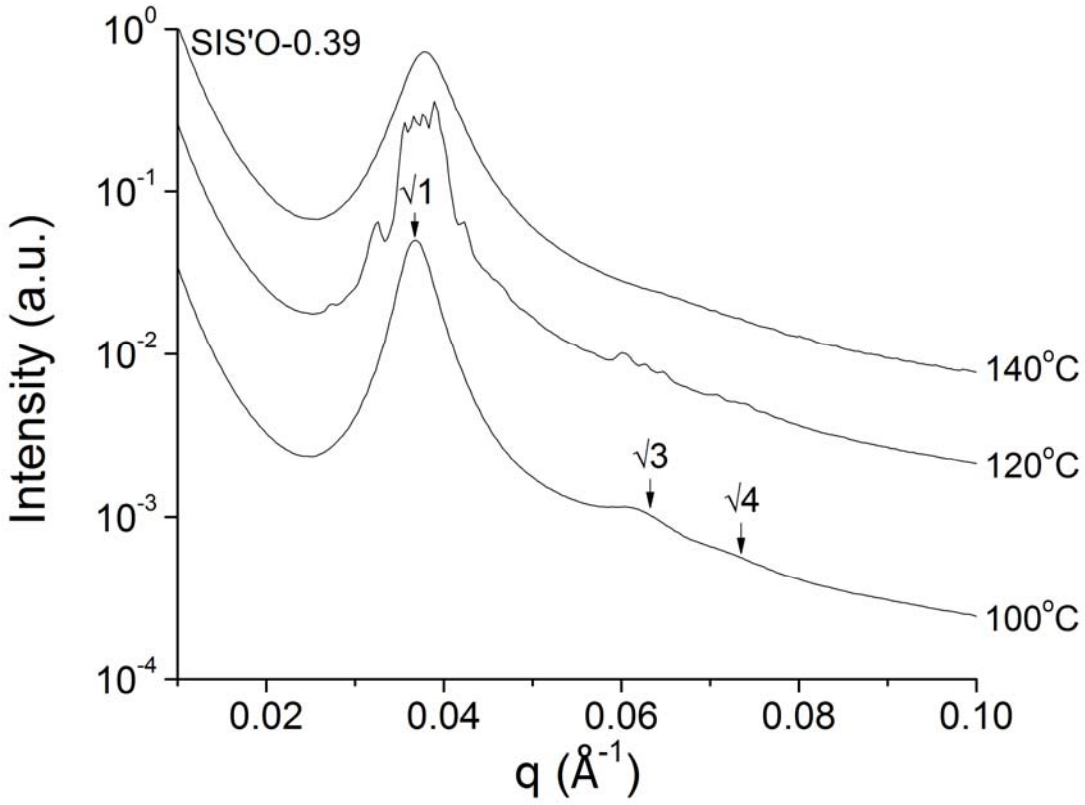

Figure 6-4 Representative synchrotron SAXS data obtained from SIS'O-0.39 with a fixed ratio of $f_S : f_I = 1 : 1$, and $\tau = 0.39$. The arrows identify the relative peak positions associated with a hexagonal symmetry at 100 °C. The tetragonal Frank-Kasper σ-phase and disordered states are identified with the results at 120 and 140 °C, respectively. Scattering patterns have been progressively shifted vertically for clarity.

into a well-ordered pattern with a six-fold symmetry (as shown by the fast-Fourier transform image in the inset) in dark matrix of the I domains. As the grain tilts away from the electron beam under the microscope, we see the projection of the black and modulated white layers. Even though the bright S and the O blocks form spheres stacking into straight lines, they do not process the wavy nature of the cylinders,consistent with

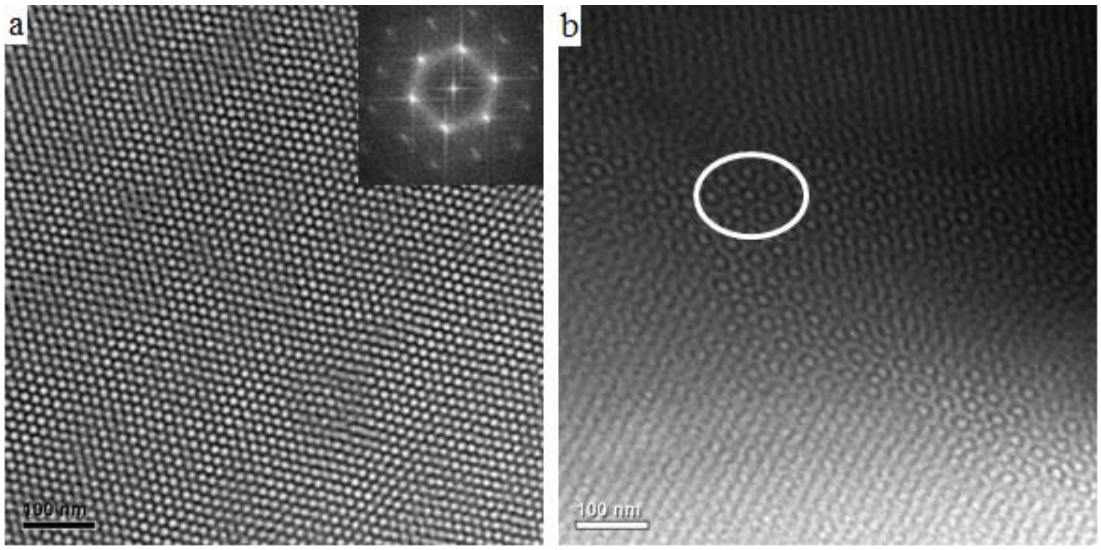

Figure 6-5 TEM micrographs obtained from OsO_4 stained asymmetric SIS'O-0.39 tetrablock copolymers annealed at (a) 100 ^{o}C and (b) 120 ^{o}C for one day, quenched in liquid nitrogen to preserve the morphologies prior to microtoming. Both images are formed by the spherical domains containing a core of the O blocks. Long-range order in (a) is associated with the simple hexagonal (P_6/mmm) packing, as shown in the fast-Fourier transform image (inset) and previously.[44] The morphology in (b) is consistent with the recently discovered Frank-Kasper σ-phase.[46] The scattered rings with the white spherical cores and the grey shells separated by the black linings are consistent with the columns of the dodecagonal units of the spheres. The characteristic σ-element with 3^2.4.3.4 tiling is identified in the white oval. The scale bars represent 100 nm.

the assignment of the simple hexagonal symmetry with a P_6/mmm space group symmetry. The well-defined long-range order presented in the TEM images seems to be contradictory to the relatively broad peaks shown in the SAXS data, possibly due to the differences in the annealing durations under the different characterization techniques.

At 120 ^{o}C, SIS'O-0.39 shows sizable well-ordered areas (Figure 6-5 (b)) containing the light rings surrounding white spherical cores and grey shells separated by the black linings. These scattered rings form a characteristic pattern in the white oval with two triangles, a square, a triangle and a square, all having the same length. This is the characteristic feature of the Frank-Kasper σ-phase, i.e., the σ-element with 3^2.4.3.4 tiling, a two-dimensional pattern vertically projected from the layers of the alternating rings surrounding a column of the spheres perpendicular to the dodecagonal stacking direction along the c-axis.[46] The SAXS and the TEM results support the assignment of the Frank-Kasper σ-phase to SIS'O-0.39 at 120 ^{o}C before it disorders at 140 ^{o}C.

SIS'O-0.50. The SIS'O-0.50 tetrablock terpolymer with τ = 0.50 is actually symmetric with equal S block lengths. This sample has a number-average molecular weight of M_n = 23.0 kg/mol and PDI = 1.04, containing 46 % S (divided equally), 46 % I and 8 % O (each ± 1%) by volume. It also forms the core-shell spheres with the O-rich cores and the S-rich shells dispersed in the mixed S and the I matrix, having a T_{ODT} = 224 ± 3 ^{o}C. It forms the liquid-like packed spheres at lower temperatures and the Frank-Kasper σ-phase at elevated temperatures before disordering. Detailed information on the synthesis and the characterization are described elsewhere.[46,47]

SIS'O-0.61 and SIS'O-0.70. Synchrotron SAXS data for SIS'O-0.61 and SIS'O-0.70 at various temperatures during the heating process are shown in Figure 6-6 (a) and (b), respectively. From 120 to 140 ^{o}C, the SAXS data for SIS'O-0.61 show two broad peaks, indicating the limited long-range structural order. We attribute these results to the liquid-like packing of the spheres,[50–57] which are corroborated by the TEM measurements

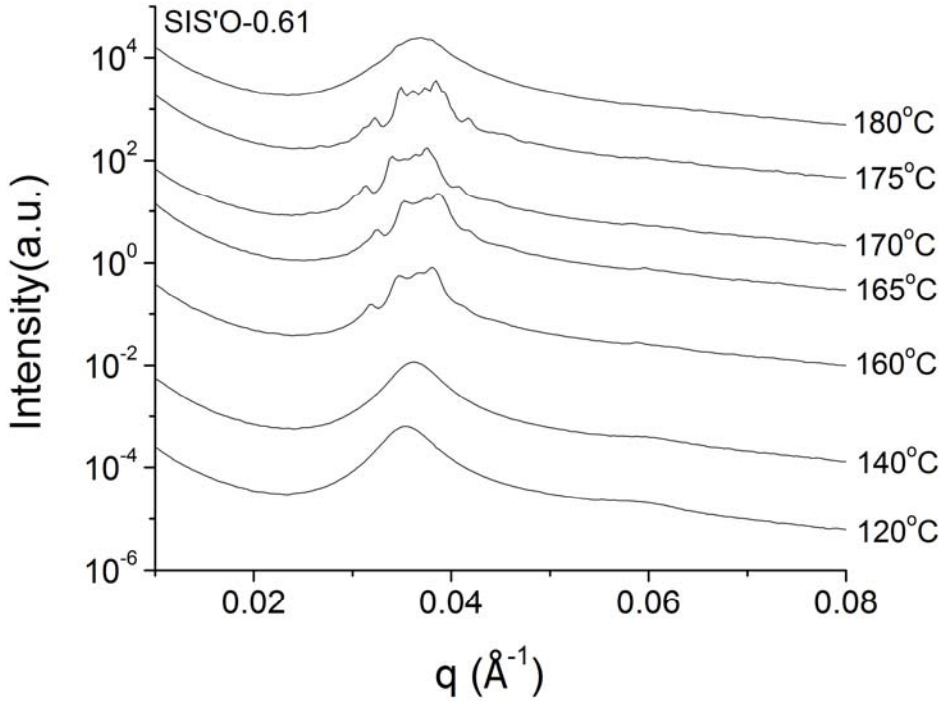

(a)

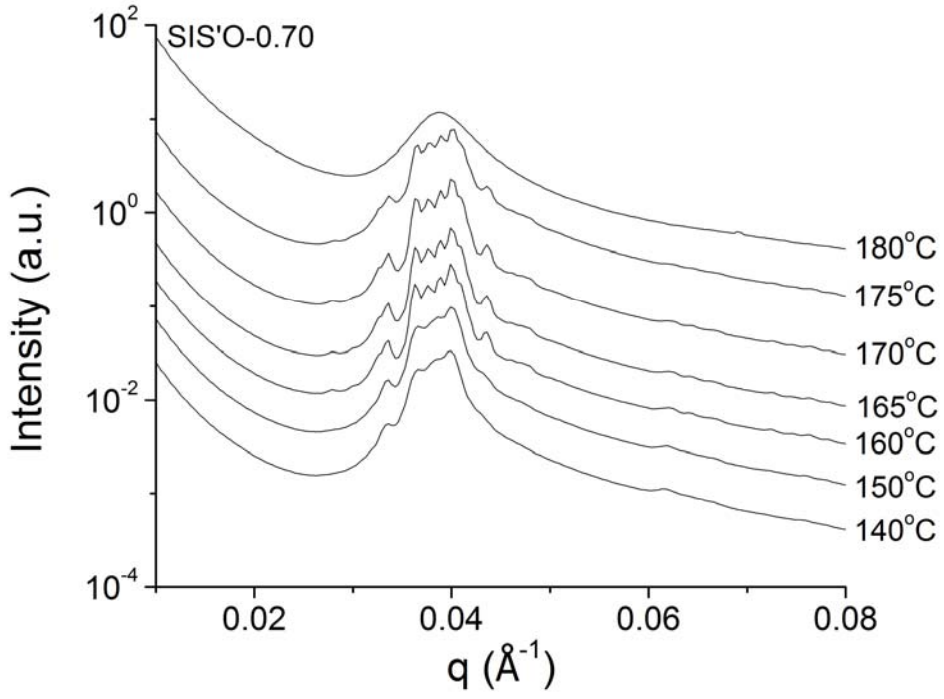

(b)

Figure 6-6 Synchrotron SAXS data for asymmetric (a) SIS'O-0.61 and (b) SIS'O-0.70 tetrablock terpolymers with $\tau = 0.61$ and 0.70, respectively. Scattering patterns have been shifted vertically for clarity.

(see Figure 6-8 (a)).

At 160 – 165 ^{o}C for SIS'O-0.61 and 140 – 150 ^{o}C for SIS'O-0.70, both samples show similar SAXS patterns with three closely spaced strong peaks and a weak peak close to this triplet at the position where the primary peak q* is used to be at lower temperatures. Higher order peaks become prominent as well. These peak positions and the relative intensity distribution of the peaks are very similar to the SAXS patterns obtained from the SISO-11 samples (see Figure 6-10), which have been identified as the QC phase (see Figure 5-14).[58,59] Upon further heating to 170 ^{o}C for SIS'O-0.61 and 160 ^{o}C for SIS'O-0.70, the characteristic scattering patterns consistent with the Frank-Kasper σ-phase[46] are obtained before both samples disorder at 180 ^{o}C with the disappearance of all the Bragg peaks. The order-disorder transition temperatures based on the SAXS for both samples are 177 ± 3 ^{o}C, coincidentally.

Figure 6-7 shows the SAXS data obtained from the SIS'O-0.61 samples during the cooling process. At 180 ^{o}C, samples are disordered as indicated by the single broad peak. After the samples are cooled to 175 ^{o}C, the SAXS patterns consistent with the Frank-Kasper σ-phase are observed. The samples remain at the σ-phase upon further cooling to 120 ^{o}C even though the QC and the LLP phases are formed at lower temperatures during the heating process as shown in Figure 6-6 (a), indicating the kinetic barrier of the σ-phase is too high to overcome.

Representative TEM images for SIS'O-0.61 and SIS'O-0.70 at various temperatures are shown in Figure 6-8 and Figure 6-9 respectively. At 120 ^{o}C, the SIS'O-0.61 samples form the liquid-like packing of the spheres (see Figure 6-8 (a)). The dark circular regions

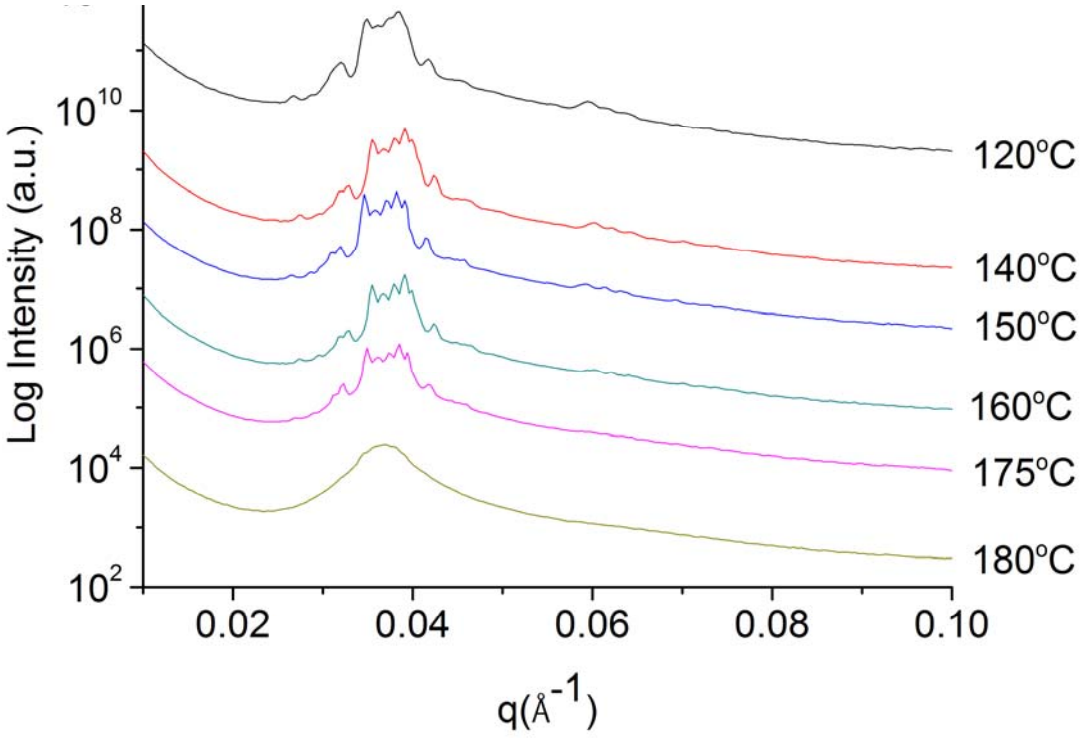

Figure 6-7 Synchrotron SAXS data obtained from the asymmetric SIS'O-0.61 samples during the cooling process. The Frank-Kasper is obtained upon cooling from the disordered state at 180 ^{o}C and remained as the σ-phase upon further cooling to 120 ^{o}C. Scattering patterns have been shifted vertically for clarity.

associated with the I blocks with the bright cores of the O blocks and the S shields appear to be dispersed without any long-range order in a grey matrix of the S and the I blocks. However, close examination reveals certain restricted regions with the short-range micro-domain periodicity.

Panel (b) and (c) are obtained after annealing the SIS'O-0.61 samples under vacuum at 160 ^{o}C for a day. Panel (c) shows the scattered rings with the white spherical cores and

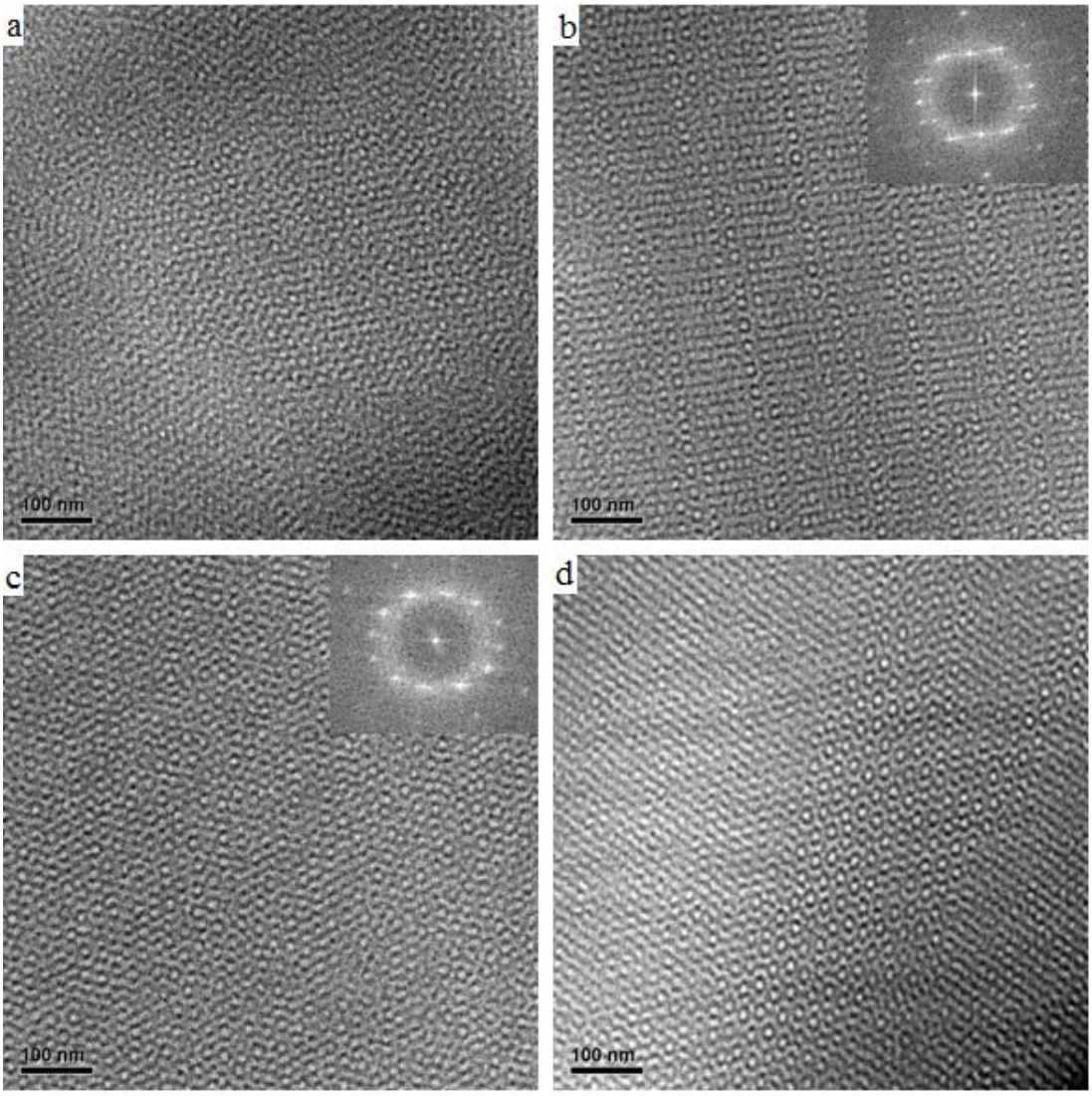

Figure 6-8 TEM images for asymmetric SIS'O-0.61 samples annealed at (a) 120 ^{o}C, (b,c) 160 ^{o}C and (d) 170 ^{o}C. Panel (a) displays limited long-range order in the specimen, with the white circle showing regions with short-range periodic order, consistent with LLP spheres. The morphology in (d) is consistent with Frank-Kasper σ-phase.[46]

grey shells separated by the black linings. On the local scale, these rings seem to have certain level of order, but not long-range orders. However, the FFT image (see the inset) reveals the presence of the long-range order as indicated by the sharp diffraction spots. Similar long-range order is also present in panel (b) with the black rings aligned into straight lines which are parallel to each other at equal distances. Note that the FFT images shown in panel (b) and (c) seem to be cubic with double diffraction spots, contradictory to the SAXS identification of a 12-fold QC phase at this temperature window.

Figure 6-9 (a) and (b) show the TEM images obtained at 140 ^{o}C for the SIS'O-0.70 samples. Panel (a) shows square arrays of dark rings with similar sizes and a bright O core at the center of each ring. The dark rings are aligned into straight lines separated at equal distance with the well-defined long-range translational order. Again, the FFT images in panel (a) and (b) suggest some cubic phase instead of the 12-fold QC phase as suggested by the SAXS data.

At 170 ^{o}C, both the SIS'O-0.61 and the SIS'O-0.70 samples show sizable well-ordered areas containing the scattered rings with the white spherical cores and grey shells separated with the black linings, consistent with the characteristic patterns formed in the Frank-Kasper σ-phase,[46] as shown in Figure 6-8 (d) and Figure 6-9 (c).

6.4 Discussion

Based on the SAXS and the TEM characterization results, the sequence of the phases associated with the asymmetric series of the SIS'O tetrablock terpolymers

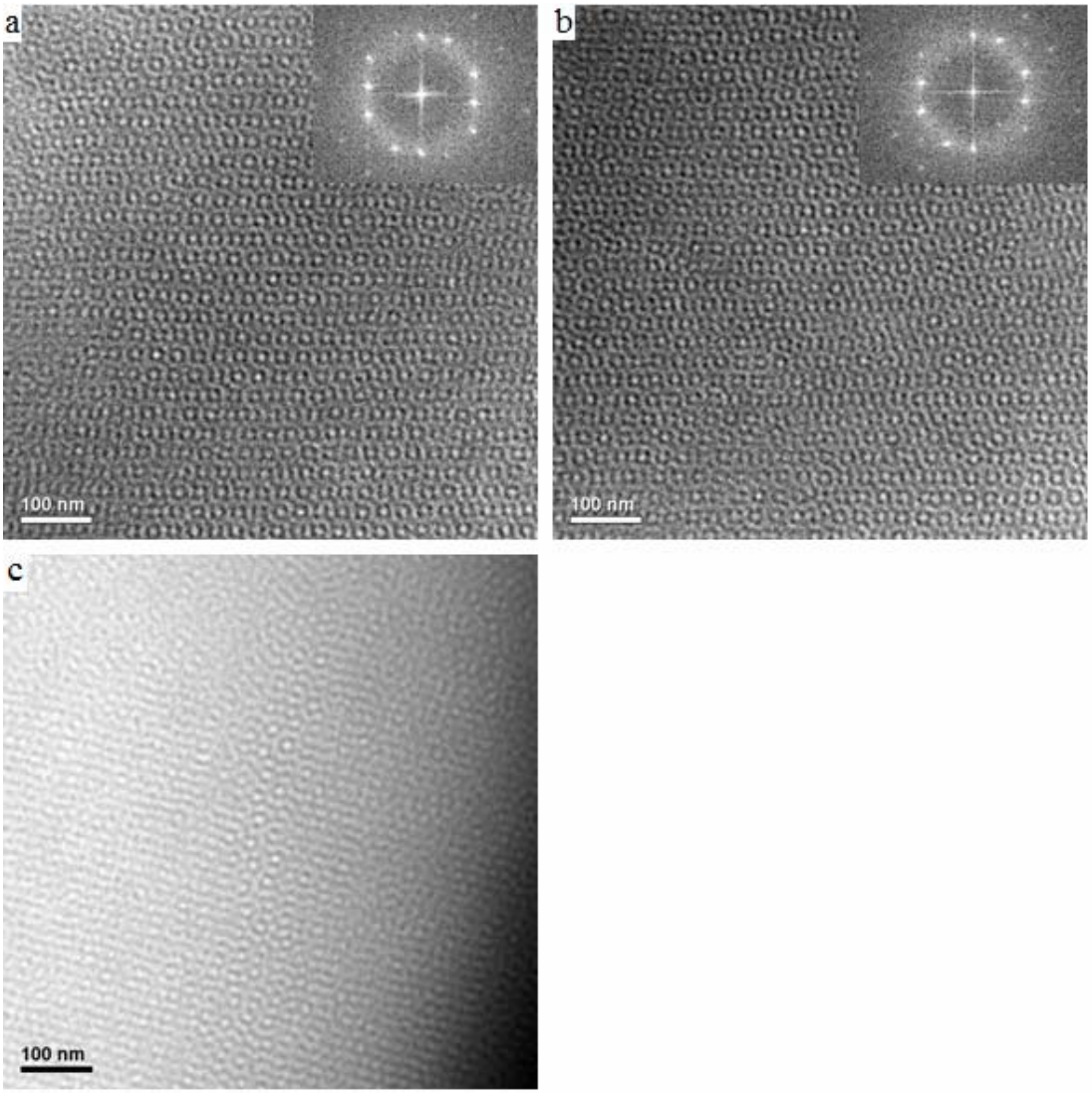

Figure 6-9 TEM micrographs obtained from OsO_4 stained SIS'O-0.70 tetrablock terpolymers after annealing for one day at (a,b) 140 ^{o}C and (c) 170 ^{o}C. All images have the spherical domains containing the cores of the O blocks with the I domains microphase separated from the brighter S and the O domains. The morphology in (c) is consistent with the Frank-Kasper σ-phase.[46]

containing equal volume fractions of the S and the I blocks is: at lower temperatures, the spheres on a hexagonal lattice at lower $\tau = 0.21 – 0.39$ and the liquid-like packed spheres at higher $\tau = 0.50 – 0.61$; at intermediate temperatures, a phase tentatively assigned as the QC phase at higher $\tau = 0.61 – 0.70$; at higher temperature near the disorder boundary, the Frank-Kasper σ-phase at intermediate to higher $\tau = 0.39 – 0.70$.

Figure 6-10 summarizes the SAXS patterns obtained from four different samples after various annealing temperatures. For easy comparison, the SAXS pattern for the Frank-Kasper σ-phase from the SIS'O-0.70 samples annealed at 170 ^{o}C is also shown at the top. The data for SIS'O-0.50 are the unreported SAXS data produced by Michael Bluemle.[60] Taking SIS'O-0.70 as the reference, the horizontal multiply factors are q/q_o = 1.22, 1.06, and 1.14 for SISO-11, SIS'O-0.61 and SIS'O-0.50, respectively.

In Figure 5-14, the SAXS patterns for SISO-11 are observed to have nearly identical peak positions and intensities as those from the certain dendrimers which have been reported to form the QC phase.[59,61,62] In Figure 6-10, four SAXS patterns after annealing SIS'O-0.70 at 150 ^{o}C, SISO-11 at 220 ^{o}C, SIS'O-0.61 at 160 ^{o}C and SIS'O-0.50 at 180 ^{o}C for about 20 – 30 minutes have almost identical peak position ratios and intensities, suggesting all of them having the 12-fold QC phase. Note that all these four samples (except for SIS'O-0.70 which the SAXS data below 140 ^{o}C is not taken) form liquid-like spheres at lower temperatures, QC phase at intermediate temperatures and the Frank-Kasper σ-phase at elevated temperatures before the sample disorders, i.e.$T_{LLP} < T_{QC} < T_{\sigma} < T_{disorder}$. Based on the SAXS data obtained during the cooling process for the LLP, QC and the Frank-Kasper σ-phase (Figure 5-7 and Figure 6-7); these are all stable phases as

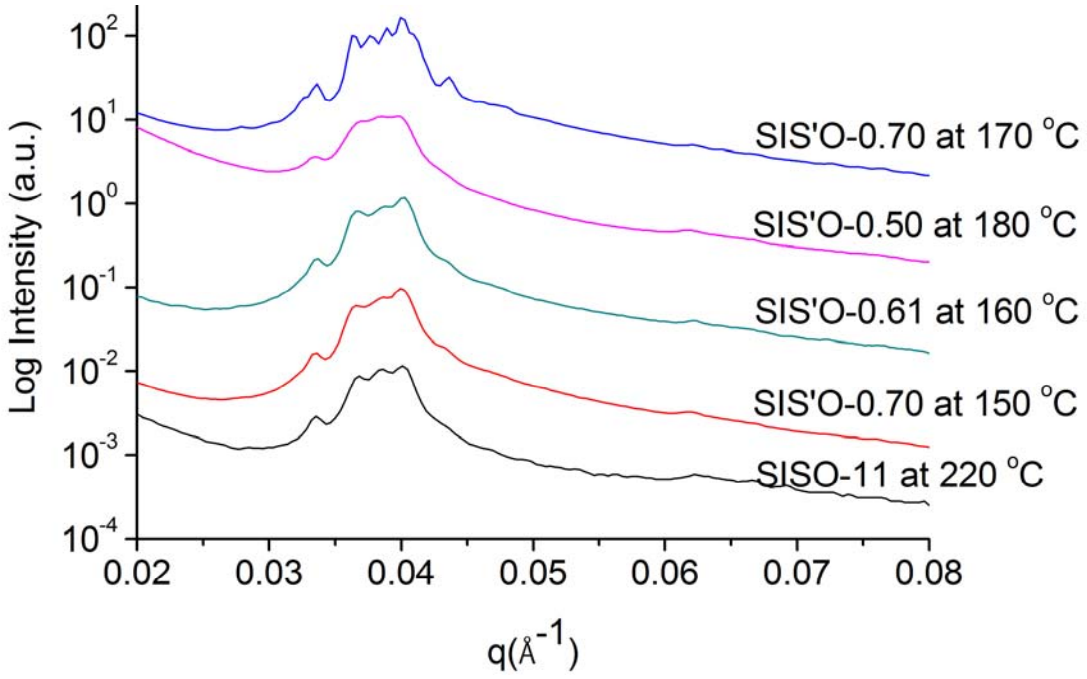

Figure 6-10 Synchrotron SAXS data for the four samples containing the $Pm\bar{3}n$ phase and one sample containing the Frank-Kasper σ-phase is shown as the top curve for easy comparison. The SAXS patterns for SIS'O-0.50 at 180 °C are the unreported data synthesized and characterized by Michael Bluemle.[60] Scattering patterns have been shifted vertically and horizontally for clarity. The horizontal multiply factors are $q/q_o = 1$, 1.22, 1.06, and 1.14 for SIS'O-0.70, SISO-11, SIS'O-0.61 and SIS'O-0.50, respectively.

indicated by the recoverability after cooling from the disordered state.

Figure 6-8 (b) and (c) and Figure 6-9 (a) and (b) show the TEM images of the SIS'O-0.61 annealed at 160 °C and SIS'O-0.70 samples annealed at 140 °C for a day. The fact that we do not see any region with a 12-fold rotational symmetry in these images, nor is it reflected in the FFT images, alters us to think of other possible phases other than the QC phase. Figure 6-11 shows the simulated TEM and FFT images for the $Pm\bar{3}n$ cubic

phase,[58,63,64] which has been observed in certain polymers and dendrimers.[59,61,62,65] These simulated images are strikingly similar to the TEM and the FFT images shown in Figure 6-9 (a). In fact, Figure 6-9 (a) shows the [001] projection of the $Pm\bar{3}n$ phase, appearing as a square array of dark rings with similar sizes and a bright O core at the center of each ring. The dark rings are aligned into straight lines separated at equal distance with the well-defined long-range translational order. Images of the other projections have weaker contrast, as expected.

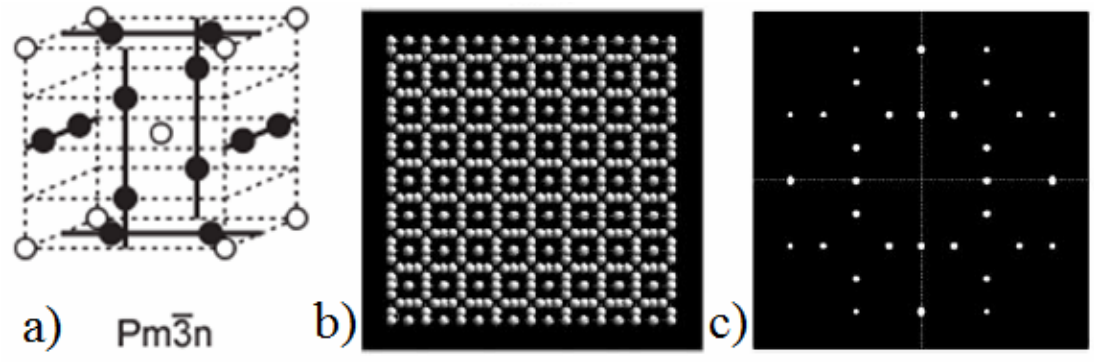

Figure 6-11 a) Unit cell of the $Pm\bar{3}n$ phase. b) Structure models viewed along the c-axis and c) the corresponding simulated diffraction patterns of the $Pm\bar{3}n$ phase. Reproduced from Ungar and Zeng.[63]

So far, we have shown that after annealing SIS'O-0.70 at 150 ^{o}C, SISO-11 at 220 ^{o}C, SIS'O-0.61 at 160 ^{o}C and SIS'O-0.50 at 180 ^{o}C for about 20 – 30 minutes, these samples exhibit almost identical SAXS patterns as those of the reported QC phase (see Figure 5-14 and 6-10),[59,61,62] suggesting these samples form QC phases after annealing for 30 minutes. However, after annealing SIS'O-0.70 at 140 ^{o}C and SIS'O-0.61 at 160 ^{o}C for

one day, these samples show TEM images that are nearly the same as the simulated results of the $Pm\bar{3}n$ phase, suggesting they form $Pm\bar{3}n$ phase after longer annealing times. Different annealing times between the SAXS and the TEM experiments (30 minutes vs. 1 day) lead to different phase formations. Lee *et. al.* discovered that poly(isoprene-b-lactide) diblocks also grow into BCC phase over approximately 30 minutes at 25 ^{o}C which is followed by a transformation to the Frank-Kasper σ-phase during the next 24 hours.[46] Even though our results do not prove that the $Pm\bar{3}n$ phase is slow to develop but this explanation is consistent with the experimental results.

In Chapter 3 – 5, we examined the phase behaviours of the symmetric SISO tetrablock terpolymers with $f_S : f_I = 2 : 3$, $f_O = 0 – 32$ % and $f_S : f_I = 3 : 2$, $f_O = 0 – 35$ %. With similar molecular weights and PEO volume fractions ($f_O = 7 – 16$ %), the isoprene-rich symmetric SISO samples form the spheres on a (simple) hexagonal lattice (HEX),[44] the dodecagonal quasicrystalline (QC)and the Frank-Kasper σ-phase with increasing temperatures,[45] similar to the asymmetric SIS'O tetrablocks with $\tau = 0.21 – 0.39$ (asymmetric SIS'O tetrablocks with lower $\tau = 0.21 – 0.32$ form the HEX spheres over a wide temperature range before the samples disorder); the styrene-rich symmetric SISO tetrablocks form the LLP spheres, the $Pm\bar{3}n$ phase and the Frank-Kasper σ-phase with increasing temperatures, similar to the asymmetric SIS'O samples with intermediate to high τ values.

This trend, together with the identical phases formed within the similar composition windows of the SIS'O tetrablock terpolymers, is promising and inspiring for us to extract the useful information regarding the interactions among various blocks with respect to the

resultant phase behaviours, especially the role of the two S blocks in this particular ABA'C type of tetrablock terpolymers. In the isoprene-rich symmetric SISO tetrablocks, both S blocks are short as compared to the isoprene block; in the asymmetric SIS'O samples with a lower τ, the terminal S block is shorter than the internal S' block. The terminal S blocks are shorter in both the isoprene-rich symmetric SISO and the asymmetric SIS'O samples with a lower τ (longer internal S' block). Similarly, the terminal S blocks are longer in both the styrene-rich symmetric SISO and the asymmetric SIS'O samples with a higher τ (shorter internal S' block). In general, the asymmetric SIS'O samples with a lower τ behave similarly to the isoprene-rich symmetric SISO counterparts and the asymmetric SIS'O samples with a higher τ behave similarly to the styrene-rich symmetric SISO counterparts. Therefore, we can speculate that the terminal S block plays a more important role in the phase formation as compared to the internal S' block in the asymmetric SIS'O tetrablock terpolymers.

In the SIS'O tetrablock terpolymers, the binary segment-segment interactions $\chi_{SI} \leq \chi_{SO} << \chi_{IO}$, the repulsion between the I and the O blocks is the greatest. Since the I and the O blocks are not directly bonded together, there is no I/O interface. The S blocks act as shields between these unfavorable interactions, leading to the formation of the core-shell spherical or the cylindrical microstructures.[44–47] Both ends of the internal S' chains are localized to the S'/O and S'/I interfaces to fulfill enthalpic requirements of minimizing the interfacial areas. In the meantime, the S' chains get stretched and compressed in order to fulfill the entropic requirements of uniform density. The lengths of the internal S' blocks affect the thickness of the shields between the I and the O

domain. On the contrary, the terminal S blocks have the freedom to move around to fill space, providing the additional latitude to novel phase formation that are not observed in the ISO triblock counterparts. As the asymmetric parameter τ changes, the length of the terminal S blocks changes, resulting in the formation of many different morphologies. When the asymmetry is very high, the shorter terminal S block is pulled into the I domain, lowering the stretching energies and the domain sizes are affected too.

Overall, the phase behaviors of the symmetric SISO and the asymmetric SIS'O tetrablock terpolymers are nearly identical. The experiments observed the same phases in the intermediate-segregation regime: the HEX spheres, the LLP spheres, the $Pm\bar{3}n$, and the Frank-Kasper σ-phase at low f_Os. The asymmetric factor introduces some new effects not present in the symmetric SISO systems. First, a modest bidispersity of the S blocks lowers the elastic energy of the S domain.[22] It is well established that the stretching energy of a bidisperse domain is less than that of a monodisperse domain.[66] The configuration of the asymmetric SIS'O tetrablocks is obtained by taking the symmetric SISO tetrablocks and transferring a small portion of the end of one S block to the end of the other. This action shifts the S block distribution away from the interface without stretching the molecules, lowering the stretching energy in the S domains of a given thickness as τ deviates from ½.

The second effect is that the high asymmetry lowers the stretching energies of the I blocks by pulling the shorter S blocks into the I domain. Even though the unfavorable interactions occur when the S and the I blocks mix, this is compensated for by the fact that the I blocks can relax. An extraction of the terminal S block allows the I domain to

shift away from the interface without further stretching the molecules. Consequently, pulling the terminal S blocks within the I domains will reduce the stretching energies of the I domains as τ approaches zero. This causes an increase in the domain spacing. These two effects of lowering stretching energies in the S and the I domains significantly change the domain sizes, cause large shifts in the phase boundaries, and influence the packing frustration.

Similar to the symmetric ABA and asymmetric ABA' systems,[8,22] asymmetry only shifts the phase boundaries in SISO/SIS'O systems, without introducing new phase formations. Similar AB diblocks and ABA triblocks copolymer melts are known to have similar phase behaviours,[12–16,19–21] no matter the ABA triblocks are symmetric or asymmetric as the asymmetry only shifts the phase boundaries.[8,67] We can view the AB diblocks as produced from cutting the symmetric ABA triblocks in the middle as polymer chains are relatively unstretched in this region, leaving the free energy of both AB and ABA systems virtually the same.[7] However, similar speculation does not work for the ISO triblocks and the SISO/SIS'O tetrablock terpolymer melts as their molecular architectures are not exactly symmetrical, e.g., symmetric OSISO pentablocks are expected, and confirm experimentally, to behave similarly to the homologous ISO triblocks,[35,38,49] but not the SISO/SIS'O systems. In the ISO system, the network morphologies such as the alternating gyroid (Q^{214}), the double gyroid(Q^{230}), and the orthorhombic with a *Fddd* symmetry (O^{70}) have been reported,[35,36,38,49,68–70] but these are not observed in the SISO/SIS'O systems so far. In the ABC triblock system, while the symmetric A and B blocks prefer a flat interface, an intermediate amount of C block

addition favours the B-C interface with certain spontaneous curvature, creating competing packing constraints. Negative interfacial Gauss curvature found in the network morphologies satisfies both conditions simultaneously under the constraint of constant density, driving the formation of the three-dimensional network formation. Changing the molecular architecture from the ISO triblocks to the SISO tetrablocks drives the preference from the hyperbolic interfaces inherent in the network morphologies to the higher, and zero Gauss, curvature surfaces present in the spheres and the cylinders.

6.5 Conclusion

The core (O) – shell (S) spheres with the simple hexagonal symmetry, liquid-like packing, $Pm\bar{3}n$ and the Frank-Kasper σ-phase have been identified in the asymmetric SIS'O tetrablock terpolymers with equal volume fractions of the S and the I blocks, f_O = 7 – 16 % and τ = 0.21 – 0.70. The asymmetric SIS'O samples with a lower τ exhibit nearly identical phase behavior with the isoprene-rich symmetric SISO samples and the asymmetric SIS'O with a higher τ exhibit nearly identical phase behavior with the styrene-rich symmetric SISO samples, suggesting that the terminal S blocks play a more important role in the phase formation as compared to the internal S' blocks. Comparing the symmetric SISO and the asymmetric SIS'O samples with similar molecular weights and compositions, they form identical phases, with the asymmetric factor only affecting the phase boundaries. The asymmetric parameter plays a key role in shifting the phase boundaries, changing domain sizes and influencing the packing frustrations.

6.6 References

(1) Lodge, T. P. *Macromolecular Chemistry and Physics* **2003**, *204*, 265.

(2) Hamley, I. W. *Developments in Block Copolymer Science and Technology*; John Wiley & Sons: Berlin, 2004.

(3) Fredrickson, G. H. *The Equilibrium Theory of Inhomogeneous Polymers*; Clarendon Press: Oxford, 2006.

(4) Semenov, A. N. *Soviet Physics, JETP* **1985**, *61*, 733.

(5) Matsen, M. W.; Bates, F. S. *Macromolecules* **1996**, *29*, 7641.

(6) Matsen, M. W.; Bates, F. S. *Journal of Chemical Physics* **1997**, *106*, 2436.

(7) Helfand, E.; Wasserman, Z. R. *Macromolecules* **1976**, *9*, 879.

(8) Matsen, M. W.; Thompson, R. B. *Journal of Chemical Physics* **1999**, *111*, 7139.

(9) Matsen, M. W.; Schick, M. *Macromolecules* **1994**, *27*, 187.

(10) Matsen, M. W. *Journal of Chemical Physics* **1995**, *102*, 3884.

(11) Watanabe, H. *Macromolecules* **1995**, *28*, 5006.

(12) Gehlsen, M. D.; Almdal, K.; Bates, F. S. *Macromolecules* **1992**, *25*, 939.

(13) Adams, J. L.; Graessley, W. W.; Register, R. A. *Macromolecules* **1994**, *27*, 6026.

(14) McKay, K. W.; Gros, W. A.; Diehl, C. F. *Journal of Applied Polymer Science* **1995**, *56*, 947.

(15) Riise, B. L.; Fredrickson, G. H.; Larson, R. G.; Pearson, D. S. *Macromolecules* **1995**, *28*, 7653.

(16) Ryu, C. Y.; Lee, M. S.; Hajduk, D. A.; Lodge, T. P. *Journal of Polymer Science*

Part B **1997**, *35*, 2811.

(17) Mayes, A. M.; Olvera de la Cruz, M. *Journal of Chemical Physics* **1989**, *91*, 7228.

(18) Mayes, A. M.; Olvera de la Cruz, M. *Journal of Chemical Physics* **1991**, *95*, 4670.

(19) Koberstein, J. T.; Russell, T. P.; Walsh, D. J.; Pottick, L. *Macromolecules* **1990**, *23*, 877.

(20) Nakatani, A. I.; Morrison, F. A.; Douglas, J. F.; Mays, J. W.; Jackson, C. L.; Muthukumar, M.; Han, C. C. *Journal of Chemical Physics* **1996**, *104*, 1589.

(21) Kim, J. K.; Lee, H. H.; Gu, Q.-J.; Chang, T.; Jeong, Y. H. *Macromolecules* **1998**, *31*, 4045.

(22) Matsen, M. W. *Journal of Chemical Physics* **2000**, *113*, 5539.

(23) Mansour, A. S.; Johnson, L. F.; Lodge, T. P.; Bates, F. S. *Journal of Polymer Science Part B: Polymer Physics* **2010**, *48*, 566.

(24) Schipper, F. J. M.; Floudas, G.; Pispas, S.; Hadjichristidis, N.; Pakula, T. *Macromolecules* **2002**, *35*, 8860.

(25) Anthamatten, M.; Hammond, P. T. *Journal of Polymer Science Part B: Polymer Physics* **2001**, *39*, 2671.

(26) Hamley, I. W.; Castelletto, V.; Yang, Z.; Price, C.; Booth, C. *Macromolecules* **2001**, *34*, 4079.

(27) Aksimentiev, A.; Holyst, R. *Macromolecular Theory and Simulations* **1999**, *8*, 328.

(28) Pochan, D. J.; Gido, S. P.; Zhou, J.; Mays, J. W.; Whitmore, M.; Ryan, A. J. *Journal of Polymer Science Part B: Polymer Physics* **1997**, *35*, 2629.

(29) Hamley, I. W.; Gehlsen, M. D.; Khandpur, A. K.; Koppi, K. A.; Rosedale, J. H.; Schulz, M. F.; Bates, F. S.; Almdal, K.; Mortensen, K. *Journal de Physique II* **1994**, *4*, 2161.

(30) Woloszczuk, S.; Banaszak, M. *European Physical Journal E* **2010**, *33*, 343.

(31) Huckstadt, H.; Gopfert, A.; Abetz, V. *Polymer* **2000**, *41*, 9089.

(32) Abetz, V.; Goldacker, T. *Macromolecular Rapid Communications* **2000**, *21*, 16.

(33) Matsushita, Y.; Suzuki, J.; Seki, M. *Physica. B, Condensed Matter* **1998**, *248*, 238.

(34) Mogi, Y.; Mori, K.; Matsushita, Y.; Noda, I. *Macromolecules* **1992**, *25*, 5412.

(35) Epps III, T. H.; Cochran, E. W.; Bailey, T. S.; Waletzko, R. S.; Hardy, C. M.; Bates, F. S. *Macromolecules* **2004**, *37*, 8325.

(36) Cochran, E. W.; Bates, F. S. *Physical Review Letters* **2004**, *93*, 087802.

(37) Mogi, Y.; Mori, K.; Kotauji, H.; Matauishita, Y.; Noda, I. *Macromolecules* **1993**, *26*, 5169.

(38) Bailey, T. S.; Hardy, C. M.; Epps III, T. H.; Bates, F. S. *Macromolecules* **2002**, *35*, 7007.

(39) Huckstadt, H.; Goldacker, T.; Gopfert, A.; Abetz, V. *Macromolecules* **2000**, *33*, 3757.

(40) Bailey, T. S.; Pham, H. D.; Bates, F. S. *Macromolecules* **2001**, *34*, 6994.

(41) Shefelbine, T. A.; Vigild, M. E.; Matsen, M. W.; Hajduk, D. A.; Hillmyer, M.

A.; Cussler, E. L.; Bates, F. S. *Journal of the American Chemical Society* **1999**, *121*, 8457.

(42) Stadler, R.; Auschra, C.; Beckmann, J.; Krappe, U.; Voight-Martin, I.; Leibler, L. *Macromolecules* **1995**, *28*, 3080.

(43) Zheng, W.; Wang, Z.-G. *Macromolecules* **1995**, *28*, 7215.

(44) Zhang, J.; Scott, S. W.; Bates, F. S. *Macromolecules* **2012**, *45*, 256.

(45) Zhang, J.; Bates, F. S. *Journal of the American Chemical Society* **2012**, *134*, 7636.

(46) Lee, S.; Bluemle, M. J.; Bates, F. S. *Science* **2010**, *330*, 349.

(47) Bluemle, M. J.; Zhang, J.; Lodge, T. P.; Bates, F. S. *Macromolecules* **2010**, *43*, 4449.

(48) Epps III, T. H.; Bailey, T. S.; Waletzko, R. S.; Bates, F. S. *Macromolecules* **2003**, *36*, 2873.

(49) Epps III, T. H.; Cochran, E. W.; Hardy, C. M.; Bailey, T. S.; Waletzko, R. S.; Bates, F. S. *Macromolecules* **2004**, *37*, 7085.

(50) Kinning, D. J.; Thomas, E. L. *Macromolecules* **1984**, *17*, 1712.

(51) Winey, K. I.; Thomas, E. L.; Fetters, L. J. *Macromolecules* **1992**, *25*, 2645.

(52) Schwab, M.; Stuehn, B. *Physical Review Letters* **1996**, *76*, 924.

(53) Adams, J. L.; Quiram, D. J.; Graessley, W. W.; Register, R. A.; Marchand, G. R. *Macromolecules* **1996**, *29*, 2929.

(54) Sakamoto, N.; Hashimoto, T.; Han, C. D.; Kim, D.; Vaidya, N. Y. *Macromolecules* **1997**, *30*, 1621.

(55) Han, C. D.; Vaidya, N. Y.; Kim, D.; Shin, G.; Yamaguchi, D.; Hashimoto, T. *Macromolecules* **2000**, *33*, 3767.

(56) Dormidontova, E. E.; Lodge, T. P. *Macromolecules* **2001**, *34*, 9143.

(57) Wang, X.; Dormidontova, E. E.; Lodge, T. P. *Macromolecules* **2002**, *35*, 9687.

(58) Zeng, X.; Ungar, G.; Liu, Y.; Percec, V.; Dulcey, A. E.; Hobbs, J. K. *Nature* **2004**, *428*, 157.

(59) Percec, V.; Imam, M. R.; Peterca, M.; Wilson, D. A.; Graf, R.; Spiess, H. W.; Balagurusamy, V. S. K.; Heiney, P. A. *The Journal of American Chemical Society* **2009**, *131*, 7662.

(60) Bluemle, M. J. *Ph. D. Thesis*; University of Minnesota: Minneapolis, 2010.

(61) Rosen, B. M.; Wilson, D. A.; Wilson, C. J.; Peterca, M.; Won, B. C.; Huang, C.; Lipski, L. R.; Zeng, X.; Ungar, G.; Heiney, P. A.; Percec, V. *The Journal of the American Chemical Society* **2009**, *131*, 17500.

(62) Hudson, S. D.; Jung, H.-T.; Kewsuwan, P.; Percec, V.; Cho, W.-D. *Liquid Crystals* **1999**, *26*, 1493.

(63) Ungar, G.; Zeng, X. *Soft Matter* **2005**, *1*, 95.

(64) Ungar, G.; Liu, Y.; Zeng, X.; Percec, V.; Cho, W. D. *Science* **2003**, *299*, 1208.

(65) Percec, V.; Ahn, C.-H.; Ungar, G.; Yeardley, D. J. P.; Moller, M.; Sheiko, S. S. *Nature* **1998**, *391*, 161.

(66) Milner, S. T.; Witten, T. A. *The Journal of Physiology (Paris)* **1988**, *49*, 1951.

(67) Matsen, M. W.; Bates, F. S. *Journal of Polymer Science Part B: Polymer Physics* **1997**, *35*, 945.

(68) Chatterjee, J.; Jain, S.; Bates, F. S. *Macromolecules* **2007**, *40*, 2882.

(69) Bluemle, M. J.; Fleury, G.; Lodge, T. P.; Bates, F. S. *Soft Matter* **2009**, *5*, 1587.

(70) Tyler, C. A.; Qin, J.; Bates, F. S.; Morse, D. C. *Macromolecules* **2007**, *40*, 4654.

7

Conclusions

The thesis focuses on the composition and the asymmetric effect on the phase behaviour of the tetrablock terpolymers using poly(styrene-*b*-isoprene-*b*-styrene-*b*-ethylene oxide) (SISO) as the model system, synthesized via a living anionic polymerization method and characterized with NMR, GPC, TEM, SAXS, DSC and DMS. The phases identified are compared with those of the well-established ISO triblock system[1–10] in order to study the effect of the molecular architecture alone on the phase behaviour, as the symmetric SISO terpolymers can be viewed as produced from splitting the S blocks of the ISO triblock in half. Six, and possibly more, types of the spherical phases are observed in this work: BCC, liquid-like packing (LLP), 12-fold

quasicrystalline (QC), $P_6/mmm, Pm\bar{3}n$, and the Frank-Kasper σ-phase. The molecular architecture is responsible in the formation of these interesting phases.

7.1 Composition Effect on Phase Behaviour

In the compositional study, two series of the symmetric SISO samples (the S blocks are divided equally) are studied with $f_S : f_I = 2 : 3, f_O = 0 – 32$ % and $f_S : f_I = 3 : 2, f_O = 0 – 35$ %. In the isoprene-rich symmetric SISO tetrablock terpolymers, core-shell geometries are formed by an O core, a shell of the internal and the terminal S blocks, in the I-rich matrix. The hexagonally ordered core-shell spherical and cylindrical morphologies (P_6/mmm and P_6/mm space group symmetries) have been identified in the bulk symmetric SISO tetrablock terpolymers with the increasing O content. Theoretical calculations based on a numerical self-consistent field theory (SCFT) for polymers predict correctly the core (O) and shell (S) domain geometries and provide valuable insights to the distribution of the block segments within the ordered structures including the asymmetric placement of the internal and the terminal S blocks within the core, shell and matrix domains, but fail to account for the simple hexagonal lattice with a P_6/mmm space group symmetry.

The temperature dependence is examined in detail using the one specimen from the symmetric isoprene-rich SISO series near the order-disorder boundary. A dodecagonal quasicrystalline (QC) phase has been identified which occurs as an intermediate state between the simple hexagonal order (P_6/mmm) and the Frank-Kasper σ-phase (P_{4_2}/mnm)

before the sample disorders, with $T_{HEX} < T_{QC} < T_{\sigma} < T_{ODT}$. The core-shell spherical domains are formed in all three ordered morphologies, with the O blocks being the core and the internal S' blocks forming the shell in an I-rich matrix, shielding the unfavourable I/O interactions. The TEM results reveal a QC morphology with a 12-fold rotational symmetry and the existence of the local dodecagonal quasicrystalline approximants that lack of any long-range translational order.

The sequence of phases reported the styrene-rich symmetric SISO tetrablock terpolymers is the disordered state ($f_O \leq 4\%$), spheres with a BCC lattice ($f_O = 9\%$), liquid-like packed (LLP) spheres ($f_O = 11 - 15\%$) and the hexagonally (HEX) ordered cylinders ($f_O = 31 - 35\%$). For the SISO samples with $f_O = 11\%$, LLP, 12-fold QC ($Pm\bar{3}n$ phase after longer annealing time of one day), σ-phase and the disordered states are formed with increasing temperatures; and for SISO samples with $f_O = 15\%$, LLP spheres and HEX cylinders are formed.

These results, together with another series with equal volume fraction of the S and the I blocks,[11,12] are summarized in Figure 7-1 (b) and compared with the well-studied ISO triblock system[5,8] (see Figure 7-1 (a)). The SISO tetrablock terpolymers exhibit dramatically different phase behaviors as that of the ISO triblocks with the ISO samples forming network morphologies such as double gyroid (Q^{230}), alternating gyroid (Q^{214}) and the *Fddd* orthorhombic structure (O^{70}) over a wide range of composition windows.[1,4,5,8,9,13,14] Changing the molecular architecture from the ISO triblocks to the SISO tetrablocks drives the preference from the hyperbolic interfaces inherent in the network morphologies to the higher, and zero Gauss, curvature surfaces present in the

core-shell spheres and cylinders. Molecular architecture plays a key role in the differences in the block copolymer phase behaviour between these two systems. The ABAC tetrablock molecular architecture offers a offer a new approach to independently control the domain shape and packing in the block copolymer melts through the manipulation of the magnitude and the sequencing of the binary segment-segment interactions ($\chi_{SI} \leq \chi_{SO} << \chi_{IO}$), which dictate the core segregation and the effective inter-domain interactions.

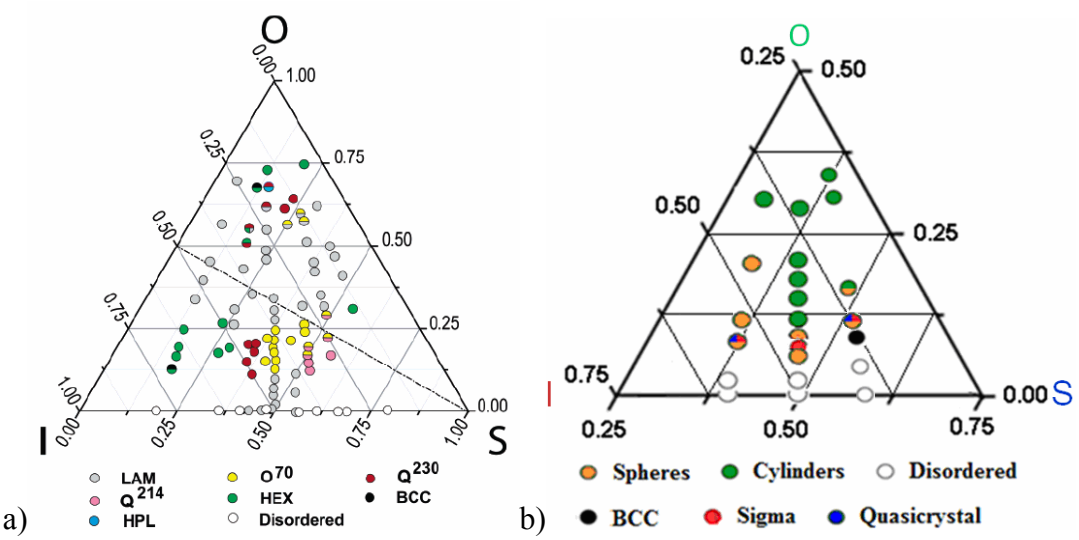

Figure 7-1 (a) Phase map for the ISO triblocks with the axes representing the volume fractions of each block in the vicinity of the order-disorder transition. The filled and open circles indicate the ordered and disordered states, respectively, within the experimental temperature range of $90 \leq T \leq 250$ ^{o}C. The samples with an OOT are represented with two different colors with the upper half showing the higher temperature state. Reproduced from Chatterjee *et al.*.[8] (b) Poly(styrene-*b*-isoprene-*b*- styrene-*b*-ethylene oxide) (SISO) phase portrait within the temperature range of $110 \leq T \leq 250$ ^{o}C.

7.2 Asymmetric Effect on Phase Behavior

In the asymmetric study, the ratios between the terminal S and the internal S' blocks in the asymmetric SIS'O samples are varied with the asymmetric parameter $\tau = N_S/(N_S+N_{S'}) = 0.21 – 0.70$ while keeping the other parameters such as f, χ and N constant. Controlling the asymmetric parameter $0 \leq \tau \leq 1$ and studying the resultant morphologies helps to elucidate the subtle factors that influence the phase behavior between the 'nonfrustrated' IS'O triblocks[1,5,13,15–19] and the 'frustrated' SIO triblocks[15,20–24]. The core-shell spheres on a hexagonal lattice ($\tau = 0.21 – 0.39$) and LLP ($\tau = 0.50 – 0.61$) have been observed at lower temperatures; the 12-fold QC phase ($\tau = 0.61 – 0.70$) with shorter annealing time of 30 minutes and the $Pm\bar{3}n$ phase after longer annealing time of one day have been observed at intermediate temperatures before the Frank-Kasper σ-phase ($\tau = 0.39 – 0.70$) is formed at the higher temperatures before the samples disorder.

Overall, the phase behaviors of the symmetric SISO and the asymmetric SIS'O tetrablock terpolymers are nearly identical. The asymmetric factor introduces some new effects not present in the symmetric SISO systems. First, a modest bidispersity of the S blocks lowers the elastic energies of the S domains.[25] Second, the high asymmetry lowers the stretching energies of the I blocks by pulling the shorter S blocks into the I domains. These two effects of lowering stretching energies in the S and I domains significantly change the domain sizes, cause large shifts in the phase boundaries, and influence the packing frustrations.

7.3 Various Spherical Phases

Most of the sphere-forming AB diblock copolymers form spherical phase with the BCC symmetry.[26] Altering the molecular architecture to ABAC type of tetrablock terpolymer increases the number of the sphere-forming phases to six and possibly more: BCC ($Im3\overline{m}$), LLP, P_6/mmm, QC, $Pm\overline{3}n$ and P_{4_2}/mnm (σ-phase). These phases (except for the BCC phase which is reported in one sample) have been discovered in several SISO samples with different compositions in this research work, indicating certain ordering tendencies. The Frank-Kasper σ-phase is also discovered in a diblock system of poly(isoprene-*b*-lactide) (IL),[12] indicating certain degree of the universal presence.[12] The formation of these interesting spherical phases indicates the great design flexibility and opportunities for the novel phase formation with the ABA'C tetrablock molecular architecture at various molecular weights and compositions. The sequence of the Flory-Huggins interaction parameters offers a wide range of spherical volume fractions due to the unfavourable I/O interactions which result in the formation of the core-shell spherical structure to eliminate the I/O interface with a shell of the internal S' block in a matrix of the terminal S (and the internal S') and I blocks.

7.4 References

(1) Bailey, T. S.; Hardy, C. M.; Epps III, T. H.; Bates, F. S. *Macromolecules* **2002**, *35*, 7007.

(2) Epps III, T. H.; Bailey, T. S.; Waletzko, R. S.; Bates, F. S. *Macromolecules*

2003, *36*, 2873.

(3) Cochran, E. W.; Morse, D. C.; Bates, F. S. *Macromolecules* **2003**, *36*, 782.

(4) Epps III, T. H.; Cochran, E. W.; Hardy, C. M.; Bailey, T. S.; Waletzko, R. S.; Bates, F. S. *Macromolecules* **2004**, *37*, 7085.

(5) Epps III, T. H.; Cochran, E. W.; Bailey, T. S.; Waletzko, R. S.; Hardy, C. M.; Bates, F. S. *Macromolecules* **2004**, *37*, 8325.

(6) Epps III, T. H.; Chatterjee, J.; Bates, F. S. *Macromolecules* **2005**, *38*, 8775.

(7) Epps III, T. H.; Bates, F. S. *Macromolecules* **2006**, *39*, 2676.

(8) Chatterjee, J.; Jain, S.; Bates, F. S. *Macromolecules* **2007**, *40*, 2882.

(9) Tyler, C. A.; Qin, J.; Bates, F. S.; Morse, D. C. *Macromolecules* **2007**, *40*, 4654.

(10) Meuler, A. J.; Ellison, C. J.; Evans, C. M.; Hillmyer, M. A.; Bates, F. S. *Macromolecules* **2007**, *40*, 7072.

(11) Bluemle, M. J.; Zhang, J.; Lodge, T. P.; Bates, F. S. *Macromolecules* **2010**, *43*, 4449.

(12) Lee, S.; Bluemle, M. J.; Bates, F. S. *Science* **2010**, *330*, 349.

(13) Cochran, E. W.; Bates, F. S. *Physical Review Letters* **2004**, *93*, 087802.

(14) Bluemle, M. J.; Fleury, G.; Lodge, T. P.; Bates, F. S. *Soft Matter* **2009**, *5*, 1587.

(15) Huckstadt, H.; Gopfert, A.; Abetz, V. *Polymer* **2000**, *41*, 9089.

(16) Abetz, V.; Goldacker, T. *Macromolecular Rapid Communications* **2000**, *21*, 16.

(17) Matsushita, Y.; Suzuki, J.; Seki, M. *Physica. B, Condensed Matter* **1998**, *248*, 238.

(18) Mogi, Y.; Mori, K.; Matsushita, Y.; Noda, I. *Macromolecules* **1992**, *25*, 5412.

(19) Mogi, Y.; Mori, K.; Kotauji, H.; Matauishita, Y.; Noda, I. *Macromolecules* **1993**, *26*, 5169.

(20) Huckstadt, H.; Goldacker, T.; Gopfert, A.; Abetz, V. *Macromolecules* **2000**, *33*, 3757.

(21) Bailey, T. S.; Pham, H. D.; Bates, F. S. *Macromolecules* **2001**, *34*, 6994.

(22) Shefelbine, T. A.; Vigild, M. E.; Matsen, M. W.; Hajduk, D. A.; Hillmyer, M. A.; Cussler, E. L.; Bates, F. S. *Journal of the American Chemical Society* **1999**, *121*, 8457.

(23) Stadler, R.; Auschra, C.; Beckmann, J.; Krappe, U.; Voight-Martin, I.; Leibler, L. *Macromolecules* **1995**, *28*, 3080.

(24) Zheng, W.; Wang, Z.-G. *Macromolecules* **1995**, *28*, 7215.

(25) Matsen, M. W. *Journal of Chemical Physics* **2000**, *113*, 5539.

(26) Leibler, L. *Macromolecules* **1980**, *13*, 1602.

Comprehensive Bibliography

Abe, E.; Saitoh, K.; Takakura, H.; Tsai, A. P.; Steinhardt, P. J.; Jeong, H.-C. *Physical Review Letters* **2000**, *84*, 4609.

Abetz, V.; Goldacker, T. *Macromolecular Rapid Communications* **2000**, *21*, 16.

Adams, J. L.; Graessley, W. W.; Register, R. A. *Macromolecules* **1994**, *27*, 6026.

Adams, J. L.; Quiram, D. J.; Graessley, W. W.; Register, R. A.; Marchand, G. R. *Macromolecules* **1996**, *29*, 2929.

Adhikari, R.; Michler, G. H. *Progress in Polymer Science* **2004**, *29*, 949.

Aksimentiev, A.; Holyst, R. *Macromolecular Theory and Simulations* **1999**, *8*, 328.

Almdal, K.; Bates, F. S.; Mortensen, K. *The Journal of Chemical Physics* **1992**, *96*, 9122.

Almdal, K.; Rosedale, J. H.; Bates, F. S. *Macromolecules* **1990**, *23*, 4336.

Alward, D. B.; Kinning, D. J.; Thomas, E. L.; Fetters, L. J. *Macromolecules* **1986**, *19*, 215.

Anthamatten, M.; Hammond, P. T. *Journal of Polymer Science Part B: Polymer Physics* **2001**, *39*, 2671.

Avgeropoulos, A.; Paraskeva, S.; Hadjichristidis, N.; Thomas, E. L. *Macromolecules* **2003**, *35*, 4030.

Bailey, T. S. *Ph.D. Dissertation;* University of Minnesota: Minneapolis, 2001.

Bailey, T. S.; Hardy, C. M.; Epps III, T. H.; Bates, F. S. *Macromolecules* **2002**, *35*, 7007.

Bailey, T. S.; Pham, H. D.; Bates, F. S. *Macromolecules* **2001**, *34*, 6994.

Bates, F. S.; Cohen, R. E.; Berney, C. V. *Macromolecules* **1982**, *15*, 589.

Bates, F. S.; Fredrickson, G. H. *Annual Review of Physical Chemistry* **1990**, *41*, 525.

Bates, F. S.; Fredrickson, G. H. *Physics Today* **1999**, *52*, 32.

Bates, F. S.; Hillmyer, M. A.; Lodge, T. P.; Bates, C. M.; Delaney, K. T.; Fredrickson, G. H. *Science* **2012**, *336*, 434.

Bates, F. S.; Rosedale, J. H.; Fredrickson, G. H. *The Journal of Chemical Physics* **1990**, *92*, 6255.

Bates, F. S.; Rosedale, J. H.; Fredrickson, G. H.; Glinka, C. J. *Physical Review Letters* **1988**, *61*, 2229.

Beckmann, J.; Auschra, C.; Stadler, R. *Macromolecular Rapid Communications* **1994**, *15*, 67.

Bindi, L.; Eiler, J. M.; Guan, Y.; Hollister, L. S.; MacPherson, G.; Steinhardt, P. J.; Yao, N. *Proceedings of the National Academy of Sciences of the United States of America* **2012**, *109*, 1396.

Bindi, L.; Steinhardt, P. J.; Yao, N.; Lu, P. J. *Science* **2009**, *324*, 5932.

Black, C. T.; Guarini, K. W.; Milkove, K. R.; Baker, S. M.; Russell, T. P.; Tuominen, M. T. *Applied Physics letters* **2001**, *79*, 409.

Bluemle, M. J. *Ph. D. Dissertation;* University of Minnesota: Minneapolis, 2010.

Bluemle, M. J.; Fleury, G.; Lodge, T. P.; Bates, F. S. *Soft Matter* **2009**, *5*, 1587.

Bluemle, M. J.; Zhang, J.; Lodge, T. P.; Bates, F. S. *Macromolecules* **2010**, *43*, 4449.

Brandrup, J.; Immergut, E. H. *Polymer Handbook*; 3rd ed.; John Wiley & Sons: New York, 1989.

Breiner, U.; Krappe, U.; Abetz, V.; Stadler, R. *Macromolecular Chemistry and Physics* **1997**, *198*, 1051.

Breiner, U.; Krappe, U.; Jakob, T.; Abetz, V.; Stadler, R. *Polymer Bulletin (Berlin)* **1998**, *40*, 219.

Breiner, U.; Krappe, U.; Stadler, R. *Macromolecular Rapid Communications* **1996**, *17*, 567.

Cahn, J. W.; Shechtman, D.; Gratias, D. *Materials Research* **1986**, *1*, 13.

Campbell, D.; White, J. R. *Polymer Characterization: Physical Techniques*; Chapman and Hall: New York, 1989.

Cavicchi, K. A.; Lodge, T. P. *Journal of Polymer Science Part B: Polymer Physics* **2003**, *41*, 715.

Ceolin, R.; Agafonov, V.; Fabre, C.; Rassat, A.; Dworkin, A.; Andre, D.; Szwarc, H.; Schierbeek, A. J.; Bernier, P.; Zahab, A. *Journal De Physique* **2004**, *428*, 157.

Chatterjee, J.; Jain, S.; Bates, F. S. *Macromolecules* **2007**, *40*, 2882.

Chin, S. S. *United State Patent* **1992**, 5118762.

Chin, S. S.; St. Clair, D. J.; Talbott, R. L. *United State Patent* **1993**, 5194500.

Cochran, E. W. *Ph.D. Dissertation;* University of Minnesota, 2004.

Cochran, E. W.; Bates, F. S. *Physical Review Letters* **2004**, *93*, 087802.

Cochran, E. W.; Garcia-Cervera, C. J.; Fredrickson, G. H. *Macromolecules* **2006**, *39*, 2449.

Cochran, E. W.; Morse, D. C.; Bates, F. S. *Macromolecules* **2003**, *36*, 782.

Colby, R. H. *Current Opinion in Colloid and Interface Science* **1996**, *1*, 454.

Cooper, W.; Hale, P. T.; Walker, J. S. *Polymer* **1974**, *15*, 175.

Cullity, B. D.; Stock, S. R. *Elements of X-Ray Diffraction*; Third.; Addison-Wesley Publishing Company, Inc: Reading, MA, 1956.

de Bruijn, N. *Nederlandse Akademie Wetenschappen Proc.* **1981**, *A84*, 39.

DeGennes, P. G. *Scaling Concepts in Polymer Physics*; Cornell University Press: Ithaca, NY, 1979.

DiVincenzo, D. P.; Steinhardt, P. J. *Quasicrystals: The State of the Art*; World Scientific: Singapore, 1991.

Dominik, L.; Martin, F.; Mojmir, S. *Physical Review Letters* **2007**, *99*, 106402.

Dormidontova, E. E.; Lodge, T. P. *Macromolecules* **2001**, *34*, 9143.

Doye, J. P. K.; Wales, D. J.; Zetterling, F. H. M.; Dzugutov, M. *Journal of Chemical Physics* **2003**, *118*, 2792.

Drolet, F.; Fredrickson, G. H. *Macromolecules* **2001**, *34*, 5317.

Drzewinski, M. A.; Cohen, R. E. *Polymeric Materials Science and Engineering* **1985**, *52*, 437.

Dzugutov, M. *Physical Review A* **1992**, *46*, R2984.

Dzugutov, M. *Physical Review Letters* **1993**, *70*, 2924.

Epps III, T. H.; Bailey, T. S.; Waletzko, R. S.; Bates, F. S. *Macromolecules* **2003**, *36*, 2873.

Epps III, T. H.; Bates, F. S. *Macromolecules* **2006**, *39*, 2676.

Epps III, T. H.; Chatterjee, J.; Bates, F. S. *Macromolecules* **2005**, *38*, 8775.

Epps III, T. H.; Cochran, E. W.; Bailey, T. S.; Waletzko, R. S.; Hardy, C. M.; Bates, F. S. *Macromolecules* **2004**, *37*, 8325.

Epps III, T. H.; Cochran, E. W.; Hardy, C. M.; Bailey, T. S.; Waletzko, R. S.; Bates, F. S. *Macromolecules* **2004**, *37*, 7085.

Fetters, L. J.; Lohse, D. J.; Richter, D.; Witten, T. A.; Zirkel, A. J. *Macromolecules* **1994**, *27*, 4639.

Fielding-Russell, G. S.; Pillai, P. S. *Polymer* **1974**, *15*, 97.

Fischer, C. A.; Simmons, E. R.; Kroll, M. S.; Lindquist, J. S. *United State Patent* **1999**, 5863977.

Floudas, G.; Vazaiou, B.; Schipper, F.; Ulrich, R.; Wiesner, U.; Iatrou, H.; Hadjichristidis, N. *Macromolecules* **2001**, *34*, 2947.

Foerster, S.; Khandpur, A. K.; Zhao, J.; Bates, F. S.; Hamley, I. W.; Ryan, A. J.; Bras, W. *Macromolecules* **1994**, *27*, 6922.

Fornasini, M. L.; Manfrinetti, P.; Mazzone, D. *Journal of Solid State Chemistry* **2006**, *179*, 2012.

Frank, F. C.; Kasper, J. S. *Acta Crystallographica* **1959**, *12*, 483.

Fredrickson, G. H. *The Equilibrium Theory of Inhomogeneous Polymers*; Clarendon Press: Oxford, 2006.

Fredrickson, G. H.; Bates, F. S. *Annual Review of Materials Science* **1996**, *26*, 501.

Fredrickson, G. H.; Helfand, E. *Journal of Chemical Physics* **1987**, *87*, 697.

Frielinghaus, H.; Hermsdorf, N.; Almdal, K.; Mortensen, K. M. L.; Corvazier, L.; Fairclough, J. P. A.; Ryan, A. J.; Hamley, I. W. *Europhysics Letters* **2001**, *53*, 680.

Gehlsen, M. D.; Almdal, K.; Bates, F. S. *Macromolecules* **1992**, *25*, 939.

Goldacker, T.; Abetz, V. *Macromolecules* **1999**, *32*, 5165.

Hadjichristidis, N.; Iatrou, H.; Pispas, S.; Pitsikalis, M. *Journal of Polymer Science Part A: Polymer Chemistry* **2000**, *38*, 3211.

Hadjichristidis, N.; Pitsikalis, M.; Iatrou, H. *Advances in Polymer Science* **2005**, *189*, 1.

Hajduk, D. A.; Harper, P. E.; Gruner, S. M.; Honeker, C. C.; Kim, G.; Thomas, E. L. *Macromolecules* **1994**, *27*, 4063.

Hajduk, D. A.; Takenouchi, H.; Hillmyer, M. A.; Bates, F. S.; Vigild, M. E.; Almdal, K. *Macromolecules* **1997**, *30*, 3788.

Hamley, I. W. *Developments in Block Copolymer Science and Technology*; John Wiley & Sons: Berlin, 2004.

Hamley, I. W.; Castelletto, V.; Yang, Z.; Price, C.; Booth, C. *Macromolecules* **2001**, *34*, 4079.

Hamley, I. W.; Gehlsen, M. D.; Khandpur, A. K.; Koppi, K. A.; Rosedale, J. H.; Schulz, M. F.; Bates, F. S.; Almdal, K.; Mortensen, K. *Journal de Physique II* **1994**, *4*, 2161.

Hamley, I. W.; Koppi, K. A.; Rosedale, J. H.; Bates, F. S.; Almdal, K.; Mortensen, K. M. L. *Macromolecules* **1993**, *26*, 5959.

Han, C. D.; Vaidya, N. Y.; Kim, D.; Shin, G.; Yamaguchi, D.; Hashimoto, T. *Macromolecules* **2000**, *33*, 3767.

Hardy, C. M.; Bates, F. S.; Kim, M.-H.; Wignall, G. D. *Macromolecules* **2002**, *35*, 3189.

Hasegawa, H.; Tanaka, H.; Yamasaki, K.; Hashimoto, T. *Macromolecules* **1987**, *20*, 1651.

Hashimoto, T.; Tsutsumi, K.; Funaki, Y. *Langmuir* **1997**, *13*, 6869.

Hashimoto, T.; Yamauchi, K.; Yamaguchi, D.; Hasegawa, H. *Macromolecular Symposia* **2003**, *201*, 65.

Hayashida, K.; Dotera, A.; Takano, A.; Matsushita, Y. *Physical Review Letters* **2007**, *98*, 195502.

Helfand, E. *Macromolecules* **1975**, *8*, 552.

Helfand, E.; Tagami, Y. *Journal of Chemical Physics* **1972**, *56*, 3592.

Helfand, E.; Wasserman, Z. R. *Macromolecules* **1976**, *9*, 879.

Herman, D. S.; Kinning, D. J.; Thomas, E. L.; Fetters, L. J. *Macromolecules* **1987**, *20*, 2940.

Hermel, T.; Hahn, S.; Chaffin, K.; Gerberich, W.; Bates, F. S. *Macromolecules* **2003**, *36*, 2190.

Hiemenz, P. C.; Lodge, T. P. *Polymer Chemistry*; Taylor & Francis Group: University of Minnesota: Minneapolis, MN, 2007.

Hillmyer, M. A.; Bates, F. S. *Macromolecules* **1996**, *29*, 6994.

Hillmyer, M. A.; Bates, F. S.; Almdal, K.; Mortensen, K.; Ryan, A. J.; Fairclough, J. P. A. *Science* **1996**, *271*, 976.

Holden, G.; Legge, N. R.; Quirk, R.; Schroeder, H. E. *Thermoplastic Elastomers*; 2nd ed.; Hanser/Gardner: Cincinnati, 1996.

Huang, Y. Y.; Hsu, J. Y.; Chen, H. L.; Hashimoto, T. *Macromolecules* **2007**, *40*, 406.

Huang, Y. Y.; Hsu, J. Y.; Chen, H. L.; Hashimoto, T. *Macromolecules* **2007**, *40*, 3700.

Huckstadt, H.; Goldacker, T.; Gopfert, A.; Abetz, V. *Macromolecules* **2000**, *33*, 3757.

Huckstadt, H.; Gopfert, A.; Abetz, V. *Polymer* **2000**, *41*, 9089.

Hudson, S. D.; Jung, H.-T.; Kewsuwan, P.; Percec, V.; Cho, W.-D. *Liquid Crystals* **1999**, *26*, 1493.

Imaizumi, K.; Ono, T.; Kota, T.; Okamota, S.; Sakurai, S. *Journal of Applied Crystallography* **2003**, *36*, 976.

International Tables for Crystallography, Volume B: Reciprocal Space; Shmueli, U., Ed.; 1st ed.; Springer, 1993.

Ishimasa, T.; Nissen, H.-U.; Fukano, Y. *Physical Review Letters* **1985**, *55*, 511.

Jaffer, K. M.; Wickham, R. A.; Shi, A.-C. *Macromolecules* **2004**, *37*, 7042.

Janot, C. *Quasicrystals: A Primer*; 2nd ed.; Oxford University Press: New York, 1994.

Jiang, A.; Yohannan, A.; Nnolim, N. O.; Tyson, T. A.; Axe, L.; Lee, S.; Cote, P. *Thin Solid Films* **2003**, *437*, 116.

Jones, H. *Proceedings of the Physical Society* **1937**, *49*, 250.

Kaga, M.; Ohta, T. *Journal of the Physical Society of Japan* **2006**, *75*, 043002.

Karatasos, K.; Anastasiadis, S.; Pakula, T.; Watanabe, H. *Macromolecules* **2000**, *33*, 523.

Kataoka, K.; Harada, A.; Nagasaki, Y. *Advanced Drug Delivery Reviews* **2001**, *47*, 113.

Keys, A. S.; Glotzer, S. C. *Physical Review Letters* **2007**, *99*, 235503.

Khandpur, A. K.; Foerster, S.; Bates, F. S.; Hamley, I. W.; Ryan, A. J.; Bras, W.; Almdal, K.; Mortensen, K. *Macromolecules* **1995**, *28*, 8796.

Kim, J. K.; Lee, H. H.; Gu, Q.-J.; Chang, T.; Jeong, Y. H. *Macromolecules* **1998**, *31*, 4045.

Kim, M. I.; Wakada, T.; Akasaka, S.; Nishitsuji, S.; Saijo, K.; Hasegawa, H.; Ito, K.; Takenaka, M. *Macromolecules* **2008**, *41*, 7667.

Kinning, D. J.; Thomas, E. L. *Macromolecules* **1984**, *17*, 1712.

Klein, H.; Audier, M.; Simonet, V.; Hippert, F.; Bellissent, R. Physica. B, *Condensed Matter* **1998**, *964*, 241.

Kleinert, H.; Maki, K. *Fortschritte der Physik* **1981**, *29*, 219.

Koberstein, J. T.; Russell, T. P.; Walsh, D. J.; Pottick, L. *Macromolecules* **1990**, *23*, 877.

Koppi, K. A.; Tirrell, M.; Bates, F. S.; Almdal, K.; Colby, R. H. *Journal de Physique II* **1992**, *2*, 1941.

Kossuth, M. B.; Morse, D. C.; Bates, F. S. *Journal of Rheology* **1999**, *43*, 167.

Krause, S. *Journal of Polymer Science, Polymer Physics Edition* **1969**, *7*, 249.

Kumar, M. N. V. R. *Journal of Pharmacy & Pharmaceutical Sciences* **2000**, *3*, 234.

Lach, R.; Adhikari, R.; Weidisch, R.; Huy, T. A.; Michler, G. H.; Grellmann, W.; Knoll, K. *Journal of Materials Science* **2004**, *39*, 1283.

Lazzari, M.; Liu, G.; Lecommandoux, S. *Block Copolymers in Nanoscience*; John Wiley & Sons: Betz-druck GmbH, Darmstadt, 2007.

Leary, D. F.; Williams, M. C. *Journal of Polymer Science, Polymer Letters Edition* **1970**, *8*, 335.

Lee, J. S.; Hirao, A.; Nakahama, S. *Macromolecules* **1989**, *22*, 2602.

Lee, S.; Bluemle, M. J.; Bates, F. S. *Science* **2010**, *330*, 349.

Leibler, L. *Macromolecules* **1980**, *13*, 1602.

Levine, D.; Steinhardt, P. J. *Physical Review Letters* **1984**, *53*, 2477.

Lifshitz, R. *Physical Review Letters* **1998**, *80*, 2717.

Liu, G. J.; Ding, J. F.; Guo, A.; Herfort, M.; BazettJones, D. *Macromolecules* **1997**, *30*, 1851.

Lodge, T. P. *Macromolecular Chemistry and Physics* **2003**, *204*, 265.

Ludwigs, S.; Boeker, A.; Voronov, A.; Rehse, N.; Magerle, R.; Krausch, G. *Nature Materials* **2003**, *2*, 744.

Macia, E. *Reports on Progress in Physics* **2006**, *69*, 397.

Macosko, C. W. *Rheology: Principles, Measurements and Applications*; Wiley-VCH: New York, 1994.

Mai, S.; Mingvanish, W.; Turner, S. C.; Chaibundit, C.; Fairclough, J. P. A.; Heatley, F.; Matsen, M. W.; Ryan, A. J.; Booth, C. *Macromolecules* **2000**, *33*, 5124.

Mansky, P.; Chaikin, P.; Thomas, E. L. *Journal of Materials Science* **1995**, *30*, 1987.

Mansour, A. S.; Johnson, L. F.; Lodge, T. P.; Bates, F. S. *Journal of Polymer Science Part B: Polymer Physics* **2010**, *48*, 566.

Matsen, M. W. *Journal of Chemical Physics* **1995**, *102*, 3884.

Matsen, M. W. *Journal of Chemical Physics* **2000**, *113*, 5539.

Matsen, M. W. *The Journal of Chemical Physics* **1998**, *108*, 785.

Matsen, M. W.; Bates, F. S. *Journal of Chemical Physics* **1997**, *106*, 2436.

Matsen, M. W.; Bates, F. S. *Journal of Polymer Science Part B: Polymer Physics* **1997**, *35*, 945.

Matsen, M. W.; Bates, F. S. *Macromolecules* **1996**, *29*, 1091.

Matsen, M. W.; Bates, F. S. *Macromolecules* **1996**, *29*, 7641.

Matsen, M. W.; Schick, M. *Macromolecules* **1994**, *27*, 187.

Matsen, M. W.; Schick, M. *Macromolecules* **1994**, *27*, 4014.

Matsen, M. W.; Schick, M. *Macromolecules* **1994**, *27*, 7157.

Matsen, M. W.; Schick, M. *Physical Review Letters* **1994**, *72*, 2660.

Matsen, M. W.; Thompson, R. B. *Journal of Chemical Physics* **1999**, *111*, 7139.

Matsushita, Y.; Nomura, M.; Watanabe, J.; Mogi, Y.; Noda, I.; Imai, M. *Macromolecules* **1995**, *28*, 6007.

Matsushita, Y.; Suzuki, J.; Seki, M. *Physica. B, Condensed Matter* **1998**, *248*, 238.

Matsushita, Y.; Tamura, M.; Noda, I. *Macromolecules* **1994**, *27*, 3680.

Mayes, A. M.; Olvera de la Cruz, M. *Journal of Chemical Physics* **1989**, *91*, 7228.

Mayes, A. M.; Olvera de la Cruz, M. *Journal of Chemical Physics* **1991**, *95*, 4670.

McKay, K. W.; Gros, W. A.; Diehl, C. F. *Journal of Applied Polymer Science* **1995**, *56*, 947.

Meier, D. J. *Journal of Polymer Science, Part C: Polymer Symposia* **1969**, *26*, 81.

Meuler, A. J.; Ellison, C. J.; Evans, C. M.; Hillmyer, M. A.; Bates, F. S. *Macromolecules* **2007**, *40*, 7072.

Meuler, A. J.; Ellison, C. J.; Hillmyer, M. A.; Bates, F. S. *Macromolecules* **2008**, *41*, 6272.

Meuler, A. J.; Fleury, G.; Hillmyer, M. A.; Bates, F. S. *Macromolecules* **2008**, *41*, 5809.

Milner, S. T.; Witten, T. A. *The Journal of Physiology (Paris)* **1988**, *49*, 1951.

Moffitt, M.; Vali, H.; Eisenberg, A. *Chemistry of Materials* **1998**, *10*, 1021.

Mogi, Y.; Mori, K.; Kotauji, H.; Matauishita, Y.; Noda, I. *Macromolecules* **1993**, *26*, 5169.

Mogi, Y.; Mori, K.; Matsushita, Y.; Noda, I. *Macromolecules* **1992**, *25*, 5412.

Mogi, Y.; Nomura, M.; Kotsuji, H.; Ohnishi, K.; Matsushita, Y.; Noda, I. *Macromolecules* **1994**, *27*, 6755.

Mori, Y.; Lim, L. S.; Bates, F. S. *Macromolecules* **2003**, *36*, 9879.

Morrison, F. A.; Winter, H. H.; Gronski, W.; Barnes, J. D. *Macromolecules* **1990**, *23*, 4200.

Nakatani, A. I.; Morrison, F. A.; Douglas, J. F.; Mays, J. W.; Jackson, C. L.; Muthukumar, M.; Han, C. C. *Journal of Chemical Physics* **1996**, *104*, 1589.

Ndoni, S.; Papadakis, C. M.; Bates, F. S.; Almdal, K. *Review of Scientific Instruments* **1995**, *66*, 1090.

Neumann, C.; Abetz, V.; Stadler, R. *Polymer Bulletin* **1996**, *36*, 43.

Neumann, C.; Loveday, D. R.; Abetz, V.; Stadler, R. *Macromolecules* **1998**, *31*, 2493.

Odian, G. *Principles of Polymerization*; Wiley: New York, 2004.

Park, M.; Harrison, C.; Chaikin, P. M.; Register, R. A.; Adamson, D. H. *Science* **1997**, *276*, 1401.

Patel, S. S.; Larson, R. G.; Winey, K. I.; Watanabe, H. *Macromolecules* **1995**, *28*, 4313.

Paterson, A. L. T. *Groupoids, Inverse Semigroups, and Their Operator Algebras*; Springer: Boston, MA, 1999.

Pennycook, S. J.; Jesson, D. E. *Ultramicroscopy* **1991**, *37*, 14.

Penrose, R. *Bulletin of the Institute of Mathematics and its Applications* **1974**, *10*, 266.

Percec, V.; Ahn, C.-H.; Ungar, G.; Yeardley, D. J. P.; Moller, M.; Sheiko, S. S. *Nature* **1998**, *391*, 161.

Percec, V.; Imam, M. R.; Peterca, M.; Wilson, D. A.; Graf, R.; Spiess, H. W.; Balagurusamy, V. S. K.; Heiney, P. A. *The Journal of American Chemical Society* **2009**, *131*, 7662.

Pochan, D. J.; Gido, S. P.; Zhou, J.; Mays, J. W.; Whitmore, M.; Ryan, A. J. *Journal of Polymer Science Part B: Polymer Physics* **1997**, *35*, 2629.

Price, C.; Lally, T. P.; Stubbersfield, R. *Polymer* **1974**, *15*, 541.

Qi, S.; Wang, Z. G. *Macromolecules* **1997**, *30*, 4491.

Qin, J.; Bates, F. S.; Morse, D. C. *Macromolecules* **2010**, *43*, 5128.

Quirk, R. P.; Ma, J.-J. *Journal of Polymer Science Part A: Polymer Chemistry* **1988**, *26*, 2031.

Riise, B. L.; Fredrickson, G. H.; Larson, R. G.; Pearson, D. S. *Macromolecules* **1995**, *28*, 7653.

Rosedale, J. H.; Bates, F. S. *Macromolecules* **1990**, *23*, 2329.

Rosen, B. M.; Wilson, D. A.; Wilson, C. J.; Peterca, M.; Won, B. C.; Huang, C.; Lipski, L. R.; Zeng, X.; Ungar, G.; Heiney, P. A.; Percec, V. *Journal of the American Chemical Society* **2009**, *131*, 17500.

Rosler, A.; Vandermeulen, G. W. M.; Klok, H.-A. *Advanced Drug Delivery Reviews* **2001**, *53*, 95.

Ryan, A. J.; Hamley, I. W.; Bras, W.; Bates, F. S. *Macromolecules* **1995**, *28*, 3860.

Ryu, C. Y.; Lee, M. S.; Hajduk, D. A.; Lodge, T. P. *Journal of Polymer Science Part B* **1997**, *35*, 2811.

Ryu, C.; Ruokolainen, J.; Fredrickson, G. H.; Kramer, E. J.; Hahn, S. *Macromolecules* **2002**, *35*, 2157.

Sakamoto, N.; Hashimoto, T.; Han, C. D.; Kim, D.; Vaidya, N. Y. *Macromolecules* **1997**, *30*, 1621.

Schipper, F. J. M.; Floudas, G.; Pispas, S.; Hadjichristidis, N.; Pakula, T. *Macromolecules* **2002**, *35*, 8860.

Schulz, M. F.; Bates, F. S.; Almdal, K.; Mortensen, K. *Physical Review Letters* **1994**, *73*, 86.

Schulz, M. F.; Khandpur, A. K.; Bates, F. S.; Almdal, K.; Mortensen, K.; Hajduk, D. A.; Gruner, S. M. *Macromolecules* **1996**, *29*, 2857.

Schwab, M.; Stuehn, B. *Physical Review Letters* **1996**, *76*, 924.

Seki, M.; Sujuki, J.; Matsushita, Y. *Journal of Applied Crystallography* **2000**, *33*, 285.

Semenov, A. N. *Macromolecules* **1989**, *22*, 2849.

Semenov, A. N. *Soviet Physics, JETP* **1985**, *61*, 733.

Shechtman, D.; Blech, I.; Gratias, D.; Cahn, J. *Physical Review Letters* **1984**, *53*, 1951.

Shefelbine, T. A.; Vigild, M. E.; Matsen, M. W.; Hajduk, D. A.; Hillmyer, M. A.; Cussler, E. L.; Bates, F. S. *Journal of the American Chemical Society* **1999**, *121*, 8457.

Sides, S. W.; Fredrickson, G. H. *Polymer* **2003**, *44*, 5859.

Silverstein, R. M.; Webster, F. X.; Kiemle, D. J. *Spectrometric Identification of Organic Compounds*; John Wiley & Sons: Hoboken, NJ, 2005.

Stadler, R.; Auschra, C.; Beckmann, J.; Krappe, U.; Voight-Martin, I.; Leibler, L. *Macromolecules* **1995**, *28*, 3080.

Stout, G. H.; Jensen, L. H. *X-Ray Structure Determination*; John Wiley & Sons: New York, 1989.

Suzuki, J.; Seki, M.; Matsushita, Y. *Journal of Chemical Physics* **2000**, *112*, 4862.

Szwarc, M. *Nature* **1956**, *178*, 1168.

Takano, A.; Soga, K.; Suzuki, J.; Matsushita, Y. *Macromolecules* **2003**, *36*, 9288.

Takenaka, M.; Wakada, T.; Akasaka, S.; Nishitsuji, S.; Saijo, K.; Shimizu, H.; Kim, M. I.; Hasegawa, H. *Macromolecules* **2007**, *40*, 4399.

Thomas, E. L.; Alward, D. B.; Kinning, D. J.; Martin, D. C.; Handlin Jr., D. L.; Fetters, L. J. *Macromolecules* **1986**, *19*, 2197.

Tsai, A. P. *Science and Technology of Advanced Materials* **2008**, *9*, 013008.

Tyler, C. A.; Morse, D. C. *Physical Review Letters* **2005**, *94*, 208302.

Tyler, C. A.; Qin, J.; Bates, F. S.; Morse, D. C. *Macromolecules* **2007**, *40*, 4654.

Ungar, G.; Liu, Y.; Zeng, X.; Percec, V.; Cho, W. D. *Science* **2003**, *299*, 1208.

Ungar, G.; Zeng, X. *Soft Matter* **2005**, *1*, 95.

Vigild, M. E.; Chu, C.; Sugiyama, M.; Chaffin, K. A.; Bates, F. S. *Macromolecules* **2001**, *34*, 951.

Wang, H. *Bell Systems Technical Journal* **1961**, *40*, 1.

Wang, J. F.; Mueller, M.; Wang, Z. G. *Journal of Chemical Physics* **2009**, *130*, 154902.

Wang, N.; Chen, H.; Kuo, K. *Physical Review Letters* **1987**, *59*, 1010.

Wang, X.; Dormidontova, E. E.; Lodge, T. P. *Macromolecules* **2002**, *35*, 9687.

Watanabe, H. *Macromolecules* **1995**, *28*, 5006.

Watanabe, H.; Sato, T.; Osaki, K. *Macromolecules* **2000**, *33*, 2545.

Wetton, R. E. *Polymer Characterization*; Blackie Academic & Professional: New York, 1993.

Whitmore, M. D. *Encyclopedia of Materials: Science and Technology*; Elsevier Science: Oxford, 2001.

Williams, D. B.; Carter, C. B. *Transmission Electron Microscopy*: A Textbook for Materials Science; Plenum Press: New York, 1996.

Williams, M. L.; Landel, R. F.; Ferry, J. D. *Journal of the American Chemical Society* **1955**, *77*, 3701.

Winey, K. I.; Thomas, E. L.; Fetters, L. J. *Macromolecules* **1992**, *25*, 2645.

Winter, H. H.; Scott, D. B.; Gronski, W.; Okamoto, S.; Hashimoto, T. *Macromolecules* **1993**, *26*, 7236.

Wolf, R. M.; Aalst, W. *Acta Crystallographica* **1972**, *28*, 111.

Woloszczuk, S.; Banaszak, M. *European Physical Journal E* **2010**, *33*, 343.

Wu, L.; Cochran, E. W.; Lodge, T. P.; Bates, F. S. *Macromolecules* **2004**, *37*, 3360.

Xie, R.; Yang, B.; Jiang, B. *Macromolecules* **1993**, *26*, 7097.

Yamamoto, A. *Acta Crystallographica* **1996**, *A52*, 509.

Yamamoto, A. *Science and Technology of Advanced Materials* **2008**, *9*, 013001.

Zeng, X.; Ungar, G.; Liu, Y.; Percec, V.; Dulcey, A. E.; Hobbs, J. K. *Nature* **2004**, *428*, 157.

Zhang, J.; Bates, F. S. *Journal of the American Chemical Society* **2012**, *134*, 7636.

Zhang, J.; Scott, S. W.; Bates, F. S. *Macromolecules* **2012**, *45*, 256.

Zhao, J.; Majumdar, B.; Schulz, M. F.; Bates, F. S.; Almdal, K.; Mortensen, K.; Hajduk, D. A.; Gruner, S. M. *Macromolecules* **1996**, *29*, 1204.

Zheng, W.; Wang, Z.-G. *Macromolecules* **1995**, *28*, 7215.

Appendix

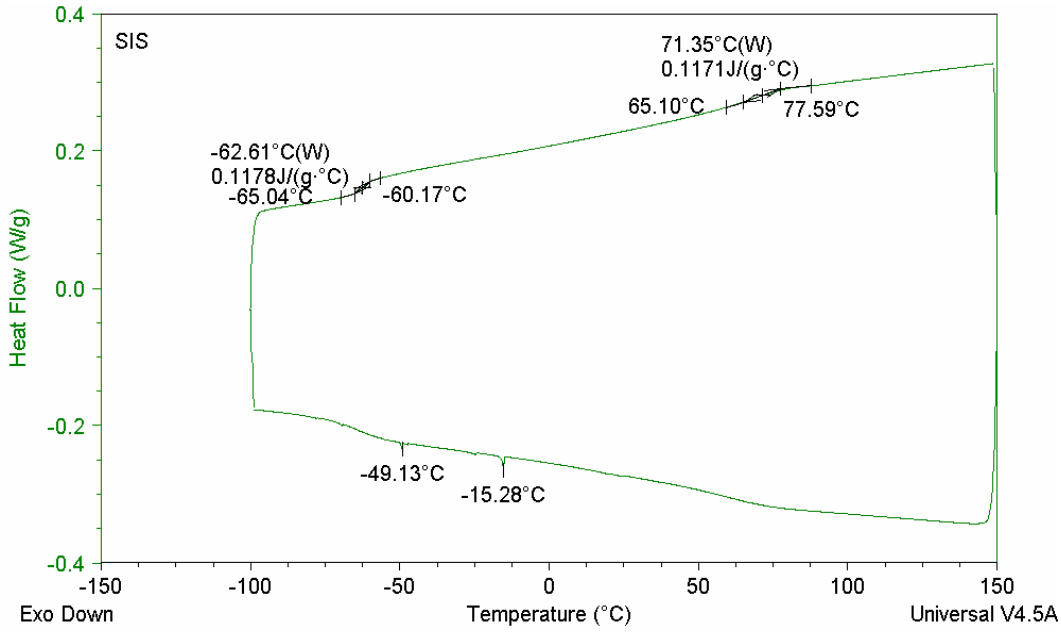

Figure A-1 The DSC data for the SIS-OH triblock precursor.

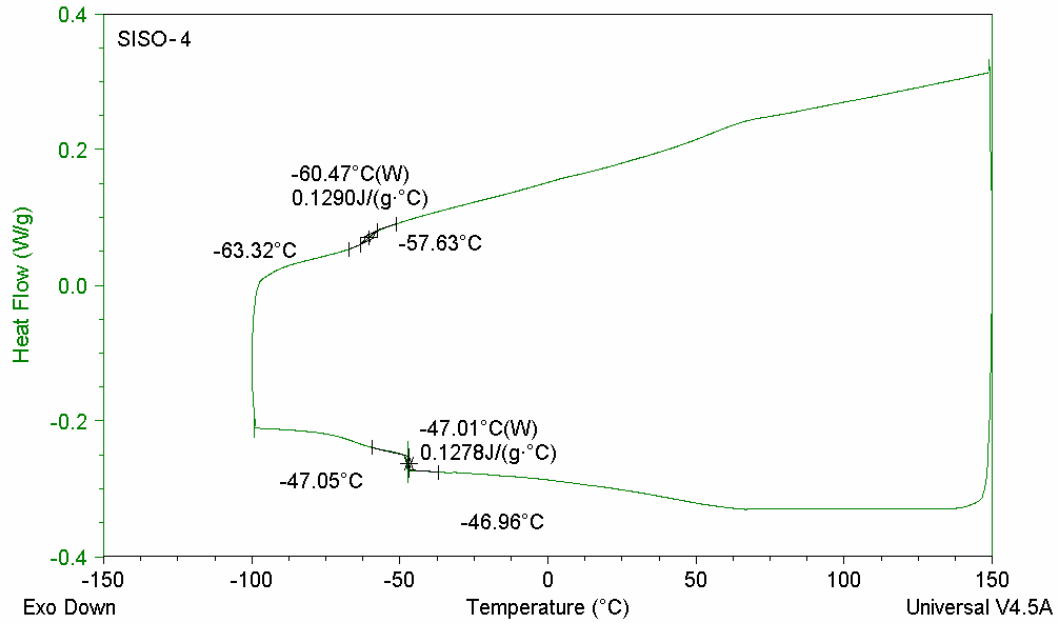

Figure A-2 The DSC data for the SISO-4 tetrablock terpolymers.

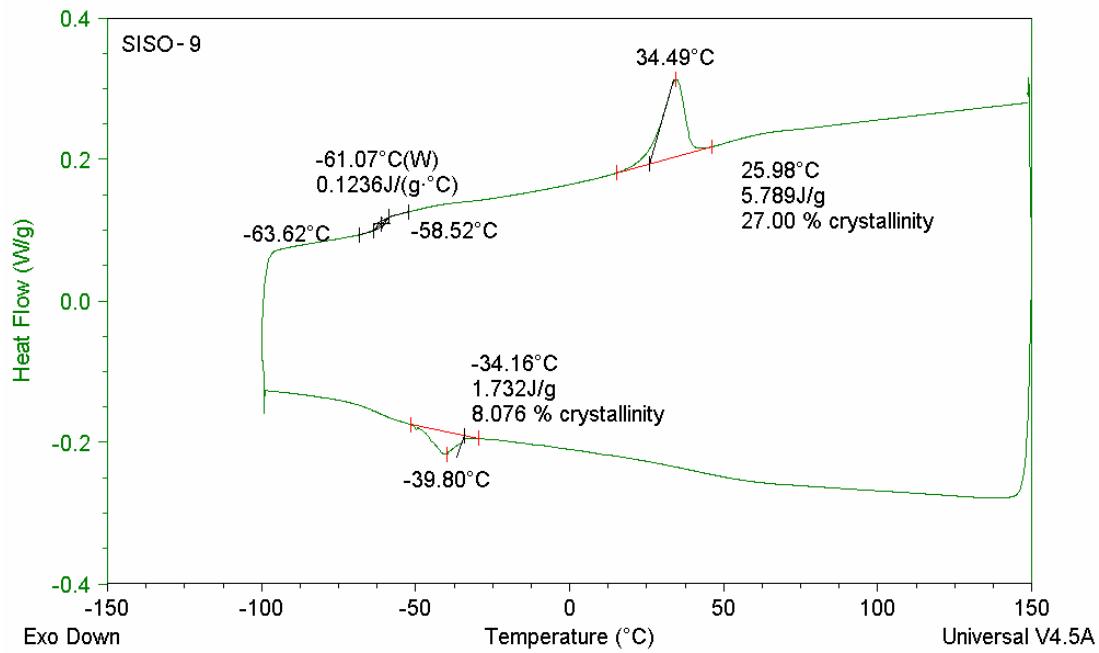

Figure A-3 The DSC data for the SISO-9 tetrablock terpolymers.

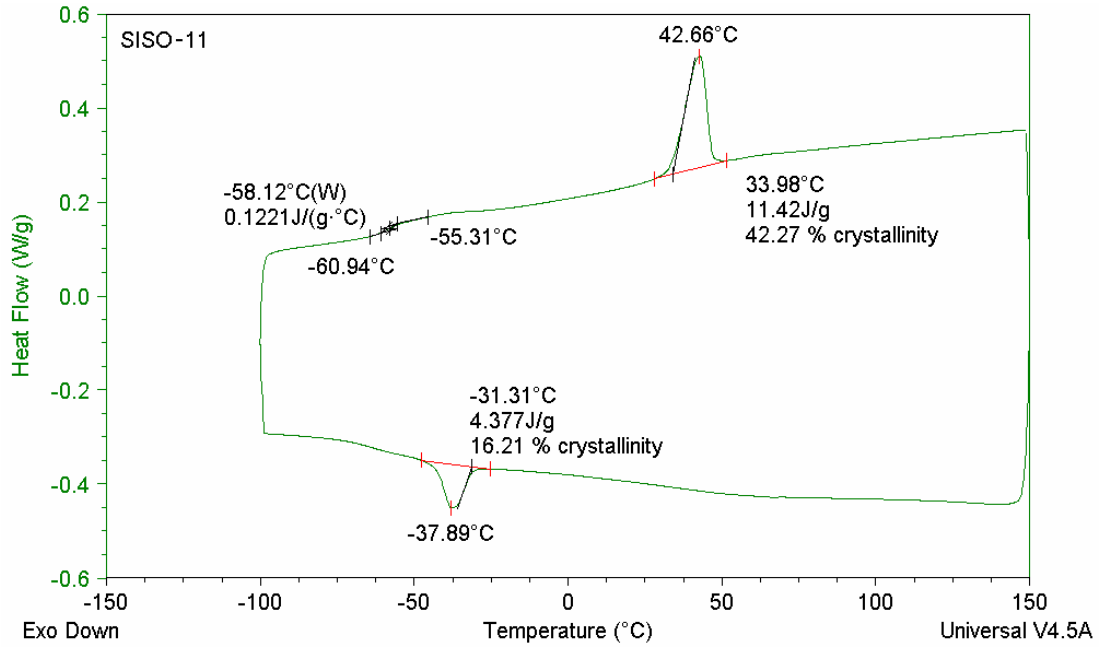

Figure A-4 The DSC data for the SISO-11 tetrablock terpolymers.

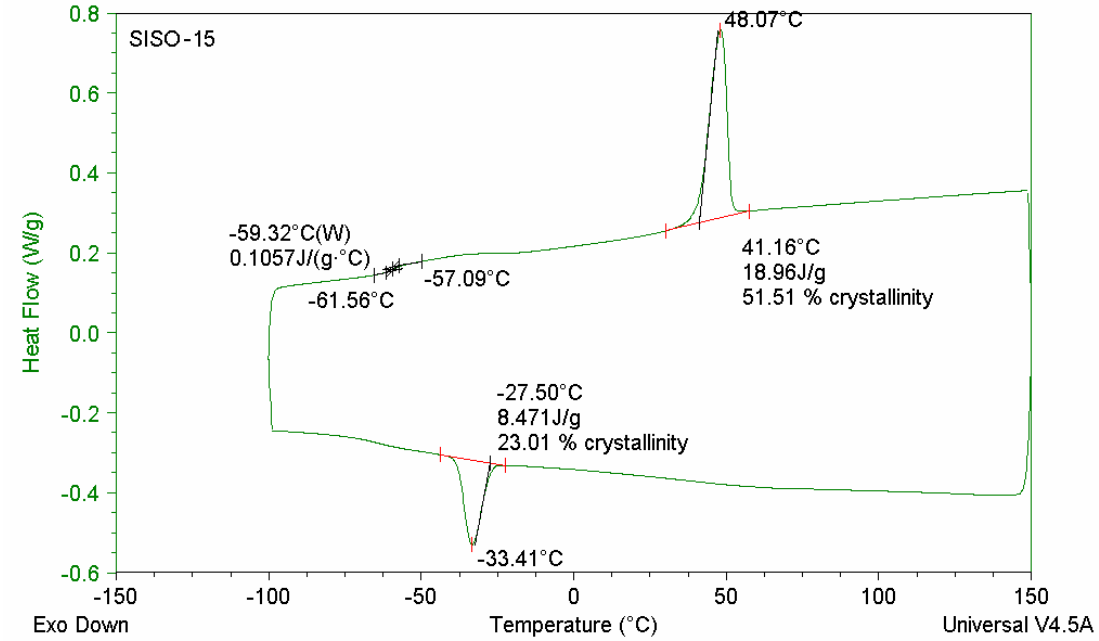

Figure A-5 The DSC data for the SISO-15 tetrablock terpolymers.

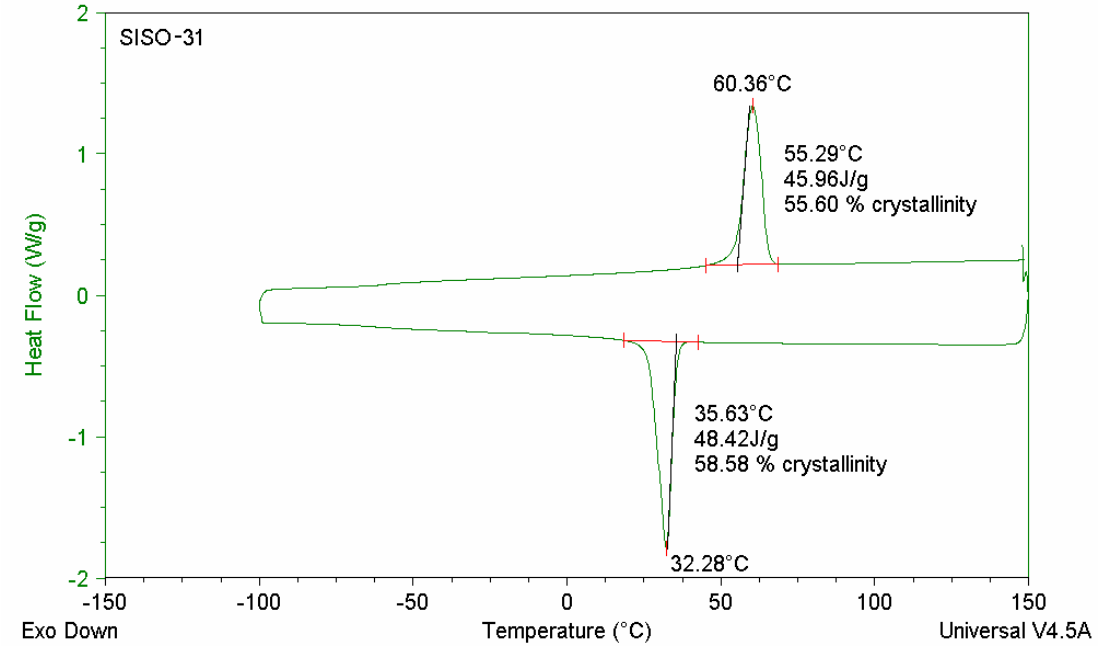

Figure A-6 The DSC data for the SISO-31 tetrablock terpolymers.

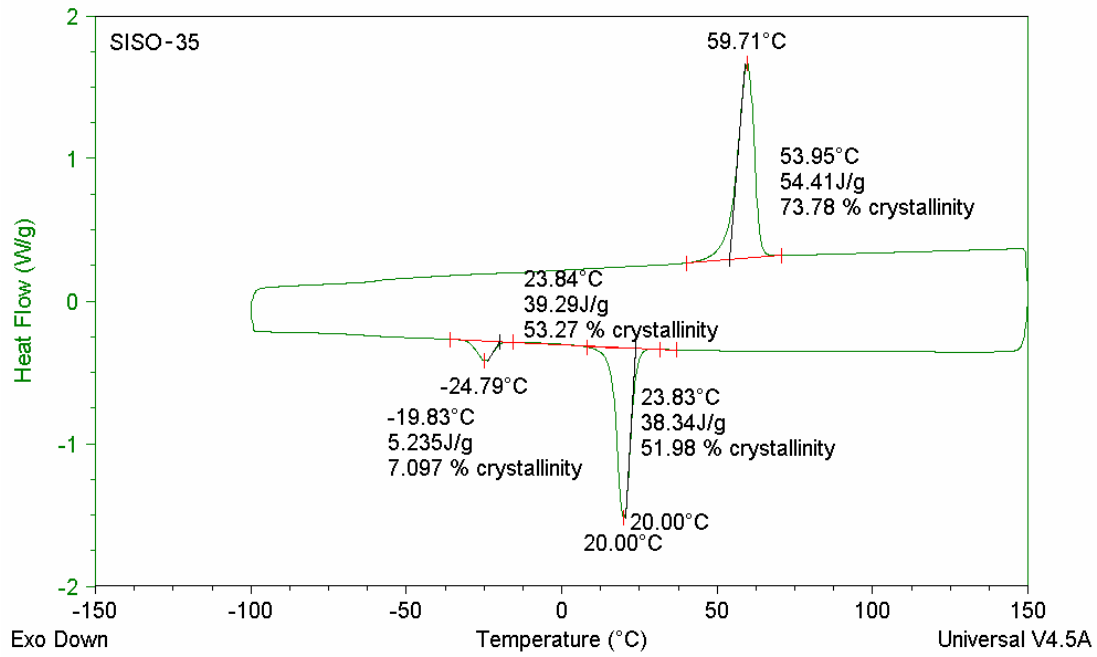

Figure A-7 The DSC data for the SISO-35 tetrablock terpolymers.